

Nonlinear waves in \mathcal{PT} -symmetric systems

Vladimir V. Konotop^{*}

*Centro de Física Teórica e Computacional and Departamento de Física,
Faculdade de Ciências, Universidade de Lisboa,
Campo Grande, Ed. C8, Lisboa 1749-016, Portugal*

Jianke Yang[†]

*Department of Mathematics and Statistics, University of Vermont,
Burlington, Vermont 05401, USA*

Dmitry A. Zezyulin[‡]

*Centro de Física Teórica e Computacional and Departamento de Física,
Faculdade de Ciências, Universidade de Lisboa,
Campo Grande, Ed. C8, Lisboa 1749-016, Portugal*

(published 18 July 2016)

Recent progress on nonlinear properties of parity-time (\mathcal{PT})-symmetric systems is comprehensively reviewed in this article. \mathcal{PT} symmetry started out in non-Hermitian quantum mechanics, where complex potentials obeying \mathcal{PT} symmetry could exhibit all-real spectra. This concept later spread out to optics, Bose-Einstein condensates, electronic circuits, and many other physical fields, where a judicious balancing of gain and loss constitutes a \mathcal{PT} -symmetric system. The natural inclusion of nonlinearity into these \mathcal{PT} systems then gave rise to a wide array of new phenomena which have no counterparts in traditional dissipative systems. Examples include the existence of continuous families of nonlinear modes and integrals of motion, stabilization of nonlinear modes above \mathcal{PT} -symmetry phase transition, symmetry breaking of nonlinear modes, distinctive soliton dynamics, and many others. In this article, nonlinear \mathcal{PT} -symmetric systems arising from various physical disciplines are presented, nonlinear properties of these systems are thoroughly elucidated, and relevant experimental results are described. In addition, emerging applications of \mathcal{PT} symmetry are pointed out.

DOI: [10.1103/RevModPhys.88.035002](https://doi.org/10.1103/RevModPhys.88.035002)

CONTENTS

I. Introduction	2	B. \mathcal{PT} lasers	11
II. Non-Hermitian Operators with Real Spectra	3	C. Atomic gases	12
A. Definition and basic properties	3	D. Plasmonic waveguides	13
1. \mathcal{PT} -symmetric parabolic potentials	4	E. Metamaterials and transformation optics	13
2. Bender-Boettcher potential	4	1. One-dimensional \mathcal{PT} -symmetric metamaterial	13
3. Two-level \mathcal{PT} -symmetric system	4	2. Transformation optics	14
B. Exceptional points	5	3. \mathcal{PT} -symmetry breaking in polarization space	14
C. \mathcal{PT} symmetry and pseudo-Hermiticity	5	F. Exciton-polariton condensates	15
D. Real spectrum and effect of perturbations	6	G. Bose-Einstein condensates	16
E. Supersymmetry and real spectra	7	H. Spin-orbit coupled Bose-Einstein condensates	16
F. Soliton theory and \mathcal{PT} -symmetric potentials	8	I. Superconductivity	17
III. \mathcal{PT} Symmetry in Nonlinear Physics	8	J. Magnetics	18
A. Optics	8	K. Electronic circuits	18
1. Paraxial optics versus quantum mechanics	8	L. Microcavities	19
2. Modeling pulse propagation through a \mathcal{PT} layer	9	M. Acoustics	19
3. Discrete optics	9	IV. \mathcal{PT} -symmetric Discrete Lattices	20
4. Nonlinearity	10	A. Formalism for discrete nonlinear systems	20
5. Synthetic photonic lattices	10	B. Discrete configurations and their linear properties	20
6. \mathcal{PT} symmetry introduced by time management	11	1. Arrays with nearest-neighbor linear interactions	20
		2. Infinite lattices with unbroken \mathcal{PT} symmetry	22
		a. An open chain with alternating coupling and dissipation	22
		b. An open chain with embedded defect	22
		c. Array of dimers	22
		3. Array of metamaterial dimers	22

^{*}vvkonotop@fc.ul.pt

[†]jyang@math.uvm.edu

[‡]dzezyulin@fc.ul.pt

C. Nonlinear stationary modes	23	1. 1D dynamics	43
1. Exact solutions and the main features of nonlinear modes	23	2. 2D dynamics	44
2. Nonlinear modes as continuous families and isolated points	23	D. Nonlinear \mathcal{PT} -symmetric lattices	45
a. Continuous families of \mathcal{PT} -symmetric solutions	23	E. Solitons in generalized lattice models	45
b. Isolated asymmetric solutions	24	1. Vector mixed-gap solitons	45
c. Isolated \mathcal{PT} -symmetric solutions	24	2. Generalized nonlinearities	46
3. Continuous families of discrete solitons	24	3. \mathcal{PT} -symmetric superlattices	46
a. Bifurcation from the linear limit	24	4. Defect solitons	46
b. Anticontinuum limit	24	F. Bragg solitons	46
4. Discrete compactons	25	VIII. \mathcal{PT} -symmetric $\chi^{(2)}$ Media	47
5. Vortices in closed arrays	26	A. Quadratic media with \mathcal{PT} -symmetric potentials	47
6. Solitons and vortices in coupled dNLS equations	27	B. \mathcal{PT} -symmetric coupler with quadratic nonlinearity	48
D. Nonlinear dynamics of \mathcal{PT} -symmetric arrays	27	IX. Partial \mathcal{PT} Symmetry	48
1. Conservative versus dissipative dynamics	27	X. Spectral Singularities	49
2. \mathcal{PT} -symmetric dimer	28	A. Spectral singularities in the linear theory	49
a. Conserved quantities, integrability, and Hamiltonian structure	28	B. Spectral singularities of a nonlinear layer	50
b. Global existence, bounded, and unbounded solutions	28	XI. \mathcal{PT} Symmetry in Klein-Gordon Models	51
c. Unidirectional propagation	28	XII. \mathcal{PT} Deformations of Nonlinear Equations	51
3. Two coupled nonlinear oscillators	28	A. Deformed KdV equation	51
4. Scattering on a \mathcal{PT} -symmetric defect	29	B. Deformed Hopf and Burgers equations	52
5. \mathcal{PT} -symmetric dimers with varying parameters	29	C. Deformed short pulse equation	53
E. Observation of \mathcal{PT} -synthetic solitons	30	D. Nonlocal NLS equation	53
V. \mathcal{PT} -symmetric Coupled NLS Equations	30	XIII. Conclusions and Perspectives	53
A. The model and its basic properties	30	Acknowledgments	53
B. Modulational instability	31	References	54
C. Bright solitons	32		
D. Breathers	32		
E. Solitons in couplers with varying parameters	33		
1. Stabilization of a soliton at an exceptional point	33		
2. Interaction of a soliton with an exceptional point	33		
3. Soliton switching by a \mathcal{PT} -symmetric defect	34		
F. Rogue waves	34		
G. Dark solitons	35		
H. Generalized \mathcal{PT} -symmetric coupled NLS equations	35		
1. Circular arrays	35		
2. Multidimensional NLS equations and wave collapse	35		
I. Localized modes in \mathcal{CPT} -symmetric BECs	36		
VI. Nonlinear Modes in Complex Potentials	36		
A. Localized potentials	36		
1. Exact solutions	36		
2. Scattering on a \mathcal{PT} -symmetric defect	37		
B. Parabolic potential	38		
C. Symmetry breaking of solitons	38		
D. Soliton families in asymmetric complex potentials	39		
VII. Nonlinear Waves in Periodic Potentials	40		
A. Linear spectrum of periodic potentials	41		
1. 1D lattice	41		
2. 2D lattices	42		
B. Solitons and their stability	42		
1. Solitons in 1D lattices	42		
2. 2D solitons	43		
3. Nonlinear periodic solutions and constant-intensity waves	43		
C. Nonlinear dynamics near the phase-transition point	43		

I. INTRODUCTION

Symmetries are the most fundamental properties of nature, which are responsible for many physical phenomena we observe. Not long ago [Bender and Boettcher \(1998\)](#) suggested that parity (\mathcal{P}) and time (\mathcal{T}) symmetries can be responsible for purely real spectra of non-Hermitian operators. While examples of such operators were known for a long time, the discovery of [Bender and Boettcher \(1998\)](#) had profound significance, because it suggested a possibility of \mathcal{PT} -symmetric modification of the conventional quantum mechanics which considers observables as Hermitian operators in the Hilbert space L^2 . This idea was further developed by [Mostafazadeh \(2002a, 2002b\)](#) who introduced and explored a general class of pseudo-Hermitian operators with special symmetries and purely real spectra. These works have since stimulated intensive research on \mathcal{PT} -symmetric operators. Developments on this front have been covered in a series of reviews ([Bender, 2005, 2007](#); [Mostafazadeh, 2010](#); [Makris et al., 2011](#)) and special issues in [Geyer, Heiss, and Znojil \(2006\)](#), [Fring, Jones, and Znojil \(2008\)](#), and [Bender et al. \(2012\)](#).

The concept of \mathcal{PT} symmetry has gone far beyond quantum mechanics and has spread to many branches of physics. [Ruschhaupt, Delgado, and Muga \(2005\)](#) noticed that if a medium where a light pulse propagates has an even refractive index profile and odd gain-loss landscape, then one can construct an optical analog of \mathcal{PT} -symmetric quantum mechanics. The real explosion of the \mathcal{PT} -symmetric optics and photonics started after the works by [El-Ganainy et al. \(2007\)](#), [Makris et al. \(2008\)](#), and [Muslimani et al. \(2008a\)](#) who suggested and elaborated paraxial \mathcal{PT} -symmetric optics. Moreover, [El-Ganainy et al. \(2007\)](#) established the concept of \mathcal{PT} -symmetric waveguide optics, by showing that discrete optics provides a simple but nontrivial framework for the

study of \mathcal{PT} -symmetric systems. The \mathcal{PT} -symmetric optical theories were soon confirmed in a series of experiments (Guo *et al.*, 2009; Rüter *et al.*, 2010; Feng *et al.*, 2011; Regensburger *et al.*, 2012). Extension of \mathcal{PT} symmetry to other branches of physics then quickly followed.

These developments suggested further extension of the theory to include *nonlinearity*, which is inherent in many fields of physics and is responsible for a wide variety of new phenomena. This study was initiated in nonlinear optics with linear \mathcal{PT} -symmetric potentials by Musslimani *et al.* (2008a). Later on optical systems with nonlinear \mathcal{PT} -symmetric potentials were also explored (Abdullaev, Kartashov *et al.*, 2011; Miroshnichenko, Malomed, and Kivshar, 2011). Presently the first experimental studies of nonlinear \mathcal{PT} -symmetric physics are already available (Peng, Özdemir, Lei *et al.* (2014); Wimmer *et al.*, 2015). From a practical point of view, important applications of \mathcal{PT} symmetry such as single-mode \mathcal{PT} lasers (Feng *et al.*, 2014; Hodaei *et al.*, 2014) and unidirectional reflectionless \mathcal{PT} -symmetric metamaterial at optical frequencies (Feng *et al.*, 2013) have also emerged.

Why are \mathcal{PT} systems interesting for physics beyond quantum mechanics? There are a number of reasons. One reason is that \mathcal{PT} systems, being dissipative in nature, exhibit many properties of conservative systems, such as all-real linear spectra and the existence of nonlinear steady states with continuous ranges of energy values. Such hybrid properties make \mathcal{PT} systems physically novel. Another reason is that \mathcal{PT} systems offer some exciting applications, such as those mentioned previously. A third reason is that loss was always considered to be a detrimental physical effect in the past. \mathcal{PT} symmetry makes loss useful, which is physically enlightening. Finally, gain and loss can be varied in time, opening new possibilities for flexible control and steering of physical processes.

In this review we describe recent developments on nonlinear \mathcal{PT} -symmetric systems. Even though reviews on linear \mathcal{PT} theories and non-Hermitian quantum mechanics have been written [see Bender (2007) and Mostafazadeh (2009a, 2010) for instance], a comprehensive review on nonlinear \mathcal{PT} -symmetric systems is still lacking. More importantly, the field of nonlinear \mathcal{PT} systems has been developing very rapidly, and a large body of knowledge has been obtained just in the past few years. Thus it is timely to write a review on this subject.¹

II. NON-HERMITIAN OPERATORS WITH REAL SPECTRA

In this section, we overview the main concepts in the theory of \mathcal{PT} -symmetric (and, more generally, non-Hermitian) linear operators. We do not intend to cover all available results of this extremely vast field, but rather to systematize the material relevant for description of nonlinear systems presented in the subsequent sections. For comprehensive reviews on non-Hermitian operators in physics and mathematics, in addition to the works listed in the Introduction, we also mention the

¹After submission of this review we became aware of the work of Suchkov *et al.* (2016) which addresses \mathcal{PT} symmetry in optical applications.

reviews by Muga *et al.* (2004), Cannata, Dedonder, and Ventura (2007), Rotter (2009), Daley (2014), and Garcia, Prodan, and Putinar (2014), as well as the monograph of Moiseyev (2011).

A. Definition and basic properties

Let $\psi(\mathbf{r}, t)$ be a complex-valued wave function of a quantum particle. Evolution of $\psi(\mathbf{r}, t)$ in space \mathbf{r} and time t is governed by the Schrödinger equation

$$i \frac{\partial \psi}{\partial t} = H\psi(\mathbf{r}, t), \quad (1)$$

where the linear operator H acts in a Hilbert space $L^2(\mathbb{R}^D)$ endowed with an inner product $\langle \psi, \phi \rangle = \int_{\mathbb{R}^D} \psi^*(\mathbf{r}, t)\phi(\mathbf{r}, t) d\mathbf{r}$, D is the space dimension, the asterisk stands for complex conjugation, and (unless stated otherwise) we consider the units where $\hbar = m = 1$ with m being the mass of the particle.

For a given linear operator H , the Hermitian conjugation H^\dagger is defined by the relation $\langle H^\dagger \psi, \phi \rangle = \langle \psi, H\phi \rangle$ for any two functions ψ and ϕ in $L^2(\mathbb{R}^D)$. An operator H is said to be Hermitian (or self-adjoint) if $H^\dagger = H$, i.e., $\langle H\psi, \phi \rangle = \langle \psi, H\phi \rangle$ [a mathematically rigorous definition of the Hermiticity (Reed and Simon, 1980) additionally requires the operator H to be densely defined, i.e., the domain of H must be a dense subset of $L^2(\mathbb{R}^D)$; for simplicity, we assume that this requirement holds for any operator we consider].

The spectrum of any Hermitian operator is purely real, while the converse is not true, i.e., Hermiticity is sufficient for reality of the spectrum but not necessary.

The two fundamental discrete symmetries in physics are given by the parity operator \mathcal{P} defined as

$$\mathcal{P}\psi(\mathbf{r}, t) = \psi(-\mathbf{r}, t), \quad (2)$$

and by the time reversal operator \mathcal{T} defined in Wigner's sense as (Wigner, 1959)

$$\mathcal{T}\psi(\mathbf{r}, t) = \psi^*(\mathbf{r}, -t). \quad (3)$$

The operator \mathcal{T} is antilinear, i.e., $\mathcal{T}(\lambda\psi + \phi) = \lambda^*\mathcal{T}\psi + \mathcal{T}\phi$, for any vectors ψ, ϕ and a complex number λ . Additionally,

$$\mathcal{P}^2 = \mathcal{T}^2 = I, \quad [\mathcal{P}, \mathcal{T}] = 0, \quad (4)$$

where I is the identity operator.

An operator H is said to be \mathcal{PT} symmetric if

$$[\mathcal{PT}, H] = 0. \quad (5)$$

Using Eq. (4), definition (5) can be rewritten as $H = \mathcal{PT}H\mathcal{PT}$.

Rapidly growing interest in \mathcal{PT} -symmetric operators was triggered by the seminal work of Bender and Boettcher (1998), where a connection between \mathcal{PT} symmetry and the reality of the spectrum was pointed out. To emphasize this connection, Bender and Boettcher (1998) introduced the notion of *unbroken \mathcal{PT} symmetry*. \mathcal{PT} symmetry of a \mathcal{PT} -symmetric operator H is said to be unbroken if any

eigenfunction of H is at the same time an eigenfunction of the \mathcal{PT} operator. In this case, the relation $H\psi = E\psi$ implies the existence of λ such that $\mathcal{PT}\psi = \lambda\psi$. From Eq. (4) it follows that there exists a real constant φ such that $\lambda = e^{i\varphi}$, i.e., any eigenvalue of the \mathcal{PT} operator is a pure phase (Bender, Boettcher, and Meisinger, 1999).

Unlike Hermiticity, \mathcal{PT} symmetry is not sufficient for the spectrum to be purely real. However, it becomes sufficient when combined with the requirement for the \mathcal{PT} symmetry to be unbroken. Indeed, let E be an eigenvalue of H with the eigenfunction ψ , i.e., $H\psi = E\psi$. Applying the \mathcal{PT} operator to both sides of this equation and utilizing Eq. (4), one obtains $H(\mathcal{PT}\psi) = E^*(\mathcal{PT}\psi)$. Then, if the \mathcal{PT} symmetry of H is unbroken, $H\psi = E^*\psi$, and hence the eigenvalue E is real. Since this procedure is applied to every eigenvalue of H , we conclude that the spectrum of H is purely real.

If the unbroken \mathcal{PT} symmetry does not hold, then the \mathcal{PT} symmetry is said to be *broken*. The broken \mathcal{PT} symmetry is typically associated with the presence of complex eigenvalues in the spectrum of H .

Unlike Hermiticity, \mathcal{PT} symmetry does not ensure the completeness of eigenvectors of the operator. Even if the spectrum of a \mathcal{PT} -symmetric operator H is entirely real, the set of eigenfunctions of H may not constitute a complete basis. The typical scenarios when the eigenvectors lose their completeness correspond to the presence of an exceptional point [see Kato (1966) and Moiseyev and Friedland (1980) and Sec. II.B] or a spectral singularity (see Sec. X.A). These features are not exclusive to \mathcal{PT} -symmetric operators and can be encountered for more general non-Hermitian operators as well.

The described connection between the \mathcal{PT} symmetry and reality of the spectrum does not involve the definition (2) of the parity operator, but rather relies on properties (4) and the fact that \mathcal{T} is antilinear. Therefore, one can also consider the generalized parity operator \mathcal{P} (Bender, Berry, and Mandilara, 2002; Mostafazadeh, 2003b, 2008), with \mathcal{P} being an arbitrary unitary linear operator $\mathcal{P}^\dagger\mathcal{P} = \mathcal{P}\mathcal{P}^\dagger = I$. Then properties (4) also imply that \mathcal{P} is self-adjoint, i.e., $\mathcal{P}^\dagger = \mathcal{P}$.

More details about the relation between \mathcal{PT} symmetry and Hermiticity can be found in Mostafazadeh (2003a, 2009a).

Now we consider a few examples.

1. \mathcal{PT} -symmetric parabolic potentials

A Schrödinger operator with a complex potential $U(x)$,

$$H = -\frac{d^2}{dx^2} + U(x), \quad U(x) = V(x) + iW(x), \quad (6)$$

is \mathcal{PT} symmetric if $U^*(x) = U(-x)$, i.e., its real and imaginary parts are even and odd, respectively:

$$V(x) = V(-x), \quad W(x) = -W(-x). \quad (7)$$

The simplest example of such a potential is the complex parabolic potential (Kato, 1966, p. 86; Znojil, 1999; Bender and Jones, 2008)

$$U(x) = (x - i\alpha)^2, \quad \alpha \in \mathbb{R}. \quad (8)$$

Its eigenvalues and eigenfunctions are

$$E_n = 2n + 1, \quad \psi_n(x) = H_n(x - i\alpha)e^{-(x - i\alpha)^2/2}, \quad (9)$$

where $n = 0, 1, \dots$, and $H_n(x)$ is the n th Hermite polynomial. Thus the \mathcal{PT} symmetry of the parabolic potential is unbroken for any α (that is E_n are real for all α).

2. Bender-Boettcher potential

Generalizing a conjecture of Bessis and Zinn-Justin, Bender and Boettcher (1998) investigated the spectrum of the potential

$$U(x) = -(ix)^N. \quad (10)$$

For $1 < N < 4$, the eigenvalue problem is posed on the real axis and the potential acquires the form $U(x) = -|x|^N \exp\{i\text{sign}(x)\pi N/2\}$. If $0 < N \leq 1$ or $N \geq 4$, then the problem must be posed on a contour lying in the complex plane.

Numerical results of Bender and Boettcher (1998) on the spectrum of this potential (Fig. 1) show that for $N \geq 2$ the spectrum is real and positive [a rigorous proof of this fact belongs to Dorey, Dunning, and Tateo (2001)]. At the lower boundary of this region, $N = 2$, this potential becomes a real parabolic potential. When $1 < N < 2$ one observes a finite number of real positive eigenvalues and an infinite number of complex-conjugate pairs of eigenvalues. As N approaches 1 from above, the lowest real eigenvalue approaches infinity, and for $N < 1$ there are no real eigenvalues. Thus \mathcal{PT} symmetry is unbroken for $N \geq 2$, but becomes *spontaneously broken* as parameter N crosses the \mathcal{PT} -symmetry-breaking threshold $N_{\text{cr}} = 2$.

3. Two-level \mathcal{PT} -symmetric system

Consider now a Hamiltonian defined by a 2×2 matrix (Bender, Berry, and Mandilara, 2002)

$$H = \begin{pmatrix} i\gamma & \kappa \\ \kappa & -i\gamma \end{pmatrix} = \kappa\sigma_1 + i\gamma\sigma_3, \quad (11)$$

where $\gamma \geq 0$ and $\kappa \geq 0$ are real parameters and hereafter we use the conventional notations for the Pauli matrices:

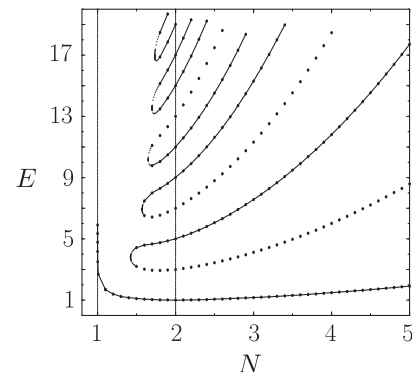


FIG. 1. Real eigenvalues of potential (10) for different N . Adapted from Bender and Boettcher, 1998.

$$\sigma_1 = \begin{pmatrix} 0 & 1 \\ 1 & 0 \end{pmatrix}, \quad \sigma_2 = \begin{pmatrix} 0 & -i \\ i & 0 \end{pmatrix}, \quad \sigma_3 = \begin{pmatrix} 1 & 0 \\ 0 & -1 \end{pmatrix}. \quad (12)$$

The Hamiltonian (11) acts in a Hilbert space which consists of two-component column vectors $\psi = (\psi_1, \psi_2)^T$ (hereafter the superscript T stands for the matrix transpose), with complex entries $\psi_{1,2}$, and the inner product is defined as $\langle \psi, \phi \rangle = \psi_1^* \phi_1 + \psi_2^* \phi_2$. The Hamiltonian (11) is \mathcal{PT} symmetric with $\mathcal{P} = \sigma_1$ and \mathcal{T} being the complex conjugation. The eigenvalues and eigenvectors of H are given by

$$E_{1,2} = \pm \sqrt{\kappa^2 - \gamma^2}, \quad \psi^{(1,2)} = \begin{pmatrix} i\gamma/\kappa \pm \sqrt{1 - \gamma^2/\kappa^2} \\ 1 \end{pmatrix}. \quad (13)$$

Thus \mathcal{PT} symmetry is unbroken (the spectrum is all real) if $\gamma \leq \kappa$ and is broken (both eigenvalues are imaginary) if $\gamma > \kappa$. At $\gamma = \kappa$, \mathcal{PT} -symmetry breaking occurs. At this point, the two eigenvalues collide, and the eigenvectors become linearly dependent. Thus \mathcal{PT} -symmetry breaking occurs at the point where the Hamiltonian is a nondiagonal Jordan block. The respective algebraic multiplicity of the eigenvalue is two, larger than its geometric multiplicity of one. Such points in the parameter space (γ, κ) are called exceptional points (Kato, 1966) or branch points (Moiseyev and Friedland, 1980).

B. Exceptional points

Transition through an exceptional point is the most typical scenario of \mathcal{PT} -symmetry breaking, which arises also in a more general context of non-Hermitian physics (Moiseyev and Friedland, 1980; Rotter, 2009; Heiss, 2012). Now we take a closer look at what happens at an exceptional point by considering a (not necessarily \mathcal{PT} -symmetric) Hamiltonian (Heiss, 2012)

$$H(\epsilon) = \begin{pmatrix} E_1 & 0 \\ 0 & E_2 \end{pmatrix} + i\epsilon \begin{pmatrix} h_{11} & h_{12} \\ h_{21} & h_{22} \end{pmatrix}, \quad (14)$$

where E_1 and E_2 are real. Eigenvalues of $H(\epsilon)$ are

$$E_{1,2}(\epsilon) = \frac{1}{2}[E_1 + E_2 + i\epsilon(h_{11} - h_{22})] \pm \frac{1}{2}\sqrt{[(h_{11} - h_{22})^2 + 4h_{12}h_{21}](\epsilon - \epsilon_1)(\epsilon_2 - \epsilon)}, \quad (15)$$

where

$$\epsilon_{1,2} = [E_1 - E_2]/[2\sqrt{h_{12}h_{21}} \mp i(h_{11} - h_{22})]. \quad (16)$$

For arbitrary parameters the spectrum of $H(\epsilon)$ contains two distinct eigenvalues. However, at $\epsilon = \epsilon_1$ (or $\epsilon = \epsilon_2$) the two eigenvalues coalesce, i.e., $E_1(\epsilon_1) = E_2(\epsilon_1)$ [or $E_1(\epsilon_2) = E_2(\epsilon_2)$], and at these points $H(\epsilon_{1,2})$ has only one linearly independent eigenvector, which means that ϵ_1 and ϵ_2 are exceptional points.

These exceptional points may be complex numbers and transition through an exceptional point requires variation of a complex parameter ϵ , i.e., is controlled by two real parameters. We simplify the consideration by imposing the conditions $h_{11} = h_{22}^*$ and $h_{12}h_{21} > 0$ (each of h_{12} and h_{21} may be complex). Then $\epsilon_{1,2}$ are real and we consider real ϵ . For definiteness we also set $\epsilon_1 < \epsilon_2$ and consider $(h_{11} - h_{22})^2 + 4h_{12}h_{21} < 0$. Then upon the increase of ϵ from zero, eigenvalues $E_{1,2}(\epsilon)$ move toward each other along the real axis and collide at $\epsilon = \epsilon_1$. At this instant phase transition occurs. After collision they move to the complex plane, then become real again at $\epsilon = \epsilon_2$ where they collide on the real axis a second time. As ϵ approaches an exceptional point functions $E_{1,2}(\epsilon)$ display a typical square root behavior $\sim \sqrt{\epsilon - \epsilon_{1,2}}$. The described restoration of unbroken \mathcal{PT} symmetry is referred to as *reentrant* \mathcal{PT} symmetry. It is noted that reentrant \mathcal{PT} symmetry resembles “bubbles of instability” in equilibria of Hamiltonian systems (MacKay, 1987).

Exceptional points are inherently different from the *degeneracy* of eigenvalues, which corresponds to the situation where two eigenvalues coalesce but their eigenvectors remain linearly independent (i.e., the eigenvalue has a diagonal Jordan block). In our case, the simplest example of degeneracy occurs when $E_1 = E_2$ and $\epsilon = 0$.

C. \mathcal{PT} symmetry and pseudo-Hermiticity

Although \mathcal{PT} symmetry itself is not sufficient to guarantee the reality of the spectrum of a Hamiltonian H , it ensures that complex eigenvalues (if any) always exist in complex-conjugate pairs. Indeed, if E is a complex eigenvalue (with nonzero imaginary part) and ψ is the corresponding eigenvector, then E^* is also an eigenvalue with eigenvector $\mathcal{PT}\psi$. This, in particular, implies that in the finite dimensional case \mathcal{PT} symmetry of a linear operator results in reality of all coefficients of the characteristic equation of the Hamiltonian. Bender and Mannheim (2010) proved that the converse is also correct: if all the coefficients of the characteristic polynomial are real, then the corresponding Hamiltonian is \mathcal{PT} symmetric.

A necessary and sufficient condition for the spectrum of a non-Hermitian Hamiltonian to be purely real can be formulated in terms of a more general property called *pseudo-Hermiticity* (Lee and Wick, 1969; Mostafazadeh, 2002a). A Hamiltonian H is said to be η -pseudo-Hermitian if there exists a Hermitian invertible linear operator η such that

$$H^\dagger = \eta H \eta^{-1}. \quad (17)$$

It is clear that if η is the identity operator, then the definition (17) is equivalent to Hermiticity, i.e., pseudo-Hermiticity is a generalization of Hermiticity. In many cases, pseudo-Hermiticity can also be considered as a generalization of \mathcal{PT} symmetry. For example, if H is a symmetric matrix Hamiltonian, then \mathcal{PT} symmetry implies $HP - \mathcal{P}H^* = 0$, and hence $H^\dagger = H^* = \mathcal{P}H\mathcal{P}$, i.e., the pseudo-Hermiticity of H . As another example, the Schrödinger operator (6) with complex potential (7) is \mathcal{P} -pseudo-Hermitian.

An immediate corollary of the pseudo-Hermiticity is that the quantity $Q = \langle \eta \psi, \psi \rangle$ is invariant under the time evolution (1) generated by the Hamiltonian H , i.e., $dQ/dt \equiv 0$ (Mostafazadeh, 2002a). In the case of the Schrödinger operator (6) and (7) this leads to a conserved quantity (Bagchi, Quesne, and Znojil, 2001)

$$Q = \int_{-\infty}^{\infty} \psi(x, t) \psi^*(-x, t) dx. \quad (18)$$

Solombrino (2002) introduced a possibly more general concept of weak pseudo-Hermiticity which does not require the operator η in Eq. (17) to be Hermitian. Whenever one considers only diagonalizable operators with discrete spectrum, the class of all pseudo-Hermitian operators coincides with the class of all weakly pseudo-Hermitian operators. Moreover, in this case (weak) pseudo-Hermiticity is equivalent to the presence of an antilinear symmetry, such as \mathcal{PT} symmetry: a diagonalizable operator H with discrete spectrum is (weakly) pseudo-Hermitian if and only if there exists an invertible antilinear operator Ω such that $\Omega^2 = I$ and $[H, \Omega] = 0$ (Mostafazadeh, 2002c; Solombrino, 2002).

The notion of the pseudo-Hermiticity allows one to formulate necessary and sufficient conditions for a Hamiltonian to possess a purely real spectrum. Let us consider the case of the discrete spectrum, and let a Hamiltonian have a complete set of biorthonormal eigenvectors $\{|\psi_n\rangle, |\phi_n\rangle\}$ defined by (Faisal and Moloney, 1981)

$$\begin{aligned} H|\psi_n\rangle &= E_n|\psi_n\rangle, & H^\dagger|\phi_n\rangle &= E_n^*|\phi_n\rangle, \\ \langle\phi_n|\psi_m\rangle &= \delta_{n,m}, & \sum_n |\psi_n\rangle\langle\phi_n| &= I. \end{aligned}$$

Then the following theorem holds.

Theorem 1 (Mostafazadeh, 2002b) Let H be a Hamiltonian that acts in a Hilbert space, has a discrete spectrum, and admits a complete set of biorthonormal eigenvectors $\{|\psi_n\rangle, |\phi_n\rangle\}$. Then the spectrum of H is real if and only if there is an invertible linear operator \mathcal{O} such that H is $\mathcal{O}\mathcal{O}^\dagger$ -pseudo-Hermitian: $H = (\mathcal{O}\mathcal{O}^\dagger)H^\dagger(\mathcal{O}\mathcal{O}^\dagger)^{-1}$.

To illustrate the application of Theorem 1, consider the \mathcal{PT} -symmetric operator (11). It possesses a complete set of biorthonormal eigenvectors unless $\epsilon = \gamma/\kappa = 1$. Since at $\epsilon < 1$ the spectrum of H is real, Theorem 1 guarantees that there exists the operator \mathcal{O} such that H is η -pseudo-Hermitian with $\eta = \mathcal{O}\mathcal{O}^\dagger$. Note that although H is \mathcal{P} -pseudo-Hermitian, this cannot be used in Theorem 1, because the parity operator $\mathcal{P} = \sigma_1$ does not admit the representation $\mathcal{P} = \mathcal{O}\mathcal{O}^\dagger$ (this can be verified straightforwardly). Therefore there must exist another operator $\eta \neq \mathcal{P}$ when the spectrum of H is purely real. By straightforward algebra one finds that

$$\eta = \frac{1}{\epsilon^2} \begin{pmatrix} 1 & i\epsilon \\ -i\epsilon & 1 \end{pmatrix}, \quad \mathcal{O} = \frac{1}{\epsilon} \begin{pmatrix} 0 & i \\ \sqrt{1-\epsilon^2} & \epsilon \end{pmatrix}.$$

Theorem 1 also indicates that no such operators exist in the broken \mathcal{PT} -symmetry case of $\epsilon > 1$.

It is noted that \mathcal{PT} symmetry is not necessary for a non-Hermitian operator to have a real spectrum. Nixon and Yang

(2016a) showed that if an operator H satisfies a weaker symmetry relation $H^\dagger\eta = \eta H$ for some operator η (not necessarily invertible), then under some mild conditions on the kernel of η , complex eigenvalues of H (if any) always come in conjugate pairs, and a real spectrum is often possible. Imposing this symmetry relation on the Schrödinger operator (6) for differential operators η , wide classes of non- \mathcal{PT} -symmetric complex potentials with all-real spectra were constructed (Nixon and Yang, 2016a). For an arbitrary real function $w(x)$, one such class of potentials is $U(x) = -w^2(x) - iw'(x)$ [see also Eq. (31)], and another class is

$$U(x) = -\left(\frac{1}{4}w^2 + \frac{w'^2 - 2w''w + c}{4w^2}\right) - iw', \quad (19)$$

where c is a free real parameter. The latter class of potentials generalizes the earlier result of Andrianov *et al.* (1999) who discovered potentials (19) with negative c using the supersymmetry (SUSY) technique (addressed in Sec. II.E).

D. Real spectrum and effect of perturbations

Since \mathcal{PT} symmetry ensures that complex eigenvalues appear as complex-conjugate pairs, one can expect that if \mathcal{PT} symmetry is unbroken and the real eigenvalues are “well separated” from each other, then the reality of the spectrum is “robust” against sufficiently small perturbations. While this intuitive expectation is not always correct, in many situations it is indeed true. In particular, this happens if a perturbed \mathcal{PT} -symmetric operator is “close” to a self-adjoint operator (Caliceti, Graffi, and Sjöstrand, 2005; Caliceti, Cannata, and Graffi, 2006). Let us consider a Hermitian operator H_0 perturbed as $H(\epsilon) = H_0 + \epsilon H_1$, where ϵ is a real parameter. We also require operators H_0 and H_1 to be pseudo-Hermitian with the same operator η ,

$$H_0^\dagger = \eta H_0 \eta^{-1}, \quad H_1^\dagger = \eta H_1 \eta^{-1}, \quad (20)$$

where $\eta^2 = I$ (for \mathcal{PT} -symmetric operators, η is a parity operator \mathcal{P}). Then according to the following theorem, the spectrum of $H(\epsilon)$ is real provided that ϵ is small enough.

Theorem 2 (Caliceti, Graffi, and Sjöstrand, 2005) Let H_0 be a self-adjoint positive operator in a Hilbert space. Let H_0 have the only discrete spectrum $\{0 \leq \lambda_0 < \lambda_1 < \dots < \lambda_n < \dots\}$, where each eigenvalue λ_j is simple, and $\delta = \inf_{j \geq 0} [\lambda_{j+1} - \lambda_j]/2 > 0$. Let also H_0 and H_1 satisfy Eq. (20), and H_1 be continuous. Then the spectrum of $H(\epsilon)$ is real if $\epsilon \in \mathbb{R}$ and $|\epsilon| < \delta/\|H_1\|$.

Here the operator norm is defined in the usual way: $\|H_1\| = \sup\{\|H_1 f\|; \|f\| = 1\}$, and the operator H_0 is said to be positive if $\langle H_0 \psi, \psi \rangle \geq 0$ for any ψ from the Hilbert space (Reed and Simon, 1980).

Theorem 2 guarantees the existence of a large class of pseudo-Hermitian operators with real spectra constructed as perturbations of a given Hermitian operator, provided the spectrum of the unperturbed operator is bounded below and its eigenvalues are well separated. As a simple example, consider the Schrödinger operator with a harmonic potential $H_0 = -d^2/dx^2 + x^2$ and \mathcal{PT} -symmetric perturbation $H_1 = iw(x)$,

with $W(x) = -W(-x)$ and $W(x) \in L^\infty(\mathbb{R})$ [recall that the L^∞ norm is defined as $\|W\|_{L^\infty} = \sup_{x \in \mathbb{R}} |W(x)|$]. Then $\delta = 1$ and the spectrum of $H_0 + \epsilon H_1$ is real at least for $|\epsilon| < 1/\|W\|_{L^\infty}$. A similar result is obtained for the power-law potentials $V(x) = x^{2m}$ with polynomial perturbations $iW(x)$, provided that the odd degree m' of polynomials $W(x)$ is less than $m - 1$ (Caliceti and Graffi, 2005).

E. Supersymmetry and real spectra

The concept of SUSY was first introduced in quantum field theories and high-energy physics [see Cooper, Khare, and Sukhatme (1995) and the references therein]. Subsequently, SUSY was utilized in quantum mechanics to construct analytically solvable potentials. This construction is based on the factorization of the Schrödinger operator into the product of two first-order operators (Infeld and Hull, 1951). Switching the order of these two first-order operators gives another Schrödinger operator with a new potential (called the *partner potential*) which shares the same spectrum as the original potential (except possibly a single discrete eigenvalue). Extending the idea of SUSY, parametric families of complex potentials with all-real spectra can be constructed (Khare and Sukhatme, 1989; Cannata, Junker, and Trost, 1998; Andrianov *et al.*, 1999; Bagchi, Mallik, and Quesne, 2001; Miri, Heinrich, and Christodoulides, 2013).

Let us employ the idea of SUSY to construct complex potentials with all-real spectra, following Khare and Sukhatme (1989), Miri, Heinrich, and Christodoulides (2013), and Yang (2014b). To this end, we consider the Schrödinger operator (6) and assume that $U(x)$ has purely real spectrum. Let E_1 and ψ_1 be an eigenvalue and its eigenfunction of H , i.e., $(H - E_1)\psi_1 = 0$. We first factorize the linear operator in this equation as

$$H - E_1 = A_- A_+, \quad A_\pm = \pm \frac{d}{dx} + Y(x), \quad (21)$$

where the function $Y(x)$ is obtained from the requirement $A_+ \psi_1 = 0$, which yields $Y(x) = -\psi_{1,x}/\psi_1$.

Now we switch operators A_+ and A_- on the right side of Eq. (21). This leads to a new Schrödinger operator defined by $H_p - E_1 = A_+ A_-$, i.e.,

$$H_p = -\frac{d^2}{dx^2} + U_p(x) \quad \text{with} \quad U_p = U + 2Y_x. \quad (22)$$

U_p is the partner potential of U and has the same spectrum as U (with the only possible exception of E_1), since operators $A_+ A_-$ and $A_- A_+$ share the same spectrum.

The partner potential U_p is real or \mathcal{PT} symmetric if U is so. In order to obtain a *non- \mathcal{PT} -symmetric* potential with all-real spectrum, we build a new factorization for the partner potential $H_p - E_1 = \tilde{A}_+ \tilde{A}_-$, with $\tilde{A}_\pm = \pm d/dx + \tilde{Y}(x)$. Equating both factorizations for $H_p - E_1$, we obtain the relation $\tilde{Y}_x + \tilde{Y}^2 = Y_x + Y^2$ which is a Riccati equation for \tilde{Y} . Decomposition $\tilde{Y} = Y + 1/f$ leads to a linear equation $f_x - 2Yf = 1$ which can be readily solved. This yields

$$\tilde{Y}(x) = -\frac{d}{dx} \ln(\tilde{\psi}_1), \quad \tilde{\psi}_1(x) = \frac{\psi_1(x)}{c + \int_0^x [\psi_1(\xi)]^2 d\xi}, \quad (23)$$

where c is an arbitrary complex constant. For this new U_p factorization, its partner potential is defined through $\tilde{H} - E_1 = A_- A_+$ and is given by $\tilde{U} = U_p - 2\tilde{Y}_x$. Utilizing the U_p and \tilde{Y} in Eqs. (22) and (23), this \tilde{U} potential is found to be

$$\tilde{U}(x) = U(x) - 2 \frac{d^2}{dx^2} \ln \left[c + \int_0^x [\psi_1(\xi)]^2 d\xi \right]. \quad (24)$$

For generic values of the complex constant c , \tilde{U} is complex and not \mathcal{PT} symmetric. In addition, its spectrum is identical to that of U . Hence if U has an all-real spectrum, so does \tilde{U} . The potential \tilde{U} is referred to as the *superpotential*; it represents a family of potentials parametrized by c .

Now we give two explicit examples of non- \mathcal{PT} -symmetric superpotentials (24) with all-real spectra. The first one is constructed from the parabolic potential $U(x) = x^2$ and its first eigenmode of $E_1 = 1$ with $\psi_1 = e^{-x^2/2}$. Then the superpotential (24) reads

$$U(x) = x^2 - 2 \frac{d^2}{dx^2} \ln \left[c + \int_0^x e^{-\xi^2} d\xi \right], \quad (25)$$

see Fig. 2(a). The spectrum of this superpotential (for any c) is $\{1, 3, 5, \dots\}$, i.e., is all real.

In the second example, the superpotential (24) is built from the \mathcal{PT} -symmetric periodic potential $U(x) = -V_0^2 e^{2ix}$ and its Bloch mode $\psi^{(1)} = I_1(V_0 e^{ix})$ with eigenvalue $E_1 = 1$. Here V_0 is a real constant, and I_n is the modified Bessel function. The resulting periodic superpotential (24) reads

$$U(x) = -V_0^2 e^{2ix} - 2 \frac{d^2}{dx^2} \ln \left[c + \int_0^x I_1^2(V_0 e^{i\xi}) d\xi \right], \quad (26)$$

see Fig. 2(b). The diffraction (dispersion) relation of this superpotential (for all c values) is the same as that of the original potential $U(x) = -V_0^2 e^{2ix}$, i.e., $E = -(k + 2m)^2$, where k is in the first Brillouin zone $k \in [-1, 1]$, and m is any non-negative integer.

If $U(x)$ is a localized real potential, then SUSY allows one to construct localized complex superpotentials (24) with all-real spectra (Miri, Heinrich, and Christodoulides, 2013; Yang, 2014b).

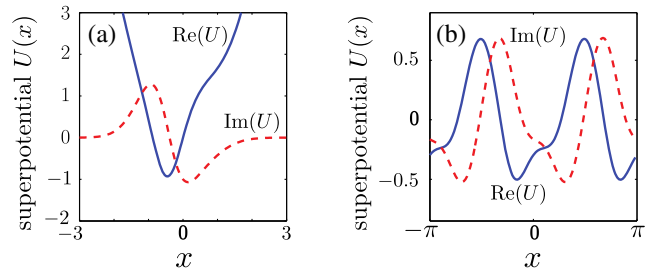


FIG. 2. (a) Superpotential (25) with $c = 1 + i$; (b) periodic superpotential (26) with $c = 0.5 - 2i$ and $V_0 = 1$. From Yang, 2014b.

Another technique allowing one to construct potentials with desirable spectrum is based on the idea of Darboux (1882) and yields similar results as those of the SUSY (Cannata, Junker, and Trost, 1998).

F. Soliton theory and \mathcal{PT} -symmetric potentials

Nonlinear integrable equations solvable by the inverse scattering transform technique play a special role in physics and mathematics. Some of those equations, like the Korteweg–de Vries (KdV) equation

$$u_t - 6uu_x + u_{xxx} = 0, \quad (27)$$

and the nonlinear Schrödinger (NLS) equation

$$i\psi_t + \psi_{xx} + g|\psi|^2\psi = 0 \quad (28)$$

with g being a real constant, constitute fundamental models describing a large variety of physical phenomena (Lamb, 1980; Ablowitz and Segur, 1981; Dodd *et al.*, 1982; Novikov *et al.*, 1984; Faddeev and Takhtadjan, 1987). The starting point of the inverse scattering transform is the representation of a nonlinear equation as a compatibility condition for two linear equations (the so-called Lax pair). Wadati (2008) noticed that the Lax representation offers a way to construct a wide class of \mathcal{PT} -symmetric (as well as complex asymmetric) potentials with purely real spectra. Indeed, let us consider the modified Korteweg–de Vries (mKdV) equation

$$w_t + 6w^2w_x + w_{xxx} = 0 \quad (29)$$

for the real function $w(x, t)$, where $x \in \mathbb{R}$ is the spatial coordinate, and $t > 0$ is time. We consider decaying functions $\lim_{|x| \rightarrow \infty} w(x, t) = 0$. Equation (29) is the compatibility condition for the Zakharov-Shabat (ZS) spectral problem (Zakharov and Shabat, 1971)

$$\phi_{1x} + i\zeta\phi_1 = w(x, t)\phi_2, \quad \phi_{2x} - i\zeta\phi_2 = -w(x, t)\phi_1, \quad (30)$$

where ζ is the spectral parameter, and the linear system

$$\begin{aligned} \phi_{1t} &= 2i\zeta(w^2 - 2\zeta^2)\phi_1 + (2i\zeta w_x - 2w^3 - w_{xx} + 4\zeta^2 w)\phi_2, \\ \phi_{2t} &= (2i\zeta w_x + 2w^3 + w_{xx} - 4\zeta^2 w)\phi_1 - 2i\zeta(w^2 - 2\zeta^2)\phi_2. \end{aligned}$$

Then the new function $\phi = \phi_2 - i\phi_1$ solves the linear Schrödinger equation $H\phi = E\phi$, where H is given by Eq. (6) with the potential (Lamb, 1980, Sec. 2.12)

$$U(x, t) = -w^2(x, t) - iw_x(x, t), \quad (31)$$

and $E = -\zeta^2$. Here time t plays the role of a parameter. If $w(x, t)$ is an even function, the potential $U(x, t)$ is \mathcal{PT} symmetric; for general real $w(x, t)$, this potential is complex and asymmetric.

Discrete eigenvalues of the ZS problem (30) are either purely imaginary or situated symmetrically with respect to the imaginary axis. Its continuous spectrum is the real axis. Thus from any solution $w(x, t)$ of the mKdV equation (29) that possesses purely imaginary discrete eigenvalues of Eq. (30),

one can obtain a complex potential $U(x, t)$ defined by Eq. (31), with purely real spectrum. Further, we notice that $w(x, t)$ depends on the parameter t , while the spectrum of the ZS problem does not depend on t . This means that t can be considered as a “deformation” parameter, and $w(x, t)$ generates a family of deformable potentials $U(x, t)$ with real spectra. As an example, we present a \mathcal{PT} -symmetric potential obtained from the two-soliton solution of the mKdV equation, with $\zeta_{1,2} = i\eta_{1,2}/2$, where $0 < \eta_1 < \eta_2$. It is generated by the function (here $t = 0$, and not indicated) (Wadati and Ohkuma, 1982; Wadati, 2008) $w(x) = 2\epsilon\Delta g(x)/f(x)$, where $\Delta = (\eta_1 + \eta_2)/(\eta_1 - \eta_2)$, $g = \eta_1 \cosh(\eta_2 x) + \eta_2 \cosh(\eta_1 x)$,

$$f = \cosh[(\eta_2 + \eta_1)x] + \frac{4\epsilon^2\eta_1\eta_2}{(\eta_1 - \eta_2)^2} + \Delta^2 \cosh[(\eta_2 - \eta_1)x],$$

and has the form

$$U(x) = -4\Delta^2(g/f)^2 - 2i\epsilon\Delta(g/f)_x. \quad (32)$$

By changing $\eta_{1,2}$ or ϵ one can modify the potential shape without violating the reality of the spectrum.

In addition we notice that the potentials of the form (31) were also discussed in the earlier literature in the context of supersymmetry (Balantekin, Seger, and Fricke, 1991; Unanyan, 1992; Andrianov *et al.*, 1999) and in application to neutrino physics (Balantekin, Fricke, and Hatchell, 1988; Nötzold, 1987).

III. \mathcal{PT} SYMMETRY IN NONLINEAR PHYSICS

Rapidly growing interest in \mathcal{PT} symmetry and particularly in its interplay with other physical phenomena, such as periodicity, discreteness, or nonlinearity, is stimulated by possibilities of extending the paradigm far beyond its quantum mechanical applications. In this section, we review suggestions on implementation of \mathcal{PT} symmetry in physical systems of different natures.

A. Optics

1. Paraxial optics versus quantum mechanics

The Schrödinger equation (1) with the Hamiltonian (6)

$$i\Psi_t + \Psi_{xx} - U(x)\Psi = 0 \quad (33)$$

has direct mathematical analogy with the theory of optical wave propagation under the paraxial approximation (El-Ganainy *et al.*, 2007; Makris *et al.*, 2008; Musslimani *et al.*, 2008a). To introduce this analogy, we consider propagation of a linear monochromatic transverse electric (TE) wave $Ee^{i\omega_0 t}$ with frequency ω_0 , in a waveguide confined to the (x, z) plane, i.e., bounded in the domain $-\ell \leq y \leq \ell$, where 2ℓ is the waveguide width, by parallel claddings (say, by Bragg mirrors). The field diffraction in such a waveguide is described by the Helmholtz equation $\nabla^2 E + k_0^2 n^2(x)E = 0$, where $k_0 = \omega_0/c$. Let the refractive index of the medium be weakly modulated along the x direction, i.e., $n(x) = n_0 + n_1(x)$, where n_0 is the constant component, and $|n_1(x)| \ll n_0$ describes the modulation. In the paraxial approximation (i.e., under small diffraction angles) the field can be

represented as $E = \psi(\xi, \zeta)\phi(y)e^{i\beta z}$, where β is the propagation constant, $\phi(y)$ describes the transverse distribution of the field and solves the equation $d^2\phi/dy^2 + k_0^2 n_0^2 \phi = \beta^2 \phi$ subject to the continuity boundary conditions at $y = \pm \ell$ (determined by the cladding), and $\psi(\xi, \zeta)$ solves Eq. (33), where $U(x) = n_0 n_1(x)/k_0^2$ and the independent variables were renamed as $\zeta = k_0 z \rightarrow t$ and $\xi = k_0 x \rightarrow x/\sqrt{2}$.

Thus variation of the dielectric permittivity $-\varepsilon(x) = -n^2(x)$ in optical applications plays the role of a potential in the Schrödinger equation, and non-Hermitian quantum mechanics can be emulated by optical media with the refractive index or permittivity [cf. Eq. (7)]

$$n(x) = n^*(-x) \quad \text{or} \quad \varepsilon(x) = \varepsilon^*(-x). \quad (34)$$

2. Modeling pulse propagation through a \mathcal{PT} layer

A simple model for refractive index (34) is provided by two cells with a gas of two-level atoms described by the Lorentz model. It was used by [Ruschhaupt, Delgado, and Muga \(2005\)](#) for description of pulse propagation through a \mathcal{PT} -symmetric layer inserted in a waveguide confined by two metallic plates parallel to the (x, y) plane and having distance $2a$ between them. If the atomic population in the left cell ($-\ell < x < 0$) is inverted, and in the right cell ($0 < x < \ell$) the atoms are in the ground state, then the dielectric permittivity for a monochromatic beam with central frequency ω reads ([Chiao, 1993](#)) $\varepsilon = 1 - f(x)\omega_p^2/(\omega^2 - \omega_0^2 + 2i\gamma\omega)$, where $f(x) = -1$ for $x \in (-\ell, 0)$ (cell with gain), $f(x) = 1$ for $x \in (0, \ell)$ (cell with loss) and zero for $|x| > \ell$, ω_p and ω_0 are the plasma and resonance frequencies, respectively, and γ is the damping constant. Assuming that the pulse frequency is close to the resonant one, i.e., $\omega - \omega_0 \ll \gamma$, and that the plasma frequency is small enough, $\omega_p \ll \gamma$, the system can be shown to obey Eq. (33) with the complex potential $U(x) \approx -i\omega_p^2 f(x)/4\gamma$ (where distance is measured in units of a/π). Accounting also for the real part of the dielectric permittivity such steplike potential can be rewritten as

$$U = \begin{cases} V_0 + i\gamma & x \in (-\ell, 0) \quad (\text{gain}), \\ V_0 - i\gamma & x \in (0, \ell) \quad (\text{absorption}), \\ 0 & |x| > \ell \quad (\text{vacuum}), \end{cases} \quad (35)$$

with V_0 and γ being real positive constants.

3. Discrete optics

Interplay between gain and loss in wave scattering attracted additional attention due to suggestions on constructing non-reciprocal optical devices ([Poladian, 1996](#)). [Greenberg and Orenstein \(2004\)](#) and [Kulishov et al. \(2005a, 2005b\)](#) considered this problem for a guiding medium with a periodic modulation of the real and imaginary parts of the refractive index $U = \delta_c \cos(2\beta_0 x) + i\delta_s \sin(2\beta_0 x)$, where δ_c and δ_s are the depths of modulations, and $\beta_0 = 2\pi/\Lambda$ is defined by the lattice period Λ . [Lin et al. \(2011\)](#) considered this phenomenon, termed as unidirectional invisibility, for the particular \mathcal{PT} -symmetric configuration. In the presence of weak constant absorption $\tilde{\gamma}$, i.e., when $U(x) \rightarrow U(x) + i\tilde{\gamma}$, one can

employ the two-mode approximation $\psi(x, t) \approx [q_1(x)e^{i\beta x} + q_2(x)e^{-i\beta x}]e^{-i\beta^2 t}$, where $q_1(x)$ and $q_2(x)$ are slowly varying amplitudes of the forward and backward propagating waves. Using this ansatz in the paraxial equation (33), in the leading order one obtains [cf. Eq. (11)]

$$i \frac{dq}{dx} = Hq, \quad q = \begin{pmatrix} q_1 \\ q_2 \end{pmatrix}, \quad H = \begin{pmatrix} -i\gamma & \kappa_{12} \\ \kappa_{21} & i\gamma \end{pmatrix}, \quad (36)$$

where $\gamma = \tilde{\gamma}/(2\beta)$, $\kappa_{12} = (\delta_s - \delta_c)e^{2ibx}/(4\beta)$, $\kappa_{21} = (\delta_s + \delta_c)e^{-2ibx}/(4\beta)$, and $b = \beta_0 - \beta$ is the phase mismatch.

System (36) is also known as the simplest model for stationary propagation of light in an optical coupler with gain and loss ([Chen, Snyder, and Payne, 1992](#)). Indeed, if one considers the real part of the dielectric permittivity (34) to have two localized and well-separated maxima, then $U(x)$ has the form of a double-well potential in quantum mechanics. The field in Eq. (33) can be searched in the form ([Landau and Lifshitz, 1977](#)) $\Psi = [q_1(z)E_1(x) + q_2(z)E_2(x)]e^{i\beta z}$, where $E_{1,2}(x)$ are the field distributions localized in the vicinity of the potential minima. Then by straightforward algebra one can show that $q_{1,2}$ solve the system (36) with properly defined matrix elements.

The link between Eqs. (33) and (36), yet in a different setting where each of the two arms of a coupler has balanced gain and loss, was established by [El-Ganainy et al. \(2007\)](#), who recognized the relevance of the model for \mathcal{PT} -symmetric optics. If \mathcal{PT} symmetry is unbroken, a medium with balanced gain and loss allows for stationary propagation of light, while the light undergoes attenuation or amplification if the \mathcal{PT} symmetry is broken. Moreover, since the existence of an exceptional point, and hence the transition between different propagation regimes, does not require the exact balance between gain and loss [Sec. II.B], one can introduce the concept of a *passive* \mathcal{PT} -symmetric coupler ([Guo et al., 2009](#)). Indeed, consider an imbalanced generalization of Eqs. (36),

$$i\dot{q}_1 = -i\gamma_1 q_1 + \kappa q_2, \quad i\dot{q}_2 = i\gamma_2 q_2 + \kappa q_1, \quad (37)$$

where $\gamma_1 \neq \gamma_2$. Hereafter the overdot stands for the derivative with respect to an evolution variable, which can be either the propagation distance or time, depending on the context. By substitution $q_{1,2}(z) = \tilde{q}_{1,2}(z)\exp[(\gamma_2 - \gamma_1)z/2]$ one verifies that $\tilde{q}_{1,2}$ solves Eq. (36) with $\gamma = (\gamma_1 + \gamma_2)/2$ and $\kappa_{12} = \kappa_{21} = \kappa$, thus reducing the dissipative system (37) to a \mathcal{PT} -symmetric one. Propagation of a $1.55 \mu\text{m}$ wavelength beam in a passive coupler fabricated on a multilayer $\text{Al}_x\text{Ga}_{1-x}\text{As}$ heterostructure with one nonlossy waveguide and another waveguide with controlled absorption was used in the experiment of

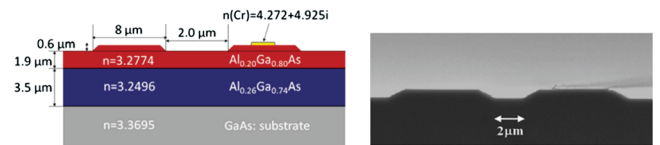


FIG. 3. Left panel: details of two-waveguide layered structure which includes the Cr stripe and features complex refractive index; right panel: scanning electron microscopy picture of the finalized device. Adapted from [Guo et al., 2009](#).

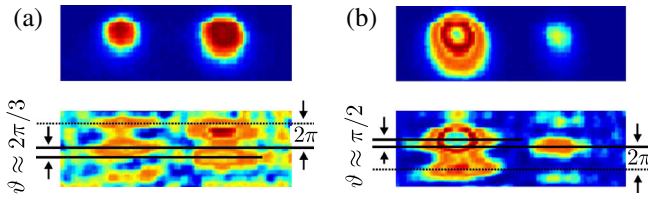


FIG. 4. Measured density distribution (upper panels) and relative phase difference between the two components (lower panels) of the \mathcal{PT} -symmetric coupler in (a) unbroken and (b) broken \mathcal{PT} symmetries. Below the \mathcal{PT} -symmetry-breaking threshold the phase difference lies in the interval $[0, \pi]$, depending on the magnitude of gain, while above the threshold this value is fixed at $\pi/2$. Adapted from Rüter *et al.*, 2010.

Guo *et al.* (2009) (see Fig. 3), where transition between broken and unbroken \mathcal{PT} symmetries was observed for the first time. Later, \mathcal{PT} -symmetry breaking was observed experimentally in different physical settings, such as the microwave billiard (implemented in a microcavity) (Bittner *et al.*, 2012) and polarization of the electromagnetic radiation interacting with a metasurface (Lawrence *et al.*, 2014).

\mathcal{PT} -symmetry phase transition in a coupler with gain and loss was observed by Rüter *et al.* (2010). In the experimental setup two waveguides were created in a photorefractive Fe-doped lithium niobate substrate. The loss was determined by excitations of electrons from Fe^{2+} centers, while gain was created by the pump light through the two-wave mixing determined by the concentration of Fe^{3+} centers. The model was described by Eqs. (37). Having the loss coefficient γ_1 fixed at the level $\gamma_1 = 3.3 \text{ cm}^{-1}$ and increasing the gain coefficient γ_2 , Rüter *et al.* (2010) observed spontaneous \mathcal{PT} -symmetry breaking as shown in Fig. 4.

System (36) also reveals other important effects observable in media with balanced gain and loss. Kulishov *et al.* (2005a) found that a finite medium with periodically modulated complex refractive index (or a coupler) of length L possesses distinct transmission and reflection properties depending on whether the light is applied at $z = 0$ or at $z = L$. This unidirectional propagation, which was also studied for the \mathcal{PT} -symmetric configuration (Lin *et al.*, 2011), is described by the entries M_{ij} of the transfer matrix $M(L)$ defined through the relation $q(L) = M(L)q(0)$. In particular, defining the left (right) transmission and reflection coefficients $t_{L(R)}$ and $r_{L(R)}$ by the conditions $q_2(L) = 0$ [$q_1(0) = 0$], one obtains

$$t_L = t_R = \frac{1}{M_{22}}, \quad r_L = -\frac{M_{21}}{M_{22}}, \quad r_R = \frac{M_{12}}{M_{22}}. \quad (38)$$

The difference in light propagation from the left and right can be described by the contrast ratio $C = (|r_L|^2 - |r_R|^2) / (|r_L|^2 + |r_R|^2)$ (Feng *et al.*, 2013). For the system (36) with $\beta_0 = \beta$ one obtains $C = 2\delta / (1 + \delta^2)$, where $\delta = \delta_s / \delta_c$. C achieves unity at $\delta = 1$. This phenomenon was observed in the experiments of Feng *et al.* (2011, 2013) at a wavelength of $1.55 \mu\text{m}$ using Si waveguides with periodic dissipation implemented by the embedded Ge/Cr structures. In order not to violate the Lorentz reciprocal theorem [see, e.g., Haus (1984)], the prediction on differences in the left and right propagations of a given mode is explained by excitation of the

orthogonal modes, when the input channel is changed to the opposite one (S. Fan *et al.*, 2012).

4. Nonlinearity

As soon as optical applications are considered, accounting for nonlinearity becomes a natural step. Considering light propagation in a Kerr-type medium, where the refractive index is a function of the field intensity $n(x, |\psi|^2) = n(x) + n_2|\psi|^2$, Eq. (33) is generalized to the NLS equation with a potential $U(x)$, i.e.,

$$i\Psi_t + \Psi_{xx} - U(x)\Psi + g|\Psi|^2\Psi = 0, \quad (39)$$

where $g = n_0 n_2 / k_0^2$ is the nonlinear coefficient which can be either positive (focusing medium) or negative (defocusing medium). Equation (39) with focusing nonlinearity and a \mathcal{PT} -symmetric periodic potential was introduced by Musslimani *et al.* (2008a). The nonlinear generalization of the coupler model (36), i.e., a nonlinear \mathcal{PT} -symmetric dimer

$$\begin{aligned} i\dot{q}_0 &= -i\gamma q_0 + \kappa q_1 + \chi|q_0|^2 q_0, \\ i\dot{q}_1 &= i\gamma q_1 + \kappa q_0 + \chi|q_1|^2 q_1 \end{aligned} \quad (40)$$

was introduced by Ramezani *et al.* (2010) and Sukhorukov, Xu, and Kivshar (2010).

5. Synthetic photonic lattices

An idea of experimental implementation of a fully discrete (discrete “time-space”) \mathcal{PT} -symmetric lattice was proposed by Miri, Regensburger *et al.* (2012) and Regensburger *et al.* (2012). Such a synthetic lattice is created in the time domain. It is produced by two fiber loops having slightly different lengths and coupled by a 50% coupler illustrated in Fig. 5. If the gain and loss are held constant in each loop, then the lattice is locally \mathcal{PT} symmetric, i.e., symmetric with respect to the \mathcal{P} inversion ($n \rightarrow -n$) combined with the complex conjugation for a fixed value of m . If gain and loss alternate on every other round trip the synthetic lattice obeys global \mathcal{PT} symmetry,

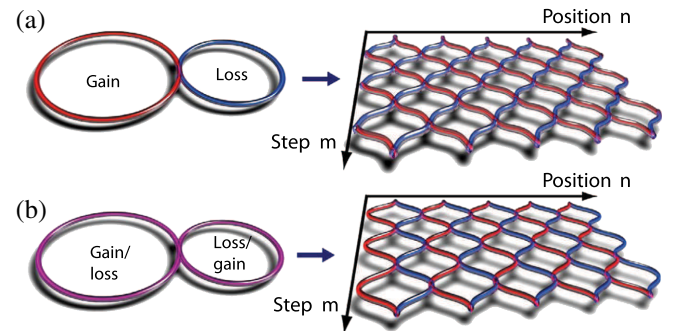


FIG. 5. Mapping of the pulse propagation in loops consisting of dispersion compensating fibers into a 2D lattice corresponding to (a) locally \mathcal{PT} -symmetric and (b) globally \mathcal{PT} -symmetric settings. Light (red) and dark (blue) segments correspond to pulses traveling during the paths with gain and with losses. Alternating gain and losses are shown by purple rings in (b). From Wimmer *et al.*, 2015.

with the above \mathcal{P} operator and \mathcal{T} operator inverting $m \rightarrow -m$ with simultaneous complex conjugation.

Pulses, whose fields are denoted by u_n^m and v_n^m , travel in shorter and longer loops, respectively (Regensburger *et al.*, 2011). Here the upper index m stands for the time interval as measured in round trips. The subindex n denotes the position of a single pulse during one cycle. The nonlinearity of the fibers leads to phase accumulation proportional to the pulse intensities. The system evolution is modeled by the nonlinear map (Wimmer *et al.*, 2015)

$$\begin{aligned} u_n^{m+1} &= \sqrt{G_u/2}(u_{n+1}^m + i v_{n+1}^m) e^{(i\Gamma/2)|u_{n+1}^m + i v_{n+1}^m|^2} e^{i\phi_n}, \\ v_n^{m+1} &= \sqrt{G_v/2}(v_{n-1}^m + i u_{n-1}^m) e^{(i\Gamma/2)|v_{n-1}^m + i u_{n-1}^m|^2}, \end{aligned} \quad (41)$$

where gain-and-loss factors $G_{u,v}$ characterize the pulse amplitudes at the coupler output. The phase function ϕ_n , controlled by the phase modulator in the experiment, is the imposed phase shift governing the \mathcal{PT} -symmetric potential (in addition to the phase shift $\pi/2$ generated by the coupler, which is also accounted for). The case $G_{u,v} = 1$ and $\phi_n = 0$ corresponds to the conservative case. The described synthetic network allowed Wimmer *et al.* (2015) to report the first observation of \mathcal{PT} -symmetric lattice solitons (see Sec. IV.E).

6. \mathcal{PT} symmetry introduced by time management

The idea of inducing \mathcal{PT} symmetry by time management can be developed further by inclusion of nonautonomous gain-and-loss coefficients $\theta(t)$ in the classical linear oscillator (Tsironis and Lazarides, 2014):

$$\ddot{q} + 2\theta(t)\dot{q} + \omega_0^2 q = 0. \quad (42)$$

If $\theta(t)$ is periodic, $\theta(t+T) = \theta(t)$, and acquires positive and negative values, e.g., $\theta = \gamma$ for $0 \leq t < T/2$ and $\theta = -\gamma$ for $T/2 \leq t < T$, then the system can feature bounded or unbounded dynamics, depending on the choice of parameters ω_0 and γ , which resembles \mathcal{PT} -symmetric behavior.

B. \mathcal{PT} lasers

One of the most important applications of \mathcal{PT} symmetry is in the design of new single-mode lasers. Laser cavities typically support a large number of closely spaced modes, which is undesirable since it leads to mode competition, random fluctuations, worse monochromaticity, and worse laser quality. Recently it was demonstrated experimentally that utilizing the concepts of \mathcal{PT} symmetry and \mathcal{PT} -symmetry breaking, new laser devices with enhanced single-mode operations and greater tunability can be realized (Feng *et al.*, 2014; Hodaei *et al.*, 2014). The basic idea is that, by strategically designing gain and loss to obey \mathcal{PT} symmetry, almost all of the modes in the laser cavity can be neutralized, except for a single lasing mode which amplifies. Hence single-mode operation is achieved.

In the experiment by Feng *et al.* (2014), the \mathcal{PT} -symmetric microring resonator was designed with 500-nm-thick InGaAsP multiple quantum wells (MQWs) on an InP substrate [Fig. 6(a)]. InGaAsP MQWs have a high material gain coefficient around 1500 nm. The gain and loss modulation,

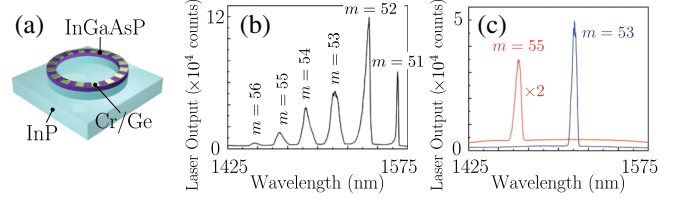


FIG. 6. (a) Schematic of the \mathcal{PT} microring laser. The diameter and width of the microring resonator are $8.9 \mu\text{m}$ and 900 nm , respectively. (b) Multimode lasing spectrum observed from the typical microring WGM laser, showing a series of lasing modes corresponding to different azimuthal orders. (c) Single-mode lasing spectra of the \mathcal{PT} microring lasers operating at the $m = 53$ and 55 azimuthal orders. Adapted from Feng *et al.*, 2014.

satisfying an exact \mathcal{PT} -symmetry operation, was periodically introduced using additional Cr-Ge structures on top of the InGaAsP MQW along the azimuthal direction (φ):

$$\Delta n = \begin{cases} n_{\text{gain}} = -in'' & \left[\frac{l\pi}{m} < \varphi < \frac{(l+1/2)\pi}{m} \right], \\ n_{\text{loss}} = in'' & \left[\frac{(l+1/2)\pi}{m} < \varphi < \frac{(l+1)\pi}{m} \right], \end{cases} \quad (43)$$

where n'' denotes the index modulation in only the imaginary part, m is the azimuthal order of the desired whispering-gallery mode (WGM) in the microring, and $l = 0, 1, 2, \dots, 2m - 1$ divides the microring into $2m$ periods. Because of the rotational symmetry of the microring, \mathcal{PT} -symmetry breaking in this resonator is thresholdless, i.e., it occurs even if the strength of gain and loss modulation is infinitesimal.

In the absence of the Cr/Ge gain-loss modulation (43), a typical multimode lasing spectrum with different WGM azimuthal orders was observed [Fig. 6(b)]. But under this \mathcal{PT} -symmetric index modulation, a single lasing mode was obtained [Fig. 6(c)]. The location of this single mode and its power efficiency are close to those without the gain-loss modulation [Fig. 6(b)].

Periodically modulated ring structures with nonzero \mathcal{PT} -symmetry breaking may support stable nonlinear vortex modes in the unbroken phase (Kartashov, Konotop, and Torner, 2015).

In a different experiment by Hodaei *et al.* (2014), a single-mode \mathcal{PT} laser was demonstrated by utilizing two adjacent microrings, one with gain and the other with loss (the active ring was based on InGaAsP quantum wells); see Fig. 7. In this case, due to linear coupling between the two microrings, \mathcal{PT} -symmetry breaking has a gain-loss threshold, which is equal to the coupling constant between the rings. When the gain-loss contrast is increased beyond this coupling constant, \mathcal{PT} -symmetry breaking occurs, and an amplifying lasing mode appears.

The experimental results are summarized in Fig. 7. When there is only one active ring, or both rings are active, a familiar multimode lasing spectrum was observed [Fig. 7(a)]. But when the two rings are placed in \mathcal{PT} configuration, a single dominant spectral peak appears, resulting in single-mode operation [Fig. 7(c)].

In both experiments, the laser design was based on a linear model by assuming a steady lasing state with a certain gain coefficient. But it should be recognized that lasing itself is an

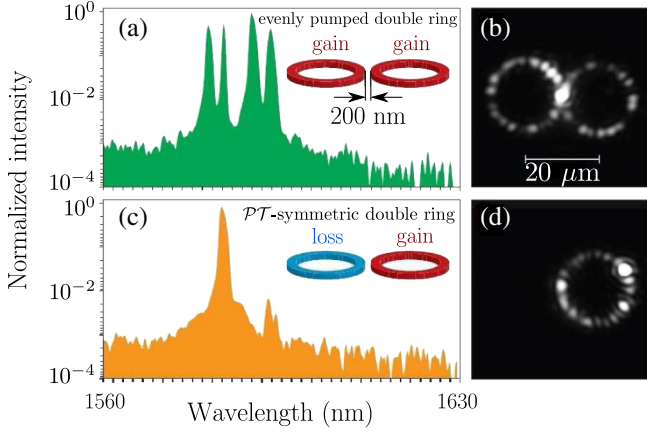


FIG. 7. (a) Spectrum obtained from an evenly pumped pair of microrings. (b) The intensity pattern shows that both resonators equally contribute. (c) Single-modal spectrum under \mathcal{PT} -symmetric conditions. (d) Lasing exclusively occurs in the active resonator. Adapted from Hodaei *et al.*, 2014.

intrinsically nonlinear process. Nonlinear modeling of these \mathcal{PT} -laser devices in the broken phase is an important open question.

C. Atomic gases

Atomic media are intrinsically dissipative. However, it was suggested by Scully (1991) and Fleischhauer *et al.* (1992) and shown experimentally by Zibrov *et al.* (1996) that by using destructive interference in the imaginary part of the dielectric susceptibility it is possible to obtain sufficiently large real refractive indices at small absorption. This is achievable in a gas of multilevel atoms subject to two far-off-resonant control fields (Yavuz, 2005; Proite *et al.*, 2008) or in a mixture of isotopes of two Λ atoms (O'Brien *et al.*, 2011; Simmons *et al.*, 2012).

The respective atomic schemes use two Raman resonances, one of which results in gain and another leads to absorption. The imaginary part of probe-field susceptibility becomes a nonmonotonic function of the frequency with positive (gain) and negative (absorbing) domains. Moreover, real and imaginary parts of the susceptibility can be designed, respectively, as even and odd functions of probe-field frequency (O'Brien *et al.*, 2011; Yavuz, 2005; Proite *et al.*, 2008; Simmons *et al.*, 2012). For a monochromatic beam the change $\omega \rightarrow -\omega$ can be viewed as the time inversion which, when accompanied by the spatial symmetry, can lead to the \mathcal{PT} -symmetric refractive index.

Hang, Huang, and Konotop (2013) considered a scheme shown in Figs. 8(a) and 8(b). Ground ($|g, s\rangle$), lower ($|a, s\rangle$), and excited ($|e, s\rangle$) atomic states of two isotopes ($s = 1, 2$) with densities $N_{1,2}$ are coupled by two strong control fields and by a probe field with the half Rabi frequencies $\Omega_{1,2}$ and Ω_p , respectively. All fields are far-off resonance, i.e., $\Delta_s \gg \Omega_s$, where $\Delta_s = \omega_{e,s} - \omega_{a,s} - \omega_c$ is the one-photon detuning, $\hbar\omega_{l,s}$ ($l = g, a,$ and e) is the energy of the state $|l, s\rangle$, and ω_p (ω_c) is the center frequency of the probe (control) field. The first scheme ($s = 1, \delta_1 > 0$) exhibits

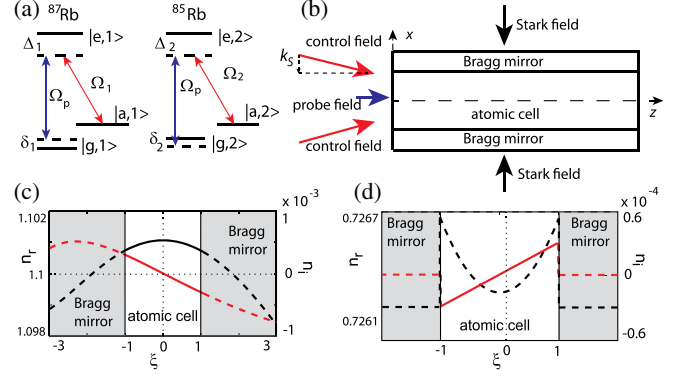


FIG. 8. (a) Isotopes of Λ atoms and Raman transitions. (b) A geometry for the atomic cell and fields applied. (c) Locally parabolic (Hang *et al.*, 2013) and (d) two-channel (Hang *et al.*, 2014) spatial distributions of the real (solid lines) and imaginary (dashed lines) parts of the refractive index.

two-photon absorption for the probe field, while the second one ($s = 2, \delta_2 < 0$) provides two-photon gain.

The mixture of isotopes is loaded in an atomic cell with Bragg cladding [Fig. 8(b)]. Spatial modulation of the susceptibility is achieved by a continuous-wave laser field (Stark field) $E_S(x) \cos(\omega_S t)$ with the amplitude E_S and frequency ω_S . Such field originates x -dependent shifts of the one-photon detunings $\Delta_s(x) = \Delta_s - (\alpha_{e,s} - \alpha_{g,s})E_S^2(x)/(4\hbar)$.

The susceptibility for the probe field is computed from the density-matrix formalism (O'Brien *et al.*, 2011):

$$\frac{\chi_p(x)}{\chi_0} = \frac{\delta_1 - i\gamma_{ag}}{(\delta_1 + \Delta_1 - i\gamma_{eg})(\delta_1 - i\gamma_{ag}) - |\Omega_1|^2} - \eta \frac{|\Omega_2|^2(\Delta_2 + i\gamma_{ag})^{-1}}{(\delta_2 + \Delta_2 - i\gamma_{eg})(\delta_2 - i\gamma_{ag}) - |\Omega_2|^2}. \quad (44)$$

Here $\chi_0 = N_1 d_{eg,1}^2 / \epsilon_0 \hbar$, and $\eta = N_2 d_{eg,2}^2 / N_1 d_{eg,1}^2$ characterizes the ratio between the densities, ϵ_0 is the vacuum permittivity, $d_{eg,s}$ stands for the dipole moment of the transition between the ground and excited states of the s th system, and γ_{ij} are dephasing rates at transitions $i \leftrightarrow j$.

A refractive index satisfying \mathcal{PT} symmetry conditions (34) can be obtained numerically using an optimization procedure (Hang, Huang, and Konotop, 2013). As an example, implementation of this algorithm in a gas of rubidium isotopes yields \mathcal{PT} -symmetric permittivity $\chi_p \approx 10^{-3}(7.5 \cos \xi + i0.394 \sin \xi)$, where $\xi = 2\pi x / \lambda_S$ and λ_S is the Stark field wavelength.

The cell confines atoms in space and can be used to cut undesirable deviations from the \mathcal{PT} symmetry. This allows for construction of refractive indexes of different shapes, such as parabolic (Hang, Huang, and Konotop, 2013) and double-hump (Hang *et al.*, 2014); see Figs. 8(c) and 8(d). The described ideas were further generalized through the use of more sophisticated atomic schemes, like four-level atoms (Li, Dou, and Huang, 2013), as well as involving nonlinear effects (Hang *et al.*, 2013, 2014). The effects of nonlinearity on the \mathcal{PT} -symmetry phase transition in finite-size systems with various profiles of the complex refractive index were studied by Walasik, Ma, and Litchinitser (2015).

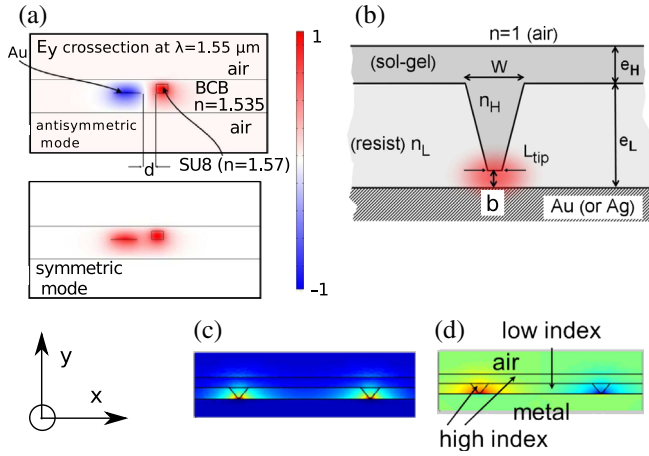


FIG. 9. (a) Antisymmetric and symmetric modes in a long-range plasmonic waveguide. The color map shows y -electric field components of the modes. (b) Cross section of a single hybrid waveguide. (c), (d) Even and odd modes in coupled waveguides, respectively. Adapted from Benisty *et al.*, 2011.

D. Plasmonic waveguides

The model (37) appears to be suitable for description of plasmonic waveguides. Such systems possess intrinsic Joule's loss due to metallic components. On the other hand, they can be combined with gain mechanisms achieved by plasmon amplification using stimulated emission of radiation (Bergman and Stockman, 2003) or with dielectric active media. These ideas were proposed by Benisty *et al.* (2011) and Lupu, Benisty, and Degiron (2013), who suggested to use long-range surface plasmon polariton waveguides based on metallic layers. Strongly confined guidance can be achieved using schemes of hybrid dielectric-plasmonic waveguides illustrated in Fig. 9.

The first device [Fig. 9(a)] is a long-range plasmonic waveguide working at the $1.55 \mu\text{m}$ wavelength. The prototypical unit (Degiron *et al.*, 2009) has an Au lossy stripe $36 \text{ nm} \times 4.6 \mu\text{m}$ cross section and SU8 stripe with gain of the $1.5 \mu\text{m} \times 2 \mu\text{m}$ cross section embedded in a transparent layer of a benzocyclobutene-based polymer (BCB). The Au stripe and SU8 waveguide are separated by the distance $d = 2.5 \mu\text{m}$. The antisymmetric and symmetric modes, which are almost TM (transverse-magnetic) polarized, are shown in the upper and lower panels, respectively.

The second hybrid model [Figs. 9(b)–9(d)] consists of two waveguides, each representing a high-index (n_H) sol-gel inverse rib optical waveguide linked to a gold (or silver) metallic plate through the low-refractive-index (n_L) filling (Benisty and Besbes, 2010). The field (at $\lambda = 633 \text{ nm}$) in the waveguide is concentrated at the tip end [the domain marked by the shaded (red) color and the transverse width b]. The figure shows calculations performed for the lossy structure. Gain can be introduced by pumping the high-index material in a limited region of the sole inverse rib and is expected to be on the order of 500 cm^{-1} . Alternately, the gain can be provided by adding organic elements to the structure (Benisty *et al.*, 2011) such as optically pumped polymer with dye (Noginov *et al.*, 2008).

Multilayered plasmonic waveguides can be made of identical parallel metallic plates separated by dielectrics. To ensure \mathcal{PT} symmetry, the dielectric layers should have alternating gain and loss (from the two sides of the metallic layer). Such a structure was theoretically studied by Alaeian and Dionne (2014a), where the calculations were performed for Ag, as a lossless metal, whose dielectric permittivity is given by $\epsilon_{\text{Ag}} = 1 - (\omega_p/\omega)^2$, and TiO_2 layers as dielectric slabs with $n = 3.2 \pm ik$, where k is tunable gain or loss. A stack of five layers of length 150 nm and width 30 nm was considered, operating at subwavelength frequencies of TM polarized plasmons. In the absence of gain and loss, the metamaterial exhibits negative index response resulting in negative diffraction. When \mathcal{PT} symmetry is imposed, Alaeian and Dionne numerically obtained several effects including double negative refraction, unidirectional invisibility, and reflection and transmission coefficients whose moduli simultaneously exceed unity. A detailed study of spectral characteristics of this stack was performed by Alaeian and Dionne (2014b). A general analysis of \mathcal{PT} symmetry in subwavelength guiding optical systems, based on the full system of Maxwell's equations, rather than the paraxial approximation, was given by Huang *et al.* (2014). In particular, it was found that, on the subwavelength scale, the broken \mathcal{PT} symmetry may be restored, while the paraxial approximation misses this possibility.

E. Metamaterials and transformation optics

1. One-dimensional \mathcal{PT} -symmetric metamaterial

Now we turn to an idea of Lazarides and Tsironis (2013) on implementation of \mathcal{PT} symmetry in metamaterials (Smith, Pendry, and Wiltshire, 2004). The simplest building block for such systems, meta-atoms, is a planar highly conductive splitting resonator (SRR) (Sarychev and Shalaev, 2004). A typical SRR is characterized by losses. To compensate these losses, one can consider coupling of a lossy SRR with one incorporating gain elements [Fig. 10(a)]. Assembling such SRR dimers in an array, one can build a \mathcal{PT} -symmetric metamaterial [Fig. 10(b)].

Each SRR can be regarded as an RLC circuit with self-inductance L , Ohmic resistance R , and capacitance C . The

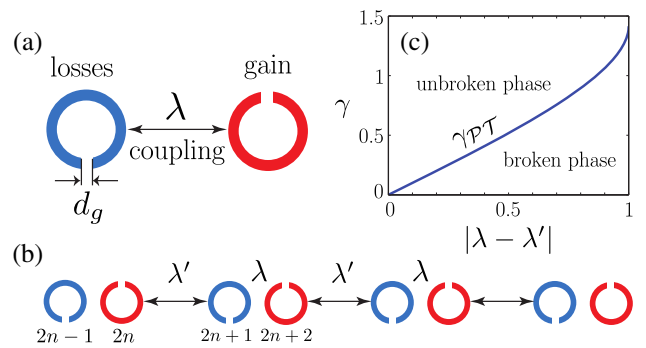


FIG. 10. (a) A \mathcal{PT} -symmetric dimer of SRRs, (b) schematic illustration of a 1D \mathcal{PT} metamaterial, and (c) domains of broken and unbroken \mathcal{PT} symmetry for the array shown in (b); the phase-transition line $\gamma_{\mathcal{PT}}$ is computed in Sec. IV.B.3. Based on ideas of Lazarides and Tsironis, 2013.

nonlinearity can be introduced by a Kerr dielectric (Zharov, Shadrivov, and Kivshar, 2003) with $\varepsilon(|\mathbf{E}|^2) = \varepsilon_0(\varepsilon_\ell + \alpha|\mathbf{E}|^2/E_c^2)$, where ε_0 is the permittivity of the vacuum, ε_ℓ is the linear dielectric permittivity, E_c is a characteristic electric field, and $\alpha = \pm 1$ is the sign of nonlinearity. The charge Q_n of the n th SRR and capacitance $C = \varepsilon(|\mathbf{E}_g|^2)A/d_g$ [where A is the area of the SRR wire cross section and d_g is the size of the gap, see Fig. 10(a)] are related as $C(U_n) = dQ_n/dU_n$, where $U_n = d_g E_{gn}$ is the voltage across the SRR's gap (Lazarides, Eleftheriou, and Tsironis, 2006). In the weakly nonlinear limit, U_n can be expressed by $U_n/U_c = q_n - \beta q_n^3 + \mathcal{O}(q_n^5)$, where $q_n = Q_n/(C_\ell U_c)$, $C_\ell = \varepsilon_0 \varepsilon_\ell A/d_g$ is the linear capacitance, $U_c = d_g E_c$, and $\beta = \alpha/(3\varepsilon_\ell)$.

The SRRs interact with each other through the near field due to magnetic dipole-dipole interactions [electric coupling in the geometry shown in Fig. 10 can be neglected (Hesmer *et al.*, 2007)]. Then dynamical equations for the charges Q_n and currents I_n read ($n = 1, 2$)

$$\frac{dQ_n}{dt} = I_n, \quad L \frac{dI_n}{dt} - (-1)^n R I_n + U_n = M \frac{dI_{3-n}}{dt} + \mathcal{E}_n,$$

where M is the mutual inductance of the SRRs determining the strength of the coupling, \mathcal{E}_n is the electromotive force induced in each SRR by the applied field, and U_n is expressed through q_n as indicated earlier. It is also taken into account that the first SRR ($n = 1$) has losses described by the resistance R , while the second SRR ($n = 2$) has gain which has the same strength as losses, i.e., $-R$.

Using the dimensionless variable $\tau = t/\sqrt{LC_\ell}$ and defining $\gamma = R\sqrt{C_\ell}/L > 0$ and $\varepsilon_n = \mathcal{E}_n/U_c$, one arrives at the system

$$\begin{aligned} \ddot{q}_1 + \lambda \ddot{q}_2 + q_1 + \gamma \dot{q}_1 &= \beta q_1^3 + \varepsilon_1(\tau), \\ \lambda \ddot{q}_1 + \ddot{q}_2 + q_2 - \gamma \dot{q}_2 &= \beta q_2^3 + \varepsilon_2(\tau), \end{aligned} \quad (45)$$

where $\dot{q}_n = dq_n/d\tau$.

In the linear limit ($\alpha = 0$) and in the absence of the external driving [$\varepsilon_n(\tau) \equiv 0$], eigenfrequencies Ω ($q_{1,2} \propto e^{i\Omega\tau}$) of the dimer (45) read

$$\Omega_\pm^2 = \frac{2 - \gamma^2 \pm \sqrt{4\lambda^2 - 4\gamma^2 + \gamma^4}}{2(1 - \lambda^2)}. \quad (46)$$

Considering $\lambda^2 < 1$, which corresponds to a typical physical setting and ensures stable dynamics in the conservative case (i.e., at $\gamma = 0$), one finds that unbroken \mathcal{PT} symmetry (with real Ω_\pm) corresponds to $0 \leq \gamma \leq \gamma_{\mathcal{PT}} = \sqrt{2 - 2\sqrt{1 - \lambda^2}}$, where $\gamma_{\mathcal{PT}}$ is the point of phase transition where the real eigenfrequencies Ω_+ and Ω_- coalesce. At $\gamma > 2$ the dimer is unstable for arbitrary coupling λ .

2. Transformation optics

Versatility of design of metamaterials allowed for development of a new area of the transformation optics. The idea (Pendry, Schurig, and Smith, 2006; Leonhardt, 2006) consists of designing a refractive index in a way to guide geometrical rays at will, in particular, avoiding a chosen domain thus making it invisible. The required refractive index can be

constructed with help of an appropriate coordinate transformation $\mathbf{r}' = \mathbf{F}(\mathbf{r})$ to Cartesian coordinates \mathbf{r}' , where electric and magnetic fields $\{\mathbf{E}, \mathbf{H}\}$ are emitted by the given sources $\{\mathbf{J}, \mathbf{M}\}$. Such coordinate transformation results in transformations of the electric and magnetic fields $\{\mathbf{E}, \mathbf{H}\}$, source current and magnetization $\{\mathbf{J}, \mathbf{M}\}$, and permittivity and permeability tensors $\{\hat{\varepsilon}, \hat{\mu}\}$, which can be obtained from the Maxwell equations (Castaldi *et al.*, 2013):

$$\{\mathbf{E}, \mathbf{H}\}(\mathbf{r}) = \Lambda^T(\mathbf{r}) \cdot \{\mathbf{E}', \mathbf{H}'\}(\mathbf{r}'), \quad (47a)$$

$$\{\mathbf{J}, \mathbf{M}\}(\mathbf{r}) = \det[\Lambda(\mathbf{r})] \Lambda^{-1}(\mathbf{r}) \cdot \{\mathbf{E}, \mathbf{H}\}(\mathbf{r}'), \quad (47b)$$

$$\hat{\varepsilon}(\mathbf{r}) = \hat{\mu}(\mathbf{r}) = \det[\Lambda(\mathbf{r})] \Lambda^{-1}(\mathbf{r}) \cdot [\Lambda^{-1}(\mathbf{r})]^T, \quad (47c)$$

where $\Lambda = \partial(x', y', z')/\partial(x, y, z)$ is the Jacobian of the transformation. In practice the so designed device performs prescribed optical transformation of the rays in a flat real space \mathbf{r} with inhomogeneous permittivity and permeability to the homogeneous space \mathbf{r}' .

Castaldi *et al.* (2013) extended these ideas for designing \mathcal{PT} -symmetric metamaterials. In the vectorial problem the requirement for \mathcal{PT} symmetry can be reduced to $\hat{\varepsilon}(\mathbf{r}) = \hat{\varepsilon}^*(-\mathbf{r})$ [or $\hat{\mu}(\mathbf{r}) = \hat{\mu}^*(-\mathbf{r})$], which can be fulfilled if the chosen transformation ensures $\Lambda(\mathbf{r}) = \Lambda^*(-\mathbf{r})$. Thus the coordinate transformation must be complex. It turns out, however, that in the described procedure a continuous transformation $\mathbf{r}' = \mathbf{F}(\mathbf{r})$ leads to \mathcal{PT} -symmetric potentials having no spontaneous \mathcal{PT} -symmetry breaking. Potentials with exceptional points can be designed using suitable discontinuous transformations.

As a simple but important example consider the transformation $x' = x$, $y' = y$, and $z' = ib(1 \mp z/d)$ where $\text{Re}z \geq 0$, $\text{Im}z = 0^+$, and $|z| \leq d$ (Castaldi *et al.*, 2013). Then for the TM polarization the relevant nonzero components of the tensors $\hat{\varepsilon}$ and $\hat{\mu}$ are given by $\varepsilon_{xx} = \mu_{xx} = \mp ib/d$ and $\varepsilon_{zz} = \pm id/b$. This transformation is particularly interesting for radiation emitted by a line source $M'_y = \delta(x')\delta(z' - ib)$ in Cartesian coordinates mapping it in the real-space source $M_y = \delta(x)\delta(z)$ in a medium with complex permittivity. The real axis $z' = 0$ is transformed into the slab boundaries $z = \mp d$. The respective metamaterial slabs can be fabricated by periodic stacking of subwavelength layers of material constituents with opposite-signed permittivities and permeabilities.

3. \mathcal{PT} -symmetry breaking in polarization space

Turning now to 2D metamaterials, we describe the direct observation of \mathcal{PT} -symmetry breaking by Lawrence *et al.* (2014) using THz time-domain spectroscopy of the metasurfaces as the one shown in Fig. 11. They explored the dependence of the transmitted field polarization $\mathbf{E} = (E_x, E_y)^T e^{i\omega t}$ on the metasurface properties defined by the Lorentzian dipoles $\mathbf{p} = (p_x, p_y)^T$, $p_{x,y} \propto e^{i\omega t}$, oriented along perpendicular directions (corresponding to the geometry of the metamolecules shown in Fig. 11), resonating at the same frequency ω_0 , and characterized by the decay rates $\gamma_y < \gamma_x \ll \omega_0$. The link between the field and the dipoles is given by the polarizability matrix written as

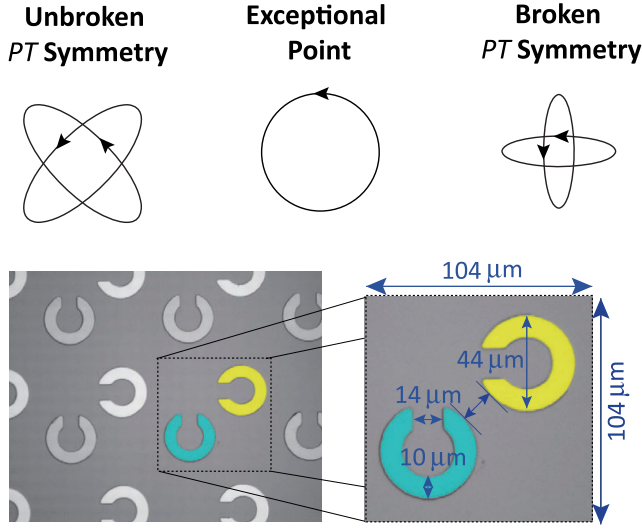


FIG. 11. Upper panels: Polarizations corresponding to unbroken and broken \mathcal{PT} -symmetric phases and to the exceptional point. Lower panel: Photograph of a \mathcal{PT} symmetric metasurface on silicon substrate composed of 300 nm thick silver [light gray (yellow)] and lead [dark gray (turquoise)] SRRs. From Lawrence *et al.*, 2014.

$$S\mathbf{p} + G_{xy}\sigma_1\mathbf{p} - i\Gamma\sigma_3\mathbf{p} = g\mathbf{E}. \quad (48)$$

Here $S = \delta + G_{xx} + i(\gamma_x + \gamma_y)/2$, $\Gamma = (\gamma_x - \gamma_y)/2$, the real coupling G_{xy} is the summation of retarded fields from all x -oriented antennas acting on an y -oriented antenna, G_{xx} is the summation of retarded coupling from all antennas oriented along the same direction, $\delta = \omega - \omega_0$ is small detuning from the resonance ($\delta \ll 1$), and g characterizes polarizability.

The eigenstates of the polarizability matrix in the left-hand side of Eq. (48) are determined by the second matrix, which in its turn has a typical structure of the \mathcal{PT} -symmetric dimer (the first term scales out the net dissipation; the considered system is passive). In the unbroken ($2G_{xy} > \Gamma$) and broken ($2G_{xy} < \Gamma$) \mathcal{PT} -symmetric phases the field is elliptically polarized but has different orientation of the axes as illustrated in Fig. 11, while at the exceptional point ($2G_{xy} = \Gamma$) the polarization is circular. These predictions were confirmed experimentally by Lawrence *et al.* (2014) on a number of metasurfaces, fabricated using photolithography, with the separation between the silver and lead SRRs in each unit cell varying from 2 to 20 μm .

F. Exciton-polariton condensates

Unlike atomic condensates existing at ultralow temperatures, where gain and losses are usually avoided, and introducing \mathcal{PT} symmetry requires special efforts (see Secs. III.G and III.H), condensates of quasiparticles are obtained in the excited states (at relatively high temperatures) and must be supported by the pump since they are usually subject to appreciable losses. Thus, on the one hand, the balance between gain and losses is fundamental for supporting these condensates, and, on the other hand, they are intrinsically nonlinear systems due to interactions among quasiparticles.

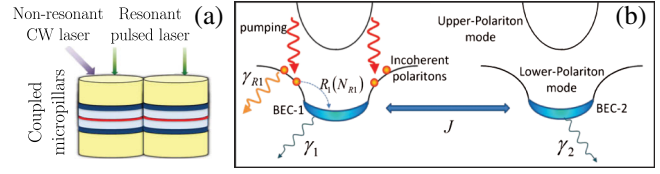


FIG. 12. (a) Semiconductor pillars pumped on the one side form a polariton Josephson junction. (b) The model for the junction: a continuous-wave laser excites high-energy excitons pumping to the reservoir. A resonant laser is used to create the required initial conditions. Adapted from Lien *et al.*, 2015.

This readily suggests that condensates of quasiparticles are natural candidates for experimental implementation and exploration of the nonlinear \mathcal{PT} -symmetric systems.

Lien *et al.* (2015) suggested a setting for implementation of \mathcal{PT} symmetry with an exciton-polariton condensate. The system consists of coupled micropillars as shown in Figs. 12(a) and 12(b). The junction is described by the Gross-Pitaevskii equation (GPE) for the vectorial wave function $\Psi = (\Psi_1, \Psi_2)^T = (\sqrt{N_1}e^{i\phi_1}, \sqrt{N_2}e^{i\phi_2})^T$: $id\Psi/dt = H\Psi$, where

$$H \equiv \begin{pmatrix} E_1 & -J \\ -J & E_2 \end{pmatrix}, \quad E_j = \epsilon_j + V_j + U_j|\Psi_j|^2, \quad (49)$$

$j = 1, 2$, ϵ_j are the single particle ground states, J characterizes tunneling between the two sides, U_j is the strength of the nonlinear interactions of quasiparticles, and the local dispersion is ignored for the wave functions of the ground state. The effective potentials in a simplified form are given by $V_1 = gN_R/A + \mathcal{G}P + (i/2)(RN_R - \gamma_1)$ and $V_2 = -(i/2)\gamma_2$, where R is a constant, $\gamma_{1,2}$ are the decay rates of the condensates, \mathcal{G} corresponds to the interaction of the condensate with high-energy excitons, the g describes interaction between the condensate and reservoir polaritons, P is the pump of the first reservoir, and N_R is the population of the first reservoir whose dynamics is determined from

$$\dot{N}_R = P - \gamma_{R1}N_R - RN_R|\Psi_1|^2 \quad (50)$$

with γ_R being the reservoir decay; the population of the second reservoir, which is not pumped, is neglected.

The model (49) and (50) admits stationary solutions (i.e., $\Psi \propto e^{-2i\Omega t}$ and N_R constant) with real frequencies

$$\Omega_{\pm} = (E_1 + E_2) \pm \sqrt{(E_1 + E_2)^2 + 4J^2}, \quad (51)$$

if a nonzero dc Josephson current $2J\sqrt{N_1N_2}\sin(\Delta\phi)$, where $\Delta\phi = \phi_2 - \phi_1$ is the relative phase, balances pump from the one side and loss from the other side. If the pump also compensates the total loss $RN_R = \gamma_1 + \gamma_2$, two analytical solutions can be derived. They exist subject to the condition $J^2 \geq \gamma_2^2/4$, which determines the unbroken \mathcal{PT} -symmetric phase, while $J^2 = \gamma_2^2/4$ corresponds to the exceptional point of the system.

Chestnov *et al.* (2016) showed that \mathcal{PT} symmetry of the coupled exciton-photon system, which can be implemented in a specific regime of pumping the exciton state and depletion of

the reservoir, enables permanent Rabi oscillations of the condensate in the external magnetic field. For a particular case of the acoustic phonon assisted pumping RN_α , where R is the pumping rate, $\alpha = \pm$ corresponds to spin projection parallel (antiparallel) to the external magnetic field, and N is the reservoir population, the system of the Boltzmann kinetic equation governing the condensate, which is supposed to be at zero momentum state, reads

$$2\dot{\chi}_\alpha = (RN_\alpha - \gamma_X)\chi_\alpha + 2i\delta_\alpha\chi_\alpha - 2i\Omega\phi_\alpha, \quad (52a)$$

$$2\dot{\phi}_\alpha = -\gamma_P\phi_\alpha - 2i\Omega\chi_\alpha, \quad (52b)$$

where ϕ_α and χ_α are the photonic and excitonic components of the condensate wave function, γ_X and γ_P are the decay rates of excitons and polaritons, 2Ω is the Rabi frequency, and $\delta_\pm = \omega_P - \omega_X - \Delta_Z$ is the effective detuning of the cavity mode and exciton frequency in the presence of the Zeeman splitting $\hbar\Delta_Z$. The evolution of the reservoir populations is described by Eq. (50) with N_R replaced by N_α .

The system (52) reveals \mathcal{PT} symmetry if the photonic gain compensates total loss $p_X = \gamma_X + \gamma_P$, and the Zeeman splitting results in the zero effective detuning, i.e., $\delta_\alpha = 0$. Then, neglecting variation of the pump $p_X N_\alpha$ on the time scale of the Rabi oscillations, for pump below some threshold value $P < P_{th}$, one obtains two eigenfrequencies of the condensate $\pm\omega_0 = \pm\sqrt{4\Omega^2 - \gamma_P^2/4}$ for the steady state solutions $\chi, \phi \propto e^{\pm i\omega_0 t}$. On the other hand, at large $P > P_{th}$ and provided the conditions for the \mathcal{PT} symmetry hold, one can obtain permanently oscillating regimes, where $\chi(t) = \chi_1 e^{i\omega_0 t} + \chi_2 e^{-i\omega_0 t}$ and $\phi(t) = \phi_1 e^{i\omega_0 t} + \phi_2 e^{-i\omega_0 t}$.

Finally, we mention that the non-Hermitian nature of exciton-polariton condensates was explored experimentally by Gao *et al.* (2015). A chaotic exciton-polariton billiard was created, which exhibits multiple exceptional points, crossing and anticrossing of energy levels, mode switching, and topological Berry phase, subject to proper changes of system parameters.

G. Bose-Einstein condensates

Bose-Einstein condensates (BECs) represent another promising area for the theoretical and experimental study of interplay between nonlinearity and phenomena originated by \mathcal{PT} symmetry. Klaiman, Günther, and Moiseyev (2008) suggested considering a BEC in a double-well potential with atoms injected into one well and removed from another well. Removal of the atoms can be achieved in different ways: by applying laser radiation or an electronic beam to ionize atoms (Gericke *et al.*, 2008; Barontini *et al.*, 2013), using inelastic interactions of atoms with the trap potential (Muga *et al.*, 2004; Cannata, Dedonder, and Ventura, 2007), or by stimulating transitions to higher levels with subsequent removal of the excited atoms from the trap. Loading of atoms ensuring exact compensation of the losses can be implemented by an atomic laser (Spreeuw *et al.*, 1995; Robins *et al.*, 2013) or by a more sophisticated technique such as combination of tilted potential wells (Kreibich *et al.*, 2013). Nonlinearity in BECs stems from two-body interactions and in the mean-field approximation results in the cubic term in the GPE

(Pitaevskii and Stringari, 2003). To describe the removal or loading of atoms within the framework of the mean-field model, one can start with the master equation in the Lindblad form (Shchesnovich and Konotop, 2010; Witthaut *et al.*, 2011; Barontini *et al.*, 2013) which shows excellent agreement with the available experimental data (Barontini *et al.*, 2013). The GPE with loading and removal of atoms reads

$$i\Psi_t = -\Delta\Psi + [V(\mathbf{r}) + iW(\mathbf{r})]\Psi - g|\Psi|^2\Psi, \quad (53)$$

where $g \sim -a_s$ characterizes the strength of two-body interactions ($g > 0$ and $g < 0$ correspond to negative and positive scattering length a_s), $V(\mathbf{r})$ and $W(\mathbf{r})$ are the real and imaginary parts of the external potential, and dimensionless units ($\hbar = 2m = 1$) are used. A 1D version of GPE (53) with \mathcal{PT} -symmetric distribution of atomic gain and losses was suggested by Yan, Xiong, and Liu (2010). In 3D, the model (53) with a \mathcal{PT} -symmetric double-well trap

$$V(\mathbf{r}) = \omega_x^2 x^2 + y^2 + z^2 + v_0 e^{-\sigma x^2}, \quad W(\mathbf{r}) = \gamma x e^{-\rho x^2} \quad (54)$$

with $\sigma = 2\rho \ln(v_0 \sigma / \omega_x^2)$ (all parameters are positive) was investigated by Dast, Haag, Cartarius, and Wunner (2013) and Dast, Haag, Cartarius, and Wunner *et al.* (2013). Cartarius and Wunner (2012) considered a 1D model with a double-well potential composed of two Dirac δ functions.

An alternative description of \mathcal{PT} -symmetric BEC models can be developed from a non-Hermitian Bose-Hubbard model, where the gain-loss coefficient γ is introduced explicitly (Graefe *et al.*, 2008; Graefe, Korsch, and Niederle, 2008; Graefe and Liverani, 2013):

$$H = i\gamma(a_2^\dagger a_2 - a_1^\dagger a_1) + v(a_1^\dagger a_2 + a_2^\dagger a_1) + c(a_1^\dagger a_1 - a_2^\dagger a_2)^2. \quad (55)$$

Here a_j and a_j^\dagger are the bosonic annihilation and creation operators for the j th mode, v is the tunneling rate, and c is the strength of two-body interactions.

H. Spin-orbit coupled Bose-Einstein condensates

Now we consider a BEC of two states, $|\uparrow\rangle$ and $|\downarrow\rangle$, belonging to the ground manifold and coupled with an excited state by laser beams, as in the Λ schemes shown in Fig. 8(a). These can be hyperfine states $|F = 1, m_F = 0\rangle$ and $|F = 1, m_F = +1\rangle$ of ^{87}Rb atoms (Lin, Jiménez-García, and Spielman, 2011) or degenerate dark states (Dalibard *et al.*, 2011). Such a system can emulate the phenomenon of spin-orbit (SO) coupling in condensed-matter physics (Stanescu, Anderson, and Galitski, 2008; Galitski and Spielman, 2013) and gives rise to a SO-coupled BEC, which was produced experimentally by Lin, Jiménez-García, and Spielman (2011).

Let atoms in the $|\downarrow\rangle$ ($|\uparrow\rangle$) state be removed (loaded into) the system with the rate $\gamma > 0$. In the absence of two-body interactions the system Hamiltonian reads (Kartashov, Konotop, and Zezyulin, 2014)

$$H = -\frac{1}{2}\frac{\partial^2}{\partial x^2} + \omega\sigma_1 + ik\sigma_1\frac{\partial}{\partial x} + i\gamma\sigma_3 + V(x). \quad (56)$$

Here κ is the strength of SO coupling, $V(x)$ is the external trap potential, ω is the strength of the linear coupling from the Zeeman field, and we have added the injection and removal of atoms to the standard model (Lin, Jiménez-García, and Spielman, 2011)

According to definitions (2) and (3), the Hamiltonian (56) acting in the Hilbert space of the vectors $\Psi = (\Psi_\uparrow, \Psi_\downarrow)^T$ is not \mathcal{PT} symmetric. However, if we define a charge (or pseudo-spin) operator \mathcal{C} : $\mathcal{C}\Psi(x, t) = \sigma_1\Psi(x, t)$, then $[\mathcal{CPT}, H] = 0$, i.e., H is \mathcal{CPT} symmetric [compare with Eq. (5)]. Interpreting the states $|\uparrow\rangle$ and $|\downarrow\rangle$ as having negative and positive energies with respect to the average chemical potential μ , one finds that \mathcal{C} indeed obeys properties of the charge operator: it exchanges the states with positive and negative energies, $\mathcal{C}^2 = 1$, $[\mathcal{C}, \mathcal{PT}] = 0$; it has eigenvalues ± 1 and changes the direction of currents [see Fig. 30 and the discussion in Sec. V.I].

In Sec. III.A, σ_1 was interpreted as the parity operator since it was obtained from \mathcal{P} defined by Eq. (2). This reflects ambiguity in definitions of symmetry operators. In particular, one can consider H as \mathcal{PT} symmetric in a more general sense, where $\tilde{\mathcal{P}} = \mathcal{C}\mathcal{P}$ is a new parity operator. We also emphasize that the \mathcal{C} operator used here should not be confused with the \mathcal{C} operator introduced by Bender, Brody, and Jones (2002) as an observable representing the signature of the \mathcal{PT} norm which allows the definition of an inner product having positive-definite signatures. Recently the \mathcal{C} operator was discussed also in an optical context (Dana, Bahabad, and Malomed, 2015).

In the model (56), \mathcal{PT} symmetry (or \mathcal{CPT} symmetry) is determined by two parameters ω/γ and $\kappa/\gamma\ell$, where ℓ is the characteristic scale of the wave function $|\partial\Psi_{\uparrow,\downarrow}/\partial x| \sim |\Psi_{\uparrow,\downarrow}|/\ell$. Thus a sufficiently broad mode ($\ell \gg \kappa/\gamma$) has effectively SO-decoupled components and cannot balance gain and loss. Since, however, $V(x)$ limits the size of the SO BEC (i.e., makes ℓ bounded), the unbroken symmetry may exist even when the homogeneous condensate is unstable, i.e., an external potential can control \mathcal{PT} -symmetry breaking.

Properties of the Hamiltonian (56) with a parabolic trap $V(x) = \nu^2 x^2/2$ are illustrated in Fig. 13. At $\gamma = 0$ the model is Hermitian and its spectrum is real:

$$\mu_{n,\pm} = \nu(n + 1/2) \pm \omega - \kappa^2/2, \quad n = 0, 1, \dots \quad (57)$$

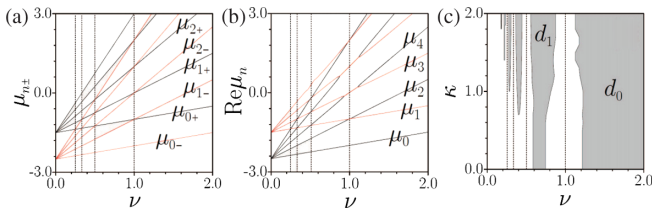


FIG. 13. (a) Spectrum (57) for $\omega = 0.5$ and $\kappa = 2$. Crossing eigenvalues occur at ν_m , $m = 1, 2, \dots$ (b) Real parts of eigenvalues for $\gamma = 0.2$, $\omega = 0.5$, and $\kappa = 2$, which merge pairwise near ν_m , and the corresponding imaginary parts become nonzero at the same time. (c) Domains of unbroken (shadowed regions) \mathcal{CPT} and broken (white regions) \mathcal{CPT} symmetries shown in the plane (κ, ν) at $\gamma = 0.2$ and $\omega = 0.5$. Dashed lines correspond to $\nu = \nu_m$. From Kartashov, Konotop, and Zezyulin, 2014.

At $\nu = \nu_m$, where $\nu_m = 2\omega/m$ with $m = 1, 2, \dots$, the spectrum contains an infinite number of double eigenvalues $\mu_{n-m,+} = \mu_{n,-}$, $n = m, m + 1, \dots$ [Fig. 13(a)]. When γ is nonzero, these double eigenvalues become complex leading to broken \mathcal{PT} symmetry [Fig. 13(b)]. For fixed $\kappa\mathcal{PT}$ symmetry is always broken in a sufficiently broad trap (small ν) [Fig. 13(c)]. As ν grows, the domains of unbroken symmetry (shadowed domains d_0, d_1, \dots) appear and alternate with the domains of broken symmetry. In a sufficiently narrow trap (large ν) the \mathcal{CPT} symmetry is unbroken for all κ (domain d_0). This stripelike structure is related to the presence of an infinite number of double eigenvalues in the spectrum (57). In Fig. 13, values of ν that correspond to the double eigenvalues are shown by dashed vertical lines, which always belong to the region of broken \mathcal{CPT} symmetry and “separate” domains d_{m-1} and d_m of unbroken symmetry.

I. Superconductivity

The Bender-Boettcher potential (10) with $N = 1$ turns out to be relevant for the pattern formation of phase slip centers in superconducting wires (Rubinstein, Sternberg, and Ma, 2007) and in the theory of fluctuation superconductivity (Chchelkatchev *et al.*, 2012).

Considering a superconducting wire in the interval $[-L, L]$ along the x axis, one can start with the time-dependent complex Ginzburg-Landau equation (Ginzburg and Landau, 1950) for the order parameter Ψ . In the dimensionless form, the model reads

$$\Psi_t + H\Psi + |\Psi|^2\Psi = 0, \quad H = -\partial^2/\partial x^2 + i\varphi - \Gamma. \quad (58)$$

Here φ is the electric potential, $1/\Gamma \propto (1 - T/T_c)^{-1}$ is the characteristic relaxation time of the order parameter, T is the temperature, and T_c is the transition temperature. The order parameter is subject to the zero boundary conditions $\Psi(\pm L) = 0$ (this choice is not crucial). The potential φ induces constant current I , i.e., $\varphi = -Ix$ (the Ohmic resistivity is set to 1).

The normal state corresponds to $\Psi = 0$, and thus the phase transition can be characterized by solutions of the linear version of Eq. (58). Setting $L = 1$ and $\Psi(x, t) = u(x)e^{(\Gamma-\lambda)t}$ one obtains the eigenvalue problem (Rubinstein, Sternberg, and Ma, 2007)

$$u_{xx} + ixIu = -\lambda u, \quad u(\pm 1) = 0, \quad (59)$$

which involves the \mathcal{PT} -symmetric potential (10) with $N = 1$. The normal state is unstable if $\Gamma < \text{Re}[\lambda(I)]$. At $I = 0$, the spectrum is real and discrete: $\lambda_n = \pi^2 n^2/4$, $n = 1, 2, \dots$. The spectrum remains real for sufficiently small I , which is guaranteed by Theorem 2. The increase of I eventually results in the collision of the eigenvalues (with the first collision occurring at $I_{\text{cr}} \approx 12.31$), followed by the emergence of complex eigenvalues.

The complex spectrum at $I > I_{\text{cr}}$ implies breaking of the Cooper pairs. On the other hand, it leads to the energy difference in the two lowest states resulting in Josephson oscillations between them and consequently in the symmetry breaking of the time averaged order parameter. These

phenomena were described and experimentally validated by Chtchelkatchev *et al.* (2012).

J. Magnetics

Gaididei (2013) suggested a way to implement a \mathcal{PT} -symmetric configuration in a double-wire magnetic structure in which a spin-polarized current j propagates along the z axis in positive and negative directions in the first and second wires, respectively. The spin-transfer torque efficiency function has the form $\varepsilon_{n,\alpha} = \eta\Lambda^2/[(\Lambda^2 + 1) - (-1)^\alpha(1 - \Lambda^2)S_{n,\alpha}^z]$, where $S_{n,\alpha}^\nu$ with $\nu = x, y, z$ is the ν th component of the spin vector $\mathbf{S}_{n,\alpha}$ of the n th site at the α th wire, η is the degree of spin polarization, $\alpha = 1, 2$, and the parameter $\Lambda \geq 1$ describes the mismatch between spacer and ferromagnet resistance (Slonczewski, 2002; Sluka *et al.*, 2011).

The magnetic energy of the system amounts to $\mathcal{E} = \mathcal{E}_1 + \mathcal{E}_2 + \mathcal{E}_{12}$, where

$$\mathcal{E}_\alpha = -J_1 \sum_n \mathbf{S}_{n,\alpha} \mathbf{S}_{n+1,\alpha} - \frac{1}{2} A \sum_n (S_{n,\alpha}^z)^2 \quad (60)$$

is the magnetic energy of the α th wire with the last term being the easy axis anisotropy (characterized by the constant A), $\mathcal{E}_{12} = -J_2 \sum_n \mathbf{S}_{n,1} \mathbf{S}_{n,2}$ represents an interaction between the wires, $S_{n,\alpha}^z$ is the z component of the spin $\mathbf{S}_{n,\alpha}$ in the α th wire, and $J_{1,2}$ are the respective exchange energies. The dynamics of the system is described by the Landau-Lifshitz equation augmented with spin-torque terms:

$$\frac{d\mathbf{S}_{n,\alpha}}{dt} = \mathbf{S}_{n,\alpha} \times \frac{\delta\mathcal{E}}{\delta\mathbf{S}_{n,\alpha}} + (-1)^\alpha j \varepsilon_{n,\alpha} \mathbf{S}_{n,\alpha} \times (\mathbf{S}_{n,\alpha} \times \hat{\mathbf{z}}), \quad (61)$$

where $\hat{\mathbf{z}}$ is a unitary vector along the z direction. The last term in Eq. (61) represents spin torques which are due to the interaction with a spin-polarized current j .

Let us consider weak deviations of spins from the ferromagnetic stationary state $\mathbf{S}_{n,\alpha} = (0, 0, 1)$. To this end we introduce complex amplitudes $\psi_{n,\alpha}$ defined by

$$\begin{aligned} S_{n,\alpha}^x &= (\psi_{n,\alpha} + \psi_{n,\alpha}^*) \sqrt{1 - |\psi_{n,\alpha}|^2}, \\ S_{n,\alpha}^y &= -i(\psi_{n,\alpha} - \psi_{n,\alpha}^*) \sqrt{1 - |\psi_{n,\alpha}|^2}, \\ S_{n,\alpha}^z &= 1 - 2|\psi_{n,\alpha}|^2, \end{aligned}$$

and consider the small-amplitude (linear) limit $|\psi_{n,\alpha}| \ll 1$. Using the Fourier transform $\psi_{n,j} = N^{-1/2} \sum_k e^{ikn+i\omega_k t} \tilde{\psi}_{k,j}$, where N is the number of spins in the chain and $\omega_k = (A + J_2) + 4J_1 \sin^2(k/2)$ is the dispersion relation of linear spin waves, one obtains a coupled \mathcal{PT} -symmetric system (36) with $q = (\tilde{\psi}_{k,1}, \tilde{\psi}_{k,2})^T$, $\gamma = j\eta/2$, and $\kappa_{12} = \kappa_{21} = J_2$.

The model can be generalized to the antiferromagnetic case $\mathbf{S}_{n,\alpha} = (0, 0, (-1)^n)$, as well as to the continuum limit.

Another model of two coupled ferromagnetic films, one with gain and the other with loss placed in an external magnetic field, was introduced by Lee, Kottos, and Shapiro (2015).

K. Electronic circuits

The concept of a passive \mathcal{PT} -symmetric system (see Sec. III.A) relies on the existence of an exceptional point which separates qualitatively different dynamical regimes. This phenomenon is well known for the simplest mechanical systems. Indeed, for a damped oscillator $\ddot{x} + 2\gamma\dot{x} + x = 0$, the exceptional point occurs at $\gamma = 1$, and it separates underdamped ($\gamma < 1$) and overdamped ($\gamma > 1$) oscillations. A \mathcal{PT} -symmetric generalization of such a system corresponds to two coupled oscillators with damping and gain:

$$\ddot{x} + 2\gamma\dot{x} + x = -2\kappa y, \quad \ddot{y} - 2\gamma\dot{y} + y = -2\kappa x. \quad (62)$$

This idea was suggested and experimentally implemented using the RLC circuits by Schindler *et al.* (2011) (Fig. 14). A mechanical realization of a dimer of oscillators was reported by Bender, Bertson *et al.* (2013).

The scheme in Fig. 14(a) obeys Kirchhoff's laws

$$\begin{aligned} I_n^C + I_n^R + I_n^L &= 0, & I_n^R &= (-1)^n \Gamma \omega_0 Q_n^C, \\ \omega_0^2 Q_1^C &= \dot{I}_1^L + \mu \dot{I}_2^L, & \omega_0^2 Q_2^C &= \dot{I}_2^L + \mu \dot{I}_1^L, \end{aligned} \quad (63)$$

where I and Q are, respectively, currents and charges in the amplified ($n = 1$) and lossy ($n = 2$) circuits with capacitor (C), resistor (R), and inductor (L); $\omega_0 = 1/\sqrt{LC}$ is the natural frequency of each isolated coil, $\mu = M/L$ characterizes inductive coupling of the coils, and $\Gamma = \sqrt{L/C}/R$ is the effective gain-loss parameter. The overdot in Eq. (63) stands for the derivative with respect to time t .

Model (62) follows directly from Eq. (63) with $x = Q_2^C$, $y = Q_1^C$, $2\gamma = \Gamma\sqrt{1 - \kappa^2}$, $\kappa = -\mu$, and the overdot for the derivative with respect to $\tau = \omega_0 t / \sqrt{1 - \kappa^2}$. Eigenfrequencies ω of Eq. (62), with $x, y \propto e^{i\omega t}$, are given by

$$\omega_\pm^2 = 1 - 2\gamma^2 \pm 2\sqrt{\kappa^2 - \gamma^2 + \gamma^4}. \quad (64)$$

Thus \mathcal{PT} symmetry is unbroken if $0 \leq \gamma \leq \gamma_{\mathcal{PT}}$, where $\gamma_{\mathcal{PT}} = \sqrt{1/2 - \sqrt{1/4 - \kappa^2}}$ is the phase-transition point. Unlike the case of a Schrödinger-type \mathcal{PT} -symmetric dimer,

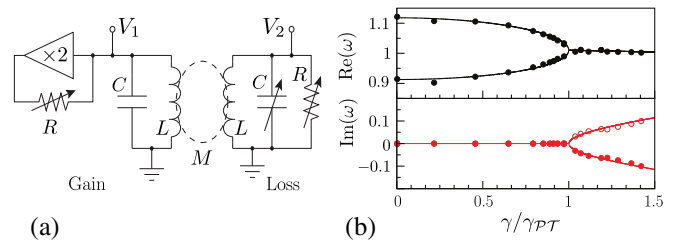


FIG. 14. (a) Electronic \mathcal{PT} -symmetric dimer. The left circuit contains the gain element due to feedback from a voltage-doubling buffer. (b) Theoretical (solid line) and experimental (circles) values of the eigenfrequency ω [open circles are reflections of the data with respect to the $\text{Im}(\omega) = 0$ axis]. Here $\omega_0 = 2 \times 10^5 \text{ s}^{-1}$ and $\mu = 0.2$. Adapted from Schindler *et al.*, 2011.

where an increase in the coupling favors unbroken symmetry [see Eq. (13)], here the increase of $|\kappa|$ eventually breaks the \mathcal{PT} symmetry. Figure 14(b) presents the comparison of theoretical and experimental results of Schindler *et al.* (2011). For further theoretical studies of the model see Bender, Gianfreda *et al.* (2013) and Nazari *et al.* (2014).

System (62) admits a Hamiltonian formulation with the Hamiltonian (Bender, Gianfreda *et al.*, 2013)

$$H = pq + \gamma(yq - xp) + (1 - \gamma^2)xy + \kappa(x^2 + y^2). \quad (65)$$

Time reversal and parity operators can be defined as (Bender, Gianfreda *et al.*, 2013)

$$\begin{aligned} \mathcal{T}: x &\rightarrow x, \quad y \rightarrow y, \quad p \rightarrow -p, \quad q \rightarrow -q, \\ \mathcal{P}: x &\rightarrow -y, \quad y \rightarrow -x, \quad p \rightarrow -q, \quad q \rightarrow -p. \end{aligned}$$

The connection between the velocities and momenta is given by

$$\dot{x} = \partial H / \partial p = q - \gamma x, \quad \dot{y} = \partial H / \partial q = p + \gamma y, \quad (66)$$

while the second pair of Hamilton equations $\dot{p} = -\partial H / \partial x$ and $\dot{q} = -\partial H / \partial y$ yields Eqs. (62).

Nonlinearity can be included in coupled circuits by taking into account the internal currents in the electric-circuit dimer. The resulting system is modeled by coupled Van der Pol oscillators and features asymmetric transport observed by Bender, Factor *et al.* (2013).

L. Microcavities

Coupled \mathcal{PT} -symmetric oscillators (66) are a fairly general model. In particular, it is possible to design an optical scheme assuring asymmetric transport in analogy with the coupled RLC circuits considered earlier (Bender, Factor *et al.*, 2013). Such a scheme extends the idea of all-silicon passive optical diode with two passive microcavities connected by an optical waveguide (L. Fan *et al.*, 2012), to a configuration with mutually balanced active and passive cavities. Experimental implementations of \mathcal{PT} -symmetric microcavities were reported by Chang *et al.* (2014), Peng, Özdemir, Rotter *et al.* (2014), and Peng, Özdemir, Lei *et al.* (2014). The prototypical experimental setup is illustrated in Fig. 15.

Nazari *et al.* (2014) suggested that the observed nonreciprocity may reside in nonlinear Fano resonances which can be captured by a model of a linear conservative array interacting with two nonlinear sites with gain (g , placed at $n = 0$) and loss (l , placed at $n = N$):

$$\begin{aligned} i\dot{\phi}_n &= -C(\phi_{n-1} + \phi_{n+1}) - V_g \phi_g \delta_{n,0} - V_l \phi_l \delta_{n,N}, \\ i\dot{\phi}_{g/l} &= -(E \mp i\gamma)\phi_{g/l} - \chi|\phi_{g/l}|^2\phi_{g/l} - V_{g/l}\phi_{0/N}. \end{aligned}$$

Here ϕ are field amplitudes, C is the coupling constant between the neighboring sites in the linear chain, $E \mp i\gamma$ models eigenmodes of the two microresonators, and $V_{g,l}$ are the coupling coefficients between the chain and the impurities. The nonlinear system interacts with the linear one at sites ϕ_0 and ϕ_N . The left incidence of a monochromatic wave, with dispersion relation $\omega(q) = 2C \cos(q)$

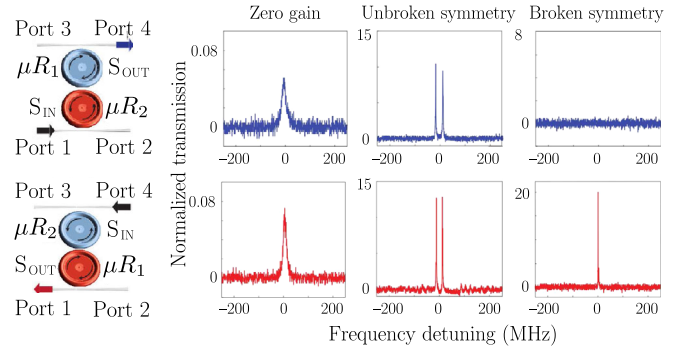


FIG. 15. Left column: the system composed of two whispering-gallery-mode resonators coupled with each other and with two fiber-taper waveguides. The resonators are silica toroids of approximately $30 \mu\text{m}$ radius. One microcavity (μR_1) is active due to E^{3+} dopants while the other (μR_2) is passive. The ions in the active microcavity are pumped by the laser in the $1.417 \mu\text{m}$ band providing gain in the $1.55 \mu\text{m}$ band. The second, third, and fourth columns show different operating regimes of the coupler. The upper and lower lines correspond to left and right incidences of light. The fourth column illustrates nonreciprocity of light propagation. From Peng, Özdemir, Lei *et al.*, 2014.

($\phi_{n,g,l} = A_{n,g,l}e^{i\omega t}$), is characterized by the reflection and transmission coefficients

$$r_L = i \frac{V_g A_g + V_l A_l e^{iqN}}{2C \sin q}, \quad t_L = I + i \frac{V_g A_g + V_l A_l e^{-iqN}}{2C \sin q},$$

where I is the input amplitude, and the amplitudes $A_{g,l}$ are found from the system

$$\begin{aligned} (E - \omega - i\gamma)A_g + \chi|A_g|^2 A_g + V_g(I + r_L) &= 0, \\ (E - \omega + i\gamma)A_l + \chi|A_l|^2 A_l + V_l e^{iqN} t_L &= 0. \end{aligned} \quad (67)$$

For the right incident wave, r_R and t_R are obtained from these expressions by the substitution $\gamma \rightarrow -\gamma$ and $V_g \leftrightarrow V_l$.

The coupled active and passive microcavities can also be studied in optomechanics, where they have promising applications such as phonon lasers (Jing *et al.*, 2014). Microcavities driven by blue- and red-detuned laser fields with mechanically connected movable mirrors were studied by Xu *et al.* (2015).

M. Acoustics

Zhu, Ramezani *et al.* (2014) extended the idea of \mathcal{PT} symmetry to the propagation of sound waves. A linear acoustic wave characterized by the pressure $P(z, t)$ in a bulk medium with z -dependent density $\rho(z)$ and bulk modulus $K(z)$ is governed by the wave equation $KP_{zz} - \rho P_{tt} = 0$. In a general situation, dissipation of sound waves can be described by a complex bulk modulus with negative imaginary part. In the meantime, by including piezoelectric elements connected with electric circuits (Popa and Cummer, 2014), it is possible to implement gain elements described by the positive imaginary part of K . Thus, by combining the elements with gain and

loss to ensure properties $K(z) = K^*(-z)$ and $\rho(z) = \rho^*(-z)$, for a monochromatic wave $P \propto e^{i\omega t}$ one obtains the linear Helmholtz equation

$$\frac{d^2 P}{dz^2} + \omega^2 U(z)P = 0, \quad U(z) = \frac{\rho(z)}{K(z)} = U^*(-z). \quad (68)$$

For a particular waveguide configuration of three gain and three loss sections separated by five passive blocks, such a medium can become unidirectionally transparent for some frequencies (Zhu, Ramezani *et al.*, 2014).

Nonlinear phenomena in the sound wave propagation can be accounted for by considering the complete strain tensor, which remains an open problem.

IV. \mathcal{PT} -SYMMETRIC DISCRETE LATTICES

In this section, we present a detailed analysis of \mathcal{PT} -symmetric lattices. Motivated by physical applications in Sec. III, our main attention will be on discrete nonlinear Schrödinger (dNLS)-type equations, although other nonlinear lattice models are also touched upon.

A. Formalism for discrete nonlinear systems

We focus on the most studied nonlinear networks where a number of waveguides is either even or infinite. For some details on arrays with an odd number of waveguides see Li and Kevrekidis (2011), K. Li *et al.* (2012), Leykam, Konotop, and Desyatnikov, 2013, and Li, Kevrekidis *et al.* (2013).

Mathematical description of the network is based on a system of ordinary differential equations

$$i\dot{\mathbf{q}} = H\mathbf{q} + F(\mathbf{q})\mathbf{q}, \quad (69)$$

where $\mathbf{q} = \mathbf{q}(z) = (q_{-N+1}, \dots, q_N)^T$ is a column vector of $2N$ elements, H is a $2N \times 2N$ symmetric matrix accounting for the linear coupling between sites, and $F(\mathbf{q})$ is a $2N \times 2N$ matrix whose elements depend on the field \mathbf{q} . In this section, we consider cubic nonlinearity where entries of matrix $F(\mathbf{q})$ are given by

$$[F(\mathbf{q})]_{pj} = \sum_{l,m=-N}^N f_{pj}^{lm} q_l^* q_m, \quad p, j = -N+1, \dots, N, \quad (70)$$

and f_{pj}^{lm} are constant coefficients.

\mathcal{PT} symmetry of H implies the following property: if $\mathbf{q}(z)$ is a solution of the underlying linear system [i.e., the system with $F(\mathbf{q}) \equiv 0$], then $\mathcal{PT}\mathbf{q}(z) = \mathcal{P}\mathbf{q}^*(-z)$ is also a solution. This is not true for the nonlinear case in general. If, however, the nonlinearity obeys the constraint

$$\mathcal{P}F^*(\mathbf{q}) = F(\mathcal{P}\mathbf{q}^*)\mathcal{P} \quad \text{for all } \mathbf{q}, \quad (71)$$

then the mentioned property holds also in the nonlinear case (K. Li *et al.*, 2012; Kevrekidis, Pelinovsky, and Tyugin, 2013b), and we say that the nonlinear system (69) is \mathcal{PT} symmetric.

B. Discrete configurations and their linear properties

1. Arrays with nearest-neighbor linear interactions

Let us start with an infinite array in which a waveguide n is linked only with its two neighbors, waveguides $n-1$ and $n+1$. The simplest \mathcal{PT} -symmetric configuration that allows for the balance between gain and loss can be assembled using the following rule: if any site of this network (say, q_n) has gain (loss) characterized by γ_n , then the site q_{-n+1} situated symmetrically with respect to the ‘‘center’’ of the chain has loss (gain) characterized by $-\gamma_n$; see Fig. 16(a). Generally speaking, linear coupling between adjacent sites can also depend on the site number. In Fig. 16 we showcase a particular case where the network has *alternating* coupling which is equal to κ between $2n$ th and $(2n+1)$ th waveguides and equal to ϵ between $(2n-1)$ th and $2n$ th waveguides. If $\kappa = \epsilon$, then the coupling becomes *homogeneous*.

Linear properties of the described array are determined by a bi-infinite tridiagonal matrix H with entries (Pelinovsky, Zezyulin, and Konotop, 2014)

$$H_{n,m} = c_n \delta_{n+1,m} + c_{n+1} \delta_{n-1,m} - (c_n + c_{n+1} - i\gamma_n) \delta_{n,n}, \quad (72)$$

where n and m run through all integers from $-\infty$ to ∞ , $c_n = \kappa$ for even n , and $c_n = \epsilon$ for odd n , and the gain-and-loss coefficients γ_n obey the property $\gamma_n = -\gamma_{-n+1}$. This lattice is \mathcal{PT} symmetric with the parity operator defined by $[\mathcal{P}\mathbf{q}(t)]_n = q_{1-n}(t)$.

Let us set the nonlinearity $F(\mathbf{q})$ as

$$[F(\mathbf{q})]_{n,m} = [(1 - \chi_n)|q_n|^2 + \chi_n|q_{1-n}|^2] \delta_{n,m}, \quad (73)$$

where the real coefficients χ_n obey the relation $\chi_n = \chi_{1-n}$. The case with $\chi_n = 0$ for all n corresponds to on-site Kerr nonlinearity, while the limit $\chi_n = 1$ for all n means nonlinear

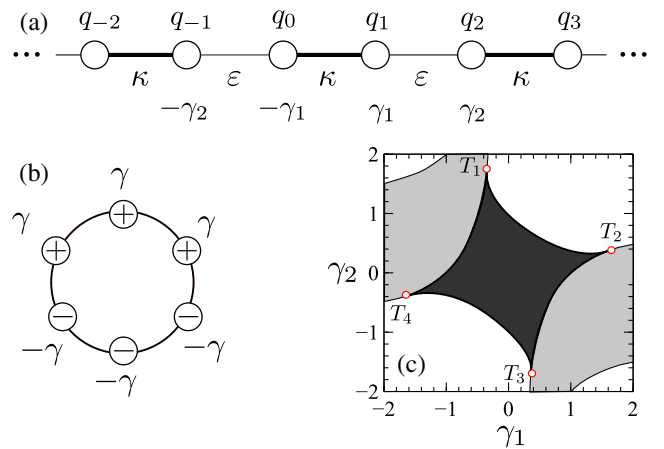


FIG. 16. (a) Infinite \mathcal{PT} -symmetric chain with alternating coupling defined by κ , ϵ and gain-loss coefficients γ_1 , γ_2 . (b) A clustered closed \mathcal{PT} -symmetric chain of six sites. (c) \mathcal{PT} -symmetry-breaking ‘‘phase diagram’’ of the open \mathcal{PT} -symmetric quadrimer (Zezyulin and Konotop, 2012b) which corresponds to the network shown in (a) truncated at q_{-1} and q_2 , with $\kappa = \epsilon = 1$.

coupling between the sites n and $1-n$. This nonlinearity satisfies Eq. (71), i.e., the corresponding nonlinear system is \mathcal{PT} symmetric.

Problem (69) can also be rewritten in terms of $q_n(t)$ as a generalized dNLS equation with gain and dissipation (Dmitriev, Sukhorukov, and Kivshar, 2010; Konotop, Pelinovsky, and Zezyulin, 2012)

$$i\dot{q}_n = c_n(q_{n+1} - q_n) + c_{n+1}(q_{n-1} - q_n) + i\gamma_n q_n + [(1 - \chi_n)|q_n|^2 + \chi_n|q_{1-n}|^2]q_n. \quad (74)$$

Imposing additional boundary conditions, one can transform the infinite system (74) into a finite array. Assuming that n in Eq. (103) runs from $-N+1$ to N for a given N and imposing zero boundary conditions, i.e., $q_{-N}(t) \equiv q_{N+1}(t) \equiv 0$, we define an *open* chain of $2N$ sites. Alternatively, one can impose periodic boundary conditions, i.e., $q_{-N} = q_N$ and $q_{-N+1} = q_{N+1}$, thus defining a *closed* chain (“necklace”) of $2N$ sites. An example of the latter configuration is shown in Fig. 16(b).

The simplest case $N = 1$ corresponds to a nonlinear \mathcal{PT} -symmetric dimer

$$\begin{aligned} i\dot{q}_0 &= q_1 - i\gamma q_0 + [(1 - \chi)|q_0|^2 + \chi|q_1|^2]q_0, \\ i\dot{q}_1 &= q_0 + i\gamma q_1 + [\chi|q_0|^2 + (1 - \chi)|q_1|^2]q_1, \end{aligned} \quad (75)$$

generalizing the model (40). In Eqs. (75), the linear coupling is set to be equal to 1, and subscripts 1 for γ and χ are omitted.

Setting $N = 2$, we obtain an array of four waveguides—a \mathcal{PT} -symmetric quadrimer. Its properties are much richer than the simplest dimer model (75). Indeed, quadrimers allow one to distinguish between open and closed geometries, to study effects of inhomogeneous couplings and gain-loss coefficients, and to observe different types of broken \mathcal{PT} symmetry [or *degrees* of \mathcal{PT} -symmetry breaking in the terminology of Joglekar *et al.* (2010) and Scott and Joglekar (2011)], such as “partially” broken symmetry (two real eigenvalues and two complex eigenvalues) and “fully” broken \mathcal{PT} symmetry (all four eigenvalues are complex). These features of \mathcal{PT} -symmetric quadrimers were systematically addressed by Bendix *et al.* (2010), Li and Kevrekidis (2011), K. Li *et al.* (2012), and Zezyulin and Konotop (2012b). As a particular example, we consider an open quadrimer with homogeneous linear coupling $\kappa = \epsilon = 1$ and arbitrary gain and losses coefficients $\gamma_{1,2}$ (Zezyulin and Konotop, 2012b), i.e.,

$$H = \begin{pmatrix} -i\gamma_2 - 2 & 1 & 0 & 0 \\ 1 & -i\gamma_1 - 2 & 1 & 0 \\ 0 & 1 & i\gamma_1 - 2 & 1 \\ 0 & 0 & 1 & i\gamma_2 - 2 \end{pmatrix}. \quad (76)$$

The \mathcal{PT} -symmetry “phase diagram” for matrix H is shown in Fig. 16(c). It features three different regions: unbroken \mathcal{PT} symmetry where the spectrum is purely real (black region), partially broken \mathcal{PT} symmetry with two real and two complex eigenvalues (gray regions), and fully broken \mathcal{PT} symmetry where all eigenvalues are complex (white regions). The

boundaries separating different regions correspond to the exceptional points. The phase diagram also contains four triple points where the three regions meet. Another feature visible in the phase diagram is the reentrant \mathcal{PT} symmetry (say after fixing $\gamma_1 = 1.2$, the \mathcal{PT} symmetry is broken at $\gamma_2 = 0$ and is restored when γ_2 increases).

In the case of arbitrary finite N , characterization of regions of unbroken and broken \mathcal{PT} symmetry is a nontrivial problem. Detailed results on this front have been obtained for several particular cases. The first case is a chain with alternating gain and loss: $\gamma_n = (-1)^{n+1}\gamma$, where γ is a constant. Such a chain can be considered as N coupled identical dimers with *inter-dimer* coupling given by κ and *intradimer* coupling given by ϵ . The second case corresponds to a clustered chain with two segments, one consisting of lossy sites and the other consisting of active sites, i.e., $\gamma_n = \text{sign}(n - 1/2)\gamma$ [see the example in Fig. 16(b)]. A systematic study of symmetry breaking in these two chains with homogeneous linear coupling ($\kappa = \epsilon = 1$) was performed by Barashenkov, Baker, and Alexeeva (2013) and Kevrekidis, Pelinovsky, and Tyugin (2013b). It was found that \mathcal{PT} symmetry is unbroken when the parameter $\gamma > 0$ is below a threshold value $\gamma_{\mathcal{PT}}$. When $\gamma > \gamma_{\mathcal{PT}}$ the \mathcal{PT} symmetry is broken. For an open alternating (*oa*) chain and alternating necklace (*an*) the symmetry-breaking thresholds are

$$\gamma_{\mathcal{PT}}^{(oa)} = \sin \frac{\pi}{2(2N+1)}, \quad \gamma_{\mathcal{PT}}^{(an)} = \begin{cases} 0, & N \text{ is even,} \\ \sin \frac{\pi}{2N}, & N \text{ is odd,} \end{cases} \quad (77)$$

while for the open clustered (*oc*) chain and clustered necklace (*cn*) only the asymptotic results at $N \rightarrow \infty$ are available (Barashenkov, Baker, and Alexeeva, 2013):

$$\gamma_{\mathcal{PT}}^{(oc)} = 8.95(2N+1)^{-2} + O((2N+1)^{-3}), \quad (78)$$

$$\gamma_{\mathcal{PT}}^{(cn)} = 2.77N^{-2} + O(N^{-3}). \quad (79)$$

In all these cases, the region of unbroken \mathcal{PT} symmetry shrinks to zero as $N \rightarrow \infty$.

Another well-studied case is a chain with a \mathcal{PT} -symmetric *impurity*, i.e., having two “defect” sites $\gamma_d = -\gamma_{1-d} = \gamma$ for some integer d (with all other sites having no gain or loss). For such a chain $\gamma_{\mathcal{PT}} = 1$ if $d = 1$ or $d = N$, and $\gamma_{\mathcal{PT}} \propto N^{-1}$ if $1 < d < N$ (Jin and Song, 2009; Joglekar *et al.*, 2010; Scott and Joglekar, 2011).

Estimates for \mathcal{PT} -symmetry-breaking thresholds for chains with arbitrary configurations of sites with gain and losses can be obtained from the perturbation theory for \mathcal{PT} -symmetric operators (Caliceti, Graffi, and Sjöstrand, 2005). For example, for an open chain with homogeneous coupling, we separate matrix H into real and imaginary parts, i.e., $H = H_0 + iG$ where H_0 is self-adjoint, and a diagonal matrix iG defines a non-self-adjoint perturbation. Then, by Theorem 2, the spectrum of H is real if

$$\max_{1 \leq n \leq N} |\gamma_n| \leq 4\sin^2[\pi(4N+2)^{-1}]. \quad (80)$$

At large N , this bound behaves as $\sim \pi^2(2N+1)^{-2}$, which is close to Eq. (78) obtained for the open clustered chain.

Pelinovsky, Zezyulin, and Konotop (2014) also found a sufficient condition for broken \mathcal{PT} symmetry in a disordered open chain with homogeneous coupling: for $\epsilon = \kappa = 1$, \mathcal{PT} symmetry is broken if $\sum_{n=1}^N \gamma_n^2 > 2N - 1$. This condition is sharp for $N = 1$. For the quadrimer case ($N = 2$), this condition ensures that \mathcal{PT} symmetry is broken outside the circle $\gamma_1^2 + \gamma_2^2 = 3$. It is interesting to notice that the triple points T_j in the diagram of Fig. 16(c) lie exactly on this circle. Thus the condition is not sharp since the regions with broken \mathcal{PT} symmetry can also be found inside the mentioned circle.

2. Infinite lattices with unbroken \mathcal{PT} symmetry

The results (77)–(80) for the finite chains indicate that \mathcal{PT} symmetry tends to be more fragile as the number of sites in the network increases, and the \mathcal{PT} -symmetry-breaking threshold can approach zero in the limit $N \rightarrow \infty$. This indeed happens in chains with \mathcal{PT} -symmetric disorder (Bendix *et al.*, 2009) and in an infinite chain with homogeneous coupling and alternating gain and loss (Dmitriev, Sukhorukov, and Kivshar, 2010; Zheng *et al.*, 2010). Pelinovsky, Kevrekidis, and Frantzeskakis (2013) demonstrated that this situation is quite general and can be encountered in different examples of infinite \mathcal{PT} -symmetric networks with extended gain and loss. There are, however, situations where an infinite linear lattice has a nonzero \mathcal{PT} -symmetry-breaking threshold. Some known examples are listed next.

a. An open chain with alternating coupling and dissipation

If $\gamma_n = (-1)^n \gamma$ and alternating coupling is characterized by the parameters κ and ϵ , as in Fig. 16(a), the linear spectrum is real if $\gamma \leq \gamma_{\mathcal{PT}} = |\kappa - \epsilon|$ and is complex otherwise (Dmitriev, Sukhorukov, and Kivshar, 2010; Zheng *et al.*, 2010).

b. An open chain with embedded defect

Consider now an infinite chain from Fig. 16(a) with homogeneous coupling $\kappa = \epsilon = 1$ and an embedded finite \mathcal{PT} -symmetric defect in a form of a dimer, i.e., $\gamma_0 = -\gamma_1 \neq 0$, and $\gamma_n = 0$ if $n \notin \{0, 1\}$. Then \mathcal{PT} symmetry is unbroken if $|\gamma_{0,1}| \leq \gamma_{\mathcal{PT}} = \sqrt{2}$ (Suchkov, Sukhorukov *et al.*, 2012; Sukhorukov *et al.*, 2012; Kevrekidis, Pelinovsky, and Tyugin, 2013b). Note that this \mathcal{PT} -symmetry-breaking threshold $\gamma_{\mathcal{PT}} = \sqrt{2}$ is larger than that for the isolated dimer ($\gamma_{\mathcal{PT}} = 1$). It is also possible to consider a defect in the form of several adjacent dimers, but the domain of the unbroken \mathcal{PT} symmetry gradually shrinks as the “width” of the defect grows.

A different case when a pair of impurities $\pm\gamma$ are separated by one or several conservative sites was addressed by Bendix *et al.* (2009), who found that the \mathcal{PT} -symmetry-breaking threshold becomes exponentially small as the distance $2d$ between the impurities tends to infinity $\gamma_{\mathcal{PT}} \approx e^{-d}$.

c. Array of dimers

If gain and loss are alternating, $\gamma_n = (-1)^n \gamma$, then the open chain in Fig. 16(a) can be viewed as an array of identical \mathcal{PT} -symmetric dimers, where the active site of each dimer is coupled to the lossy site of the adjacent one. Bendix *et al.*

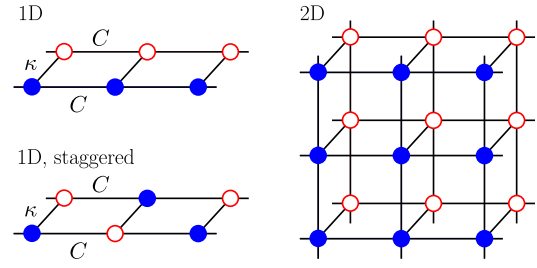


FIG. 17. 1D and 2D arrays of identical \mathcal{PT} -symmetric dimers. Interdimer and intradimer couplings are characterized by κ and C . Open red and filled blue circles correspond to the sites with gain and losses, respectively. Based on ideas of Bendix *et al.* (2010) (1D), Chen *et al.* (2014) (2D), and D’Ambroise, Kevrekidis, and Malomed (2015) (1D, staggered).

(2010) proposed another assembling of \mathcal{PT} -symmetric dimers in an array which possess unbroken \mathcal{PT} symmetry even if all couplings are equal. Such an array is illustrated in Fig. 17 (1D). This setup is described by the system

$$\begin{aligned} i\dot{u}_n &= i\gamma u_n + \kappa v_n + C(u_{n-1} + u_{n+1}) - \chi|u_n|^2 u_n, \\ i\dot{v}_n &= -i\gamma v_n + \kappa u_n + C(v_{n-1} + v_{n+1}) - \chi|v_n|^2 v_n, \end{aligned} \quad (81)$$

where $\kappa > 0$ and $C > 0$ describe interdimer and intradimer couplings, and χ is the coefficient used to account the effect of the Kerr nonlinearity. In the linear case ($\chi = 0$), the condition of unbroken \mathcal{PT} symmetry for Eq. (81) is $\gamma \leq \gamma_{\mathcal{PT}} = \kappa$, i.e., \mathcal{PT} -symmetry breaking does not depend on C (Bendix *et al.*, 2010). The nonlinear system with $\chi \neq 0$ supports propagation of solitons (Suchkov *et al.*, 2011). Inverting gain and loss in a half of the chain produces a model with the *domain wall*. Scattering of linear waves in the latter system was studied by Suchkov, Dmitriev *et al.* (2012).

For a *staggered* modification shown in Fig. 17 (1D, staggered) with the orientations of the dimers alternating between the adjacent sites, \mathcal{PT} symmetry is unbroken if $\gamma \leq \gamma_{\mathcal{PT}} = \kappa - 2C$, where $\kappa, C, \gamma > 0$ (D’Ambroise, Kevrekidis, and Malomed, 2015).

3. Array of metamaterial dimers

Now we turn to a different type of an infinite \mathcal{PT} -symmetric chain—the model of 1D metamaterials which consists of \mathcal{PT} -symmetric dimers of SRRs discussed in Sec. III.E [see Figs. 10(a) and 10(b)]. Assuming that n enumerates the dimers (q_{2n-1}, q_{2n}) in the array, where odd and even SRRs have loss and gain, respectively [Fig. 10(b)], and neglecting electric coupling, the model describing the metamaterial can be written in the following dimensionless form (Lazarides and Tsironis, 2013):

$$\begin{aligned} \lambda' \ddot{q}_{2n} + \ddot{q}_{2n+1} + \lambda \ddot{q}_{2n+2} + q_{2n+1} + \gamma \dot{q}_{2n+1} + \alpha q_{2n+1}^2 + \beta q_{2n+1}^3 \\ = \epsilon_0 \sin(\Omega\tau), \\ \lambda \ddot{q}_{2n-1} + \ddot{q}_{2n} + \lambda' \ddot{q}_{2n+1} + q_{2n} - \gamma \dot{q}_{2n} + \alpha q_{2n}^2 + \beta q_{2n}^3 \\ = \epsilon_0 \sin(\Omega\tau), \end{aligned} \quad (82)$$

where λ' and λ describe interdimer and intradimer couplings. It is assumed the driving force is the same for all SRRs and has

frequency Ω , and the nonlinearity is generalized to include quadratic terms.

The dispersion relation for the array (82) in the linear limit ($\alpha = \beta = 0$) and in the absence of the driving force ($\epsilon_0 = 0$) is readily found from the substitution $(q_{2n-1}, q_{2n}) \sim (A, B) \exp[i(2nk - \Omega\tau)]$ with constants A and B (Wang and Aceves, 2013):

$$\Omega_k^2 = \frac{2 - \gamma^2 \pm \sqrt{\gamma^4 - 4\gamma^2 + 4(\lambda - \lambda')^2 + 16\lambda\lambda' \cos^2 k}}{2[1 - (\lambda - \lambda')^2 - 4\lambda\lambda' \cos^2 k]}.$$

At $\lambda' = 0$ (i.e., when all dimers are decoupled), this formula recovers the eigenfrequencies of \mathcal{PT} -symmetric SRR dimer (46). In the case of equal coupling $\lambda = \lambda'$, \mathcal{PT} symmetry of the array is broken. The most unstable mode is the one with $k = \pi/2$ corresponding to out-of-phase oscillating dimers (i.e., with π -phase shift for the nearest SRRs). Thus \mathcal{PT} -symmetry breaking occurs at $\gamma_{\mathcal{PT}} = \sqrt{2 - 2\sqrt{1 - (\lambda - \lambda')^2}}$ and $\gamma_{\mathcal{PT}} \sim |\lambda - \lambda'| \rightarrow 0$ as $\lambda' \rightarrow \lambda$. Domains of broken and unbroken \mathcal{PT} -symmetric phases are shown in Fig. 10(c).

Wang and Aceves (2013) considered the dynamics of metamaterial dimers in the long-wavelength and small-amplitude limits and derived coupled-mode equations supporting Bragg soliton solutions (see Sec. VII.F).

C. Nonlinear stationary modes

An important class of solutions of Eq. (69) consists of nonlinear stationary modes. They have the form $\mathbf{q}(z) = e^{-iEz}\mathbf{w}$, where E is a real parameter and \mathbf{w} is a z -independent vector solving the algebraic system

$$E\mathbf{w} = H\mathbf{w} + F(\mathbf{w})\mathbf{w}. \quad (83)$$

Note that the equality $F(\mathbf{w}) = F(\mathbf{q})$ follows from Eq. (70).

1. Exact solutions and the main features of nonlinear modes

In some simple cases (like dimer or quadrimer models) solutions of system (83) can be found explicitly (Li and Kevrekidis, 2011; Miroshnichenko, Malomed, and Kivshar, 2011; Graefe, 2012; Rodrigues *et al.*, 2013). For the \mathcal{PT} -symmetric dimer (40), this system is

$$\begin{aligned} Ew_0 &= \kappa w_1 - i\gamma w_0 + |w_0|^2 w_0, \\ Ew_1 &= \kappa w_0 + i\gamma w_1 + |w_1|^2 w_1. \end{aligned} \quad (84)$$

Using polar representations $w_{0,1} = A_{0,1} e^{i\phi_{0,1}}$, $A_{0,1} \geq 0$, one can see that in addition to the trivial solution $A_0 = A_1 = 0$, other nonlinear modes are determined by

$$A_0^2 = A_1^2 = E \pm \sqrt{\kappa^2 - \gamma^2}, \quad \sin(\phi_1 - \phi_0) = \gamma/\kappa. \quad (85)$$

This result reveals several features. First, there exist two branches of nonlinear modes [corresponding to “+” and “−” signs in Eq. (85)] when $\gamma < \kappa$. At the exceptional point $\kappa = \gamma$, these two branches coalesce, and above the phase transition ($\gamma > \kappa$), nonlinear modes do not exist. Below the phase

transition, these modes constitute two *continuous families*: even if parameters of the model γ and κ are fixed, one still can find a continuous set of solutions by varying the free parameter E . Amplitudes of the nonlinear modes tend to infinity as E increases. On the other hand, amplitudes of the modes vanish at $E = \pm\sqrt{\kappa^2 - \gamma^2}$, which corresponds to the eigenvalues of the linear problem. Therefore both solution families bifurcate from the linear limit. Any nonlinear mode is \mathcal{PT} invariant (up to a gauge transformation $w \rightarrow w^{i\theta}$), i.e., $\mathcal{PT}w = w$, which in the case at hand means $w_1 = w_0^*$.

Linear stability of a nonlinear mode is examined by linearizing Eq. (69) in the vicinity of the stationary solution \mathbf{w} and evaluating eigenvalues of the resulting linear problem. For the dimer model, the branch corresponding to the “−” sign is stable only if $E^2 \leq 4(\kappa^2 - \gamma^2)$, while the “+” branch is always stable (Li and Kevrekidis, 2011).

The example of a dimer showcases several prototypical properties of discrete nonlinear modes, but not all of them. Indeed, for quadrimer models ($N = 2$) nonlinear modes (including stable ones) can exist even if \mathcal{PT} symmetry of the underlying linear system is broken. Furthermore, there exist nonlinear modes that do not bifurcate from the linear limit and in the limit $E \rightarrow \infty$ some families of nonlinear modes can disappear (Li and Kevrekidis, 2011; K. Li *et al.*, 2012; Zezyulin and Konotop, 2012b; Kevrekidis, Pelinovsky, and Tyugin, 2013b; Li, Zezyulin, Konotop, and Kevrekidis, 2013).

2. Nonlinear modes as continuous families and isolated points

As emphasized, nonlinear modes of the \mathcal{PT} -symmetric nonlinear dimer exist as continuous families. This property is typical for conservative systems, but is quite unusual for systems with gain and loss. On the other hand, \mathcal{PT} -symmetric arrays can also feature properties of dissipative systems (Akhmediev and Ankiewicz, 2005), i.e., they can admit another type of solutions which are *isolated points*. For such solutions, E is no longer a free parameter but is determined by the balance between dissipation and gain, i.e., by the system parameters. This feature can be illustrated in a \mathcal{PT} -symmetric dimer with nonlinear gain and loss (Miroshnichenko, Malomed, and Kivshar, 2011)

$$\begin{aligned} i\dot{q}_0 &= \kappa q_1 - i\gamma q_0 + i\Gamma|q_0|^2 q_0 + |q_0|^2 q_0, \\ i\dot{q}_1 &= \kappa q_0 + i\gamma q_1 - i\Gamma|q_1|^2 q_1 + |q_1|^2 q_1, \end{aligned} \quad (86)$$

where in addition to linear gain and loss ($\gamma \geq 0$) one also has \mathcal{PT} -symmetric nonlinear gain and loss characterized by $\Gamma \geq 0$. Looking for stationary nonlinear modes in the form of $q_{0,1} = A_{0,1} e^{i\phi_{0,1}} e^{-iEz}$, one can classify possible solutions into three groups (Miroshnichenko, Malomed, and Kivshar, 2011; Duanmu *et al.*, 2013; Chen *et al.*, 2015):

a. Continuous families of \mathcal{PT} -symmetric solutions

In this case E is a free parameter, $A_0^2 = A_1^2 \neq \gamma/\Gamma$, $A_0 = A_1$ are determined from the equation

$$(1 + \Gamma^2)A_0^4 - 2(E + \gamma\Gamma)A_0^2 + \gamma^2 + E^2 - \kappa^2 = 0,$$

and phases $\phi_{0,1}$ can be computed from A_0 .

b. Isolated asymmetric solutions

For solutions of this type, $E = \gamma/\Gamma$, $A_0^2 \neq A_1^2$, and $A_0^2 + A_1^2 = \gamma/\Gamma$. Note that these solutions have no counterparts in the dimer model without nonlinear dissipation ($\Gamma = 0$), because they require $\gamma/\Gamma > 0$ and exist only due to the competition between linear and nonlinear dissipation and gain.

c. Isolated \mathcal{PT} -symmetric solutions

In this case, E is determined from $(2\Gamma E - \gamma)^2 / (2\kappa\Gamma)^2 + (\gamma/2\kappa)^2 = 1$, and $A_0^2 = A_1^2$, $A_0^2 + A_1^2 = \gamma/\Gamma$. These modes exist only if both linear and nonlinear gain and loss are present.

A similar classification of solutions can be elaborated for quadrimers with nonlinear gain and loss (Li, Kevrekidis, and Malomed, 2014).

3. Continuous families of discrete solitons

In a general case, families of nonlinear modes and their stability analysis require numerical treatments. However, in some limiting cases the problem can be investigated by means of an asymptotic expansion or by the technique of analytical continuation.

a. Bifurcation from the linear limit

If the underlying linear problem possesses a real eigenvalue, one can search for a family of nonlinear modes of Eq. (83) bifurcating from this eigenvalue. Let us consider the case when \tilde{E} is a simple real eigenvalue of H and $\tilde{\mathbf{w}}$ is the corresponding eigenvector, i.e., $H\tilde{\mathbf{w}} = \tilde{E}\tilde{\mathbf{w}}$. Up to a phase multiplier $e^{i\varphi}$ (see discussion in Sec. II), the eigenvector can be chosen to be \mathcal{PT} invariant, i.e., $\mathcal{PT}\tilde{\mathbf{w}} = \tilde{\mathbf{w}}$. This property implies that the product $\langle \tilde{\mathbf{w}}^*, \tilde{\mathbf{w}} \rangle$ is real.

In the vicinity of the linear limit nonlinear modes bifurcating from the eigenstate $\tilde{\mathbf{w}}$ can be searched using the perturbation expansion (Zezyulin and Konotop, 2012b)

$$\mathbf{w} = \epsilon\tilde{\mathbf{w}} + \epsilon^3\mathbf{w}^{(3)} + o(\epsilon^3), \quad E = \tilde{E} + \epsilon^2 E^{(2)} + o(\epsilon^2), \quad (87)$$

where ϵ is a small real parameter, $\epsilon \ll 1$. The coefficients $\mathbf{w}^{(3)}$ and $E^{(2)}$ of the expansions are to be determined.

Substituting expansions (87) into Eq. (83) and noticing from Eq. (70) that $F(\mathbf{w}) = \epsilon^2 F(\tilde{\mathbf{w}}) + O(\epsilon^3)$, one obtains $E^{(2)}\tilde{\mathbf{w}} = (H - \tilde{E})\mathbf{w}^{(3)} + F(\tilde{\mathbf{w}})\tilde{\mathbf{w}}$. This equation allows one to compute $E^{(2)} = \langle \tilde{\mathbf{w}}^*, F(\tilde{\mathbf{w}})\tilde{\mathbf{w}} \rangle / \langle \tilde{\mathbf{w}}^*, \tilde{\mathbf{w}} \rangle$ (Zezyulin and Konotop, 2012b, 2013). Bifurcation of a family of nonlinear modes is possible only if $E^{(2)}$ is real. Hence, bearing in mind that $\langle \tilde{\mathbf{w}}^*, \tilde{\mathbf{w}} \rangle$ is real, one obtains a necessary condition for a family of nonlinear modes to bifurcate from a simple eigenstate \tilde{E} : $\text{Im}\langle \tilde{\mathbf{w}}^*, F(\tilde{\mathbf{w}})\tilde{\mathbf{w}} \rangle = 0$. If the nonlinearity is \mathcal{PT} symmetric, i.e., Eq. (71) holds, then this condition is satisfied automatically.

Validity of formal perturbation expansions (87) for the particular case of the open chain with Kerr nonlinearity was proven by Kevrekidis, Pelinovsky, and Tyugin (2013b) using the standard Lyapunov-Schmidt method. Dohnal and Siegl

(2015) developed a more general analysis and proved existence of nonlinear stationary modes bifurcating from a simple eigenvalue in systems with antilinear symmetry. Expansions (87), however, must be modified if the eigenvalue \tilde{E} is not simple. Nonlinear modes bifurcating from *semisimple* eigenvalues (i.e., eigenvalues with equal algebraic and geometric multiplicities) were addressed by Li, Zezyulin, Konotop, and Kevrekidis (2013) and Zezyulin and Konotop (2013). Bifurcations from double and triple eigenvalues (with algebraic multiplicity larger than the geometric one) were studied by Zezyulin and Konotop (2013).

b. Anticontinuum limit

Existence of continuous families can also be rigorously proven in the so-called anticontinuum limit (ACL), developed in the seminal work of MacKay and Aubry (1994) for a conservative dNLS equation. The method consists of continuation from the limit of strong nonlinearity where the linear coupling can be neglected and exact solutions of effectively decoupled oscillators can be found. The solution family is constructed using analytical continuation.

This idea can be extended to infinite \mathcal{PT} -symmetric arrays (Konotop, Pelinovsky, and Zezyulin, 2012) as well as to finite \mathcal{PT} -symmetric chains and \mathcal{PT} -symmetric defects embedded in finite chains (Kevrekidis, Pelinovsky, and Tyugin, 2013b; Pelinovsky, Zezyulin, and Konotop, 2014). As an example, let us consider the system (74) with all coupling coefficients c_n scaled to unity and zero boundary conditions $q_{-N} = q_{N+1} = 0$. Substituting $q_n = w_n e^{-i(E-2)z}$ yields the following system of algebraic equations ($-N+1 \leq n \leq N$):

$$Ew_n = w_{n+1} + w_{n-1} + i\gamma_n w_n + [(1 - \chi_n)|w_n|^2 + \chi_n|w_{1-n}|^2]w_n, \quad (88)$$

with $w_{-N} = w_{N+1} = 0$. Looking for \mathcal{PT} -invariant stationary modes, $\mathcal{PT}\mathbf{w} = \mathbf{w}$, we obtain $w_n = w_{1-n}^*$, which reduces Eq. (88) to the system of N equations ($1 \leq n \leq N$)

$$Ew_n = w_{n+1} + w_{n-1} + i\gamma_n w_n + |w_n|^2 w_n, \quad (89)$$

with boundary conditions $w_0 = w_{N+1}^* = 0$. Note that the coefficients χ_n are not present in Eq. (89).

To enable the consideration of ACL, we rescale variables as $E = 1/\delta$ and $w_n = W_n/\delta^{1/2}$ with $\delta \geq 0$, and rewrite Eq. (89) in the form

$$(1 - |W_n|^2)W_n = \delta(W_{n+1} + W_{n-1} + i\gamma_n W_n), \quad (90)$$

where the boundary conditions now read $W_0 = W_{N+1}^* = 0$. In the limit $\delta \rightarrow 0$ (i.e., $E \rightarrow \infty$), Eq. (90) becomes decoupled and can be solved analytically. The solutions obtained for $\delta = 0$ can then be analytically continued to the $\delta > 0$ case by the implicit function theorem. Using this approach, Pelinovsky, Zezyulin, and Konotop (2014) proved that if the coefficients $\gamma_1, \gamma_2, \dots, \gamma_N$ satisfy constraints

$$\left| \sum_{n=K}^N \gamma_n \right| < 1 \quad \text{for all } K = 1, 2, \dots, N, \quad (91)$$

then in the limit $E \rightarrow \infty$ there exist 2^N unique \mathcal{PT} -invariant nonlinear modes such that

$$||w_n|^2 - E| \leq C \quad \text{for each } n = 1, 2, \dots, N, \quad (92)$$

where C is a positive E -independent constant.

The modes described by Eq. (92) are characterized by unbounded amplitudes $|w_n|^2$ at all sites $n = 1, 2, \dots, N$ when $E \rightarrow \infty$. They, however, do not exhaust all possible nonlinear modes, and for a proper choice of the coefficients $\gamma_1, \gamma_2, \dots, \gamma_N$ one can also construct 2^M ($M = 1, 2, \dots, N - 1$) solutions whose amplitudes in the limit of $E \rightarrow \infty$ grow unbounded only at $2M$ central sites but vanish for other $2N - 2M$ sites, i.e.,

$$\begin{aligned} ||w_n|^2 - E| &\leq C \quad \text{for all } n = 1, 2, \dots, M, \\ |w_n|^2 &\leq CE^{-1} \quad \text{for all } n = M + 1, M + 2, \dots, N, \end{aligned}$$

where again C is a positive constant which does not depend on E .

Pelinovsky, Zezyulin, and Konotop (2014) proved that under certain (not very restrictive) conditions on coefficients $\gamma_1, \gamma_2, \dots, \gamma_N$ the system (88) admits altogether $2^{N+1} - 2$ \mathcal{PT} -invariant stationary solutions (unique up to a gauge transformation) for all sufficiently large E .

ACL can also be used to classify linear stability of nonlinear modes in the limit $E \rightarrow \infty$. Stability can be affected by the choice of nonlinear coefficients χ_n [recall that χ_n do not enter the stationary system (89)]. Pelinovsky, Zezyulin, and Konotop (2014) showed that 2^N nonlinear modes that exist in the limit $E \rightarrow \infty$ under the conditions (91) contain exactly one spectrally stable mode if $\chi_n < 1/2$ for all $n = 1, 2, \dots$, and exactly two spectrally stable modes if $\chi_n = 1/2$ for all n .

The ACL approach can also be used in infinite \mathcal{PT} -symmetric lattices to prove the existence of discrete solitons, i.e., nonlinear modes satisfying boundary conditions $|w_n| \rightarrow 0$ as $|n| \rightarrow \infty$ (Konotop, Pelinovsky, and Zezyulin, 2012). Consider an infinite network (74) with Kerr nonlinearity ($\chi_n = 0$), alternating gain and loss $\gamma_n = (-1)^n \gamma$, and alternating coupling constants: $c_n = \kappa$ for even n and $c_n = \epsilon$ for odd n (n runs through all integers from $-\infty$ to ∞). In this case, the ACL can be introduced as the limit $\epsilon \rightarrow 0$, when the infinite chain decouples into a set of identical \mathcal{PT} -symmetric dimers. Each dimer bears either the trivial zero solution or one of the two nonzero solutions defined by Eq. (85). In the simplest situation, only one dimer is excited (with a nonzero amplitude) in the ACL, while all other dimers have zero amplitudes. Using the implicit function theorem, one can prove that the obtained configuration can be continued analytically from the limit $\epsilon = 0$ to $\epsilon > 0$. The obtained solution for $\epsilon > 0$ represents a discrete \mathcal{PT} -symmetric soliton. Depending on the choice of sign in Eq. (85), one can construct two types of solutions, termed below as “+” solitons and “-” solitons. These solitons can be continued to finite values of ϵ numerically, up to a certain threshold value of ϵ at which the Jacobian matrix of the implicit function theorem becomes degenerate and further continuation is not possible. An example of the bifurcation diagram is shown in Fig. 18(a), where the branch of - solitons terminates at some critical value of ϵ , and power

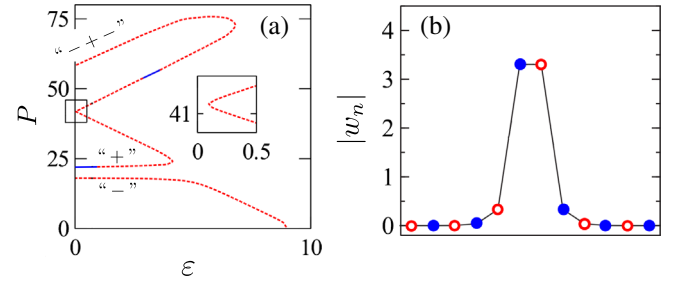


FIG. 18. (a) Bifurcations of discrete \mathcal{PT} -symmetric solitons from the ACL which corresponds to $\epsilon = 0$. Solid blue and dashed red fragments correspond to stable and unstable solitons, respectively. (b) Profile of an unstable soliton on the homogeneous lattice $\epsilon = \kappa$. Open (red) and filled (blue) circles correspond to the sites with gain and losses, respectively. For both panels, $\kappa = 1$, $\gamma = 0.1$, and $\mu = 10$. Adapted from Konotop, Pelinovsky, and Zezyulin, 2012.

$P = \sum_n |w_n|^2$ of solitons vanishes. The branch of + solitons merges with another branch of solitons designated as $- + -$. In the ACL, solitons of the $- + -$ branch reduce to the configuration where all decoupled dimers bear zero amplitude, except for three consecutive dimers, the central one having amplitude (85) with the + sign and the two others having the - sign. Solutions from the + branch are stable for sufficiently small ϵ , but lose stability at $\epsilon = \kappa - \gamma$, i.e., at the point of \mathcal{PT} -symmetry breaking. However, the (unstable) discrete solitons can be continued to the region of broken \mathcal{PT} symmetry, and even up to the case where $\kappa = \epsilon = 1$ when the coupling becomes homogeneous [Fig. 18(b)]. Stable solitons in the infinite chain with homogeneous coupling can also be found if the chain includes only a finite number of sites with gain and loss (i.e., a \mathcal{PT} -symmetric defect) (Kevrekidis, Pelinovsky, and Tyugin, 2013b). If the defect consists of only two sites, localized modes can be obtained analytically (Dmitriev *et al.*, 2011; Zhang *et al.*, 2014).

Discrete solitons in a lattice with saturable nonlinearity have been considered by Song *et al.* (2014).

4. Discrete compactons

Compactons were introduced by Rosenau and Hyman (1993) and Rosenau (1994) as excitations whose field is concentrated on a finite support and is exactly zero outside this region. Such objects cannot exist in systems with linear dispersion. However, linear dispersion can be completely suppressed in specially designed \mathcal{PT} -symmetric arrays of waveguides (Yulin and Konotop, 2013). Indeed let us consider an infinite network shown in Fig. 19(a). It consists of lossy (u_n), active (v_n), and conservative (w_n) waveguides. The coupling coefficients are κ (real and positive) and $\kappa_1 = \tilde{\kappa} e^{i\phi/2}$ with real $\tilde{\kappa}$ and ϕ . Gain and loss are described by the single parameter γ . The array is governed by the dynamical system

$$\begin{aligned} i\dot{u}_n &= \kappa v_n - i\gamma u_n + \kappa_1 (w_{n-1} + w_n) + \chi |u_n|^2 u_n, \\ i\dot{v}_n &= \kappa u_n + i\gamma v_n + \kappa_1^* (w_{n-1} + w_n) + \chi |v_n|^2 v_n, \\ i\dot{w}_n &= \kappa_1 (u_n + u_{n+1}) + \kappa_1^* (v_n + v_{n+1}) + \chi |w_n|^2 w_n, \end{aligned} \quad (93)$$

where χ is the coefficient of Kerr nonlinearity.

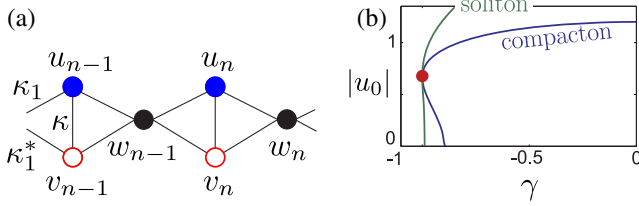


FIG. 19. (a) Array of waveguides that supports discrete compactons. (b) Bifurcation diagram of branches of compactons and solitons for $\kappa = 1$, $\tilde{\kappa} = 0.25$, and $\chi = 1$. The point where the branches intersect is indicated by a dot. Adapted from Yulin and Konotop, 2013.

The linear dispersion relation is obtained by the ansatz $(u_n, v_n, w_n) = (u, v, w)e^{i(bz - kn)}$ with $\chi = 0$:

$$b^3 - (\kappa^2 - \gamma^2)b - 8\tilde{\kappa}^2[b \cos \phi + \gamma \sin \phi + \kappa] \cos^2(k/2) = 0.$$

In order to have a (linear) compacton, there must exist a dispersion branch where the propagation constant b is independent of k . This is possible if $\gamma = -\kappa \sin \phi$. Then there is a k -independent dispersion branch $b = -\kappa \cos \phi$ which describes the dipole mode with $w_{\text{dip}} = 0$ and

$$u_{\text{dip}} = \alpha v_{\text{dip}}, \quad \alpha = \frac{\kappa^2 - \tilde{\kappa}^2(1 + i \cos k)}{\tilde{\kappa}^2(1 + i \cos k) - \kappa^2 \cos \phi} e^{i\phi}. \quad (94)$$

This mode corresponds to the excitation of only one ‘‘cell’’ (say at $n = 0$), i.e., represents a linear compacton.

In the presence of nonlinearity, one can construct a continuous family of nonlinear solutions bifurcating from the dipole mode (94). The nonlinear solutions persist as compactons if one follows along the line $\gamma = -\kappa \sin \phi$. A bifurcation diagram for nonlinear \mathcal{PT} -symmetric compactons with $\chi = 1$ is illustrated in Fig. 19(b). Moving along the bifurcation curve, one arrives at another bifurcation point (indicated by a red dot) where the compacton branch intersects a branch of conventional nonlinear \mathcal{PT} -symmetric modes. At this intersection point the compacton and soliton coexist.

5. Vortices in closed arrays

A discrete circular array of N waveguides representing a system with rotational symmetry supports vortex modes (Desyatnikov, Dennis, and Ferrando, 2011). These objects are characterized by the phase $\sim \exp(i2\pi mn/N)$ with $m = (1/2\pi) \sum_{n=1}^N \text{Arg}(q_n^* q_{n+1})$ being the topological charge (TC) and $n = 1, 2, \dots, N$ being the waveguide number. The charge-flipping transformation $m \leftrightarrow -m$ can be viewed as complex conjugation or time reversion. Discrete vortices persist in arrays with embedded \mathcal{PT} -symmetric defects similar to the one illustrated in Fig. 20(a) (Leykam, Konotop, and Desyatnikov, 2013). Interplay between nonlinearity and gain and loss breaks the \mathcal{PT} symmetry and thus degeneracy of the vortex modes.

Propagation of the monochromatic fields $q_n(z)$ ($n = 1, \dots, N$) is governed by the system ($\chi = \pm 1$)

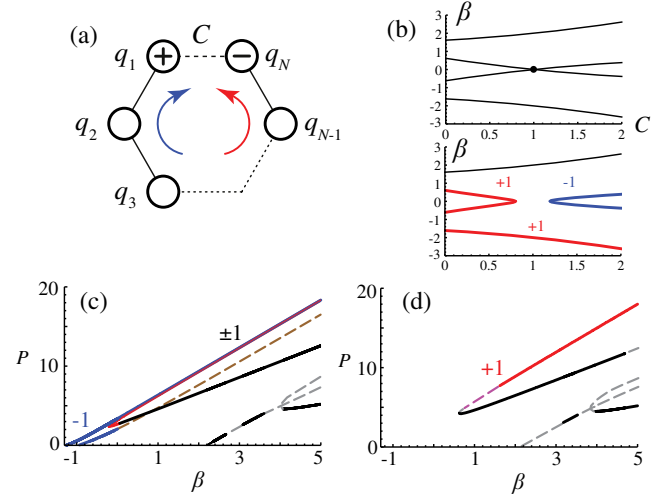


FIG. 20. (a) Array of N waveguides with one active ($n = 1$) and one lossy ($n = N$) waveguide. Phase circulation direction is indicated by anticlockwise (red, $m > 0$) and clockwise (blue, $m < 0$) arrows. (b) Linear propagation constants β vs C for a conservative ($\gamma = 0$, upper panel) and \mathcal{PT} -symmetric ($\gamma = 0.2 < \gamma_{\mathcal{PT}}$, lower panel) ring of $N = 4$ waveguides. Degenerate vortex modes occur at the intersection marked by the black dot. Curves labeled with ‘‘+1’’ and ‘‘-1’’ consist of the modes with the respective TC. Stable (unstable) nonlinear modes of $N = 3$ ring are shown with solid (dashed) lines for (c) $C = 1.3$, $\gamma = 0.2 < \gamma_{\mathcal{PT}}$ and (d) $C = 1.3$, $\gamma = 0.6 > \gamma_{\mathcal{PT}}$. TCs are indicated next to the curves, $m = +1$ in red (purple), $m = -1$ in blue (brown), and $m = 0$ in black (gray). Adapted from Leykam, Konotop, and Desyatnikov, 2013.

$$\begin{aligned} i\dot{q}_1 + Cq_N + q_2 - i\gamma q_1 + \chi|q_1|^2 q_1 &= 0, \\ i\dot{q}_n + q_{n-1} + q_{n+1} + \chi|q_n|^2 q_n &= 0, \\ i\dot{q}_N + Cq_1 + q_{N-1} + i\gamma q_N + \chi|q_N|^2 q_N &= 0, \end{aligned} \quad (95)$$

subject to the cyclic boundary conditions $q_{n+N} = q_n$.

The equations for linear stationary solutions $q_n = w_n e^{i\beta z}$ can be cast in the general form $\beta \mathbf{w} = H \mathbf{w}$, where $H = H_0 + i\gamma H_1$, H_0 is a matrix describing the array without dissipation and loss, and H_1 has the only nonzero entries $(H_1)_{11} = (H_1)_{NN} = \gamma$. H is \mathcal{PT} symmetric, and the \mathcal{PT} -symmetry-breaking threshold is $\gamma_{\mathcal{PT}} = |C - 1|$ (Sukhorukov et al., 2012; Leykam, Konotop, and Desyatnikov, 2013). The spectrum of the linear problem for a ring with $N = 4$ is illustrated in Fig. 20(b). At $\gamma = 0$ vortex modes exist only at $C = 1$, and they are degenerate (i.e., the modes with opposite TCs have the same energy). At $\gamma > 0$ the degeneracy is broken and vortex branches with $|m| = 1$ appear.

Typical families of nonlinear modes in an array with $N = 3$ and $C > 1$ are shown in Figs. 20(c) and 20(d) for unbroken and broken \mathcal{PT} symmetries, respectively. For $\gamma < \gamma_{\mathcal{PT}}$ nonlinear $m = -1$ modes bifurcate from the linear modes, and a pair of $m = +1$ vortices is created from a saddle-node bifurcation [Fig. 20(c)]. For $\gamma > \gamma_{\mathcal{PT}}$ the $m = -1$ modes are destroyed, while the saddle-node bifurcation for $m = +1$ remains [Fig. 20(d)].

Finally we note that stable vortices as well as lifting of their degeneracy were also reported in continuous azimuthally

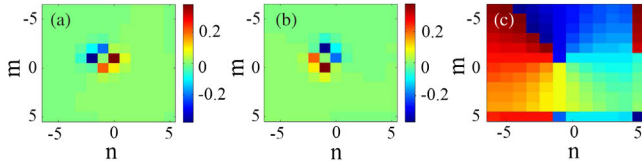


FIG. 21. (a) Real and (b) imaginary parts, and the (c) phase structure, of field $u_{m,n}$ for a typical stable on-site \mathcal{PT} -symmetric vortex soliton with $(C, \kappa, \gamma) = (-0.03, -1, 0.4)$. From *Chen et al.*, 2014.

modulated \mathcal{PT} -symmetric rings (*Kartashov, Konotop, and Torner*, 2015).

6. Solitons and vortices in coupled dNLS equations

\mathcal{PT} -symmetric dimers in an infinite array (81) are described by two coupled 1D dNLS equations, whose soliton solutions were reported by *Suchkov et al.* (2011). A natural extension of that model is an infinite 2D array of coupled dimers, i.e., in a plane as shown schematically in Fig. 17(b). This leads to a model of coupled 2D dNLS equations (*Chen et al.*, 2014)

$$\begin{aligned} i\dot{u}_{n,m} &= i\gamma u_{n,m} + \kappa v_{n,m} + C\Delta^{(2)}u_{n,m} - |u_{n,m}|^2 u_{n,m}, \\ i\dot{v}_{n,m} &= -i\gamma v_{n,m} + \kappa u_{n,m} + C\Delta^{(2)}v_{n,m} - |v_{n,m}|^2 v_{n,m}, \end{aligned}$$

where $\Delta^{(2)}$ is a 2D second-order difference operator, i.e., $\Delta^{(2)}u_{n,m} = u_{n-1,m} + u_{n+1,m} + u_{n,m-1} + u_{n,m+1} - 4u_{n,m}$. If $\gamma < \kappa$ (i.e., \mathcal{PT} symmetry is unbroken), the system admits solutions with $v_{n,m} = e^{i\delta}u_{n,m}$, where

$$\delta = -\arcsin(\gamma/\kappa) \quad \text{or} \quad \delta = \pi + \arcsin(\gamma/\kappa), \quad (96)$$

and $u_{n,m}$ satisfies a single conservative 2D dNLS equation

$$i\dot{u}_{n,m} = \kappa \cos(\delta)u_{n,m} + C\Delta^{(2)}u_{n,m} - |u_{n,m}|^2 u_{n,m}.$$

Each nonlinear mode of the latter equation yields two solutions of the original system corresponding to two different δ in Eq. (96). A conservative 2D dNLS equation admits on- and off-site vortex solitons characterized by nontrivial phase circulations along a closed contour (*Malomed and Kevrekidis*, 2001; *Kevrekidis*, 2009). Their counterparts in the 2D \mathcal{PT} -symmetric system were considered by *Chen et al.* (2014), who found that off-site vortices are unstable for almost any C , while on-site vortices can be stable in a wide range of parameters. An example of a stable \mathcal{PT} -symmetric vortex is shown in Fig. 21.

D. Nonlinear dynamics of \mathcal{PT} -symmetric arrays

1. Conservative versus dissipative dynamics

\mathcal{PT} -symmetric dynamical systems generally do not conserve energy, which allows them to possess unbounded solutions (which are forbidden in conservative discrete lattices). The unbounded growth is a typical scenario of evolution of an unstable \mathcal{PT} -symmetric stationary mode subjected to a small initial perturbation. Alternatively, unstable

\mathcal{PT} -symmetric modes break up into long-lived transient structures, but typically do not evolve to an attractor (in this way \mathcal{PT} -symmetric dynamics has some features of conservative and Hamiltonian systems). If the initial conditions correspond to a slightly perturbed stable nonlinear mode, then the evolution also resembles that in a conservative system, i.e., the amplitude of the perturbation remains nearly constant. Numerical evidences of such behavior can be found in *Li and Kevrekidis* (2011), *K. Li et al.* (2012), *Li, Zezyulin, Konotop, and Kevrekidis* (2013), and *Pelinovsky, Zezyulin, and Konotop* (2014) for finite lattices, and in *Kevrekidis, Pelinovsky, and Tyugin* (2013b) and *Zhang et al.* (2014) for infinite chains. Explanation of this behavior might stem from the symplectic structure of the linear operator that describes evolution of small perturbations of stationary states (*Alexeeva et al.*, 2012) (see Sec. V.A). Despite the absence of energy conservation, \mathcal{PT} -symmetric systems can conserve other quantities (*Ramezani et al.*, 2010) and admit a Hamiltonian representation. A variety of completely integrable Hamiltonian \mathcal{PT} -symmetric dimers were reported by *Barashenkov* (2014), *Barashenkov and Gianfreda* (2014), and *Barashenkov, Pelinovsky, and Dubard* (2015). In fact, some such systems have been known much earlier outside the domain of the \mathcal{PT} symmetry (*Jørgensen, Christiansen, and Abou-Hayt*, 1993; *Jørgensen and Christiansen*, 1994).

The best studied case corresponds to a finite \mathcal{PT} -symmetric open chain with Kerr nonlinearity and alternating gain and loss. *Kevrekidis, Pelinovsky, and Tyugin* (2013a) proved that solutions of the underlying configuration exist globally (i.e., do not blow up in finite time) for any initial condition. At the same time, there exist initial conditions that evolve to exponentially growing solutions, even if \mathcal{PT} symmetry of the underlying linear system is unbroken [see Eq. (77)]. More results on nonlinear dynamics of \mathcal{PT} -symmetric oligomers (including categorization of different dynamical scenarios) can be found in *Dmitriev et al.* (2011), *Li and Kevrekidis* (2011), *D'Ambroise, Kevrekidis, and Lepri* (2012), *K. Li et al.* (2012), *Suchkov, Sukhorukov et al.* (2012), *Duanmu et al.* (2013), *Li, Kevrekidis et al.* (2013), *Li, Zezyulin, Konotop, and Kevrekidis* (2013), *Rodrigues et al.* (2013), *D'Ambroise, Malomed, and Kevrekidis* (2014), *Zhang et al.* (2014), and *Xu, Kevrekidis, and Saxena* (2015).

Dynamics of solitons in infinite \mathcal{PT} -symmetric chains was discussed by *Dmitriev, Sukhorukov, and Kivshar* (2010) and *Suchkov et al.* (2011). Scattering on a \mathcal{PT} -symmetric defect embedded in an infinite conservative chain was studied by *Dmitriev et al.* (2011), *D'Ambroise, Kevrekidis, and Lepri* (2012), *Suchkov, Sukhorukov et al.* (2012), *D'Ambroise et al.* (2014), and *Zhang et al.* (2014).

We also mention the possibility for the existence of conserved quantities in \mathcal{PT} -symmetric networks with an arbitrary number of sites. Recall that any linear \mathcal{PT} -symmetric (and hence \mathcal{P} -pseudo-Hermitian) system admits an integral of motion $Q = \langle \mathcal{P}\mathbf{q}, \mathbf{q} \rangle$ (see Sec. II.C). This quantity is not conserved in a nonlinear system (69) with generic nonlinearity $F(\mathbf{q})$. However if the nonlinear operator $F(\mathbf{q})$ is pseudo-Hermitian, i.e.,

$$F^\dagger(\mathbf{q}) = \mathcal{P}F(\mathbf{q})\mathcal{P} \quad \text{for any } \mathbf{q}, \quad (97)$$

then the nonlinear system (69) also conserves the same quantity Q (Zezyulin and Konotop, 2013). This observation allows one to construct nonlinear arrays with at least one integral of motion. Note that if $\mathcal{PF}^*(\mathbf{q}) = F(\mathbf{q})\mathcal{P}$ for all \mathbf{q} and $F(\mathbf{q})$ is a symmetric matrix, i.e., $F^T(\mathbf{q}) = F(\mathbf{q})$ for any \mathbf{q} , then Eq. (97) automatically holds.

2. \mathcal{PT} -symmetric dimer

Dynamics of the nonlinear dimer model (75) can be conveniently described using Stokes variables

$$\begin{aligned} S_0 &= |q_0|^2 + |q_1|^2, & S_1 &= q_0 q_1^* + q_0^* q_1, \\ S_2 &= i(q_0 q_1^* - q_0^* q_1), & S_3 &= |q_1|^2 - |q_0|^2, \end{aligned} \quad (98)$$

which satisfy the identity $S_0^2 = S_1^2 + S_2^2 + S_3^2$. From system (75) one obtains

$$\begin{aligned} \dot{S}_0 &= 2\gamma S_3, & \dot{S}_1 &= (1 - 2\chi)S_2 S_3, \\ \dot{S}_2 &= 2S_3 - (1 - 2\chi)S_1 S_3, & \dot{S}_3 &= 2\gamma S_0 - 2S_2. \end{aligned} \quad (99)$$

a. Conserved quantities, integrability, and Hamiltonian structure

Ramezani *et al.* (2010) discovered that the \mathcal{PT} -symmetric dimer (75) with $\chi = 0$ admits two integrals of motion. Indeed, using the new variable $r = \sqrt{S_1^2 + S_2^2}/2$, the first conserved quantity is found to be $\rho = \sqrt{r^2 - S_1} + 1$. The second constant of motion J is obtained from $2\rho \sin[(J - S_0)/(2\gamma)] = S_1 - 2$. Pickton and Susanto (2013) used the integrals ρ and J to construct the phase portrait and to classify the behavior of all solutions of the system. Further, Barashenkov (2014) found that the dimer model admits a Hamiltonian representation, and the Hamiltonian

$$H = -2 \left(\sqrt{\rho^2 + 1} + 2\rho \sin \theta \cosh P_\theta + \gamma \theta \right) \quad (100)$$

is expressed in terms of polar coordinates ρ and θ , defined as $\rho \sin \theta = S_1/2 - 1$ and $\rho \cos \theta = -S_2/2$, and momentum P_θ , defined by $2r \sinh P_\theta = S_3$ and $2r \cosh P_\theta = S_0$ (since ρ is a conserved quantity, the conjugate momentum P_ρ does not enter the Hamiltonian). The Hamiltonian equations read

$$\begin{aligned} \dot{\theta} &= \frac{\partial H}{\partial P_\theta} = -S_3, & \dot{P}_\theta &= -\frac{\partial H}{\partial \theta} = 2 \left(\gamma + \frac{\rho \cos \theta}{r} \cosh P_\theta \right), \\ \dot{\rho} &= \frac{\partial H}{\partial P_\rho} = 0, & \dot{P}_\rho &= -\frac{\partial H}{\partial \rho} = 2 \frac{\rho + \sin \theta}{r} \cosh P_\theta. \end{aligned}$$

The \mathcal{PT} -symmetric dimer (75) with $\chi = 1/2$ is also integrable (Pelinovsky, Zezyulin, and Konotop, 2014). In this case substitution $q_{0,1} = p_{0,1} \exp[(1/2i) \int (|p_0|^2 + |p_1|^2) dz]$ transforms the model into a linear system: $i\dot{p}_0 = -i\gamma p_0 + p_1$, $i\dot{p}_1 = i\gamma p_1 + p_0$, meaning that all solutions are bounded for $\gamma < 1$ and generically unbounded for $\gamma \geq 1$.

b. Global existence, bounded, and unbounded solutions

Turning back to the general model (99) with arbitrary χ , one concludes that solutions for any initial condition exist globally

as Gronwall's inequality implies that $S_0(z) \leq S_0(0)e^{2\gamma|z|}$ for all z .

For $\chi = 0$ and $\gamma < 1$, there exist sufficiently small initial conditions with globally bounded solutions (Kevrekidis, Pelinovsky, and Tyugin, 2013a). On the other hand, for $\chi \neq 1/2$ the system admits infinitely growing solutions, even in the case of unbroken \mathcal{PT} symmetry (Kevrekidis, Pelinovsky, and Tyugin, 2013a; Pelinovsky, Zezyulin, and Konotop, 2014). For $\chi = 0$, Barashenkov, Jackson, and Flach (2013) found an exact unbounded solution $q_{0,1} = \exp\{\mp \gamma(z - z_0) - i/\gamma \sinh[2\gamma(z - z_0)]\}$, where z_0 is a free parameter. For $\gamma > 1$, all trajectories are generically unbounded, except for initial conditions that lie on the stable manifold of the saddle point $q_0 = q_1 = 0$ (Barashenkov, Jackson, and Flach, 2013).

c. Unidirectional propagation

A linear \mathcal{PT} -symmetric coupler displays nonreciprocal behavior characterized by the field growth in the two arms (see Sec. III.A). The nonlinearity changes the situation leading to effectively *unidirectional* light propagation (Ramezani *et al.*, 2010; Sukhorukov, Xu, and Kivshar, 2010), i.e., to a light diode functionality. More specifically, if the nonlinearity coefficient χ exceeds some threshold value χ_{th} , the output radiation almost entirely concentrates in the arm with gain [the q_1 component in Eq. (40)] independent of which arm the input radiation is applied; while for the nonlinearity below the critical value, the output radiation is distributed between the two arms. The critical nonlinearity $\chi_{th} = 4 - 2\pi\gamma$ was estimated from the heuristic argument that for energy exchange to occur, there must exist a maximum of S_0 , i.e., a point z where relations $\dot{S}_0 = 0$ and $\ddot{S}_0 < 0$ hold simultaneously (Ramezani *et al.*, 2010). A description of possible evolution scenarios can be found in Sukhorukov, Xu, and Kivshar (2010).

3. Two coupled nonlinear oscillators

Now we turn to nonlinear generalizations of the coupled oscillator model (62). These studies were initiated by Cuevas *et al.* (2013), who considered periodic orbits of the model

$$\begin{aligned} \ddot{x} + 2\gamma\dot{x} + x + 2\kappa y + x^3 &= 0, \\ \ddot{y} - 2\gamma\dot{y} + y + 2\kappa x + y^3 &= 0, \end{aligned}$$

and showed that, under the so-called rotating wave approximation, this model is reduced to the nonlinear \mathcal{PT} -symmetric dimer (40).

Another way to generalize the linear coupled oscillator model (62) is based on a nonlinear extension of the Hamiltonian (65):

$$\begin{aligned} H &= pq + \gamma(yq - xp) + (1 - \gamma^2)xy + \kappa(x^2 + y^2) \\ &+ \sum_{n,m} g_{nm} x^n y^m, \end{aligned} \quad (101)$$

which preserves the same Hamiltonian structure as described in Sec. III.L for the linear case. By choosing $g_{nm} = \delta_{n,1}\delta_{m,3} + \delta_{n,1}\delta_{m,3}$, one obtains the relation between momenta and velocities given by Eq. (66), as well as the following dynamical equations (Barashenkov and Gianfreda, 2014):

$$\begin{aligned} \ddot{x} + 2\gamma\dot{x} + x + 2\kappa y + x^3 + 3xy^2 &= 0, \\ \ddot{y} - 2\gamma\dot{y} + y + 2\kappa x + y^3 + 3yx^2 &= 0. \end{aligned} \quad (102)$$

This system leads to a new integrable nonlinear \mathcal{PT} -symmetric dimer. It was derived by Barashenkov and Gianfreda (2014) using a multiple-scale perturbation expansion under the scaling $2\kappa = 3K\epsilon^2$ and $2\gamma = \Gamma\epsilon^2$, where $\epsilon \ll 1$ is a small parameter, and $K, \Gamma = O(1)$. Looking for a solution of Eq. (102) in the form of perturbation expansions $x = \epsilon x_1 + \epsilon^3 x_3 + \dots$ and $y = \epsilon y_1 + \epsilon^3 y_3 + \dots$, and using the scaled time variables $T_{2n} = \epsilon^{2n} t$ ($n = 0, 1, \dots$), one obtains the leading order solution as $x_1 = \sqrt{K} q_0 e^{iT_0} + \text{c.c.}$, $y_1 = \sqrt{K} q_1 e^{iT_0} + \text{c.c.}$, where $q_{0,1}$ solve the equations

$$\begin{aligned} i\dot{q}_0 + q_1 + (|q_0|^2 + 2|q_1|^2)q_0 + q_1^2 q_0^* &= -i\Gamma q_0, \\ i\dot{q}_1 + q_0 + (|q_1|^2 + 2|q_0|^2)q_1 + q_0^2 q_1^* &= i\Gamma q_1. \end{aligned} \quad (103)$$

Here the overdot denotes the derivative with respect to $\tau = 3KT_2/2$, and gain and loss are characterized by $\Gamma = \gamma/(3K)$. The system (103) is Hamiltonian, i.e., can be obtained from the equations of motion $i\dot{q}_0 = -\partial H/\partial q_1^*$ and $i\dot{q}_1 = -\partial H/\partial q_0^*$, with the Hamiltonian H as

$$H = (|q_0|^2 + |q_1|^2)(1 + q_0^* q_1 + q_0 q_1^*) + i\Gamma(q_1^* q_0 - q_0^* q_1). \quad (104)$$

The system also conserves the quantity $S_1 = q_0 q_1^* + q_0^* q_1$ and is therefore integrable.

Another interesting feature of the system (103) is the existence of stable nonlinear stationary modes for any value of Γ , even for $|\Gamma| > 1$ when stable propagation of linear waves is not possible. Another modification of a \mathcal{PT} -symmetric dimer with a similar property was reported by Cuevas-Maraver *et al.* (2015). Moreover, it is possible to find a family of dimers for which all nonlinear trajectories remain bounded, irrespectively of the value of the gain-loss coefficient Γ (Barashenkov, Pelinovsky, and Dubard, 2015). This phenomenon can be termed as nonlinearity-induced \mathcal{PT} -symmetry restoration.

4. Scattering on a \mathcal{PT} -symmetric defect

An infinite conservative lattice with a \mathcal{PT} -symmetric defect supports propagation of linear modes which undergo scattering by the defect (Dmitriev *et al.*, 2011; Suchkov, Sukhorukov *et al.*, 2012). The simplest case corresponds to a \mathcal{PT} -symmetric dimer embedded in a conservative lattice. It can be represented schematically by a chain in Fig. 16(a), where all $\gamma_n = 0$ except for $\gamma_1 = \gamma$, and all coupling constants are equal: $\kappa = \epsilon = 1$, except for the one between q_0 and q_1 which is equal to some constant C . If all couplings are equal, i.e., $C = 1$, the transmission and reflection coefficients of a plane wave in the linear limit $\chi = 0$ incident from the left are

$$T(k) = \frac{2ie^{-ik} \sin k}{e^{-2ik} + \gamma^2 - 1}, \quad R(k) = \frac{-\gamma^2 + 2\gamma \sin k}{e^{-2ik} + \gamma^2 - 1},$$

where real k is the Bloch-wave number of the incident wave.

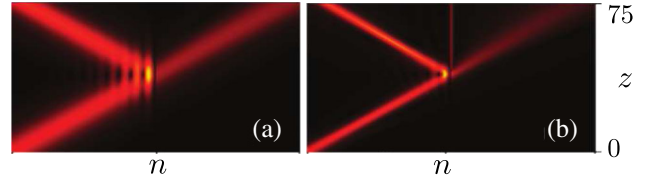


FIG. 22. Two scenarios of discrete soliton scattering on a \mathcal{PT} -symmetric dimer defect. (a), (b) Feature the same model parameters, but different amplitudes of the incident discrete soliton: $A = 0.2$ vs $A = 0.5$. In both panels, n runs from $n = -75$ to $n = 75$. Adapted from Suchkov, Sukhorukov *et al.*, 2012.

Since $|T(k)|^2$ and $|R(k)|^2$ can be larger than unity, the reflected and/or transmitted waves can be amplified after the scattering. This property is verified in the nonlinear case as well. Numerical study shows that the \mathcal{PT} -symmetric dimer defect can substantially amplify the incident soliton (Suchkov, Sukhorukov *et al.*, 2012). It was also found that soliton scattering can occur without [Fig. 22(a)] or with [Fig. 22(b)] excitation of an internal localized mode, depending on the amplitude of the incident soliton. Defect modes localized on a nonlinear \mathcal{PT} -symmetric dimer were described by Zhang *et al.* (2014).

Asymmetric scattering of left and right incident plane waves by nonlinear \mathcal{PT} -symmetric defects embedded in a linear conservative infinite chain was considered by D'Ambroise, Kevrekidis, and Lepri (2012). Scattering by a nonlinear defect embedded in a linear ladder configuration, similar to that shown in Fig. 17(a), was described by D'Ambroise *et al.* (2014).

5. \mathcal{PT} -symmetric dimers with varying parameters

A practically relevant issue is the management of nonlinear systems by means of varying parameters. D'Ambroise, Malomed, and Kevrekidis (2014) numerically investigated the effect of time-periodic gain on dynamics of the nonlinear dimer (40) with periodic coupling $\kappa = V_0 + V_1 \cos(\omega z)$. In the linear limit, such a system is characterized by the presence of parametric resonance, and its long-term linear behavior is determined by the Floquet multipliers. On the plane of parameters (V_0, V_1) one can distinguish regions of stable and unstable dynamics. The inclusion of nonlinearity significantly affects the dynamics, i.e., the same initial data can be bounded in the linear case and unbounded in the nonlinear case and vice versa. The effect of the varying gain-loss profile was investigated by Horne *et al.* (2013) and Battelli *et al.* (2015).

Another question of practical relevance is the effect of *random* modulations of system parameters which preserve the \mathcal{PT} symmetry only on average. Considering the \mathcal{PT} -symmetric dimer (40) with coupling $\kappa + K(z)$ and gain-loss coefficients $\gamma + \Gamma_{1,2}(z)$, where $K(z)$ and $\Gamma_{1,2}(z)$ are delta-correlated white noises, Konotop and Zezyulin (2014a) demonstrated that the statistically averaged intensity of the field in the coupler grows exponentially. The growth occurs independently of whether the average \mathcal{PT} symmetry is broken or not, but the broken \mathcal{PT} symmetry boosts the growth rate.

Stability regions for the model of coupled oscillators (62) with periodically modulated gain-loss coefficients were investigated by Psiachos, Lazarides, and Tsironis (2014).

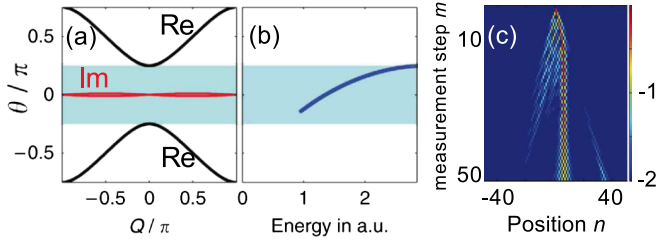


FIG. 23. Solitons in locally \mathcal{PT} -symmetric lattices. (a) The linear dispersion relation (105) with $G = 1.1$. Black and red lines with labels “Re” and “Im” correspond to real and imaginary parts of θ , respectively. (b) Family of solitons in gap of the spectrum (shaded blue domain) on the diagram θ vs E . (c) Formation and propagation of a discrete soliton as the input power $P \approx 120$ mW. The color bar shows \log_{10} (intensity). Adapted from Wimmer *et al.*, 2015.

E. Observation of \mathcal{PT} -synthetic solitons

Now we turn to the experimental observation of solitons in \mathcal{PT} -symmetric synthetic lattices reported by Wimmer *et al.* (2015). The experimental setting was briefly described in Sec. III.A (see Fig. 5). It is modeled by the nonlinear map (41), meaning that the temporal (i.e., evolution) coordinate (m in this case) is also discrete.

Discrete solitons in lattices with local symmetry [see Fig. 5(a)] are described by the model (41) with $G_u = 1/G_v = G$ and $\phi_n = 0$. Neglecting the nonlinearity in the map (41) and using the ansatz $(u_n^m, v_n^m) \sim e^{i(Qn + \theta m)}$, one obtains the linear dispersion relation

$$\theta = \pm \arccos \{ \cos [Q - (i/2) \ln G] / \sqrt{2} \} \quad (105)$$

illustrated in Fig. 23(a). Although the imaginary part of θ is not exactly zero in the infinite lattice, numerical results of Wimmer *et al.* (2015) show that in the finite lattice the eigenvalues remain real as long as the gain does not exceed a certain critical value.

When nonlinearity is taken into account, increasing of the input power leads to a formation of a discrete soliton, as shown in Fig. 23(c). A stationary soliton is of the form $(u_n^m, v_n^m) = (U_n, V_n) e^{i\theta m}$ and can be characterized by the energy $E = \sum_n (|U_n|^2 + |V_n|^2)$. One can identify a family of stationary solitons which can be visualized on the plane (θ, E) ; see Fig. 23(b).

Discrete solitons in lattices with global \mathcal{PT} symmetry [see Fig. 5(b)] are described by the map (41) where the phase alternates as n varies according to the following rule: $\phi_n = \phi_0$ for $\text{mod}(n + 3, 4) < 2$, and $\phi_n = -\phi_0$ otherwise. The spectrum of the linear lattice in this case is determined by

$$\cos(4Q) = 3 \cos^2(2\theta) + 8 \cosh(\ln G) \cos(\phi_0) \cos(2\theta) + \cosh(2 \ln G) - 4 \sin^2(\phi_0). \quad (106)$$

The examples of the numerical solution of the obtained equation are shown in Figs. 24(a) and 24(b). Formation and propagation of a discrete soliton at large intensity of a broad

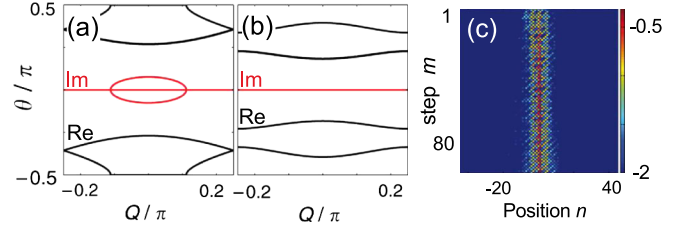


FIG. 24. Band-gap spectrum (106) for (a) the broken \mathcal{PT} symmetry at $G = 1.4$, $\phi_0 = 0$, and (b) unbroken \mathcal{PT} symmetry at $G = 1.4$, $\phi_0 = 0.4\pi$. Black and red lines with labels Re and Im show real and imaginary parts of θ . (c) Formation of a broad single-hump soliton for $G = 1.4$ and $\phi_0 = -0.4\pi$. The color bar shows \log_{10} (intensity). Adapted from Wimmer *et al.*, 2015.

Gaussian pulse applied to the network input are shown in Fig. 24(c).

V. \mathcal{PT} -SYMMETRIC COUPLED NLS EQUATIONS

A. The model and its basic properties

Generalization of discrete \mathcal{PT} -symmetric networks is given by *distributed couplers*, modeled by two linearly coupled NLS equations with gain and loss

$$\begin{aligned} i\psi_{1,z} &= -\psi_{1,xx} - \kappa\psi_2 + i\gamma\psi_1 + (\chi|\psi_1|^2 + \tilde{\chi}|\psi_2|^2)\psi_1, \\ i\psi_{2,z} &= -\psi_{2,xx} - \kappa\psi_1 - i\gamma\psi_2 + (\tilde{\chi}|\psi_1|^2 + \chi|\psi_2|^2)\psi_2, \end{aligned} \quad (107)$$

where all coefficients are real and we assume $\kappa \geq 0$ and $\gamma \geq 0$. Following optical terminology, the terms with χ and $\tilde{\chi}$ are referred to as self-phase modulation (SPM) and cross-phase modulation (XPM), respectively.

The model (107) is \mathcal{PT} symmetric with the parity operator $\mathcal{P} = \sigma_1$. This means that for a given solution $\psi_{1,2}(x, z)$ of Eq. (107) there exists a solution $\psi_1^{(\mathcal{PT})}(x, z) = \psi_2^*(x, -z)$ and $\psi_2^{(\mathcal{PT})}(x, z) = \psi_1^*(x, -z)$.

Using substitution $\psi_{1,2} \sim e^{ikx - ibz}$, we obtain the dispersion relation of the underlying linear system ($\chi = \tilde{\chi} = 0$) as $b = k^2 \pm \sqrt{\kappa^2 - \gamma^2}$. Thus \mathcal{PT} symmetry is unbroken for $\gamma \leq \kappa$, and $\gamma = \gamma_{\mathcal{PT}} = \kappa$ is the exceptional point.

In the context of optical applications, model (107) with $\chi = 0$ was introduced by Driben and Malomed (2011b) for constant gain-and-loss coefficient γ , by Abdullaev, Konotop *et al.* (2011) for a \mathcal{PT} -symmetric defect with localized $\gamma = \gamma(z)$, and by Driben and Malomed (2011a) for periodic $\gamma(z)$ and $\kappa(z)$. Pelinovsky, Zezyulin, and Konotop (2015) proved that the Cauchy problem for Eq. (107) has a unique global solution in the energy space $(\psi_1, \psi_2) \in H^1(\mathbb{R}) \times H^1(\mathbb{R})$, with the H^1 norm defined by $\|\psi\|_{H^1}^2 = \int_{\mathbb{R}} (|\psi|^2 + |\psi_x|^2) dx$. This global existence, however, does not rule out the possibility of indefinitely growing total H^1 norm, $\|\psi_1\|_{H^1} + \|\psi_2\|_{H^1}$. In the particular case of $\chi = \tilde{\chi}$, Eqs. (107) represent a \mathcal{PT} -symmetric extension of the exactly integrable model introduced by Manakov (1973). In this case, the system can be conveniently treated in terms of integral Stokes variables [cf. Eq. (98)]

$$S_0 = \int_{\mathbb{R}} (|\psi_1|^2 + |\psi_2|^2) dx, \quad S_1 = \int_{\mathbb{R}} (\psi_1^* \psi_2 + \psi_2^* \psi_1) dx,$$

$$S_2 = i \int_{\mathbb{R}} (\psi_1^* \psi_2 - \psi_2^* \psi_1) dx, \quad S_3 = \int_{\mathbb{R}} (|\psi_1|^2 - |\psi_2|^2) dx,$$

which for $\chi = \tilde{\chi}$ solve

$$\dot{S}_0 = 2\gamma S_3, \quad \dot{S}_1 = 0, \quad \dot{S}_2 = -2\kappa S_3,$$

$$\dot{S}_3 = 2\gamma S_0 + 2\kappa S_2,$$

where the overdot stands for the derivative with respect to z . Thus the model conserves two quantities: S_1 and $C = \kappa S_0 + \gamma S_2$, which allows one to obtain a general solution

$$S_0 = \kappa C / \omega^2 + A_1 \cos(2\omega z) + A_2 \sin(2\omega z), \quad (108)$$

with $\omega = \sqrt{\kappa^2 - \gamma^2}$ and constant C and $A_{1,2}$. Hence the total power $S_0(z)$ is bounded for $\gamma < \kappa$ and generically unbounded otherwise. On the basis of numerical simulations, [Pelinovsky, Zezyulin, and Konotop \(2015\)](#) also conjectured that the H^1 norm of all solutions in the system with $\chi = \tilde{\chi}$ is also bounded for $\gamma < \kappa$.

Let us also point out that if $\gamma \leq \kappa$, then substitution

$$\psi_2 = e^{i\delta} \psi_1, \quad \delta = \arcsin \gamma / \kappa \quad \text{or} \quad \delta = \pi - \arcsin \gamma / \kappa \quad (109)$$

reduces Eq. (107) to a single conservative NLS equation for function $\psi_1(x, z)$ ([Driben and Malomed, 2011b](#); [Alexeeva et al., 2012](#); [Bludov et al., 2013](#)):

$$i\psi_{1,z} = -\psi_{1,xx} + (\chi + \tilde{\chi})|\psi_1|^2\psi_1 - \kappa \cos(\delta)\psi_1. \quad (110)$$

B. Modulational instability

The system (107) admits a solution in the form of a carrier-wave (CW) background ([Bludov, Konotop, and Malomed, 2013](#))

$$\psi_j^{\text{CW}} = \rho e^{ikx - ibz + i(-1)^j \delta / 2}, \quad b = k^2 + \rho^2(\chi + \tilde{\chi}) - \cos \delta, \quad (111)$$

where k and ρ are constants. To study its linear stability, we use the standard substitution,

$$\psi_j = \psi_j^{\text{CW}} + \rho(\eta_j e^{-i(\beta z - \kappa x)} + \nu_j^* e^{i(\beta^* z - \kappa x)}) e^{ikx - ibz},$$

with $|\eta_j|, |\nu_j| \ll 1$. The linearization gives two branches $\beta_{1,2}(\kappa)$ of the stability eigenvalues:

$$\beta_1 = 2k\kappa \pm \kappa \sqrt{\kappa^2 + 2\rho^2(\chi + \tilde{\chi})}, \quad (112)$$

$$\beta_2 = 2k\kappa \pm \sqrt{(\kappa^2 + 2\cos \delta)[\kappa^2 + 2\cos \delta + 2\rho^2(\chi - \tilde{\chi})]}, \quad (113)$$

which feature several sources of modulational instability (MI). One source of MI stems from Eq. (112) and corresponds to

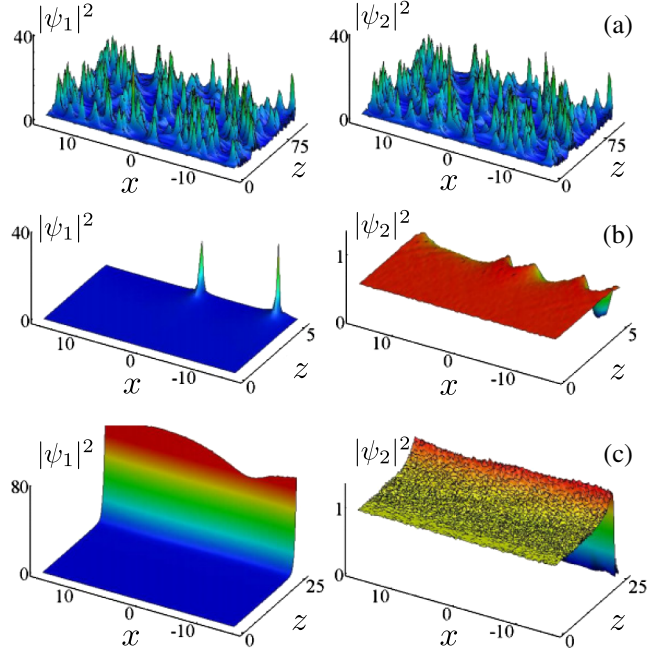


FIG. 25. Intensity evolution of the field components $|\psi_1|^2$ and $|\psi_2|^2$ (left and right columns) of the plane wave with (a) $\rho = 1.604$, $\chi = 0.5$, and $\tilde{\chi} = -1$; (b) $\rho = 0.76$, $\chi = -1.5$, and $\tilde{\chi} = 1$; and (c) $\rho = 0.98$, $\chi = 0.25$, and $\tilde{\chi} = 1$. For all panels, $k = 0$, $\delta = \pi/4$. Adapted from [Bludov, Konotop, and Malomed, 2013](#).

$$\chi + \tilde{\chi} < 0. \quad (114)$$

This is the MI due to long-wavelength excitations; it is not influenced by gain and loss and is present also in a conservative system of NLS equations without linear coupling. Another source of MI stems from Eq. (113):

$$\cos \delta < \max\{0, \rho^2(\chi - \tilde{\chi})\}, \quad (115)$$

and arises due to the linear coupling and is significantly affected by the gain and loss.

Different origins of the MI manifest themselves through different dynamical scenarios illustrated in Fig. 25. In Fig. 25(a), XPM nonlinearity is focusing, and we observe a “standard” scenario of MI which is very similar to its Hamiltonian counterpart where the power is distributed between the two waveguides. If the XPM is defocusing, but the condition (114) is satisfied, one observes relatively fast power transfer from the lossy waveguide to the active one, accompanied by fast growing peaks [Fig. 25(b)]. Such behavior is induced by the focusing SPM, and therefore is not significantly changed even when one passes from the domain of parameters (114) [Fig. 25(b)] to the one defined by Eq. (115) (not shown in Fig. 25). The third distinctive scenario of the MI takes place when both XPM and SPM are defocusing [Fig. 25(c)]. In this case, the MI occurs only due to the imbalance between the gain and loss, induced by the nonlinearity and resulting in nearly homogeneous growth (decay) of the field in the waveguide with gain (loss), respectively.

C. Bright solitons

When a CW background is unstable, a system can admit solitonic solutions. Using substitution (109), one can find a one-soliton exact solution which for $\tilde{\chi} = 0$ and $\chi = -2$ reads (Driben and Malomed, 2011b)

$$\psi_1^s = e^{i\delta - ibz} \frac{a}{\cosh(ax)}, \quad \psi_2^s = e^{-ibz} \frac{a}{\cosh(ax)}, \quad (116)$$

where the propagation constant $b = -a^2 - \cos \delta$, amplitude $a > 0$, and we set $\kappa = 1$. Equation (116) actually describes two types of solutions which can be termed *symmetric* ($0 < \delta < \pi/2$) and *antisymmetric* ($\pi/2 < \delta < \pi$) in accordance with the respective conservative limits $\delta = 0$ and $\delta = \pi$ (Wright, Stegeman, and Wabnitz, 1989). Bright solitons in the presence of SPM and XPM, i.e., for nonzero χ and $\tilde{\chi}$, were considered by Bludov *et al.* (2013).

Driben and Malomed (2011b) found that the symmetric soliton is stable for

$$a^2 < a_{\max}^2 = 2\sqrt{1 - \gamma^2}/3, \quad (117)$$

which agrees with the known result for the conservative case $\gamma = 0$ (Wright, Stegeman, and Wabnitz, 1989). At $\gamma > 0$, the condition (117) can be obtained from the linear-stability analysis (Alexeeva *et al.*, 2012) which starts with the substitution

$$\begin{aligned} \psi_1 &= \psi_1^s + e^{i\delta - ibz} (p + q)/\sqrt{2}, \\ \psi_2 &= \psi_2^s + e^{-ibz} (p - q)/\sqrt{2}, \end{aligned}$$

where $p = \text{Re}[p_1(x)e^{\mu z}] + i\text{Re}[p_2(x)e^{\mu z}]$, $q = \text{Re}[q_1(x)e^{\mu z}] + i\text{Re}[q_2(x)e^{\mu z}]$, $\mu = \nu - i\omega$, and $p_{1,2}$, $q_{1,2}$ are complex functions. The linearization with respect to p and q gives the eigenvalue problem

$$(L - \cos \delta)\mathbf{p} + 2\gamma J\mathbf{q} = \mu J\mathbf{p}, \quad (L + \cos \delta)\mathbf{q} = \mu J\mathbf{q}, \quad (118)$$

where $\mathbf{p} = (p_1, p_2)^T$, $\mathbf{q} = (q_1, q_2)^T$, and $J = -i\sigma_2$ [see Eq. (12)],

$$L = \begin{pmatrix} L_+ & 0 \\ 0 & L_- \end{pmatrix}, \quad L_{\pm} = -\frac{d^2}{dx^2} - b - (4 \pm 2)|\psi_2^s|^2.$$

In fact, the stability analysis reduces to the second equation in Eq. (118), since the first equation has a bounded solution \mathbf{p} for any bounded \mathbf{q} and $\mu \neq 0$. The obtained symplectic eigenvalue problem pertains to Hamiltonian evolution, and thus scenarios of evolution of instabilities are expected to be characteristic of conservative systems, despite the presence of gain and loss.

For the soliton (116), by introducing $X = ax$, $\lambda = \mu/a^2$, and $\eta = \cos \delta/a^2$, the second equation in Eq. (118) can be rewritten as

$$(L_- + \eta)(L_+ + \eta)q_1 = -\lambda^2 q_1, \quad (119)$$

where $L_{\pm} = -d^2/dX^2 + 1 - (4 \pm 2)\text{sech}^2 X$. For the symmetric soliton (116) with $\cos \delta > 0$, the lowest eigenvalue of L_- is

zero, and hence $L_- + \eta$ is positive definite and the inverse $(L_- + \eta)^{-1}$ exists. The symmetry of the eigenvalue problem (119) implies that if λ is an eigenvalue, so are $-\lambda$ and $\pm\lambda^*$. Hence stability of the solitons requires that the minimal eigenvalue expressed through the Rayleigh quotient

$$-\lambda^2 = \min\{\langle q_1, (L_+ + \eta)q_1 \rangle / \langle q_1, (L_- + \eta)^{-1}q_1 \rangle\}$$

must be positive. This occurs if the lowest eigenvalue of the operator $L_+ + \eta$, i.e., $\nu = -3 + \eta$, is positive. Recalling the definition of η one recovers Eq. (117).

Numerical studies of antisymmetric solitons show that all such solutions are unstable (Driben and Malomed, 2011b; Alexeeva *et al.*, 2012). However, lifetimes of the solitons with small amplitudes are exponentially long so for some purposes they can be regarded as stable. Dynamics of unstable solitons, either symmetric or antisymmetric, is divided into two asymptotic regimes: unbounded growth and formation of breathers. Unbounded growth typically occurs when amplitudes of unstable solitons are sufficiently large.

While bright solitons (116) correspond to the most fundamental localized excitations in nonlinear \mathcal{PT} -symmetric couplers, Li, Li, and Malomed (2014) demonstrated that the model also supports stable propagation of ‘‘supersolitons’’ (Novoa *et al.*, 2008), i.e., localized excitations consisting of many identical solitons which feature Newton-cradle-like dynamics. Dynamics and stability of a 2-soliton solution, i.e., the input $\psi_1(z=0) = e^{i\delta}\psi_2(z=0) = 2a/\cosh(ax)$, in a \mathcal{PT} -symmetric coupler, as well as switching of a 2-soliton initial pulse applied to only one of the arms were considered by Driben and Malomed (2012).

D. Breathers

In numerical studies of soliton stabilization at the exceptional point (see Sec. V.E.1), Driben and Malomed (2011a) found breathers featuring persistent irregular oscillations. In further studies of bright solitons Alexeeva *et al.* (2012) found two main scenarios of the development of instabilities: unbounded growth of a soliton amplitude and emergence of periodic breatherlike excitations. This naturally poses a question on the existence of breathers in \mathcal{PT} -symmetric coupled NLS equations (107). We address this question following Barashenkov *et al.* (2012), for the case of $\chi = -2$, $\tilde{\chi} = 0$, and $\kappa = 1$, in Eq. (107). First, let us observe that the global rotation

$$\begin{pmatrix} q_1 \\ q_2 \end{pmatrix} = U \begin{pmatrix} \psi_1 \\ \psi_2 \end{pmatrix}, \quad U = \frac{1}{2\cos \delta} \begin{pmatrix} e^{i\delta} & -1 \\ e^{-i\delta} & 1 \end{pmatrix}, \quad (120)$$

where δ is defined by Eq. (109), transforms Eq. (107) into a new system of two NLS-like equations without any linear dissipation and coupling. In the limit of small amplitudes $|q_{1,2}| \ll 1$, the new system decouples into two linear equations: $iq_{j,z} = -q_{j,xx} \pm \cos(\delta)q_j$, where $j = 1, 2$. Thus at small amplitudes one can look for a solution of the nonlinear problem in the form of a multiple-scale expansion

$$q_j = \sqrt{\epsilon} e^{(-1)^j i \cos(\delta)z} (A_j + \epsilon A_j^{(1)} + \dots), \quad (121)$$

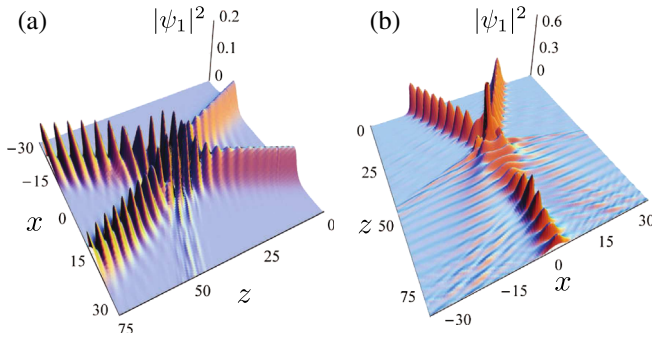


FIG. 26. (a) Collision of antisymmetric (initially left) and symmetric (initially right) solitons for $\gamma = 0.5$ and $a = 0.3$. A pair of breathers emerge from the collision. (b) Inelastic collision of two breathers for $\gamma = 0.3$ and $a = 0.3$. Adapted from Barashenkov *et al.*, 2012.

where $A_j^{(n)}$ depend on $Z = \epsilon z$, $X = \sqrt{\epsilon}x$, as well as the rest of the scale variables $Z_n = \epsilon^{n+1}z$ and $X_n = \epsilon^{n+1/2}x$ with $n = 1, 2, \dots$. Substituting Eq. (121) into the nonlinear equations for $q_{1,2}$, collecting all terms with the same power of ϵ , and eliminating the secular terms, one obtains

$$iA_{j,Z} + A_{j,XX} + 2(|A_j|^2 + 2|A_{3-j}|^2)A_j = 0, \quad (122)$$

where $j = 1, 2$. This system has two obvious solutions: $(A_1, 0)$ and $(0, A_2)$ which in terms of the original functions $\psi_{1,2}$ yield antisymmetric and symmetric bright solitons. The system (122) also admits vector solitons with $A_1 = A_2$. Taking the latter solution and inverting rotation (120), one obtains a breather

$$\begin{pmatrix} \psi_1 \\ \psi_2 \end{pmatrix} = \frac{2a \exp(ia^2z)}{\sqrt{3} \cosh(ax)} \begin{pmatrix} \cos[\cos(\delta)z] \\ i \sin[\delta + \cos(\delta)z] \end{pmatrix}, \quad (123)$$

where the amplitude a must be small enough ($a \sim \epsilon^{1/2} \ll 1$). The frequency of the breather in the leading order is determined by $\cos(\delta) = \sqrt{1 - \gamma^2}$.

Linear-stability analysis and numerical simulations indicate that breathers are stable. Moreover, breathers appear to be rather common objects which are excited when unstable solitons break up (Alexeeva *et al.*, 2012), after interaction of symmetric and antisymmetric solitons [Fig. 26(a)], and after interaction of a soliton with a defect (Bludov *et al.*, 2014). Numerical studies of interaction of breathers show appreciable inelastic effects as illustrated in Fig. 26(b) (Barashenkov *et al.*, 2012; Rysaeva, Suchkov, and Dmitriev, 2014).

E. Solitons in couplers with varying parameters

1. Stabilization of a soliton at an exceptional point

The exceptional point of the linearized ($\chi = \tilde{\chi} = 0$) system (107) corresponds to $\gamma_{\mathcal{PT}} = \kappa$. It is evident from the substitution (109) that at this point symmetric and antisymmetric solitons merge into the same solution with $\psi_2 = i\psi_1$ which appears to be unstable. However, by introducing simultaneous periodic modulations of the gain, loss, and coupling, i.e., by considering the model

$$\begin{aligned} i\psi_{1,z} &= -\psi_{1,xx} + f(z)(\psi_2 + i\psi_1) + \chi|\psi_1|^2\psi_1, \\ i\psi_{2,z} &= -\psi_{2,xx} + f(z)(\psi_1 - i\psi_2) + \chi|\psi_2|^2\psi_2, \end{aligned} \quad (124)$$

where $f(z)$ describes the modulations, the soliton can be stabilized. This fact was established by Driben and Malomed (2011a) who studied numerically the case $f(z) = f_0 \sin(2\pi z/L)$, where f_0 and L are the amplitude and period of the modulation. It was found that the soliton can indeed be stabilized and can even become an attractor with a significantly broad basin.

The existence of stable solitons at the exceptional point was also reported by Li and Xie (2014) for the case where the coupling constant is modulated periodically whereas the dissipation is constant (or vice versa).

2. Interaction of a soliton with an exceptional point

By modulating the coupling constant one can implement a situation where the coupled waveguides have parameters corresponding to the exceptional point or to the broken \mathcal{PT} symmetry only at a single point or on a finite segment of the propagation distance. Such a localized modulation of the coupling can be referred to as a *coupling defect*. Following Bludov *et al.* (2014), now we consider the interaction of a bright vector soliton with a coupling defect of the form $\kappa(z) = \kappa_0 - (\kappa_0 - \kappa_{\min})e^{-z^2/\ell^2}$, where κ_{\min} and κ_0 are the minimum and maximum of the coupling, and ℓ is a defect-length parameter. We consider the system (107) in the absence of XPM ($\tilde{\chi} = 0$), set $\chi = -1$, and take $\gamma = 1$ without loss of generality. The introduced defect is centered at $z = 0$, where the strength of coupling $\kappa(0) = \kappa_{\min}$ is the weakest. Thus when $\kappa_{\min} = 1$, the exceptional point is achieved at $z = 0$. Far from the defect the NLS equations are homogeneous, and thus one can consider incidence of a soliton initially given by Eq. (116) on the defect. Numerical simulations revealed various scenarios visualized in Fig. 27.

If the defect length ℓ exceeds some critical value $\ell_{\text{cr}}(\kappa_{\min})$ (which depends on κ_{\min}), then the soliton energy grows without bound after interaction with the defect, i.e., the soliton cannot “overcome” the defect. If ℓ is below $\ell_{\text{cr}}(\kappa_{\min})$, then

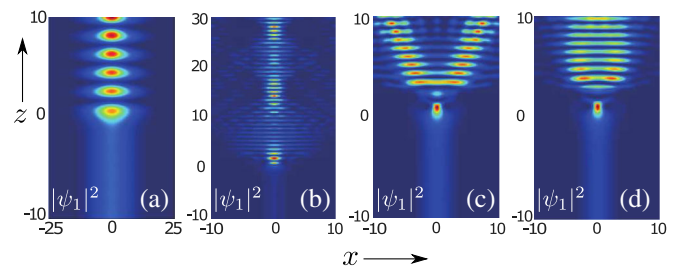


FIG. 27. (a) Symmetric soliton passing the defect at $\kappa_0 = 2$, $\ell = 1$ (in this case $\ell_{\text{cr}} \approx 7$). The interaction of an antisymmetric soliton with the defect at $\kappa_0 = 4$, (b) $\ell = 1.1$, (c) $\ell = 2.2$, and (d) $\ell = 2.7$ (in this case $\ell_{\text{cr}} \approx 3.4$). In (b) broadening is repeated with period ≈ 10 while the breather period ≈ 0.8 . In all panels the initial conditions are taken in the form (116) with $a = 1/\sqrt{2}$, the defect is centered at $z = 0$, and $\kappa_{\min} = 1$. Only the first component $|\psi_1|^2$ is shown; the behavior of $|\psi_2|^2$ is similar. Adapted from Bludov *et al.*, 2014.

after passing the defect a symmetric soliton is transformed into a breather propagating along the homogeneous coupler [Fig. 27(a)]. When an antisymmetric soliton interacts with the coupling defect, possible scenarios include the emergence of (quasi)breathers with periodic broadening of the shape [Fig. 27(b)], splitting of a soliton into two outgoing breathers [Fig. 27(c)], as well as splitting of the soliton into two breathers which after some distance start moving toward each other [Fig. 27(d)].

3. Soliton switching by a \mathcal{PT} -symmetric defect

Now we turn to propagation of a soliton in a coupler having constant coupling but localized gain-loss defects. The problem is modeled by

$$\begin{aligned} i\psi_{1,z} &= -\psi_{1,xx} - \psi_2 - i\gamma_1(z)\psi_1 - |\psi_1|^2\psi_1, \\ i\psi_{2,z} &= -\psi_{2,xx} - \psi_1 - i\gamma_2(z)\psi_2 - |\psi_2|^2\psi_2, \end{aligned} \quad (125)$$

where the coefficients $\gamma_1(z)$ and $\gamma_2(z)$ are arbitrary so far.

Soliton switching can be described by the Lagrangian approach [see Pare and Florjanczyk (1990) for the conservative coupler]. This approach relies on the ansatz $\psi_j = A_j e^{i\phi_j} / \cosh(ax)$ [cf. Eqs. (116)] where amplitudes $A_{1,2}$ and phases $\phi_{1,2}$ are considered as slow functions of the propagation distance z . The Lagrangian equations are (Abdullaev, Konotop *et al.*, 2011)

$$F_z = -(\gamma_1 - \gamma_2)(1 - F^2) + 2\sqrt{1 - F^2} \sin(\phi), \quad (126a)$$

$$\phi_z = \delta F Q - 2F \cos(\phi) / \sqrt{1 - F^2}, \quad (126b)$$

$$Q_z = -\gamma_1 Q(1 + F) - \gamma_2 Q(1 - F). \quad (126c)$$

Here $F = (P_1 - P_2) / (P_1 + P_2)$ is the relative distribution of the power [$P_{1,2}(z) = \int_{-\infty}^{\infty} |\psi_{1,2}|^2 dx$] between the two arms of the coupler, $Q(z) = [P_1(z) + P_2(z)] / [P_1(0) + P_2(0)]$ is the total power normalized to the input one, $\phi = \phi_1 - \phi_2$ is the relative phase, and $\delta = a[P_1(0) + P_2(0)]/3$. Equations (126) are similar to those describing a coupler operating in the stationary regime (Abdullaev, Konotop, and Shchesnovich, 2011). Thus one can expect various types of dissipative dynamics of a soliton, reproducing light propagation in the x -independent dimer model. One of such effects, the switching of a soliton by a dissipative defect localized on the distance interval $[z_a, z_b]$, is illustrated in Fig. 28(a). The input soliton is mainly concentrated in the dissipative arm ($P_1 \gg P_2$), but the output is concentrated in the active arm, resembling unidirectional propagation described in Sec. IV.D.2. By adding a new defect with inverted gain and loss the switching can be repeated [see the inset of Fig. 28(a)].

Note that \mathcal{PT} symmetry is not necessary for switching since it can be achieved even in a purely dissipative coupler [Fig. 28(b)]. Moreover, decay of the total power can be strongly suppressed by increasing the strength of the dissipative defect. This phenomena can be termed a *macroscopic Zeno effect* (Shchesnovich and Konotop, 2010) which is a macroscopic (mean-field) manifestation of the well-known quantum Zeno effect (Facchi and Pascazio, 2008; Daley,

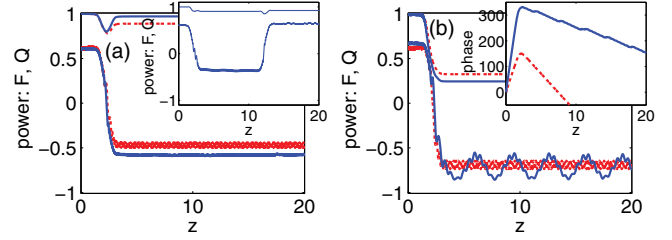


FIG. 28. (a) Soliton switching between arms by the \mathcal{PT} -symmetric segment $\gamma_2(z) = -\gamma_1(z) = \Gamma(\arctan[5(z - z_a)] - \arctan[5(z - z_b)])^2$ with $\Gamma = 0.065$, $z_a = 1.5$, and $z_b = 3.0$. In the inset of (a) a gain-loss segment is added at $z \sim 10$. The parameters were engineered in order to keep $Q(z) \approx 1$. (b) The same as in (a) but with the only dissipative segment included in the first arm [$\gamma_2(z) \equiv 0$] and with $\Gamma = 0.135$. The inset shows the relative phase. In both panels $\psi_1(0) = 20\text{sech}(10\sqrt{2}x)$ and $\psi_2(0) = 5\text{sech}(5x/\sqrt{2})$ [i.e., $F(0) = 3/5$]. Adapted from Abdullaev, Konotop *et al.*, 2011.

Barontini *et al.* (2013). A macroscopic Zeno effect in a BEC subject to an ionizing electronic beam was experimentally observed by Barontini *et al.* (2013).

F. Rogue waves

In the regime of MI, the system (107) supports another type of localized excitation known as a rogue wave (Kharif, Pelinovsky, and Slunyaev, 2009). Here we are interested in deterministic rogue waves, which are nonlinear excitations propagating on a nonzero background and localized in space and time. The simplest rogue-wave solution is the Peregrine soliton of the NLS equation (Peregrine, 1983). In order to construct a counterpart of the Peregrine soliton in the \mathcal{PT} -symmetric coupled NLS equations (107), one can employ the reduction (109) and (110). Then if the condition of the MI (114) is satisfied, the exact Peregrine soliton of Eqs. (107) reads (Bludov *et al.*, 2013)

$$\begin{aligned} \psi_j(x, z) &= \rho e^{(-1)^j i\delta/2 - ibz} \\ &\times \left[1 - \frac{4[1 - 2i(\chi + \tilde{\chi})\rho^2 z]}{1 - 2(\chi + \tilde{\chi})\rho^2 x^2 + 4(\chi + \tilde{\chi})^2 \rho^4 z^2} \right]. \end{aligned} \quad (127)$$

When $|z| \rightarrow \infty$ or $|x| \rightarrow \infty$, this solution approaches the constant background given by Eq. (111) with $k = 0$.

The analytical solution (127) is illustrated in Fig. 29. Direct numerical simulations on the dynamics of Peregrine solitons subject to different initial conditions were performed by Bludov *et al.* (2013). In a generic situation due to the instability an emergence of a single peak follows by the development of the modulational instability, reflecting different scenarios corresponding to different relations among the nonlinear parameters described in Sec. V.B. An example of such evolution is shown in Figs. 29(b) and 29(c).

The system (107) also admits more complex rogue-wave solutions called higher-order rogue waves. They can be readily obtained from higher-order rogue waves of the NLS equation through the reduction (109) and (110) (Akhmediev, Ankiewicz, and Soto-Crespo, 2009; Dubard *et al.*, 2010; Guo,

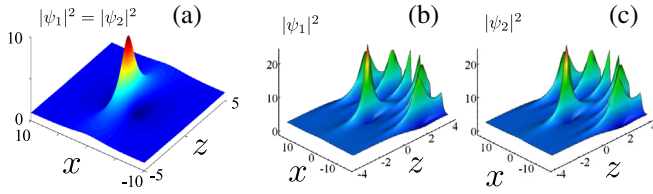


FIG. 29. (a) Vector Peregrine soliton (127) with $\rho = 1, \chi = 0.5$, and $\tilde{\chi} = -1$. (b), (c) Intensities of the Peregrine solitons for $\rho = 1.604, \chi = 0.5, \tilde{\chi} = -1$, and $\delta = \pi/4$, initiated with slightly perturbed initial conditions at $z = z_{\text{ini}} = -4$. The shown scenario of the evolution corresponds to the scenario of MI shown in Fig. 25(a). Adapted from Bludov *et al.*, 2013.

Ling, and Liu, 2012; Ohta and Yang, 2012; Dai and Huang, 2014).

G. Dark solitons

Dark solitons in coupled \mathcal{PT} -symmetric NLS equations can exist if the CW background is stable (Bludov, Konotop, and Malomed, 2013). Under substitution (109) we again obtain Eq. (110), but now we assume $\chi + \tilde{\chi} > 0$. Dark-soliton solutions of the NLS equation are well known (Tsuzuki, 1971; Faddeev and Takhtadjan, 1987). In the particular case of zero velocity, the respective soliton (also known as a black soliton) reads $\psi^{\text{ds}}(x, z) = u_0(x)e^{-ibz}$, where

$$u_0(x) = \rho \tanh[\rho \sqrt{(\tilde{\chi} + \chi)/2x}]. \quad (128)$$

As in the case of bright solitons (see Sec. V.C), the linear stability of a slightly perturbed soliton (with perturbations $\propto e^{i\lambda z}$) is reduced to two separate eigenvalue problems (Bludov, Konotop, and Malomed, 2013): $L_{1,2}\psi = \Lambda_{1,2}\psi$, where $\Lambda = \lambda^2$, and the operators are defined by

$$L_1 = (L_+ - L)(L_- + \cos\delta), \quad L_2 = (L_- - \cos\delta)(L_+ + L),$$

with $L \equiv 2\chi u_0^2 - \cos\delta$ and

$$L_{\pm} = -\frac{d^2}{dx^2} - b + [(2 \pm 1)\chi_1 + \chi]u_0^2.$$

The dark soliton is linearly stable if all eigenvalues $\Lambda_{1,2}$ are real and positive. The eigenvalue problem for L_2 is the well-studied stability problem for the black soliton in the conservative defocusing medium. It is known that $L_+ + L$ is positive definite, and $L_- - \cos\delta$ has only one negative eigenvalue and one zero eigenvalue (Barashenkov, 1996). It is also known that the minimal eigenvalue of L_2 is positive (Chen, 1996). Thus, L_2 does not give instability, and the analysis is reduced to the study of operator L_1 .

The linear stability of \mathcal{PT} -symmetric dark solitons was studied by Bludov, Konotop, and Malomed (2013). Stable dark solitons are robust and their collision is almost elastic. If the system has a weak imbalance between gain γ_1 and loss γ_2 in the two waveguides, dark solitons can still survive for a long time.

H. Generalized \mathcal{PT} -symmetric coupled NLS equations

These studies do not exhaust rich dynamics governed by coupled \mathcal{PT} -symmetric NLS equations, including, in particular, resonant mode interactions (Wasak *et al.*, 2015). Furthermore, generalizations of the model itself are possible, which are considered in this section.

1. Circular arrays

As in Sec. IV where a dimer model was generalized to \mathcal{PT} -symmetric oligomers, two coupled \mathcal{PT} -symmetric NLS equations can be generalized to an array of N waveguides. Barashenkov, Baker, and Alexeeva (2013) studied NLS equations assembled in open and closed \mathcal{PT} -symmetric arrays with alternating and clustered gain-loss configurations (see Sec. IV.B.1). Here we consider the alternating closed (necklace) configuration, modeled by

$$i\psi_{n,z} + \psi_{n,xx} + 2|\psi_n|^2\psi_n + \psi_{n-1} + \psi_{n+1} = 2i(-1)^n\gamma\psi_n, \quad (129)$$

with $n = 1, \dots, 2N$, under boundary conditions $\psi_{2N+1} = \psi_1$ and $\psi_{2N} = \psi_0$. The \mathcal{PT} -symmetry-breaking threshold of this system is not affected by the dispersive terms $\psi_{n,xx}$. Therefore the linear waves are stable if $\gamma < \gamma_{\mathcal{PT}}^{(an)}$ in Eq. (77). [Note that in a system with alternating dispersion, i.e., with alternating signs in front of the second derivative, \mathcal{PT} symmetry is always broken (Gupta and Sarma, 2014b).]

If \mathcal{PT} symmetry is unbroken, a solitonic solution can be searched in the form $\psi_n = e^{i\phi_n + ia^2z} \text{sech}(ax)$, where phases ϕ_n are determined from

$$e^{-i\phi_{n-1}} + e^{i\phi_n} = 2i(-1)^n\gamma, \quad \phi_n = \phi_{n+1} - \phi_n.$$

These equations yield $\phi_n = (-1)^n \arcsin \gamma + \pi n + \phi$, where ϕ is a constant phase (appearing due to the phase invariance of the system).

2. Multidimensional NLS equations and wave collapse

Another extension of the \mathcal{PT} -symmetric coupler model is coupled \mathcal{PT} -symmetric multidimensional NLS equations with more general nonlinearities, i.e.,

$$\begin{aligned} i\psi_{1,z} &= -\nabla^2\psi_1 - \kappa\psi_2 - F_1(|\psi_1|, |\psi_2|)\psi_1 + i\gamma\psi_1, \\ i\psi_{2,z} &= -\nabla^2\psi_2 - \kappa\psi_1 - F_2(|\psi_1|, |\psi_2|)\psi_2 - i\gamma\psi_2, \end{aligned} \quad (130)$$

where $x \in \mathbb{R}^D$, $\nabla = (\partial/\partial x_1, \dots, \partial/\partial x_D)$, and $F_j(\cdot, \cdot)$ describe the nonlinearities.

Starting with the case of cubic nonlinearities $F_1 = \chi|\psi_1|^2 + \tilde{\chi}|\psi_2|^2$ and $F_2 = \tilde{\chi}|\psi_2|^2 + \chi|\psi_1|^2$, we recall that for focusing SPM and XPM ($\chi, \tilde{\chi} \geq 0$), solutions of a single NLS equation with $D \geq 2$ suffer finite-time blowup for a wide range of initial conditions (Sulem and Sulem, 2000), even in the presence of linear dissipation (Tsutsumi, 1984). For the \mathcal{PT} -symmetric system (130) with critical dimensionality $D = 2$, no exact result on the global existence or blowup of the solution is available for general coefficients κ, γ, χ , and $\tilde{\chi}$. However, a

sufficient condition for global existence can be formulated in the particular case of $\gamma < \kappa$ and $\chi = \tilde{\chi}$. In this case, extending the arguments presented in Sec. V.A on the 2D case, one can show that there exists *a priori* upper bound $S_{\max} = \sup_z S_0(z) < \infty$ for the Stokes component $S_0(z) = \|\psi_1\|_{L^2(\mathbb{R}^2)}^2 + \|\psi_2\|_{L^2(\mathbb{R}^2)}^2$. The value of S_{\max} depends on the initial conditions. Using this fact, Pelinovsky, Zezyulin, and Konotop (2015) showed that if $\chi = \tilde{\chi} = 1$ and the initial conditions satisfy the requirement $S_{\max} < \frac{1}{2}\|R\|_{L^2}^2$, then a global solution in $H^1(\mathbb{R}^2) \times H^1(\mathbb{R}^2)$ does exist. Here $R = R(x)$ is the (unstable) Townes soliton (Chiao, Garmire, and Townes, 1964), i.e., the localized positive solution of the 2D stationary problem $\nabla^2 R - R + R^3 = 0$.

The study of 2D bright solitons within the framework of Eq. (130) with focusing cubic nonlinearity and defocusing quintic nonlinearity, i.e., $F_j = |\psi_j|^2 - |\psi_j|^4$ ($j = 1, 2$), was reported by Burlak and Malomed (2013). Using the substitution (109), the system is reduced to a single 2D NLS equation whose radially symmetric solutions provide the shapes for \mathcal{PT} -symmetric solitons. It was found that the 2D solitons can be dynamically stable for $\gamma < \gamma_C$, where γ_C is some critical value which depends on the coupling strength. Solitons in a closed array of three 2D waveguides with the cubic-quintic nonlinearity were studied by Feijoo, Zezyulin, and Konotop (2015).

In the supercritical case $D \geq 3$, the \mathcal{PT} -symmetric coupled NLS equations with cubic nonlinearity may undergo a finite-time blowup, whose sufficient conditions were established by Dias *et al.* (2014). Numerical studies reveal that the model features different evolution scenarios, including decay of the initial pulses, growth of the solution in the active or lossy component, or both.

I. Localized modes in \mathcal{CPT} -symmetric BECs

Following Kartashov, Konotop, and Zezyulin (2014) we now turn to the NLS equations with gain and loss and linear SO-type coupling discussed in Sec. III.H. The two-body interactions can be approximated by almost equal nonlinear coefficients [in an experiment the difference was less than 1% (Lin, Jiménez-García, and Spielman, 2011)]. This leads to the coupled GPEs $i\Psi_t = H\Psi - \chi(\Psi^\dagger\Psi)\Psi$, where the linear Hamiltonian H is given by Eq. (56).

Stationary modes $\Psi = e^{-i\mu t}\psi(x)$ can bifurcate from the linear eigenstates. From properties of the underlying linear system, one can identify two fundamental (one-hump) nonlinear modes, two two-hump modes, etc. The SO coupling induces nonzero currents

$$j_{\uparrow\downarrow} = \frac{1}{2i} \left(\Psi_{\uparrow\downarrow}^* \frac{\partial \Psi_{\uparrow\downarrow}}{\partial x} - \frac{\partial \Psi_{\uparrow\downarrow}^*}{\partial x} \Psi_{\uparrow\downarrow} \right),$$

whose directions in the $|\uparrow\rangle$ and $|\downarrow\rangle$ components coincide. At the same time, directions of the currents in the two fundamental modes are opposite (the same being true for the two-hump modes, three-hump modes, etc). Families of nonlinear modes (see Fig. 30) consist of alternating intervals of stable and unstable segments, and stable nonlinear modes exist for both attractive and repulsive nonlinearities. Moreover, stable

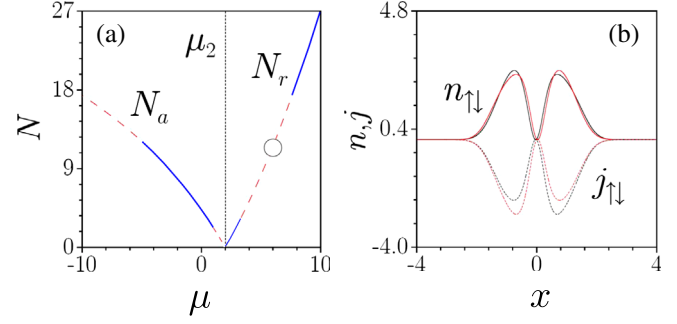


FIG. 30. (a) Families of nonlinear modes of a SO BEC in a parabolic trap $V(x) = \nu^2 x^2/2$ bifurcating from the linear mode μ_2 (see Fig. 13) for $\kappa = 1$, $\nu = 2$, $\gamma = 0.2$, and $\omega = 0.5$. Solid blue (dashed red) curves correspond to stable (unstable) modes. Here $N = \int_{-\infty}^{\infty} \Psi^\dagger \Psi dx$, and curves with labels N_a and N_r correspond to attractive and repulsive nonlinearities, respectively. The circle in (a) corresponds to a two-hump nonlinear mode shown in (b). Here $n_{\uparrow\downarrow} = |\psi_{\uparrow\downarrow}|^2$. Adapted from Kartashov, Konotop, and Zezyulin, 2014.

nonlinear modes exist even if the \mathcal{CPT} symmetry of the linear problem is broken. \mathcal{CPT} symmetry (specifically, the property $\mathcal{CPT}\sigma_3 = -\sigma_3\mathcal{CPT}$) implies that the nonlinear modes have zero (pseudo)magnetization $M = \int_{-\infty}^{\infty} \Psi^\dagger \sigma_3 \Psi dx = 0$.

VI. NONLINEAR MODES IN COMPLEX POTENTIALS

In this section, we consider nonlinear modes supported by complex potentials $U(x)$ in the NLS equation (39). More specifically, we focus on potentials which are either localized $U(x) \rightarrow 0$ or unbounded $U(x) \rightarrow \infty$ as $x \rightarrow \pm\infty$. Stationary nonlinear modes in this equation are of the form $\Psi(x, t) = \psi(x)e^{i\mu t}$, where μ is a real propagation parameter and $\psi(x)$ solves

$$\psi_{xx} - U(x)\psi + g|\psi|^2\psi = \mu\psi, \quad (131)$$

subject to the zero boundary conditions $\lim_{|x| \rightarrow \infty} \psi = 0$.

If the underlying linear equation, i.e., Eq. (131) with $g = 0$, admits a guided mode with a real propagation constant, then a question of interest is the possibility for nonlinear modes to bifurcate from that mode.

A. Localized potentials

1. Exact solutions

Starting with localized potentials, we note that linear spectra of some of them are available analytically (Cooper, Khare, and Sukhatme, 1995; Znojil, 2000). Moreover, many of such potentials admit exact expressions for nonlinear modes. The first known example corresponds to a \mathcal{PT} -symmetric Scarff II potential

$$U(x) = -V_1 \text{sech}^2 x - iV_2 \text{sech} x \tanh x, \quad (132)$$

with $V_1 > 0$ and $V_2 \neq 0$, which is a complexification of the real Scarff II potential (Cooper, Khare, and Sukhatme, 1995). The spectrum of Eq. (132) was found analytically by Ahmed (2001a, 2001b) through a transformation of the corresponding

Schrödinger equation to the Gauss hypergeometric equation and by Bagchi and Quesne (2000, 2002) using complex Lie algebras. If $|V_2| < V_{\text{cr}} = V_1 + 1/4$, then the discrete spectrum consists of a sequence of real eigenvalues. At $|V_2| = V_{\text{cr}}$ the real eigenvalues merge pairwise and split into complex-conjugate pairs as $|V_2|$ exceeds V_{cr} , i.e., \mathcal{PT} symmetry becomes broken.

The nonlinear model (131) and (132) admits an exact particular solution for the focusing ($g > 0$) and defocusing ($g < 0$) nonlinearities at $\mu = 1$ (Muslimani *et al.*, 2008a; Shi *et al.*, 2011):

$$\psi = \sqrt{\frac{V_1 - (V_2/3)^2 - 2}{g}} \frac{\exp[i(V_2/3) \arctan(\sinh x)]}{\cosh x}. \quad (133)$$

In Eq. (133) it is assumed that parameters $V_{1,2}$ and g are chosen so that the expression under the radical is positive.

The nonlinear mode (133) is \mathcal{PT} symmetric, i.e., $\psi(x) = \psi^*(-x)$. This mode belongs to a continuous family of localized \mathcal{PT} -symmetric modes (fundamental solitons) which can be obtained numerically by varying the propagation constant μ at fixed model parameters V_1 , V_2 , and g . A numerical study of fundamental and multipole solitons and their stability in the potential (132) was performed for focusing (Muslimani *et al.*, 2008a) and defocusing (Shi *et al.*, 2011; Chen, Hu, and Qi, 2014) Kerr nonlinearities, as well as for nonlocal nonlinearity (Shi *et al.*, 2012).

A \mathcal{PT} -symmetric extension of the Rosen-Morse II potential $U(x) = -V_1 \text{sech}^2 x + iV_2 \tanh x$ is another potential which admits explicit expressions for particular nonlinear modes (Midya and Roychoudhury, 2013). Note that in this case only the real part of the potential vanishes as $x \rightarrow \pm\infty$, while the imaginary part approaches constant values. The linear spectrum of this Rosen-Morse II potential was obtained by Lévai and Magyar (2009). Explicit expressions for nonlinear modes in a more sophisticated potential $U(x) = -V_1 \text{sech}^2 x + V_2^2 \text{sech}^4 x + 4iV_2 \text{sech}^2 x \tanh x$ were reported by Muslimani *et al.* (2008b) and generalized by Khare, Al-Marzoug, and Bahlouli (2012) and Midya and Roychoudhury (2014). More generally, potentials allowing for exact solutions can be constructed systematically using the “inverse engineering” approach (Abdullaev *et al.*, 2010) which consists of assuming the given field pattern and finding a potential shape sustaining such a pattern, or using the similarity transformation (Serkin and Hasegawa, 2000; Pérez-García, Torres, and Konotop, 2006) reducing a nonautonomous NLS equation [with a potential $U(x, t)$ and time-dependent coefficients] to the autonomous NLS equation (39) (Chen, Dai, and Wang, 2014; Dai, Wang, and Zhou, 2014; Dai and Wang, 2014a, 2014c; Xu and Dai, 2014).

Exact particular solutions are also available in multidimensional \mathcal{PT} -symmetric potentials (see also Sec. IX), including 2D and 3D versions of Scarff and Rosen-Morse potentials (Dai, Wang, and Zhou, 2014; Dai and Wang, 2014b, 2014c; Hu and Chen, 2014; Wang, Dai, and Wang, 2014a, 2014b).

One more example admitting explicit nonlinear solutions is \mathcal{PT} deformation of a parabolic potential (Midya, 2015; Yan, Wen, and Konotop, 2015)

$$U(x) = \Omega^2 x^2 - V_0 e^{-2x^2} + i\gamma x e^{-x^2}. \quad (134)$$

A numerical study of the linear spectrum for the \mathcal{PT} -symmetric Gaussian potential [which corresponds to $\Omega = 0$ in Eq. (134)] was performed by Ahmed (2001a), and nonlinear modes were computed numerically by Hu *et al.* (2011) and Jisha, Devassy *et al.* (2014). More complex exactly solvable \mathcal{PT} extensions of the parabolic potential have been discussed by Yan, Xiong, and Liu (2010), Yan (2013), and Yan, Wen, and Konotop (2015).

Kartashov, Malomed, and Torner (2014) demonstrated that stable solitons in the *defocusing* nonlinearity can be found in the absence of any real symmetric part, i.e., when $U(x) = i\gamma x e^{-x^2}$, provided that the nonlinearity is spatially modulated, and its profile grows rapidly enough as $x \rightarrow \pm\infty$, e.g., $g = g(x) = -(g_1 + g_2 x^2) e^{x^2}$. The existence of bright solitons in such self-defocusing nonlinearity can be explained by “nonlinearizability” of the respective NLS equation at the soliton tails. For $\gamma = 0$ the exact soliton solution can be found in the analytical form.

Exact solutions have been also found for some double-well (Wen and Yan, 2015; Yan, Wen, and Konotop, 2015) and multiwell (Yan, Wen, and Hang, 2015) \mathcal{PT} -symmetric potentials.

2. Scattering on a \mathcal{PT} -symmetric defect

A localized \mathcal{PT} -symmetric potential can be viewed as a defect which scatters an incident wave. For certain cases, including the \mathcal{PT} -symmetric Scarff II potential (132), the scattering data for the linear problem can be found in an explicit form (Lévai, Cannata, and Ventura, 2001; Cannata, Dedonder, and Ventura, 2007). In the nonlinear setting, one can consider incidence of a soliton on a \mathcal{PT} -symmetric defect. The numerical study of soliton scattering by Eq. (132) reveals several dynamical scenarios (Nazari, Nazari, and Moravvej-Farshi, 2012; Karjanto *et al.*, 2015). They include swinging and self-trapping of the normally incident soliton, as well as nonreciprocity of left and right incidences. Asymmetric evolution of two simultaneously launched solitons on a

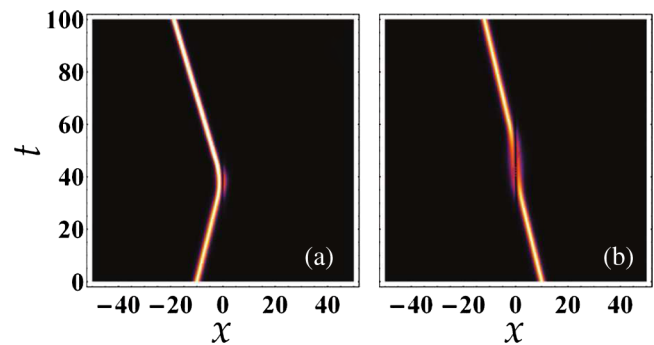


FIG. 31. Scattering of a soliton by the potential $U(x) = -V_0^2 \text{sech}(V_0 x) + iW_0 x \text{sech}(V_0 x)$ with $V_0 = W_0 = -2$. (a) Almost perfect reflection of the soliton moving from the left. (b) Almost perfect transmission of the soliton moving from the right. In both cases the velocity of the incident soliton is $|v_0| = 0.25$, and the initial position is at $|x_0| = 10$. From Al Khawaja *et al.*, 2013.

\mathcal{PT} -symmetric defect was reported by Nazari *et al.* (2013). It was also found by Al Khawaja *et al.* (2013) and Al-Marzoug (2014) that in a certain range of the parameters of the potential and the incident soliton, one can observe a unidirectional soliton flow, i.e., the soliton moving from the left to the right is almost perfectly reflected, while the soliton moving in the opposite direction is almost perfectly transmitted (see Fig. 31). Unidirectional transmission, amplification, and destruction of gap solitons (supported by a real periodic potential) on a \mathcal{PT} -symmetric defect was also observed by Abdullaev, Brazhnyi, and Salerno (2013).

B. Parabolic potential

Now we turn to stationary nonlinear modes of Eq. (131) with a parabolic \mathcal{PT} -symmetric potential (8). Linear eigenmodes of this potential are given by $\tilde{\mu}_n = -(2n + 1)$, $n = 0, 1, \dots$, and the eigenfunctions $\tilde{\psi}_n(x)$ can be expressed in terms of Hermite polynomials [see Eqs. (9)]. We first look for *small-amplitude* nonlinear modes bifurcating from the linear eigenstates $\tilde{\psi}_n(x)$. In this case, the nonlinear modes can be constructed by an asymptotic expansion

$$\begin{aligned} \psi_n(x) &= \varepsilon \tilde{\psi}_n + \varepsilon^3 \psi_n^{(3)} + o(\varepsilon^3), \\ \mu &= \tilde{\mu}_n + g\varepsilon^2 \mu_n^{(2)} + o(\varepsilon^2), \end{aligned} \quad (135)$$

where $\varepsilon \ll 1$ is a small real parameter. Substituting this expansion into Eq. (131) and collecting terms of order ε^3 one obtains an equation for $\psi_n^{(3)}$:

$$(\psi_n^{(3)})_{xx} - \tilde{\mu}_n \psi_n^{(3)} - (x - i\alpha)^2 \psi_n^{(3)} = g\mu_n^{(2)} \tilde{\psi}_n - g|\tilde{\psi}_n|^2 \tilde{\psi}_n.$$

The solvability condition (Fredholm alternative) for this equation requires its right-hand side to be orthogonal to the kernel of the adjoint operator in the left-hand side, i.e., orthogonal to $\tilde{\psi}_n^*$. This allows one to compute $\mu_n^{(2)}$ as (Zezyulin and Konotop, 2012a; Yang, 2014b)

$$\mu_n^{(2)} = \frac{\int_{-\infty}^{\infty} \tilde{\psi}_n^3(x) \tilde{\psi}_n^*(x) dx}{\int_{-\infty}^{\infty} \tilde{\psi}_n^2(x) dx}. \quad (136)$$

For expansions (135) to be meaningful, $\mu_n^{(2)}$ must be real (a similar constraint also arises for discrete systems in Sec. IV.C.3.a). When $\alpha = 0$, the eigenfunctions $\tilde{\psi}_n(x)$ are real valued, hence the coefficients $\mu_n^{(2)}$ are positive for all n . When $\alpha \neq 0$, $\tilde{\psi}_n(x)$ are complex valued. However, parity of their real and imaginary parts ensures that the coefficient $\mu_n^{(2)}$ is still real for any n and α . Thus for each n one can identify a continuous family of nonlinear modes $\psi_n(x)$ bifurcating from the n th linear eigenstate $\tilde{\psi}_n(x)$.

Further analysis of these nonlinear modes can be performed numerically. The continuous families can be visualized as curves $gP_n(\mu)$, where $P_n = \int_{-\infty}^{\infty} |\psi_n|^2 dx$ is the power of the n th mode; see Fig. 32. Each point above (below) the axis $gP = 0$ corresponds to a nonlinear mode under focusing (defocusing) nonlinearity. A striking difference between the two panels in Fig. 32 is *coalescence* of nonlinear modes bifurcating from different linear eigenstates, which does not occur in the conservative parabolic potential ($\alpha = 0$) (Kivshar,

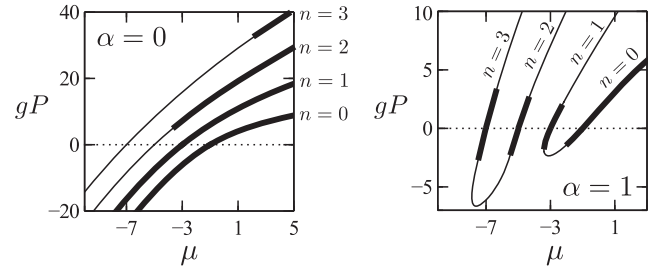


FIG. 32. Families of nonlinear modes in the conservative ($\alpha = 0$) and \mathcal{PT} -symmetric ($\alpha = 1$) parabolic potential (8) and focusing ($g = 1$) and defocusing ($g = -1$) nonlinearities. Bold segments on the power curves correspond to stable nonlinear modes. Adapted from Zezyulin and Konotop, 2012a.

Alexander, and Turitsyn, 2001; Kevrekidis *et al.*, 2005), but becomes possible in its \mathcal{PT} -symmetric counterpart ($\alpha \neq 0$) (Zezyulin and Konotop, 2012a). This coalescence can be described in terms of a saddle-node bifurcation (Gallo and Pelinovsky, 2014). A similar scenario of collisions of nonlinear modes can be observed if instead of the propagation constant μ one varies parameters of the \mathcal{PT} -symmetric potential. Such collisions were observed in the \mathcal{PT} -symmetric potential (134) with $V_0 = 0$ and varying values of γ at a fixed propagation constant (Achilleos *et al.*, 2012) (see Fig. 33), in a \mathcal{PT} -symmetric double-well potential (Cartarius *et al.*, 2012; Dast, Haag, Cartarius, and Wunner, 2013; Dast, Haag, Cartarius, and Wunner *et al.*, 2013), and in a slab waveguide with a piecewise constant complex potential (Tsoy, Tadjimuratov, and Abdullaev, 2012). In a way this behavior is reminiscent of linear \mathcal{PT} phase transition: cf. the \mathcal{PT} -symmetry-breaking diagram in Fig. 1.

C. Symmetry breaking of solitons

The continuous families of nonlinear modes discussed above are \mathcal{PT} symmetric, i.e., satisfy $\mathcal{PT}\psi = \psi$ (up to a phase shift $\psi \rightarrow \psi e^{i\theta}$, $\theta \in \mathbb{R}$). This observation raises a question: can \mathcal{PT} -symmetric systems admit continuous families of non- \mathcal{PT} -symmetric solitons? In conservative systems continuous families of asymmetric solutions can exist due to symmetry-breaking bifurcations, where asymmetric solitons

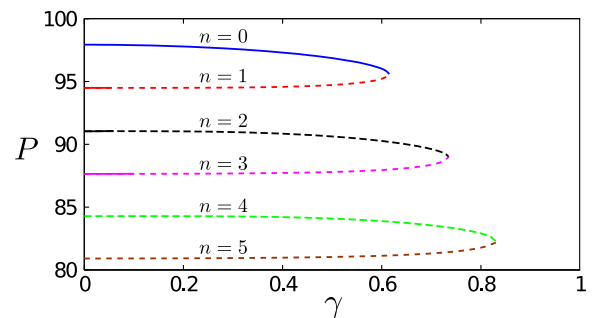


FIG. 33. The power P as a function of the strength γ of the imaginary potential in Eq. (134) with $V_0 = 0$. The bifurcation diagram shows the merging of different solution branches through saddle-node bifurcations. Solid (dashed) lines indicate dynamically stable (unstable) solutions. Here $g = -1$, $\Omega \approx 0.07$, and $\mu = -3$. Adapted from Achilleos *et al.*, 2012.

bifurcate out from the base family of symmetric solitons as the power (L^2 norm) of symmetric solitons exceeds a certain threshold. This symmetry breaking usually occurs in a double- (or multi)well real potential or in a periodic potential (Jackson and Weinstein, 2004; Kirr *et al.*, 2008; Sacchetti, 2009; Akylas, Hwang, and Yang, 2011; Yang, 2012; Malomed, 2013). However, most of the studies of double-well and periodic \mathcal{PT} -symmetric potentials (Muslimani *et al.*, 2008a; Cartarius and Wunner, 2012; Cartarius *et al.*, 2012; C. Li *et al.*, 2012; Nixon, Ge, and Yang, 2012; Dast, Haag, Cartarius, and Wunner, 2013; Dast, Haag, Cartarius, and Wunner *et al.*, 2013; Maytevarunyoo, Malomed, and Reksabutr, 2013; Rodrigues *et al.*, 2013) did not report non- \mathcal{PT} -symmetric nonlinear modes with real propagation constants. Indeed, continuous families of non- \mathcal{PT} -symmetric solitons cannot be expected intuitively, since it is “difficult” for those solitons to balance gain and loss. This intuition is supported by mathematical analysis of Yang (2014a), who showed that for non- \mathcal{PT} -symmetric soliton families to exist in a \mathcal{PT} -symmetric potential infinitely many nontrivial conditions must be satisfied simultaneously, which is generically impossible. However, in a generalized Wadati potential (31)

$$U(x) = -[w^2(x) + \alpha w(x) + iw'(x)], \quad (137)$$

where $w(x)$ is a real and even function and α is a real constant, symmetry breaking of solitons can occur, and continuous families of non- \mathcal{PT} -symmetric solitons are possible (Yang, 2014d). As an example, we consider

$$w(x) = A_- e^{-(x+x_0)^2} + A_+ e^{-(x-x_0)^2}, \quad (138)$$

where A_{\pm} and x_0 are constants. When $A_- = A_+$, this function generates a \mathcal{PT} -symmetric double-well potential $U(x)$ plotted in Fig. 34(a). The linear spectrum of this potential is all real (see Sec. II.F) and contains three positive isolated eigenvalues, the largest being ≈ 3.6614 . From this largest discrete eigenmode, a family of \mathcal{PT} -symmetric solitons bifurcates out. Under focusing nonlinearity ($g = 1$), the power curve of this family is shown in Fig. 34(b), and the soliton profile at the marked point c is displayed in Fig. 34(c). At the propagation constant $\mu_c \approx 3.9287$ of this base power branch, a family of non- \mathcal{PT} -symmetric solitons bifurcates out. The power curve of this non- \mathcal{PT} -symmetric family is also shown in Fig. 34(b). At the marked point d of the bifurcated power branch, the non- \mathcal{PT} -symmetric solution is displayed in Fig. 34(d). Most of the energy in this soliton resides on the right side of the potential.

From Eq. (131) one can see that if $\psi(x)$ is a solution, so is $\psi^*(-x)$. Thus for each of the non- \mathcal{PT} -symmetric solitons $\psi(x)$ in Fig. 34(b), there is a companion soliton $\psi^*(-x)$ whose energy resides primarily on the left side of the potential. Thus this symmetry-breaking bifurcation is pitchfork type.

Linear-stability analysis shows that the base family of \mathcal{PT} -symmetric solitons is stable before the bifurcation point ($\mu < \mu_c$) and becomes unstable when $\mu > \mu_c$ due to the presence of a real positive eigenvalue. However, the bifurcated family of non- \mathcal{PT} -symmetric solitons is stable. To corroborate these linear-stability results, in Figs. 34(e) and 34(f) we show direct simulations of soliton evolutions under initial 1% random-noise perturbations. It is seen from Fig. 34(e) that the

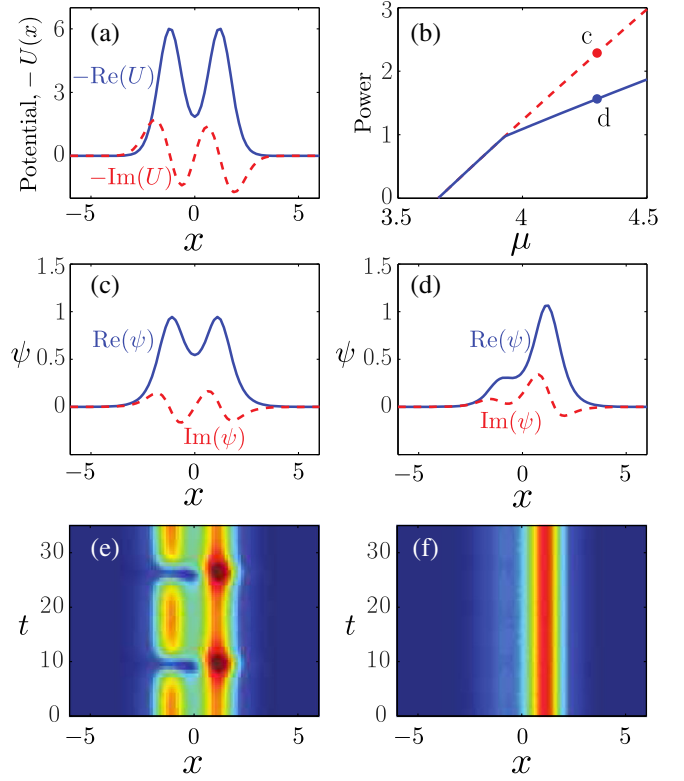


FIG. 34. (a) Inverted plot of the \mathcal{PT} -symmetric potential (137) generated by Eq. (138) with $A_- = A_+ = 2$, $x_0 = 1.2$, $x_0 = 1.2$, and $\alpha = 1$. (b) Power diagram for nonlinear modes with $g = 1$ (solid blue: stable solitons; dashed red: unstable solitons). (c), (d) \mathcal{PT} -symmetric and asymmetric solitons corresponding to points c and d on the power diagram with $\mu = 4.3$. (e), (f) Evolution of the solitons shown in (c) and (d) under 1% random-noise perturbations. Adapted from Yang, 2014d.

\mathcal{PT} -symmetric soliton in Fig. 34(c) breaks up and becomes non- \mathcal{PT} -symmetric. Upon further propagation, the solution bounces back to almost \mathcal{PT} symmetric again, followed by another breakup. In contrast, Fig. 34(f) shows that the asymmetric soliton in Fig. 34(d) is stable against perturbations.

Note that this symmetry-breaking bifurcation also occurs for many other potentials of the form (137), including periodic potentials (Yang, 2014d).

D. Soliton families in asymmetric complex potentials

In a generic complex non- \mathcal{PT} -symmetric potential [$U(x) \neq U^*(-x)$], continuous families of solitons are not expected even if $U(x)$ has all-real linear spectra (Yang, 2014b). Indeed, let us suppose that $U(x)$ is a complex potential which admits a simple isolated real eigenvalue $\tilde{\mu}_n$, with the corresponding localized eigenfunction $\tilde{\psi}_n(x)$. If a soliton family bifurcates out from this linear eigenmode, then in the small-amplitude limit one can expand these solitons into a perturbation series analogous to Eq. (135) and, following the analysis of Sec. VI.B, we recover that the bifurcation of the continuous family from the real eigenvalue $\tilde{\mu}_n$ is possible only if the coefficient $\mu_n^{(2)}$ defined by Eq. (136) is real. As seen in Sec. VI.B on the example of a parabolic potential, if $U(x)$ is \mathcal{PT} symmetric, the reality of $\mu_n^{(2)}$ is satisfied automatically.

However, for a generic complex potential $U(x)$ this condition is likely to fail. Moreover, reality of $\mu_n^{(2)}$ is only the first condition for a soliton family to bifurcate out from a linear mode. As we pursue this perturbation calculation to higher orders, infinitely many more nontrivial conditions would need to be met (Yang, 2014b). This shows that in a generic non- \mathcal{PT} -symmetric potential $U(x)$ soliton families should not exist.

These generic arguments, however, do not apply if the system has hidden symmetries. Tsoy, Allayarov, and Abdullaev (2014) found numerically that continuous families of nonlinear modes do exist in a one-hump asymmetric Wadati potential (137) generated by $w(x) = \eta / \cosh[a(x)x]$, where η is a real constant and $a(x)$ is a step function: $a(x) = a_-$ at $x < 0$, and $a(x) = a_+$ at $x > 0$, with a_{\pm} being real unequal constants. An explanation for this observation given by Konotop and Zezyulin (2014b) consists of the existence of an additional conservation law. Indeed, using the polar representation for the stationary nonlinear mode $\psi(x) = \rho(x)e^{i\int v(x)dx}$, we rewrite the stationary equation (131) with potential (137) in the hydrodynamic form (without loss of generality, we assume $\alpha = 0$ in this section)

$$\begin{aligned} \rho_{xx} - \mu\rho + w^2\rho + g\rho^3 - v^2\rho &= 0, \\ 2\rho_x v + \rho v_x + w_x \rho &= 0. \end{aligned} \quad (139)$$

It is straightforward to verify that these equations admit a conserved quantity

$$I = \rho_x^2 + \rho^2(v+w)^2 - \mu\rho^2 + g\rho^4/2, \quad dI/dx \equiv 0. \quad (140)$$

Because of the existence of this integral of motion, for each value of the propagation constant μ , all localized nonlinear modes can be identified through a solution of a system of two equations with two real unknowns (“shooting constants”) which determine the asymptotic behavior of $\psi(x)$ at $x \rightarrow \pm\infty$. This observation allows one to confirm the existence of continuous families of nonlinear modes using a shooting-type argument: the number of constraints (matching conditions at $x = 0$) is equal to the number of available free parameters. Using this approach, Konotop and Zezyulin (2014b) found families of nonlinear modes in an asymmetric complex double-hump potential defined by Eq. (138) with $A_- \neq A_+$, as illustrated in Fig. 35.

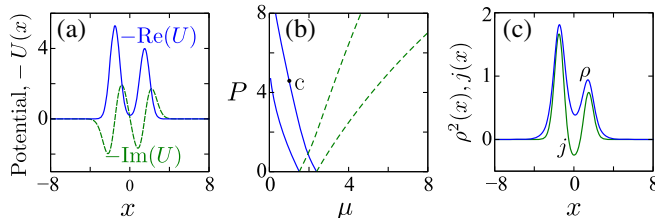


FIG. 35. (a) Inverted plot of the asymmetric potential $U(x)$ for $w(x)$ defined by Eqs. (137) and (138) with $A_- = 2.3$, $A_+ = 2$, $x_0 = 1.5$, and $\alpha = 0$. (b) Power diagram for nonlinear modes. Solid blue (dashed green) lines correspond to defocusing (focusing) nonlinearity. (c) Intensity ρ^2 and current $j = v\rho^2$ for the nonlinear mode marked as c in (b). Adapted from Konotop and Zezyulin, 2014b.

Bifurcation of soliton families from linear modes in asymmetric complex potentials was also studied analytically by Nixon and Yang (2016b). Under a weak assumption, it was shown that the stationary equation (131) admits a constant of motion if and only if the complex potential $U(x)$ is of Wadati type (137). Using this constant of motion, the soliton equation (139) was reduced to a second-order equation for the amplitude of the soliton. From this new soliton equation, it was shown by perturbation methods that continuous families of solitons bifurcate out from linear eigenmodes. It was also found that these results hold not only for the cubic nonlinearity, but also for all nonlinearities of the form $F(|\Psi|^2)\Psi$ in Eq. (39), where $F(\cdot)$ is an arbitrary real-valued function.

VII. NONLINEAR WAVES IN PERIODIC POTENTIALS

In this section, we review properties of solitons in 1D and 2D \mathcal{PT} -symmetric periodic potentials. For the 1D case, we explore the NLS equation (39) with a potential $U(x) \equiv U_{1D}(x)$, where $U_{1D}(x)$ is a periodic and \mathcal{PT} -symmetric function, while in 2D the model is

$$i\Psi_t + \Psi_{xx} + \Psi_{yy} - U_{2D}(x, y)\Psi + g|\Psi|^2\Psi = 0, \quad (141)$$

where $U_{2D}(x, y)$ is periodic in x and y and satisfies the \mathcal{PT} -symmetry condition $U_{2D}^*(x, y) = U_{2D}(-x, -y)$.

Similar to their real-valued counterparts, \mathcal{PT} -symmetric periodic potentials feature band-gap spectra (Bender, Dunne, and Meisinger, 1999; Jones, 1999). For many familiar \mathcal{PT} -symmetric periodic potentials, it has been shown that when the imaginary component of the potential is below a certain threshold, then all the spectral bands lie on the real axis, and the spectrum of the potential is all real. Above this threshold, phase transition occurs, and complex eigenvalues appear (Musslimani *et al.*, 2008a; Makris *et al.*, 2011; Nixon, Ge, and Yang, 2012). Sometimes, this threshold is zero, meaning that complex eigenvalues exist for any imaginary strength of the periodic potential (Musslimani *et al.*, 2008b).

In \mathcal{PT} -symmetric periodic potentials, special periodic solutions can be found analytically (Musslimani *et al.*, 2008b; Abdullaev *et al.*, 2010). Continuous families of bright solitons were found numerically by C. Li *et al.* (2012), Nixon, Ge, and Yang (2012), and Zeng and Lan (2012) in pure periodic potentials, and by Lu and Zhang (2011) and Wang and Wang (2011) in a \mathcal{PT} -symmetric periodic potential with local defects. Some of these soliton families bifurcate out from edges of Bloch bands, while others do not. Above the phase transition, these solitons are all unstable; but below the phase transition, they can be stable in certain parameter regions. In addition to soliton families, distinctive linear diffraction patterns were reported by Makris *et al.* (2010) and Regensburger *et al.* (2012), and periodic bound states were reported by Nixon, Zhu, and Yang (2012). The localization-delocalization transition of light propagating in quasi-periodic \mathcal{PT} -symmetric lattices was numerically obtained by Hang *et al.* (2015).

In two dimensions, a distinctive pyramid diffraction pattern was reported in both linear and nonlinear regimes near the phase transition (Nixon and Yang, 2013). In addition to these results, other interesting phenomena such as nonreciprocal

Bloch oscillations (Longhi, 2009b), rectification and dynamical localization (Kartashov *et al.*, 2016), and unidirectional propagation discussed in Secs. III.A and IV.D.2 have also been found in linear \mathcal{PT} -symmetric periodic potentials.

A. Linear spectrum of periodic potentials

1. 1D lattice

Spectral properties of one-dimensional Schrödinger operators with complex periodic potentials have been intensively studied [for a recent review, see Djakov and Mityagin (2006) and Makris *et al.* (2008)]. In particular, Gasyimov (1980) considered the Schrödinger operator $H = -d^2/dx^2 + U_{1D}(x)$, where

$$U_{1D}(x) = \sum_{n=1}^{\infty} u_n e^{inx}, \quad \sum_{n=1}^{\infty} |u_n| < \infty \quad (142)$$

is the 2π -periodic potential which becomes \mathcal{PT} symmetric if all coefficients u_n are real. It was proven that the spectrum of H is real and fills the semiaxis $[0, \infty)$. Eigenfunctions of H constitute a complete basis in a properly defined linear space.

We illustrate the typical properties of linear periodic \mathcal{PT} -symmetric lattices using as an example the potential in the form

$$U_{1D}(x) = -V_0[\cos^2(x) + iW_0 \sin(2x)]. \quad (143)$$

For this π -periodic lattice, V_0 characterizes the strength of the real component of the potential, and $W_0 \neq 0$ is the relative magnitude of the imaginary component.

Linear modes of Eq. (33) with the potential (143) are

$$\Psi(x, t) = \psi(x) e^{-i\mu t}, \quad \psi(x) = p(x; k) e^{ikx}, \quad (144)$$

where $\psi(x)$ is a Bloch mode solving the eigenvalue problem

$$\mu\psi + \psi_{xx} + V_0[\cos^2 x + iW_0 \sin(2x)]\psi = 0, \quad (145)$$

$p(x; k)$ is a π -periodic function in x , k is the wave number in the irreducible Brillouin zone (BZ) $-1 \leq k \leq 1$, and μ is the propagation constant. The function $\mu = \mu(k)$ is the diffraction (or dispersive) relation, and all admissible values of μ constitute the Bloch bands. The dispersion relations $\mu = \mu(k)$ for three values of W_0 are displayed in Fig. 36. At $W_0 = 0.4$, \mathcal{PT} symmetry is unbroken, and the Bloch bands are all real and separated by gaps. At $W_0 = 1/2$ (the exceptional point), all Bloch bands touch each other and gaps disappear. When $W_0 > 1/2$, \mathcal{PT} symmetry is broken, and complex eigenvalues appear in the Bloch bands.

At $W_0 = 1/2$, one can introduce the variable transformation $\xi = i\sqrt{V_0/2}e^{ix}$ which reduces Eq. (145) to the Bessel equation,

$$\xi^2 \psi_{\xi\xi} + \xi \psi_{\xi} + (\xi^2 - \mu - V_0/2)\psi = 0, \quad (146)$$

whose solution is $\psi(x) = J_k(i\sqrt{V_0/2}e^{ix})$, where $k = \pm\sqrt{\mu + V_0/2}$ (Berry, 1998; Bender, Dunne, and Meisinger, 1999; Graefe and Jones, 2011; Midya, Roy, and

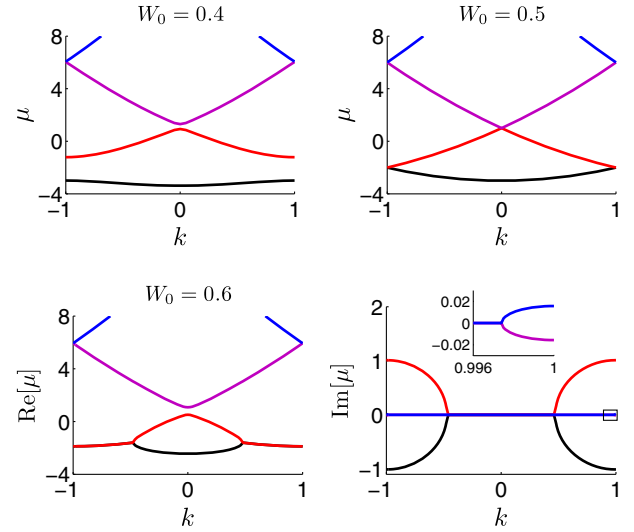


FIG. 36. Diffraction relations of 1D \mathcal{PT} lattice (143) for three values of W_0 ($V_0 = 6$). The inset in the lower right panel is an amplification of the small boxed region near $k = 1$ and $\text{Im}[\mu] = 0$ of the same panel. From Nixon, Ge, and Yang, 2012.

Roychoudhury, 2010; Nixon, Ge, and Yang, 2012). Using a power-series expansion of the Bessel function, the solution can be rewritten as $\psi(x) = e^{ikx} \tilde{p}(x; k)$, where $\tilde{p}(x; k)$ is a π -periodic function of x . In order for this solution to be a Bloch mode, k should be real. If we also restrict k to be in the first BZ $-1 \leq k \leq 1$, then the exact diffraction relation is $\mu = -V_0/2 + (k + 2m)^2$, where $m = 0, \pm 1, \pm 2, \dots$. This diffraction function matches that shown in Fig. 36 for $W_0 = 0.5$. It shows that all Bloch bands are real valued. In addition, these Bloch bands are connected at either the center ($k = 0$) or edge ($k = \pm 1$) of the BZ, where $\mu = -V_0/2 + n^2$, and $n = 0, 1, 2, \dots$

We now consider the case where W_0 is near $1/2$, i.e., $V_0(W_0 - 1/2) \equiv \epsilon \ll 1$. In this case, Eq. (145) becomes

$$(\mu + V_0/2)\psi + \psi_{xx} + V_0/2(e^{2ix})\psi + \epsilon i \sin(2x)\psi = 0.$$

Since complex eigenvalues first appear near band intersections we only need to calculate the eigenvalue at $k = 0$ and ± 1 , where the Bloch modes are π or 2π periodic. These solutions and the associated μ values can be expanded as a power series in $\epsilon^{1/2}$,

$$\begin{aligned} \mu &= -V_0/2 + n_0^2 + \epsilon^{1/2}n_1 + \epsilon n_2 + \dots, \\ \psi &= \psi_0 + \epsilon^{1/2}\psi_1 + \epsilon\psi_2 + \dots, \end{aligned} \quad (147)$$

where $n_0 = 0, 1, 2, \dots$, and the coefficients n_1, n_2, n_3, \dots are constants shown in Table I (Nixon, Ge, and Yang, 2012). When $n_0 = 1, 3$, the coefficient n_1 or n_3 is imaginary, thus complex eigenvalues bifurcate out simultaneously above the phase-transition point ($\epsilon > 0$). The imaginary part of these complex eigenvalues at $n_0 = 3$ ($\sim \epsilon^{3/2}$) is much smaller than that at $n_0 = 1$ ($\sim \epsilon^{1/2}$), and no complex eigenvalues bifurcate out when $n_0 = 0, 2$. Continuing these calculations to higher n_0 values, one can find that the coefficient n_{2m+1} is always imaginary for $n_0 = 2m + 1$, where $m = 0, 1, 2, \dots$. Thus

TABLE I. Coefficients in the μ expansion (147).

n_0	n_1	n_2	n_3
0	0	$V_0/8$	0
1	$\pm iV_0^{1/2}/2$	$V_0/32$	$\pm i(V_0^{-1/2}/4 + V_0^{3/2}/2^9)$
2	0	$-5V_0/48, V_0/48$	0
3	0	$-V_0/64$	$\pm iV_0^{3/2}/2^9$
N	0	$-V_0/8(N^2 - 1)^{-1}$	0

complex eigenvalues bifurcate out simultaneously from all odd values of n_0 at the phase-transition point $W_0 = 1/2$.

Table I also shows that below the phase-transition point ($W_0 < 1/2$, or $\epsilon < 0$), the eigenvalue μ is real for all integers n_0 .

2. 2D lattices

In 2D, we focus on the separable potential

$$U_{2D}(x, y) = U_{1D}(x) + U_{1D}(y), \quad (148)$$

whose linear spectrum can be obtained directly from the spectrum of the 1D problem (143). In this case, $\mu = \mu(k_1) + \mu(k_2)$ is the 2D diffraction relation, k_1, k_2 are Bloch wave numbers in the x and y directions which are located inside the first BZ, and

$$\Psi(x, y, t) = e^{ik_1x + ik_2y - i\mu t} p(x; k_1) p(y; k_2), \quad (149)$$

where $p(x; k)$ is the 1D π -periodic function as given in Eq. (144). This diffraction relation shows that complex eigenvalues appear in the 2D \mathcal{PT} lattice if and only if complex eigenvalues appear in the 1D \mathcal{PT} lattice (143). Thus Bloch bands in the 2D potential (148) are all real when $W_0 \leq 1/2$, and a phase transition occurs at $W_0 = 1/2$ above which complex eigenvalues arise.

B. Solitons and their stability

Solitons in \mathcal{PT} -symmetric periodic potentials exist as continuous families (Muslimani *et al.*, 2008a; C. Li *et al.*, 2012; Nixon, Ge, and Yang, 2012). The simplest soliton families are those that bifurcate out from edges of Bloch bands, and they can be established analytically by exponential asymptotics methods (Nixon and Yang, 2014). In addition to these simplest soliton families, an infinite number of other soliton families were reported numerically (C. Li *et al.*, 2012; Nixon, Ge, and Yang, 2012).

1. Solitons in 1D lattices

Let us consider the 1D NLS equation (39) with \mathcal{PT} -symmetric periodic potential (143). Solitons are searched in the form $\Psi(x, t) = e^{-i\mu t} \psi(x)$, where $\psi(x)$ is a stationary localized wave function solving Eq. (131), and μ is a real propagation constant. In full analogy with the conservative case (Brazhnyi and Konotop, 2004; Yang, 2010; Pelinovsky, 2011), exponentially decaying soliton solutions (alias *gap solitons*) exist when μ lies inside band gaps of the underlying linear system. For broken \mathcal{PT} symmetry, all solitons are

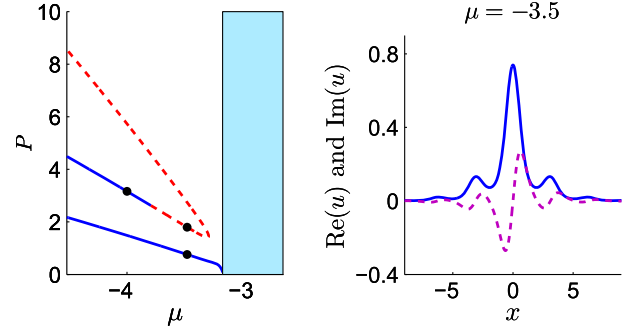


FIG. 37. 1D solitons in the semi-infinite gap of Eq. (143) under focusing nonlinearity ($g = 1$) for $V_0 = 6$ and $W_0 = 0.45$. (left) Power curves of these solitons; solid blue and dashed red lines represent stable and unstable solitons, respectively; the shaded region is the first Bloch band. (right) A fundamental soliton at $\mu = -3.5$ (marked by a dot on the lower curve of the left panel); the solid blue line is for the real part and the dashed pink line for the imaginary part. From Nixon, Ge, and Yang, 2012.

unstable since small tails of solitons will be amplified. Thus next we consider only the unbroken \mathcal{PT} -symmetry case where $W_0 \leq 1/2$.

In Fig. 37 (left) we illustrate two families of solitons in the semi-infinite gap under focusing nonlinearity (Nixon, Ge, and Yang, 2012). The lower power curve is for the fundamental solitons which are \mathcal{PT} symmetric, i.e., $\psi^*(x) = \psi(-x)$, and whose real parts possess a single dominant peak. The profile of such a soliton at $\mu = -3.5$ is displayed in Fig. 37 (right). This soliton family bifurcates out of the first Bloch band, and in the vicinity of the bifurcation the solitons can be described as low-amplitude Bloch-wave packets. The entire family of fundamental solitons is linearly stable.

The upper power curve in Fig. 37 consists of dipole solitons. This power curve features double branches which terminate through a saddle-node bifurcation before reaching the first Bloch band. Profiles of two such solitons on the lower power branch are displayed in Fig. 38 (two left panels). The real parts of these dipole solitons possess two dominant peaks of opposite sign. This however does not violate \mathcal{PT} symmetry, as due to phase invariance we have that $\phi(x) = \psi(x)e^{i\pi/2}$ is a \mathcal{PT} -symmetric solution.

Dipole solitons are linearly stable only in a certain portion of their existence region. Specifically, only dipole solitons on the lower branch with $\mu \leq \mu_a \approx -3.8$ are stable (see Fig. 37,

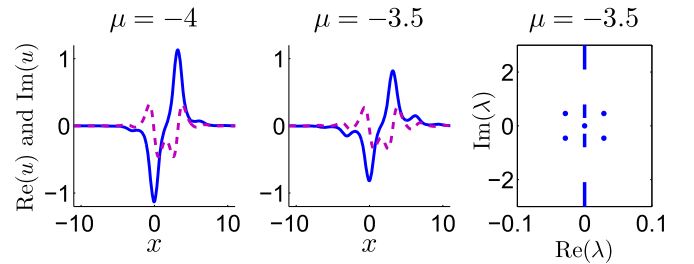


FIG. 38. Two left panels: dipole solitons at the marked points of the lower power curve in Fig. 37. Right panel: linear-stability spectrum for the dipole soliton in the middle panel. From Nixon, Ge, and Yang, 2012.

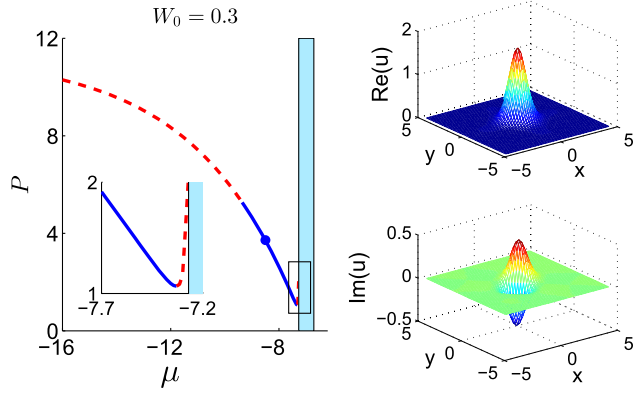


FIG. 39. (Left) Power curve of fundamental 2D solitons in the semi-infinite gap under focusing nonlinearity ($g = 1$) for $V_0 = 6$ and $W_0 = 0.3$. The inset is amplification of the power curve near the first Bloch band in the same panel. Solid blue lines indicate stable solitons, while dashed red lines indicate unstable solitons. (Right) Real and imaginary parts of the soliton $\psi(x, y)$ at $\mu = -8.5$ (marked by a dot on the power curve). From Nixon, Ge, and Yang, 2012.

left panel). For dipole solitons in this region, their spectra are entirely imaginary. At $\mu = \mu_a$, stability switching occurs where a quadruple of complex eigenvalues bifurcates off the edge of the continuous spectrum (see Fig. 38, right panel). Within this unstable region, there is a second eigenvalue bifurcation at $\mu \approx -3.4$ of the lower branch (near and on the left side of the power minimum) where a pair of real eigenvalues bifurcate out from zero.

Beside these soliton families, the model also admits other types of solitons such as truncated-Bloch-mode solitons (C. Li *et al.*, 2012) which are stable in certain parameter regimes. Stable dissipative solitons exist at the surface between a homogeneous Kerr medium and a truncated lattice (143) supported by the linear dissipation (He, Mihalache *et al.*, 2012).

2. 2D solitons

Solitons and their stability in 2D \mathcal{PT} -symmetric periodic potentials (148) have also been studied (Nixon, Ge, and Yang, 2012). These solitons are of the form $\Psi(x, y, t) = e^{-i\mu t}\psi(x, y)$. Figure 39 (left panel) shows fundamental 2D solitons in the semi-infinite gap under focusing nonlinearity ($g = 1$). Similar to the conservative case, there exists a threshold power (L^2 norm) necessary for the existence of such solitons. The profiles of the solitons possess \mathcal{PT} symmetry, $\psi^*(x, y) = \psi(-x, -y)$, and their real parts have a single dominant peak [Fig. 39, right panel]. These fundamental solitons are stable only in a finite μ interval, even though their existence region is infinite. For large negative values of μ , the instability is due to a quadruple of complex eigenvalues, whereas for μ values near the first band, the instability is due to a pair of real eigenvalues.

Beside the fundamental solitons in Fig. 39, other types of solitons such as vortex solitons and multipole solitons have also been reported in 2D \mathcal{PT} -symmetric lattices (Zhu, Wang *et al.*, 2013; Li *et al.*, 2014; Ren *et al.*, 2014; Wang *et al.*, 2015).

3. Nonlinear periodic solutions and constant-intensity waves

As mentioned earlier, a \mathcal{PT} -symmetry threshold can be zero. This fact, however, does not prohibit the existence of nonlinear periodic solutions, which do not require the propagation constant to belong to a band gap of the linear spectrum. For instance, the phase transition for the \mathcal{PT} -symmetric periodic potential $U_{1D}(x) = -[V_0 \sin^2 x + 3iW_0 \sin x]$, where V_0 and W_0 are real constants, has zero threshold (complex eigenvalues appear in Bloch bands for any nonzero W_0). However, in the presence of focusing nonlinearity, it admits a stationary x -periodic solution found in exact form by Musslimani *et al.* (2008b),

$$\Psi(x, t) = \sqrt{V_0 + W_0^2} \cos x e^{iW_0 \sin x - i\mu t}, \quad \mu = 1 - V_0,$$

provided that $V_0 > -W_0^2$. These periodic solutions may be stable, even though the periodic potential is above the phase transition (Lumer *et al.*, 2013). Examples of stable periodic solutions in defocusing medium can also be found (Abdullaev *et al.*, 2010).

The complex Wadati potentials $U_{1D}(x) = -[w^2(x) + iw_x(x)]$ (see also Secs. VI.C and VI.D) support exact constant-intensity solutions $\Psi = A \exp[-i \int w(x) dx + igA^2 t]$, where A is a real amplitude (Makris *et al.*, 2015). These solutions can be generalized to the 2D case, where the \mathcal{PT} -symmetric potential reads $U_{2D}(x, y) = -|\mathbf{W}|^2 - i\nabla \cdot \mathbf{W}$, with a vector potential $\mathbf{W} = (W_1, W_2)$ constrained by the condition $(W_1)_y = (W_2)_x$. Then the 2D exact solutions have the form $\Psi(x, y, t) = A \exp[-i \int_C \mathbf{W} \cdot d\mathbf{r} + igA^2 t]$, where C is a smooth open curve between any two points in the (x, y) plane. The constant-amplitude solutions were explored by Makris *et al.* (2015) in the context of modulational instability.

C. Nonlinear dynamics near the phase-transition point

Beyond the question of stationary modes, a more general question is how an initial wave evolves in a \mathcal{PT} -symmetric periodic potential. Here we review linear and nonlinear dynamics of wave packets near the phase-transition point, investigated analytically by Nixon, Zhu, and Yang (2012) and Nixon and Yang (2013), and describe new phenomena such as wave blowup, periodic bound states, and linear or nonlinear pyramid diffraction patterns.

1. 1D dynamics

We first consider the model (39) with the potential (143), which in this section is rewritten as $U(x) = U_{1D}(x) = -V_0^2[\cos(2x) + iW_0 \sin(2x)]$. For this form of the potential, the phase transition occurs at $W_0 = 1$. At this phase-transition point, the diffraction relation is $\mu = (k + 2m)^2$, where k is in the first BZ $k \in [-1, 1]$, and m is any non-negative integer (see Fig. 36 for $W_0 = 1/2$).

At $k = 0$ and ± 1 , adjacent Bloch bands intersect each other. At these intersection points, Bloch solutions are degenerate and π or 2π periodic in x . Posed as an eigenvalue problem for $\Psi = \phi(x)e^{-i\mu t}$ in the linear equation (33), we get $L\phi = -\mu\phi$, where $L \equiv \partial_x^2 - U(x)|_{W_0=1}$. Then at these band-intersection points, the eigenvalues are $\mu = n^2$, where n is any positive

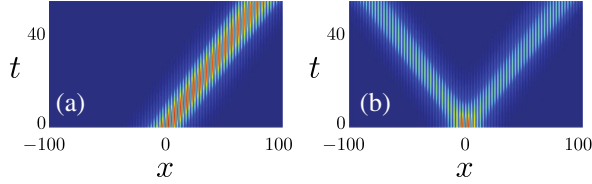


FIG. 40. (a) Linear unidirectional wave packet and (b) linear wave packet splitting at the phase-transition point $W_0 = 1$. Other parameters are $\epsilon = 0.1$, $\mu = 1$, and $V_0 = \sqrt{6}$. From Nixon, Zhu, and Yang, 2012.

integer. These eigenvalues all have geometric multiplicity 1 and algebraic multiplicity 2, thus there exists a generalized eigenfunction $\phi^{\mathbb{S}}$ satisfying $(L + \mu)\phi^{\mathbb{S}} = \phi$ [for construction of the complete basis at an exceptional point see Gasymov (1980) and Graefe and Jones (2011)].

To study nonlinear dynamics of wave packets near the phase-transition point (i.e., $W_0 \sim 1$), one can use the asymptotic expansion $\Psi = e^{-i\mu t}[cA(X, T)\phi(x) + \epsilon^2\psi_1 + \dots]$, where $A(X, T)$ is an envelope of the degenerate Bloch mode $\phi(x)$, $X = \epsilon x$, $T = \epsilon t$ are slow variables, and $0 < \epsilon \ll 1$. From the multiple-scale perturbation analysis one finds that near $n = 1$ and $W_0 = 1 - c\epsilon^2$, where c is a constant, the envelope is governed by a nonlinear Klein-Gordon (KG) equation,

$$A_{TT} - 4A_{XX} + \alpha A + \gamma|A|^2A = 0. \quad (150)$$

Here $\alpha = cV_0^4/2$ and $\gamma = (2g/\pi) \int_{-\pi}^{\pi} |\phi|^2 \phi^2 dx$ are real constants. At higher n values, similar envelope equations can be derived under appropriate scalings of $W_0(\epsilon)$.

Envelope dynamics in the nonlinear KG equation (150) proves to closely mimic the corresponding wave packet dynamics in the original \mathcal{PT} model (39).

First, at the phase-transition point ($c = 0$), solutions for the left and right propagating waves (resembling solutions of the wave equation $A_{TT} - 4A_{XX} = 0$) can be found in the original linear \mathcal{PT} model (39) with $g = 0$. Two examples are shown in Fig. 40. The spreading-shelf solutions in this wave equation were reported experimentally by Regensburger *et al.* (2012).

Next we consider envelope solutions in the KG equation (150) with self-defocusing nonlinearity ($\gamma < 0$) near the lowest band-intersection point ($n = 1$). Nixon, Zhu, and Yang (2012) numerically found that below the phase-transition point ($c > 0$) envelope solutions blow up to infinity [first panel in Fig. 41]. With the full model (39), similar growing

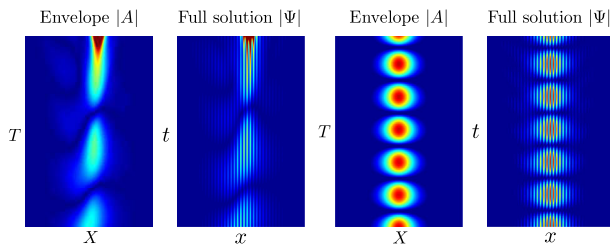


FIG. 41. Nonlinear wave packet solutions below the phase-transition point ($c = 1$) under self-defocusing nonlinearity. From left to right: a blowup solution in the envelope equation and the full equation; a periodic bound state in the envelope equation and the full equation. From Nixon, Zhu, and Yang, 2012.

solutions were found and displayed in Fig. 41 (second panel). With the full model, this blowup may eventually be suppressed, but that is already beyond the asymptotic regime of the KG model (150). Under self-defocusing nonlinearity Eq. (150) also admits breatherlike solutions shown in the third panel of Fig. 41, as well as stationary solitons $A(X, T) = F(X)e^{i\omega T}$ with $\omega \in [-\sqrt{\alpha}, \sqrt{\alpha}]$. The corresponding breather solution in the full model is shown in the fourth panel of Fig. 41.

If the nonlinearity is self-focusing ($g = 1$), envelope solutions do not blow up, periodic bound states cannot be found, and stationary solitary waves do not exist in the envelope equation. In this case, breathers as well as nonlinear diffracting solutions similar to the linear diffracting pattern reported by Makris *et al.* (2010) can be found. Dynamics near the breaking point appears to be rich even in the linear limit, allowing, in particular, for the resonant mode conversion (Vysloukh and Kartashov, 2014).

2. 2D dynamics

Next we consider dynamics of wave packets in a 2D \mathcal{PT} -symmetric periodic potential near the phase-transition point (Nixon and Yang, 2013). The mathematical model is taken as Eq. (141) with $U_{2D}(x, y) = U_{1D}(x) + U_{1D}(y)$, where $U_{1D}(x)$ is the same periodic potential used in the 1D dynamics. At the phase-transition point $W_0 = 1$, the linear diffraction relation reads $\mu = (k_x + 2m_1)^2 + (k_y + 2m_2)^2$, where (k_x, k_y) are Bloch wave numbers in the first BZ $-1 \leq k_x, k_y \leq 1$, and $m_{1,2}$ are non-negative integers. The most complex degeneracies occur at points $k_x = 0, \pm 1$ and $k_y = 0, \pm 1$, where the diffraction surface intersects itself fourfold as illustrated in Fig. 42. When a linear Bloch wave $\Psi = \phi(x, y)e^{-i\mu t}$ is chosen at one of these degeneracies, $\phi(x, y)$ satisfies an eigenvalue equation $L\phi = -\mu\phi$, where $L = \nabla^2 - U(x, y)|_{W_0=1}$, $\mu = n_1^2 + n_2^2$, and (n_1, n_2) are any pair of positive integers.

We conduct the analysis at the lowest intersection point $\mu = 2$. The perturbation expansion for the wave packet near this point is $\Psi = \epsilon^{3/2}e^{-i\mu t}[A(X, Y, T)\phi^{01}(x, y) + \epsilon\psi_1 + \dots]$, where ϕ^{01} is the Bloch mode at the point $(k_x, k_y, \mu) = (1, 1, 2)$, $(X, Y, T) = (\epsilon x, \epsilon y, \epsilon t)$ are slow variables, and $0 < \epsilon \ll 1$. Near the phase-transition point we express $W_0 = 1 - \eta\epsilon^2/V_0^2$, where η measures the deviation from phase transition. Through a perturbation calculation we obtain (Nixon and Yang, 2013)

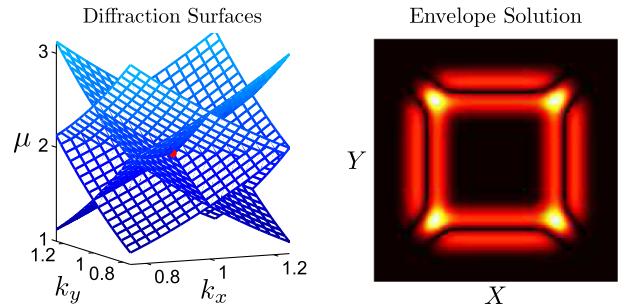


FIG. 42. (Left) Diffraction relation near intersection point $(k_x, k_y, \mu) = (1, 1, 2)$ (marked by red dot). (Right) Linear pyramid diffraction of initial Gaussian envelope at phase-transition point in the envelope equation (151). From Nixon and Yang, 2013.

$$\begin{aligned} \partial_T^4 A - 8(\partial_X^2 + \partial_Y^2)\partial_T^2 A + 16(\partial_X^2 - \partial_Y^2)^2 A \\ + \alpha\partial_T^2 A + i\tilde{g}\partial_T(|A|^2 A) = 0, \end{aligned} \quad (151)$$

where $\alpha = 2V_0^2\eta$ and \tilde{g} is a real constant. Equation (151) reveals important physical features, which are demonstrated next using the initial conditions

$$A = A_0 e^{-(X^2+Y^2)}, \quad A_T = A_{TT} = 0, \quad \partial_T^3 A = -i\tilde{g}|A|^2 A \quad (152)$$

in the envelope equation [and the corresponding initial conditions in the full equation (141)]. Further, we take $V_0^2 = 6$, $\epsilon = 0.1$, and $\eta = 0$ or 1 (at or below the phase transition, respectively), which yields $\alpha = 12\eta$ and $\tilde{g} \approx 7.3g$.

In the linear limit $g = 0$ and at the phase-transition point $\alpha = 0$, Eq. (151) becomes linear and is readily solved. Its general solution corresponds to an expanding square wave front propagating with speeds ± 2 in both X and Y directions, which is termed *pyramid diffraction*. For the initial conditions (152), this pattern is illustrated in Fig. 42.

In the presence of nonlinearity ($\tilde{g} \approx 7.3g$) and below the phase transition, the wave packet diffracts away if its initial amplitude is below a certain threshold value, as displayed in the upper left panel of Fig. 43. If the initial amplitude is above this threshold, the envelope solution blows up to infinity in finite time. For example, with the initial condition (152), the envelope solution in Eq. (151) blows up when $A_0 > 3.2$ (Fig. 43, upper middle and right panels). Remarkably, this blowup is independent of the sign of nonlinearity, a fact which is clear from the envelope equation (151), since a sign change in \tilde{g} can be accounted for by taking the complex conjugate of this equation. In the full equation (141), it was confirmed that similar growth occurs for both signs of the nonlinearity as well (see Fig. 43, lower row) at initial stages of evolution, although the finite-time blowup is ruled out in the defocusing medium at longer times.

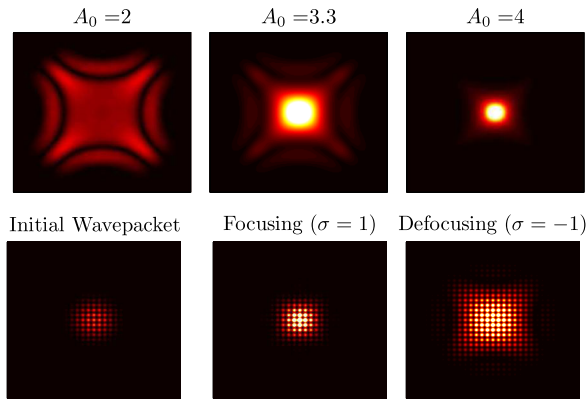


FIG. 43. Nonlinear dynamics of wave packets below phase transition. Upper row: envelope solutions in Eq. (151) at $T \approx 2$ for three values of A_0 in Eq. (152). Lower row: solutions of the full equation (141) for the initial wave packet with $A_0 = 6$ (left) at later times under focusing (middle) and defocusing (right) nonlinearities. From Nixon and Yang, 2013.

D. Nonlinear \mathcal{PT} -symmetric lattices

So far we considered nonlinear models whose linear parts obey \mathcal{PT} symmetry. Now we turn to wave propagation in a nonlinear \mathcal{PT} -symmetric lattice governed by

$$i\Psi_t + \Psi_{xx} + g[1 + U_{NL}(x)]|\Psi|^2\Psi = 0, \quad (153)$$

where $U_{NL}(x) = U_{NL}^*(-x)$ is a \mathcal{PT} -symmetric nonlinear potential. Equation (153) can be considered as a \mathcal{PT} -symmetric deformation of conservative nonlinear lattice models studied intensively during the last decade [see Kartashov, Malomed, and Torner (2011) for a review]. This model with a periodic \mathcal{PT} -symmetric potential $U_{NL}(x) = V_0 \cos(x) + iW_0 \sin(x)$ was introduced by Abdullaev, Kartashov *et al.* (2011). It supports continuous families of stable solitons [a detailed linear-stability analysis was performed by Zezyulin, Kartashov, and Konotop (2011)]. Interestingly, stable solitons can be found even if periodic modulation of the real part of the potential is absent, i.e., $V_0 = 0$. Stable solitons also exist in nonperiodic nonlinear landscapes, such as $U_{NL}(x) = iW_0 \tanh x$ or $U_{NL}(x) = iW_0 x$.

Further natural generalization is a model of combined linear and nonlinear \mathcal{PT} -symmetric lattices (He *et al.*, 2012b):

$$i\Psi_t + \Psi_{xx} - U_L(x)\Psi + g[1 + U_{NL}(x)]|\Psi|^2\Psi = 0, \quad (154)$$

where $U_L(x) = U_L^*(-x)$ and $U_{NL}(x) = U_{NL}^*(-x)$. The presence of both linear and nonlinear modulations enriches the problem and makes it possible to consider a general case where linear and nonlinear modulations are different from each other and the special case where the two lattices are identical (He *et al.*, 2012b). Stable gap solitons can be found in both cases, as well as in the case of real-valued functions $U_{NL}(x)$ (He and Mihalache, 2012; He *et al.*, 2012a; Meng and Liu, 2013). It is of interest to consider in-phase modulations, i.e., $U_L(x) = U_{NL}(x)$ (He *et al.*, 2012b) and out-of-phase modulations, i.e., $U_L(x) = -U_{NL}(x)$. The latter type of modulation can support stable fundamental and multipole solitons whose counterparts in in-phase lattices are unstable (Huang, Li, and Dong, 2013).

E. Solitons in generalized lattice models

The basic \mathcal{PT} -symmetric nonlinear models described allow for numerous generalizations accounting for more complex forms of nonlinearities and periodic lattices, as well as for multicomponent situations. Such generalized models also support a variety of solitons whose properties were studied systematically. Here we provide a succinct review of the available results [some generalizations were also summarized by He and Malomed (2013)].

1. Vector mixed-gap solitons

A model describing two incoherently coupled fields ($\Psi_{1,2}$) in a \mathcal{PT} -symmetric lattice $U(x)$,

$$i\frac{\partial\Psi_{1,2}}{\partial t} + \frac{\partial^2\Psi_{1,2}}{\partial x^2} - U(x)\Psi_{1,2} + (|\Psi_1|^2 + |\Psi_2|^2)\Psi_{1,2} = 0,$$

was studied by Kartashov (2013). Since the model does not include linear coupling between the two fields, it supports the so-called mixed-gap solitons characterized by different propagation constants for the two field components $\Psi_j(x, t) = e^{-i\mu_j t} \psi_j(x)$, where $\mu_1 \neq \mu_2$ lie in different gaps of the \mathcal{PT} -symmetric potential. A further generalization of this model accounting for both linear and nonlinear periodic lattices was considered by Zhu, Cao *et al.* (2014).

2. Generalized nonlinearities

A \mathcal{PT} -symmetric lattice model with a more general form of nonlinearity is

$$i\Psi_t + \Psi_{xx} - U(x)\Psi + F(x, |\Psi|^2)\Psi = 0. \quad (155)$$

The case of nonlocal nonlinearity corresponds to $F(x, |\Psi|^2) = g(x) \int_{-\infty}^{\infty} K(x-y) |\Psi(y)|^2 dy$, where $K(x) \geq 0$ is a kernel function describing nonlocal properties of the medium and $g(x)$ is the nonlinear coefficient. Stable nonlocal gap solitons were found for both self-focusing [$g(x) \equiv 1$] (H. Li *et al.*, 2012) and self-defocusing [$g(x) \equiv -1$] (Zhu, Li *et al.*, 2013; Jisha, Alberucci *et al.*, 2014) nonlocal nonlinearities. A spatially modulated nonlocal nonlinearity with a periodic function $g(x)$ was also considered (Yin *et al.*, 2012). ‘‘Accessible solitons’’ (Snyder and Mitchell, 1997) in a strongly nonlocal 2D \mathcal{PT} -symmetric medium were reported by Zhong, Belić, and Huang (2012).

Saturating nonlinearity $F(x, |\Psi|^2) = g|\Psi|^2/(1 + |\Psi|^2)$ also supports gap solitons (Cao *et al.*, 2014; Hong and Jung, 2015). Multistable solitons in \mathcal{PT} -symmetric lattices in the presence of cubic-quintic nonlinearity $F(x, |\Psi|^2) = g_1|\Psi|^2 + g_2|\Psi|^4$ were reported by Li, Liu, and Dong (2012). He and Mihalache (2013) studied soliton propagation in the cubic-quintic Ginzburg-Landau model with a \mathcal{PT} -symmetric lattice.

3. \mathcal{PT} -symmetric superlattices

Superlattices are combinations of several periodic potentials with different periods. Zhu *et al.* (2011) considered a \mathcal{PT} -symmetric superlattice with the potential $U(x)$ having real and imaginary parts $V(x) = \varepsilon \sin^2(x + \pi/2) + (1 - \varepsilon) \sin^2[2(x + \pi/2)]$ and $W(x) = W_0 \sin(2x)$ and found that such a superlattice supports stable gap solitons. The extension of this study to the case where both real and imaginary parts of the complex potential are dual-periodic superlattices was addressed by H.-C. Wang *et al.* (2014).

4. Defect solitons

Periodic lattices or superlattices locally perturbed by a defect can support defect solitons. As an example, one can consider a periodic lattice whose real part is given as $V(x) = \cos^2(x)[1 + \varepsilon f_D(x)]$, where $f_D(x)$ is a localized function and the coefficient ε controls the defect strength (Wang and Wang, 2011). If the imaginary part is an unperturbed periodic function, say, $W(x) = W_0 \sin(2x)$, then the resulting \mathcal{PT} -symmetric defect lattice is known to support stable defect solitons under self-focusing (Wang and Wang, 2011; Hu and Hu, 2012) and self-defocusing (Hu and Hu, 2013a) nonlinearities. Further developments in this directions

include defect solitons in superlattices (Lu and Zhang, 2011; Hu, Lu *et al.*, 2012; S.-M. Hu and Hu, 2013; Fang *et al.*, 2014; H. Wang *et al.*, 2014), as well as in nonlocal (Hu, Lu *et al.*, 2012; Hu, Ma *et al.*, 2012; Fang *et al.*, 2014), saturable (Hu and Hu, 2013b), and \mathcal{PT} -symmetric (Wang *et al.*, 2012; H. Wang *et al.*, 2014) nonlinearities. Defect solitons in 2D \mathcal{PT} -symmetric lattices were reported by Xie *et al.* (2014).

Finishing this review of generalized \mathcal{PT} -symmetric lattice models, we also mention other possibilities such as chirped (quasiperiodic) \mathcal{PT} lattices (Chun-Yan, Chang-Ming, and Liang-Wei, 2013) and effects of higher-order diffraction on \mathcal{PT} models (Ge *et al.*, 2014).

F. Bragg solitons

The NLS-type models considered above do not account for waves reflected from the periodic structure, i.e., they are only valid away from the Bragg resonance. If a stop gap is relatively narrow and the carrier-wave frequency falls inside that gap, the interference of forward and backward propagating waves

$$E = E_f(z, t)e^{i(\beta_0 z - \omega_0 t)} + E_b(z, t)e^{-i(\beta_0 z + \omega_0 t)} \quad (156)$$

must be considered. Here ω_0 is the carrier-wave frequency and $\beta_0 = n_0 \omega_0 / c$ is the unperturbed propagation constant. Then under Kerr nonlinearity the medium supports the so-called *Bragg solitons* (Acevez and Wabnitz, 1989; Christodoulides and Joseph, 1989). Bragg solitons persist also in the case of a periodic \mathcal{PT} -symmetric grating and are described by the coupled equations (Miri, Aceves *et al.*, 2012):

$$\begin{aligned} \frac{i}{v} \frac{\partial E_f}{\partial t} + i \frac{\partial E_f}{\partial z} + (\kappa + g)E_b + \gamma(|E_f|^2 + 2|E_b|^2)E_f &= 0, \\ \frac{i}{v} \frac{\partial E_b}{\partial t} - i \frac{\partial E_b}{\partial z} + (\kappa - g)E_f + \gamma(2|E_f|^2 + |E_b|^2)E_b &= 0, \end{aligned} \quad (157)$$

where $v = c/n_0$, κ is the coupling arising from the real Bragg grating itself, g is the antisymmetric coupling arising from the complex \mathcal{PT} -symmetric potential, and γ is a nonlinear coefficient.

In the linear limit ($\gamma = 0$), the substitution $E_{f,b} = \Psi_{f,b} e^{i(Kz - \Omega t)}$ yields the dispersion relation $\Omega^2 = v^2(K^2 + \kappa^2 - g^2)$. Thus \mathcal{PT} symmetry is unbroken (Ω is real for any K) if $g \leq \kappa$; the case $g = \kappa$ corresponds to the exceptional point, and \mathcal{PT} symmetry is broken if $g > \kappa$. When \mathcal{PT} symmetry is unbroken, the nonlinear model (157) supports traveling soliton solutions

$$E_{f,b} = \pm \alpha \sqrt{\frac{\kappa_\rho}{2\gamma}} \Delta^{\mp 1} \sin(\sigma) \operatorname{sech}\left(\theta \mp \frac{\sigma}{2}\right) e^{i\eta(z,t)}, \quad (158)$$

where $\kappa_\rho = \sqrt{\kappa^2 - g^2}$, $\theta = \kappa_\rho \sin(\sigma)(z - mvt)/\sqrt{1 - m^2}$, $m = (1 - \Delta^4)/(1 + \Delta^4)$, and $\Delta, \sigma \in (0, \pi)$ are free parameters. The amplitude α and phase $\eta(z, t)$ can also be found in analytical form (Miri, Aceves *et al.*, 2012).

The nonlinear model (157) also supports plane wave solutions whose modulational instability was classified by

Sarma (2014) in different parameter regimes. Families of more general traveling-wave solutions (including bright solitons in forward waves and dark solitons in backward waves) were reported by Gupta and Sarma (2014a).

VIII. \mathcal{PT} -SYMMETRIC $\chi^{(2)}$ MEDIA

In this section, we consider \mathcal{PT} -symmetric optical media with quadratic (i.e., $\chi^{(2)}$) nonlinearity. Our main concern is the existence and stability of nonlinear modes. We have seen before that the existence of continuous solution families requires not only balance between linear gain and loss, but also a specific form of nonlinearity. This balance can be achieved either in spatially extended systems or in linearly coupled multicomponent systems. $\chi^{(2)}$ media appear as a special case since they arise due to frequency conversion and intrinsically have two components having “different nonlinearities.” In addition, they do not allow linear coupling between the two components due to different frequencies. Therefore \mathcal{PT} -symmetric optics of quadratic media can be developed either on the basis of coupled extended systems where one (or each) component is subject to gain and loss or as a combination of (at least two) \mathcal{PT} -symmetric models where the first two components are linearly coupled with the second two components. Next we consider the respective examples.

A. Quadratic media with \mathcal{PT} -symmetric potentials

The dimensionless mathematical model for quadratic media with \mathcal{PT} -symmetric potentials reads

$$iq_{1,z} = -q_{1,xx} + V(x)q_1 + 2q_1^*q_2, \quad (159a)$$

$$iq_{2,z} = -(1/2)q_{2,xx} + 2[\tilde{V}(x) + \beta]q_2 + q_1^2, \quad (159b)$$

where q_1 and q_2 are the fundamental-frequency (FF) and second-harmonic (SH) fields, β is the mismatch parameter, and $V(x)$, $\tilde{V}(x)$ are \mathcal{PT} -symmetric potentials. Stationary localized solutions of Eq. (159) are searched in the form $q_1 = w_1(x)e^{ibz}$ and $q_2 = w_2(x)e^{2ibz}$, where w_1, w_2 can be required to obey the symmetries $\{w_1(x), w_2(x)\} = \{w_1^*(-x), w_2^*(-x)\}$ or $\{w_1(x), w_2(x)\} = \{-w_1^*(-x), w_2^*(x)\}$. In the so-called cascade limit corresponding to large β for which the approximate solution $w_2 \approx -w_1^2/2\beta$ of Eq. (159b) is valid (Stegeman, Hagan, and Torner, 1996), Eq. (159a) for the FF is reduced to the stationary NLS equation (131) with a \mathcal{PT} -symmetric potential. This suggests the existence of localized modes in the model (159) with \mathcal{PT} -symmetric potentials. Such modes indeed were found (Moreira *et al.*, 2012) in the case of the Scarff II potential (132) for the FF and $\tilde{V} = 2V_1/\cosh^2 x$ for the SH. On the other hand, exact sech-shaped or cnoidal-shaped solutions can be found by “inverse engineering” (Abdullaev and Umarov, 2014; Truong Vu *et al.*, 2015).

Another case where stationary modes in \mathcal{PT} -symmetric quadratic media were found (Moreira, Konotop, and Malomed, 2013) corresponds to the periodic \mathcal{PT} -symmetric potential $V(x)$ given by Eq. (143) in the FF and a real periodic potential $\tilde{V}(x) = \tilde{V}_1 \cos^2(2x)$ in the SH. The resulting

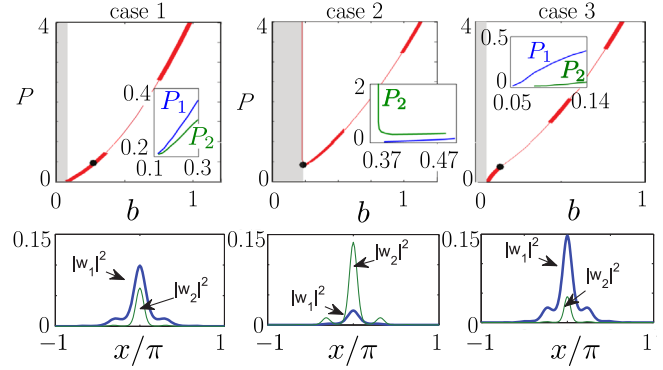


FIG. 44. Upper panels: families of fundamental solitons in the semi-infinite gap. Left, center, and right panels correspond to cases 1, 2, and 3 with $\beta = -0.316, 0,$ and $-0.5134,$ respectively. Thick and thin lines correspond to stable and unstable solitons. Shaded regions denote bands of the FF and/or SH. Insets show powers of the FF (P_1) and SH (P_2) fields close to the band edge. Lower panels: intensities of stable fundamental solitons indicated by black circles in the respective upper panels: $b = 1.25$ (case 1), 1.43 (case 2), and 1.21 (case 3). Other parameters are $V_0 = \tilde{V}_0 = 2$ and $W_0 = 0.35$. Adapted from Moreira, Konotop, and Malomed, 2013.

periodic model supports families of gap solitons which bifurcate from band edges of the underlying linear model. Such bifurcations are always characterized by vanishing fields in the FF ($w_1 \rightarrow 0$), while the asymptotics of SH may be different. More precisely, there exist three possibilities for bifurcation of gap solitons from band edges.

Case 1: Both components are of the same order, i.e., $w_2 \sim w_1$ and $w_1 \rightarrow 0$. In this case (see left column of Fig. 44), in the vicinity of the bifurcation the nonlinearity is negligible, and both components are governed by linear equations: the FF is described by a solution of the stationary equation (145) with the pair (μ, ψ) replaced by (b, w_1) , i.e., $w_1 \sim \psi$, while $w_2 \sim \tilde{\psi}$, where $\tilde{\psi}$ solves the linear Mathieu equation with the potential $\tilde{V}(x)$. For the existence of a gap soliton, the propagation constant b should belong to the gaps of both FF and SH, which requires a nonempty overlap of the stop gaps of both components; such an overlap can be termed a *total gap*. Moreover, the adopted scaling implies that band edges of FF and SH should coincide exactly. This constraint makes this case uncommon, although in practice it can always be achieved by adjusting the mismatch parameter β .

Case 2: The SH field remains finite: $w_2 = \mathcal{O}(1)$ and $w_1 \rightarrow 0$. In this case (see middle column of Fig. 44), the vicinity of the total gap must coincide with the respective SH gap edge. Then, while the FF component is vanishing ($w_1 \rightarrow 0$) as b approaches the total gap edge, the amplitude of the SH w_2 remains finite and its width increases (i.e., the SH in this limit becomes delocalized). This explains divergent powers of the SH P_2 (shown in the inset in the middle panel of Fig. 44) and, respectively, the divergence of the total power.

Case 3: The SH amplitude scales as the square of the FF amplitude: $w_2 = \mathcal{O}(w_1^2)$ and $w_1 \rightarrow 0$. This case (see right column of Fig. 44) takes place when an edge of the total gap, from which gap solitons bifurcate, is determined by one of the

respective edges of the gap of the FF. Then in the small-amplitude limit the SH is determined by the field distribution in the FF and the total power vanishes at the bifurcation point.

B. \mathcal{PT} -symmetric coupler with quadratic nonlinearity

A model of a \mathcal{PT} -symmetric coupler with $\chi^{(2)}$ nonlinearity, introduced by Li, Zezyulin, Kevrekidis *et al.* (2013), reads

$$\begin{aligned} i\dot{u}_1 &= k_1 u_2 - 2u_1^* v_1 + i\gamma_1 u_1, \\ i\dot{v}_1 &= k_2 v_2 - u_1^2 - \beta v_1 + i\gamma_2 v_1, \\ i\dot{u}_2 &= k_1 u_1 - 2u_2^* v_2 - i\gamma_1 u_2, \\ i\dot{v}_2 &= k_2 v_1 - u_2^2 - \beta v_2 - i\gamma_2 v_2. \end{aligned} \quad (160)$$

Here two modes propagate in each waveguide: the FF u_j and the SH v_j , and $j = 1, 2$ enumerates the coupler arm. The linear coupling between two FFs (two SHs) is described by k_1 (k_2), the gain (loss) strength in the arms is given by γ_j , and β is the mismatch parameter.

Stationary modes of Eq. (160) are searched in the form $(u_1, v_1, u_2, v_2)^T = e^{-i\Lambda b z} \mathbf{w}$, where $\Lambda = \text{diag}(1, 2, 1, 2)$, b is the propagation constant, and $\mathbf{w} = (w^{(1)}, w^{(2)}, w^{(3)}, w^{(4)})^T$ solves the stationary nonlinear problem $E\Lambda\mathbf{w} = H\mathbf{w} - F(\mathbf{w})\mathbf{w}$, where the matrix H describes the linear part of the system (160) and the matrix function $F(\mathbf{w})$ has $F_{1,2} = 2[w^{(1)}]^*$, $F_{2,1} = w^{(1)}$, $F_{3,4} = 2[w^{(3)}]^*$, and $F_{4,3} = w^{(3)}$ with other entries being zero. H is \mathcal{PT} symmetric with $\mathcal{P} = \sigma_1 \otimes \sigma_0$.

From a physical point of view Eq. (160) represents a coupler with each of the arms guiding two modes; from a mathematical point of view, it is a quadrimer similar to the one considered in Sec. IV.B. Eigenvalues of H are given by

$$\tilde{b}_{1,2} = \pm \sqrt{k_1^2 - \gamma_1^2}, \quad \tilde{b}_{3,4} = \frac{1}{2} \left(-\beta \pm \sqrt{k_2^2 - \gamma_2^2} \right),$$

and its eigenvectors are

$$\begin{aligned} \tilde{\mathbf{w}}_1 &= (e^{i\theta_1}, 0, e^{-i\theta_1}, 0)^T, & \tilde{\mathbf{w}}_2 &= i(e^{-i\theta_1}, 0, -e^{i\theta_1}, 0)^T, \\ \tilde{\mathbf{w}}_3 &= (0, e^{i\theta_2}, 0, e^{-i\theta_2})^T, & \tilde{\mathbf{w}}_4 &= i(0, e^{-i\theta_2}, 0, -e^{-i\theta_2})^T, \end{aligned}$$

where $\theta_{1,2} = (1/2) \arctan(\gamma_{1,2}/\sqrt{k_{1,2}^2 - \gamma_{1,2}^2})$. If \mathcal{PT} symmetry is unbroken, i.e., $|\gamma_{1,2}| < k_{1,2}$, then eigenvectors $\tilde{\mathbf{w}}_j$ are \mathcal{PT} invariant, i.e., $\mathcal{PT} \tilde{\mathbf{w}} = \tilde{\mathbf{w}}$.

In the nonlinear problem, one looks for nonlinear modes obtained by continuation from the linear eigenvectors (see Sec. IV.C.3.a). Note that $F(\tilde{\mathbf{w}}_{3,4}) = 0$, which means that the eigenvectors $\tilde{\mathbf{w}}_{3,4}$ also solve the nonlinear problem (160). As a result, one can construct nonlinear modes of two different types. For the first type, one looks for nonlinear continuation of $\tilde{\mathbf{w}}_{1,2}$ in the form of expansions $\mathbf{w}_j = \varepsilon \tilde{\mathbf{w}}_j + \varepsilon^2 \mathbf{W}_j + \dots$ and $b_j = \tilde{b}_j + \varepsilon b_j^{(2)} + \dots$, where the coefficients \mathbf{W}_j and $b_j^{(2)}$ ($j = 1, 2$) are computed from the solvability conditions at higher orders. This is the standard expansion: in the linear limit ($\varepsilon = 0$), the power of nonlinear modes $P = |w^{(1)}|^2 + |w^{(3)}|^2 + 2(|w^{(1)}|^2 + |w^{(3)}|^2)$ (which corresponds to the Manley-Rowe invariant of the conservative coupler with

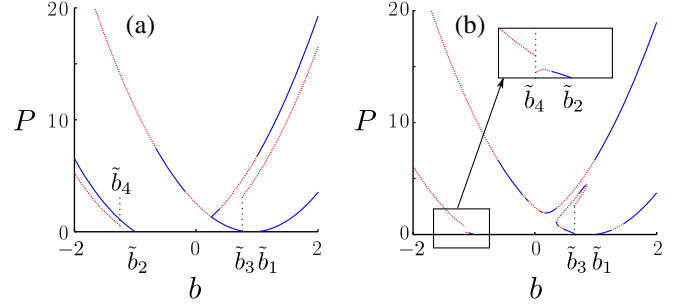


FIG. 45. Families of nonlinear modes in $\chi^{(2)}$ coupler (160) for (a) $k_1 = 1$, $k_2 = 2$, $\beta = 0.5$, and $\gamma_{1,2} = 0$; and (b) $\gamma_1 = 0.1$ and $\gamma_2 = 0.9$. Solid blue and dashed red segments correspond to stable and unstable modes, respectively. Adapted from Li, Zezyulin, Kevrekidis *et al.*, 2013.

$\gamma_{1,2} = 0$) vanishes. For modes of the second type, which bifurcate from $\tilde{\mathbf{w}}_{3,4}$, the expansions are of the form $\mathbf{w}_j = \alpha_j \tilde{\mathbf{w}}_j + \varepsilon \mathbf{W}_j + \dots$, $b_j = \tilde{b}_j + \varepsilon^2 b_j^{(2)} + \dots$, where α_j ($j = 3, 4$) are (generally nonzero) coefficients. In this case, at $\varepsilon = 0$ the mode amplitudes do not vanish. Admissible values of the coefficients α_j are found from compatibility conditions that arise from the underlying expansions. Generally speaking there exist two admissible values of α_j , thus $\tilde{\mathbf{w}}_3$ and $\tilde{\mathbf{w}}_4$ admit two continuous families of nonlinear modes (Li, Zezyulin, Kevrekidis *et al.*, 2013).

The numerical results are illustrated in Fig. 45. In both conservative and \mathcal{PT} -symmetric cases there are two solution families bifurcating from the eigenstates $\tilde{\mathbf{w}}_1$ and $\tilde{\mathbf{w}}_2$. These bifurcations take place at the limit $P = 0$. Bifurcations of nonlinear modes from $\tilde{\mathbf{w}}_{3,4}$ occur at finite P (in some cases these values of P are quite small and hardly distinguishable from $P = 0$ on the scale of the figure). In the conservative case, either $\tilde{\mathbf{w}}_3$ or $\tilde{\mathbf{w}}_4$ gives rise to one physically distinct family. In the \mathcal{PT} -symmetric case two distinct solution families originate from either of $\tilde{\mathbf{w}}_3$ or $\tilde{\mathbf{w}}_4$.

IX. PARTIAL \mathcal{PT} SYMMETRY

Multidimensional complex potentials considered so far obey the \mathcal{PT} symmetry with the canonical \mathcal{P} operator (2) resulting in inversion of all spatial variables. Now we discuss situations where the complex potential is not \mathcal{PT} symmetric in this sense but is *partially \mathcal{PT} symmetric* meaning that the potential is invariant under complex conjugation and reflection in a *single* spatial direction. Such potentials can still admit all-real spectra and support continuous families of solitons (Yang, 2014c; Kartashov, Konotop, and Torner, 2015).

The mathematical model we use is a 2D NLS equation (141) with a potential $U_{2D}(x, y)$ which is partially \mathcal{PT} symmetric with respect to x :

$$U_{2D}^*(x, y) = U_{2D}(-x, y). \quad (161)$$

No symmetry is assumed in the y direction.

First, we argue that the linear spectrum of a partially \mathcal{PT} -symmetric potential can be all real. If the potential is separable, i.e., $U_{2D} = U_{2D}^0 = V_1(x) + V_2(y)$, then the partial

\mathcal{PT} -symmetry condition (161) implies that $V_1^*(x) = V_1(-x)$, $V_2^*(y) = V_2(y)$, and its eigenvalues are $\lambda = \Lambda_1 + \Lambda_2$, where Λ_j are eigenvalues of 1D potentials $V_j(x)$. Since $V_1(x)$ is \mathcal{PT} symmetric, its eigenvalues Λ_1 can be all real. Since $V_2(y)$ is strictly real, i.e., the respective Hamiltonian is Hermitian, its eigenvalues Λ_2 are all real as well. Thus eigenvalues λ of the separable potential $U_{2D}(x, y)$ can be all real.

Next, we consider a separable potential with all-real spectra perturbed by a localized potential $U_{2D}^p(x, y)$: $U_{2D} = U_{2D}^0 + \epsilon U_{2D}^p$, where ϵ is a small real parameter, and both U_{2D}^0 and U_{2D}^p satisfy the partial \mathcal{PT} symmetry (161). Since U_{2D}^p is localized, the continuous spectrum of the perturbed potential U_{2D} coincides with that of U_{2D}^0 and is thus all real. Regarding isolated eigenvalues of U_{2D} , they can be shown to be real as well by a perturbation calculation (Bender and Jones, 2008; Yang, 2014c).

Partially \mathcal{PT} -symmetric potentials possess some typical feature of standard \mathcal{PT} -symmetric potentials, such as a phase transition in the linear case and the existence of continuous families of stationary solitons in the nonlinear case. One can show that from each simple real discrete eigenvalue $\tilde{\mu}_n$ of a partially \mathcal{PT} -symmetric potential, a continuous family of solitons bifurcates out under both focusing and defocusing nonlinearities. Indeed, introducing small-amplitude expansions for nonlinear modes bifurcating from a linear eigenvalue $\tilde{\mu}_n$ with an eigenfunction $\tilde{\psi}_n(x, y)$, similar to those in Eqs. (135), one can show that bifurcations are governed by the coefficient $\mu_n^{(2)}$ defined by Eq. (136), where the integrals should be taken over $dx dy$. For a real eigenvalue $\tilde{\mu}_n$, its eigenfunction $\tilde{\psi}_n$ inherits the partial \mathcal{PT} symmetry of the potential. Thus both integrals in the expression for $\mu_n^{(2)}$ are real, so $\mu_n^{(2)}$ is also real. Pursuing the perturbation calculation to higher orders, one can construct a perturbation solution to all powers of ϵ , and thus a continuous family of solitons, parametrized by μ , bifurcates out from the linear eigenmode $(\tilde{\mu}_n, \tilde{\psi}_n)$.

The existence of soliton families can be verified numerically. For this purpose, we take the partially \mathcal{PT} -symmetric potential

$$U_{2D} = -3(e^{-|r-r_+|^2} + e^{-|r-r_-|^2}) - 2(e^{-|r+r_+|^2} + e^{-|r+r_-|^2}) + i\gamma(-e^{-|r+r_-|^2} + e^{-|r+r_+|^2} - 2e^{-|r-r_+|^2} + 2e^{-|r-r_-|^2}),$$

where $\mathbf{r}_\pm = (\pm x_0, y_0)$. (162)

For $\gamma = 0.1$ and $x_0 = y_0 = 1.5$, this potential has three discrete eigenmodes, from each of which a soliton family bifurcates out. Soliton families bifurcated from the first and second linear eigenmodes of the potential under focusing nonlinearity ($g = 1$) are displayed in Fig. 46(a). Interestingly, these two power curves are connected through a fold bifurcation and have an upper bound. The profile of a stable soliton on the power curve is displayed in Figs. 46(b) and 46(c).

Results of numerical linear-stability analysis show that most solitons of the upper power branch are stable. This is surprising, since in conservative potentials solitons on the upper power branch are generally less stable. The increased stability of the upper power branch here is due to the complex

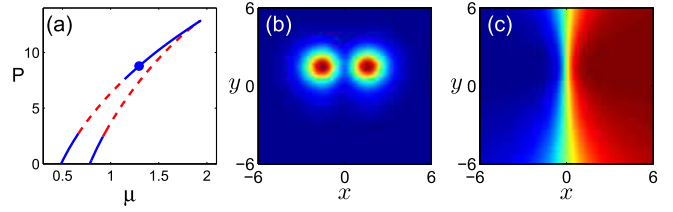


FIG. 46. (a) Power diagram of soliton families in the potential (162) under focusing nonlinearity (solid blue segments are stable and dashed red unstable); (b), (c) amplitude and phase fields of the soliton at the marked point of the power curve. Adapted from Yang, 2014c.

partially \mathcal{PT} -symmetric potential (162), which stabilizes solitons at higher powers.

Solitons in Fig. 46 are partially \mathcal{PT} symmetric as the underlying potential (162) itself. In special classes of partially \mathcal{PT} -symmetric potentials, symmetry breaking of solitons can occur, where families of nonpartially \mathcal{PT} -symmetric solitons can bifurcate out from the base branch of partially \mathcal{PT} -symmetric solitons (Yang, 2015). This situation is analogous to 1D \mathcal{PT} -symmetric potentials [see Sec. VI.C and Yang (2014d)].

X. SPECTRAL SINGULARITIES

A. Spectral singularities in the linear theory

A non-Hermitian Hamiltonian at an exceptional point does not admit a complete biorthonormal basis and cannot be diagonalized. Alternatively, completeness of the basis is lost if the continuum spectrum features a *spectral singularity* (Naimark, 1954), which may be relevant for physical applications (Longhi, 2009a, 2009b, 2010; Mostafazadeh and Mehri-Dehnavi, 2009; Mostafazadeh, 2009b, 2009c, 2011a, 2011b); see also Mostafazadeh (2015) for a recent review.

Consider an eigenvalue problem $H\tilde{\psi}_k = k^2\tilde{\psi}_k$ for the Schrödinger operator (6) with a localized complex potential $\lim_{x \rightarrow \pm\infty} |U(x)| = 0$ (the tilde stands for eigenstates of the linear problem). The associated Jost solutions $\tilde{\psi}_{k\pm}(x)$ are defined by their asymptotics $\tilde{\psi}_{k\pm}(x) \sim e^{\pm ikx}$ for $x \rightarrow \pm\infty$, while an arbitrary eigenfunction of the continuous spectrum has asymptotics $\tilde{\psi}_k(x) \rightarrow A_{\pm}e^{ikx} + B_{\pm}e^{-ikx}$ at $x \rightarrow \pm\infty$. The constants A_{\pm} and B_{\pm} are not independent: the link among them defines the transfer matrix $M(k)$:

$$(A_+, B_+)^T = M(k)(A_-, B_-)^T. \quad (163)$$

The Wronskian of the Jost solutions $W[\tilde{\psi}_{k-}, \tilde{\psi}_{k+}] = 2ikM_{22}(k)$ is x independent and $\det M(k) = 1$. If $M_{22}(k_*) = 0$ for some real $k_* \neq 0$, then the number $k_*^2 > 0$ is said to be a spectral singularity (Mostafazadeh and Mehri-Dehnavi, 2009). The explicit form of the Wronskian implies that the linear dependence of the Jost solutions is necessary and sufficient for the spectral singularity (Mostafazadeh, 2013a). Note that bound states of H , if any, are also defined by the roots of $M_{22}(k)$ which, however, are located in the upper half plane of the complex k : $\text{Im}(k) > 0$.

Spectral singularities are known for a number of particular cases, including the steplike potential (35) (Mostafazadeh, 2009b, 2011a, 2014), δ -function potentials (Mostafazadeh and Mehri-Dehnavi, 2009), \mathcal{PT} -symmetric Scarff II potentials (Ahmed, 2009), and special types of periodic potentials (Gasymov, 1980; Longhi, 2010).

Consider now a monochromatic wave incident on the potential $U(x)$ either from the left or from the right and suppose that there exists a real k_* solving $M_{22}(k_*) = 0$, i.e., there exists a spectral singularity. The relations (38) among the scattering characteristics still hold. Thus at the spectral singularity the reflection and transmission coefficients diverge, behaving like zero-width resonances (Mostafazadeh, 2009b). It follows from Eq. (163) that there exists a solution with $A_-(k_*) = B_+(k_*) = 0$. This is a solution where only radiation propagating away from the potential exists, i.e., it means that the potential operates as a laser (Longhi, 2010; Mostafazadeh, 2011a).

On the other hand, if a medium allows for a zero of $M_{11}(\tilde{k}_*) = 0$ with real \tilde{k}_* , then there exists a solution with $A_+(\tilde{k}_*) = B_-(\tilde{k}_*) = 0$ meaning the absence of radiation propagating away from the potential. Such a medium operates as a coherent perfect absorber (CPA), which was predicted by Chong *et al.* (2010) and observed experimentally by Wan *et al.* (2011). $(\tilde{k}_*)^2$ is referred to as time-reversed spectral singularity (Longhi, 2011; Mostafazadeh, 2015). Realization of a CPA using a pair of passive resonators was reported by Sun *et al.* (2014). They observed complete absorption of light when the system was in a (passive) \mathcal{PT} -symmetric phase; however, the complete absorption was not observed when the \mathcal{PT} phase was broken.

In a generic case, there may exist either spectral singularities or time-reversed spectral singularities, or both with $k_* \neq \tilde{k}_*$. However, if a complex potential is \mathcal{PT} symmetric, then for each k^* there exist $\tilde{k}_* = k_*$ giving origin to so-called self-dual spectral singularity. Such a potential can operate either as a laser or as an absorber, i.e., as a CPA laser (Longhi, 2010; Chong, Ge, and Stone, 2011; Mostafazadeh, 2012). Furthermore, the interplay between \mathcal{PT} symmetry and Fano resonances can result in singularities emerging from the coincidence of two independent singularities and having highly directional responses (Ramezani *et al.*, 2014).

B. Spectral singularities of a nonlinear layer

Generalization of spectral singularities to nonlinear media is justified by at least two reasons. First, in a realistic system infinite transmission or reflection coefficients are the idealization, and regularizing mechanisms must be involved, nonlinearity being one of them. Second, the nonlinearity is expected to become a dominating mechanism at large field amplitudes.

Effects of nonlinearity on spectral singularities were considered by Mostafazadeh (2013a, 2013b, 2014) for the nonlinear eigenvalue problem

$$H^{nl}\psi_k = k^2\psi_k, \quad H^{nl}\psi \equiv -\psi'' + U(x)\psi + F(\psi', \psi, x)\psi, \quad (164)$$

where $\psi(x)$ is a complex-valued function, $U(x)$ is a rapidly decaying complex potential, and $F(\psi', \psi, x)$ describes the nonlinearity, which is confined to the interval $[0, 1]$: $F(\psi', \psi, x) \equiv 0$ for $x < 0$ and $x > 1$. In this case one can still exploit Jost solutions $\tilde{\psi}_{k\pm}$ of the underlying linear problem and define a nonlinear spectral singularity as follows (Mostafazadeh, 2013a): a positive real number k^2 is a spectral singularity of H^{nl} if there exists a solution ψ_k of the nonlinear problem (164) such that $\lim_{x \rightarrow \pm\infty} \psi_k(x) = C_{\pm} \tilde{\psi}_{k\pm}(x)$, where C_{\pm} are complex numbers.

Continuity of the field and its derivative at the boundaries of the nonlinear medium requires

$$\psi_k(0) = \psi_{k-}(0), \quad \psi'_k(0) = \psi'_{k-}(0), \quad (165a)$$

$$\psi_k(1) = \psi_{k+}(1), \quad \psi'_k(1) = \psi'_{k+}(1). \quad (165b)$$

This suggests an algorithm for obtaining spectral singularities (Mostafazadeh, 2013a, 2013b). Consider a solution $\psi_{k-}(x)$ [or $\psi_{k+}(x)$] of Eq. (164) on the semiaxis $x \in [0, \infty)$ [or $x \in (-\infty, 1]$] with the ‘‘initial’’ conditions (165a) [or (165b)]. Compute k ensuring the asymptotics $\psi_k(x) \sim C_+ e^{ikx}$ as $x \rightarrow \infty$ [or $\psi_k(x) \sim C_- e^{-ikx}$ as $x \rightarrow -\infty$]. If the problem has a real solution for either of $\psi_k(x)$, the respective k then yields a spectral singularity k^2 .

Let us consider an example of a non- \mathcal{PT} -symmetric potential $U(x) = \zeta\delta(x-a)$, where ζ is a complex number, $a \in (0, 1)$ is the position of the defect inside the nonlinear layer, and Kerr nonlinearity $F \equiv \chi|\psi|^2$ with real χ for $x \in (0, 1)$ and $F \equiv 0$ otherwise (Mostafazadeh, 2013a). Assuming $\chi|\psi|^2$ to be small, one finds that a nonlinear spectral singularity occurs at k satisfying $\zeta \approx 2ik + i\chi|A_-|^2(e^{2ik(1-a)} + e^{2ika} - 2)/(2k)$ [at $\chi = 0$ one recovers the linear spectral singularity (Mostafazadeh and Mehri-Dehnavi, 2009)]. The field intensity can be found from

$$\chi|A_-|^2 \approx -k\text{Re}(\zeta)/(\cos[k(1-2a)]\sin k), \quad (166)$$

which is valid for $\text{Re}(\zeta) \ll 1$ and $k \neq \pi m, \pi(m+1/2)/(1-2a)$. The obtained nonlinear spectral singularities obey parity symmetry, i.e., they are invariant under the transformation $a \rightarrow 1-a$; they are amplitude dependent and sensitive to the location of the defect a . One also observes that the right-hand side of Eq. (166) has a minimal value, which means that no singularities arise if the amplitude is below a certain threshold.

A nonlinear \mathcal{PT} -symmetric bilayered structure with the potential (35) was considered by Mostafazadeh (2014). It was found that for $V_0 = 1$ the lossy layer results in a decrease of the lasing threshold of the gain. On the other hand, when $V_0 - 1 \gg \gamma$ the threshold value of the gain-loss coefficient, considered as a function of the real part of the refractive index, has a minimum (for a homogeneous active layer the lasing threshold decreases with V_0).

From these examples, one can conclude that while the cubic nonlinearity makes the spectral singularity amplitude dependent, it does not regularize the scattering characteristics. Similar conclusions can be reached from the study of steplike potentials (35) (Mostafazadeh, 2013b, 2014).

However, regularization of the spectral singularity is indeed possible. It was obtained by Liu, Gupta, and Agarwal (2014) for a \mathcal{PT} -symmetric bilayered structure with saturable nonlinearity modeled by

$$\frac{d^2\psi}{dx^2} + k^2\xi(x)\frac{(\delta + i)\psi}{1 + \delta^2 + \alpha|\psi|^2} = 0, \quad (167)$$

where $\xi(x) = -1$ for $x \in (-L, 0)$ and $\xi(x) = 1$ for $x \in (0, L)$, and δ, α are real constants.

The described algorithm of obtaining nonlinear spectral singularities relies on the solution of the scattering problem where the output radiation is fixed, rather than on the solution of a problem with the fixed amplitude of the incident wave. These are two different statements of the nonlinear scattering problem, referred to as the *fixed-output* and *fixed-input* problems [see, e.g., Konotop and Vázquez (1994) and references therein]. The fixed-input problem manifests multi-stability phenomenon, while the fixed-output problem does not. In the numerical study of transmission-coefficient dependence on the input intensity, bistability was reported by Liu, Gupta, and Agarwal (2014).

XI. \mathcal{PT} SYMMETRY IN KLEIN-GORDON MODELS

\mathcal{PT} symmetry can be introduced in KG models which in the conservative case read

$$u_{tt} - u_{xx} + f(u) = 0, \quad (168)$$

where $f(u)$ is a nonlinear function of the field $u(x, t)$. The two celebrated examples are the sine-Gordon (SG) equation given by $f(u) = \sin(u)$ and the ϕ^4 model given by $f(u) = 2(u^3 - u)$. Now the \mathcal{PT} symmetry is defined by the transformation $(x, t) \rightarrow (-x, -t)$. To preserve this symmetry, gain and loss can be introduced by adding a spatially inhomogeneous dissipative term $\gamma(x)u_t$ with $\gamma(x)$ being an odd function: $\gamma(x) = -\gamma(-x)$ (Demirkaya *et al.*, 2013, 2014). This yields the model

$$u_{tt} - u_{xx} + \gamma(x)u_t + f(u) = 0, \quad (169)$$

where lossy and gain domains correspond to regions with $\gamma(x) > 0$ and $\gamma(x) < 0$, respectively.

For the \mathcal{PT} -symmetric KG model (169), the Galilean invariance is broken. Therefore, unlike its conservative counterpart (168), the model does not admit traveling-wave solutions. Nevertheless, stationary solutions are not affected by the dissipation and gain and are given by $u = \phi(x)$, where $\phi(x)$ solves $\phi_{xx} = f(\phi)$. The most interesting solution is the kink, which is a topological object given by $\phi(x) = 4 \arctan(e^{x-x_0})$ in the SG model, and $\phi(x) = \tanh(x - x_0)$ in the ϕ^4 model (x_0 stands for the position of the kink center).

To study linear stability of these kinks, one substitutes $u(t, x) = \phi(x) + v(x)e^{\lambda t}$, with $v(x) \ll 1$, into Eq. (169) and obtains a linear eigenvalue problem

$$\lambda^2 v + \lambda\gamma(x)v - v_{xx} + f'(\phi)v = 0. \quad (170)$$

Demirkaya *et al.* (2014) performed a general analysis of Eq. (170) as well as a numerical study of stability for $\gamma(x) = \epsilon x e^{-x^2/2}$, where the constant ϵ characterizes the strength of gain and loss. The main findings for SG and ϕ^4 kinks can be summarized as follows. The linear-stability spectrum is unaffected by $\gamma(x)$ (except for a possible shift of the discrete spectrum along the imaginary axis) if the kink center x_0 coincides with the boundary between the domains with gain and loss, i.e., with $x = 0$. If, however, the kink center is shifted to the lossy or to the gain region, then the kink becomes spectrally stable and unstable, respectively. Behavior of kinks in \mathcal{PT} -symmetric SG and ϕ^4 models can also be described by means of a generalized collective coordinate method which was developed by Kevrekidis (2014) on the basis of a proposition of Galley (2013) who suggested an approach to formulation of the Lagrangian and Hamiltonian dynamics of generic nonconservative systems.

The conservative SG equation is also known to admit a breather solution

$$\phi = 4 \arctan \frac{\sigma \cos[a(t - t_0)]}{a \cosh[\sigma(x - x_0)]},$$

where $\sigma = \sqrt{a}$, $0 < a < 1$, x_0 is the center of the breather, and t_0 is a constant. Lu, Kevrekidis, and Cuevas-Maraver (2014) addressed the existence and stability of breathers in the \mathcal{PT} -symmetric SG model. Unlike kinks, breathers are always affected by the gain and loss because of their time-periodic nature. This, in particular, makes their persistence in the \mathcal{PT} -symmetric model possible only if they are centered at the boundary between the gain and loss. Numerical analysis shows that even for a small amplitude of the gain and loss $|\gamma(x)|$ the breather becomes unstable through a Hopf bifurcation. It was also found that if a breather is initially centered at the lossy side, then it will decay away. If, however, the breather is initially shifted toward the gain region, then its energy will grow until a pair of a kink and an antikink is nucleated.

XII. \mathcal{PT} DEFORMATIONS OF NONLINEAR EQUATIONS

The nonlinear models we considered so far were constructed by adding nonlinear terms (physically, by accounting for nonlinear interactions) to linear models with complex potentials, dissipation, or gain. In this section, we address another possibility, where the so-called \mathcal{PT} deformation (alias \mathcal{PT} extension) is performed by extending purely real coefficients of a nonlinear equation to the complex plane.

A. Deformed KdV equation

The idea was formulated by Bender *et al.* (2007) and can be described as follows. Consider wave dynamics governed by the KdV equation

$$u_t + uu_x + u_{xxx} = 0. \quad (171)$$

Now under parity transformation ($x \rightarrow -x$), u also has to change its sign $u \rightarrow -u$. Since we are dealing with a classical Hamiltonian system, the time reversal operator \mathcal{T} results in the

change $t \rightarrow -t$ with simultaneous change $u \mapsto -u$. Then in order to continue u from the real axis to the complex plane, one can “borrow” from the quantum mechanics the rule of changing $i \rightarrow -i$ when applying time reversal. This suggests to introduce a \mathcal{PT} -symmetric extension of the KdV equation as (Bender *et al.*, 2007)

$$u_t - iu(iu_x)^\varepsilon + u_{xxx} = 0, \quad \varepsilon \in \mathbb{R}. \quad (172)$$

Obviously, both Eqs. (171) and (172) are invariant under the \mathcal{PT} transformation. At $\varepsilon = 1$, Eq. (172) reduces to Eq. (171). Other physically relevant cases include $\varepsilon = 0$, which leads to the dispersive equation $v_t + v_{xxx} = 0$ with $v = e^{-it}u$, and $\varepsilon = 3$, which leads to the nonlinear equation $u_t - u(u_x)^3 + u_{xxx} = 0$ (Fushchych, Serov, and Amerov, 1991; Bender *et al.*, 2007).

Another \mathcal{PT} deformation of the KdV equation can be obtained using the Hamiltonian formulation. The original KdV equation (171) can be written in a Hamiltonian form as

$$u_t = \frac{\partial}{\partial x} \frac{\delta H}{\delta u(x)} = \{u, H\}, \quad (173)$$

where

$$H(t) = \int_{-\infty}^{\infty} \mathcal{H}(x, t) dx, \quad \mathcal{H}(x, t) = \frac{1}{2} u_x^2 + u^3. \quad (174)$$

Fring (2007) considered a \mathcal{PT} -symmetric generalization of the Hamiltonian density $\mathcal{H}(x, t)$ as

$$\mathcal{H}(x, t) = -(1 + \varepsilon)^{-1} (iu_x)^{\varepsilon+1} + u^3, \quad (175)$$

which satisfies the relation $\mathcal{H}(u(x)) = \mathcal{H}^*(u(-x))$. The latter property ensures that the energy on each symmetric interval $[-a, a]$ is real:

$$E = \int_{-a}^a \mathcal{H}(u(x)) dx = \int_{-a}^a \mathcal{H}^*(u(x)) dx = E^*. \quad (176)$$

Equation (173) with the Hamiltonian (175) yields another \mathcal{PT} deformed KdV equation (Fring, 2007)

$$u_t - 6uu_x + i\varepsilon(\varepsilon - 1)(iu_x)^{\varepsilon-2} u_{xx}^2 + \varepsilon(iu_x)^{\varepsilon-1} u_{xxx} = 0. \quad (177)$$

While the physical relevance of models like Eq. (172) or (177) for arbitrary values of the deformable parameter ε remains an open question, the systems themselves possess some interesting properties which justify the attracted interest. One of them is the existence of integrals of motion, which is a nontrivial issue for nonconservative systems. In particular, model (172) with $\varepsilon = 3$ admits two integrals of motion (Bender *et al.*, 2007)

$$I_{\pm} = \int dx \int_0^{2^{1/3}u(x,t)} ds [\text{Bi}(s) \pm \sqrt{3}\text{Ai}(s)], \quad (178)$$

where $\text{Ai}(\cdot)$ and $\text{Bi}(\cdot)$ are the Airy functions. The quantity I_{\pm} is strictly positive [when $u(x, t)$ is not identically zero] and therefore can be interpreted as the energy.

For other \mathcal{PT} deformations of the KdV equation, as well as for examples of their solutions, see Bagchi and Fring (2008)

and Cavaglia, Fring, and Bagchi (2011). General aspects of preservation of integrability under \mathcal{PT} -symmetric deformations were considered by Assis and Fring (2009, 2010) by means of the Painlevé analysis.

B. Deformed Hopf and Burgers equations

Cavaglia and Fring (2012) studied a \mathcal{PT} -deformed Hopf equation

$$u_t - if(u)(iu_x)^\varepsilon = 0, \quad (179)$$

where $f(u)$ is a well-behaved function, and ε is a real rational number. For $\varepsilon = 1$, Eq. (179) reduces to the real-valued Hopf equation

$$w_t + f(w)w_x = 0. \quad (180)$$

This deformation extends the earlier results of Bender and Feinberg (2008) on the \mathcal{PT} deformation $v_t - iv(iv_x)^\varepsilon = 0$ of the inviscid Burgers equation $w_t + ww_x = 0$.

The \mathcal{PT} -deformed Hopf equation (179) can be obtained from its original version (180) for arbitrary rational ε through an explicit map, i.e., change of variables (Curtright and Fairlie, 2008; Cavaglia and Fring, 2012). For the particular case of $f(w) = w^n$, the map reads $w \mapsto \sqrt[n]{\varepsilon u(iu_x)^n}$. This direct mapping allows for the straightforward analysis of wave dynamics in the deformed model on the basis of the knowledge about the “seed” real nonlinear equation. We illustrate this on the example of shock formation (Bender and Feinberg, 2008; Cavaglia and Fring, 2012). Suppose the initial condition to the Hopf equation (180) is $w(x_0, 0) = w_0(x_0)$, and consider a characteristic, i.e., a curve in the plane (x, t) for which $w(x, t) = w_0(x_0)$. The characteristic has the form $x = f(w_0)t + x_0$. At the point of gradient catastrophe two characteristics cross and w_x tends to infinity. Then by computing

$$w_x = w'_0(x_0) \frac{dx_0}{dx} = \frac{w'_0(x_0)}{1 + t[df(w_0)/dx_0]} \quad (181)$$

and utilizing the described map, one finds that for $f(w) = w^n$ the earliest time for shock formation in the \mathcal{PT} -deformed Hopf equation (179) is

$$t_s^w = -e^{-1/n} \left[\frac{d}{dx_0} [u_0^{1/n} (iu_{x_0})^{(n-1)/n}] \right]^{-1}. \quad (182)$$

Requiring the time t_s^w to be real, one finds that this condition is satisfied under the replacement $u_0 \rightarrow i^\alpha \tilde{u}_0$, where $\tilde{u}_0 \in \mathbb{R}$, $\alpha = (4m \pm 1)n/\varepsilon$, and $m \in \mathbb{Z}$. Thus for certain combinations of ε and n one cannot observe shock wave formation for real solutions of the deformed equation (179). On the other hand, the deformed model offers other possibilities for singularities of the solutions to occur (Cavaglia and Fring, 2012). Such possibilities correspond to a curvature catastrophe. For the inviscid Burgers equation [$f(w) = w$] this phenomenon stems from the relation $w_x = i\varepsilon(iu_x)^{\varepsilon-2} [u_x^2 + (\varepsilon - 1)uu_{xx}]$, meaning that the shock of the u field ($u_x \rightarrow \infty$) always corresponds to the shock of w . In the meantime, the converse is not

necessarily true because $w_x \rightarrow \infty$ can also occur when $u_{xx} \rightarrow \infty$.

For \mathcal{PT} -symmetric deformations of the Burgers equation see Yan (2008, 2013).

C. Deformed short pulse equation

\mathcal{PT} deformation of yet another model, the short pulse equation $u_{xt} = u + \frac{1}{2}(u^2 u_x)_x$ (Schäfer and Wayne, 2004), was constructed by Yan (2012):

$$i[(iu_x)^\sigma]_t = u + bu^m + ic[u^n(iu_x)^\varepsilon]_x. \quad (183)$$

Here the parameters b, c, σ, n, m , and ε are all real. For their specific choices Eq. (183) admits soliton, kink, or compacton solutions.

D. Nonlocal NLS equation

The NLS equation (28) belongs to the so-called Ablowitz-Kaup-Newell-Segur (AKNS) scheme (Ablowitz *et al.*, 1973), which allows one to obtain a wide class of equations integrable by the inverse scattering transform. More specifically, the NLS equation (28) with $g = 2$ is a particular case of the more general integrable system (Ablowitz and Segur, 1981; Novikov *et al.*, 1984)

$$i\psi_t + \psi_{xx} + 2\phi\psi^2 = 0, \quad i\phi_t - \phi_{xx} - 2\psi\phi^2 = 0, \quad (184)$$

subject to the reduction $\phi(x, t) = \psi^*(x, t)$.

Ablowitz and Musslimani (2013) considered yet another reduction $\phi(x, t) = \pm\psi^*(-x, t)$ leading to the following equation with nonlocal nonlinearity ($\sigma = \pm 1$):

$$i\psi_t(x, t) = \psi_{xx}(x, t) + 2\sigma\psi(x, t)\psi^*(-x, t)\psi(x, t). \quad (185)$$

Note that in this equation the nonlinear term can be represented as $F(\psi)\psi$, where $F(\phi) = 2\sigma\phi(x, t)\phi^*(-x, t)$. For any ψ , the nonlinearity satisfies the identity $[F(\psi)]^* = \mathcal{P}F(\psi)\mathcal{P}$, and thus commutes with \mathcal{PT} and can be termed as \mathcal{PT} symmetric or \mathcal{P} -pseudo-Hermitian in the sense of the definition (97). In the discrete case this property guarantees the existence of at least one integral of motion. For the continuous model (185), one can find an infinite number of conserved quantities. The first one is given by Eq. (18), and the second and third ones read

$$Q_2 = \int_{-\infty}^{\infty} [\psi_x(x, t)\psi^*(-x, t) + \psi(x, t)\psi_x^*(-x, t)]dx, \quad (186)$$

$$Q_3 = \int_{-\infty}^{\infty} [\psi_x(x, t)\psi_x^*(-x, t) - \sigma\psi^2(x, t)\psi^{*2}(-x, t)]dx. \quad (187)$$

The one-soliton solution for Eq. (185) reads

$$\psi(x, t) = -\frac{2(\eta + \bar{\eta})e^{i\bar{\theta}}e^{-4i\bar{\eta}^2 t}e^{-2\bar{\eta}x}}{1 + e^{i(\bar{\theta} + \theta)}e^{4i(\eta^2 - \bar{\eta}^2)t}e^{-2(\bar{\eta} + \eta)x}}, \quad (188)$$

where $\eta, \bar{\eta}(> 0)$, θ and $\bar{\theta}$ are constants.

Being a particular case of the model (184), Eq. (185) is only the first equation in a hierarchy of integrable nonlocal models. It can be generalized to the vectorial case and to include a wider class of symmetries through the reductions of the type $\phi(x, t) = \psi^*(\varepsilon_1 x, \varepsilon_2 t)$, where ε_1 and ε_2 take values ± 1 (Yan, 2015).

Furthermore, one can construct a discrete analog of Eq. (185), which was reported by Ablowitz and Musslimani (2014) and Yan (2015).

XIII. CONCLUSIONS AND PERSPECTIVES

In this article, we reviewed recent progress on nonlinear wave dynamics in \mathcal{PT} -symmetric systems. We showed that the interplay between nonlinearity and \mathcal{PT} symmetry creates a host of new phenomena which sets nonlinear \mathcal{PT} -symmetric systems apart from traditional conservative or dissipative systems. For instance, even though \mathcal{PT} systems contain gain and loss and are dissipative in nature, they admit continuous families of nonlinear modes and integrals of motion—properties which are common in conservative systems but rare in dissipative systems. \mathcal{PT} -symmetry breaking of nonlinear modes in certain types of \mathcal{PT} systems is another surprising property which is highly nonintuitive. Stabilization of nonlinear modes in \mathcal{PT} -symmetric systems above phase transition is a fascinating property as well.

Most of the materials reviewed in this article are on theoretical aspects of \mathcal{PT} -symmetric systems. But a number of experimental validations of the main concepts as well as several practical applications were also described. Since \mathcal{PT} symmetry is prevalent in a wide range of physical systems, further experimental studies are expected to continue. A reason \mathcal{PT} symmetry can be physically useful is that it allows for overcoming losses while still preserving guidance properties of the system. In addition, under \mathcal{PT} symmetry, the gain and loss can be varied, thus paving the way for optimal and flexible control of wave-guiding systems. Exciting applications of \mathcal{PT} symmetry have already appeared. They include optical switches, unidirectional reflectionless \mathcal{PT} -symmetric metamaterials at optical frequencies, single-mode \mathcal{PT} -symmetric microring lasers, CPA lasers, and phonon lasers. In those applications, the effects of nonlinearity can be an important issue. For instance, it is well known that lasing is an intrinsic nonlinear process. Thus studies of nonlinear effects in those emerging applications are important open questions.

We anticipate that nonlinear \mathcal{PT} systems may find further applications in the near future, especially because the paradigm is relevant practically to all branches of contemporary physics. We also expect growing interest in this subject from the mathematical community, which is justified by the novelty and beauty of properties of \mathcal{PT} -symmetric models and, more generally, of non-Hermitian systems.

ACKNOWLEDGMENTS

We are indebted to our colleagues F. Kh. Abdullaev, Y. V. Bludov, C. Hang, G. Huang, Y. V. Kartashov, P. G. Kevrekidis, B. A. Malomed, D. E. Pelinovsky, and Z. Yan for fruitful collaboration and for enlightening discussions on several

topics of the present review. The work of V. V. K. and D. A. Z. was supported by the FCT (Portugal) through the Grant No. PTDC/FIS-OPT/1918/2012, and the work of J. Y. was supported in part by AFOSR (Grant No. USAF 9550-12-1-0244) and the NSF (Grant No. DMS-1311730).

REFERENCES

- Abdullaev, F. Kh., V. A. Brazhnyi, and M. Salerno, 2013, *Phys. Rev. A* **88**, 043829.
- Abdullaev, F. Kh., Y. V. Kartashov, V. V. Konotop, and D. A. Zezyulin, 2011, *Phys. Rev. A* **83**, 041805.
- Abdullaev, F. Kh., V. V. Konotop, M. Ögren, and M. P. Sørensen, 2011, *Opt. Lett.* **36**, 4566.
- Abdullaev, F. Kh., V. V. Konotop, M. Salerno, and A. V. Yulin, 2010, *Phys. Rev. E* **82**, 056606.
- Abdullaev, F. Kh., V. V. Konotop, and V. S. Shchesnovich, 2011, *Phys. Rev. A* **83**, 043811.
- Abdullaev, F. Kh., and B. A. Umarov, 2014, *J. Phys. Conf. Ser.* **553**, 012001.
- Ablowitz, M. J., D. J. Kaup, A. C. Newell, and H. Segur, 1973, *Phys. Rev. Lett.* **31**, 125.
- Ablowitz, M. J., and Z. H. Musslimani, 2013, *Phys. Rev. Lett.* **110**, 064105.
- Ablowitz, M. J., and Z. H. Musslimani, 2014, *Phys. Rev. E* **90**, 032912.
- Ablowitz, M. J., and H. Segur, 1981, *Solitons and the Inverse Scattering Transform* (SIAM, Philadelphia).
- Acevez, A. B., and S. Wabnitz, 1989, *Phys. Lett. A* **141**, 37.
- Achilleos, V., P. G. Kevrekidis, D. J. Frantzeskakis, and R. Carretero-González, 2012, *Phys. Rev. A* **86**, 013808.
- Ahmed, Z., 2001a, *Phys. Lett. A* **282**, 343.
- Ahmed, Z., 2001b, *Phys. Lett. A* **287**, 295.
- Ahmed, Z., 2009, *J. Phys. A* **42**, 472005.
- Akhmediev, N., and A. Ankiewicz, 2005, Eds., *Dissipative Solitons* (Springer, Berlin).
- Akhmediev, N. N., A. Ankiewicz, and J. M. Soto-Crespo, 2009, *Phys. Rev. E* **80**, 026601.
- Akylas, T. R., G. Hwang, and J. Yang, 2011, *Proc. R. Soc. A* **468**, 116.
- Alaician, H., and J. A. Dionne, 2014a, *Phys. Rev. B* **89**, 075136.
- Alaician, H., and J. A. Dionne, 2014b, *Phys. Rev. A* **89**, 033829.
- Alexeeva, N. V., I. V. Barashenkov, A. A. Sukhorukov, and Yu. S. Kivshar, 2012, *Phys. Rev. A* **85**, 063837.
- Al Khawaja, U., S. M. Al-Marzoug, H. Bahlouli, and Yu. S. Kivshar, 2013, *Phys. Rev. A* **88**, 023830.
- Al-Marzoug, S. M., 2014, *Opt. Express* **22**, 22080.
- Andrianov, A. A., M. V. Ioffe, F. Cannata, and J. P. Dedonder, 1999, *Int. J. Mod. Phys. A* **14**, 2675.
- Assis, P. E. G., and A. Fring, 2009, *J. Phys. A* **42**, 105206.
- Assis, P. E. G., and A. Fring, 2010, *Pramana J. Phys.* **74**, 857.
- Bagchi, B., and A. Fring, 2008, *J. Phys. A* **41**, 392004.
- Bagchi, B., S. Mallik, and C. Quesne, 2001, *Int. J. Mod. Phys. A* **16**, 2859.
- Bagchi, B., and C. Quesne, 2000, *Phys. Lett. A* **273**, 285.
- Bagchi, B., and C. Quesne, 2002, *Phys. Lett. A* **300**, 18.
- Bagchi, B., C. Quesne, and M. Znojil, 2001, *Mod. Phys. Lett. A* **16**, 2047.
- Balantekin, A. B., S. H. Fricke, and P. J. Hatchell, 1988, *Phys. Rev. D* **38**, 935.
- Balantekin, A. B., J. E. Seger, and S. H. Fricke, 1991, *Int. J. Mod. Phys. A* **06**, 695.
- Barashenkov, I. V., 1996, *Phys. Rev. Lett.* **77**, 1193.
- Barashenkov, I. V., 2014, *Phys. Rev. A* **90**, 045802.
- Barashenkov, I. V., L. Baker, and N. V. Alexeeva, 2013, *Phys. Rev. A* **87**, 033819.
- Barashenkov, I. V., and M. Gianfreda, 2014, *J. Phys. A* **47**, 282001.
- Barashenkov, I. V., G. S. Jackson, and S. Flach, 2013, *Phys. Rev. A* **88**, 053817.
- Barashenkov, I. V., D. E. Pelinovsky, and P. Dubard, 2015, *J. Phys. A* **48**, 325201.
- Barashenkov, I. V., S. V. Suchkov, A. A. Sukhorukov, S. V. Dmitriev, and Yu. S. Kivshar, 2012, *Phys. Rev. A* **86**, 053809.
- Barontini, G., R. Labouvie, F. Stubenrauch, A. Vogler, V. Guarrera, and H. Ott, 2013, *Phys. Rev. Lett.* **110**, 035302.
- Battelli, F., J. Diblik, M. Fečkan, J. Pickton, M. Pospíšil, and H. Susanto, 2015, *Nonlinear Dyn.* **81**, 353.
- Bender, C. M., 2005, *Contemp. Phys.* **46**, 277.
- Bender, C. M., 2007, *Rep. Prog. Phys.* **70**, 947.
- Bender, C. M., B. K. Berntson, D. Parker, and E. Samuel, 2013, *Am. J. Phys.* **81**, 173.
- Bender, C. M., M. Berry, and A. Mandilara, 2002, *J. Phys. A* **35**, L467.
- Bender, C. M., and S. Boettcher, 1998, *Phys. Rev. Lett.* **80**, 5243.
- Bender, C. M., S. Boettcher, and P. N. Meisinger, 1999, *J. Math. Phys. (N.Y.)* **40**, 2201.
- Bender, C. M., D. C. Brody, J. Chen, and E. Furlan, 2007, *J. Phys. A* **40**, F153.
- Bender, C. M., D. C. Brody, and H. F. Jones, 2002, *Phys. Rev. Lett.* **89**, 270401.
- Bender, C. M., G. V. Dunne, and P. N. Meisinger, 1999, *Phys. Lett. A* **252**, 272.
- Bender, C. M., and J. Feinberg, 2008, *J. Phys. A* **41**, 244004.
- Bender, C. M., A. Fring, U. Günther, and H. Jones, 2012, Eds., *J. Phys. A: Math. Theor. Special Issue*, Vol. **44**.
- Bender, C. M., M. Gianfreda, Ş. K. Özdemir, B. Peng, and L. Yang, 2013, *Phys. Rev. A* **88**, 062111.
- Bender, C. M., and H. F. Jones, 2008, *J. Phys. A* **41**, 244006.
- Bender, C. M., and P. D. Mannheim, 2010, *Phys. Lett. A* **374**, 1616.
- Bender, N., S. Factor, J. D. Bodyfelt, H. Ramezani, D. N. Christodoulides, F. M. Ellis, and T. Kottos, 2013, *Phys. Rev. Lett.* **110**, 234101.
- Bendix, O., R. Fleischmann, T. Kottos, and B. Shapiro, 2009, *Phys. Rev. Lett.* **103**, 030402.
- Bendix, O., R. Fleischmann, T. Kottos, and B. Shapiro, 2010, *J. Phys. A* **43**, 265305.
- Benisty, H., and M. Besbes, 2010, *J. Appl. Phys.* **108**, 063108.
- Benisty, H., *et al.*, 2011, *Opt. Express* **19**, 18004.
- Bergman, G. J., and M. I. Stockman, 2003, *Phys. Rev. Lett.* **90**, 027402.
- Berry, M. V., 1998, *J. Phys. A* **31**, 3493.
- Bittner, S., B. Dietz, U. Günther, H. L. Harney, M. Miski-Oglu, A. Richter, and F. Schäfer, 2012, *Phys. Rev. Lett.* **108**, 024101.
- Bludov, Yu. V., R. Driben, V. V. Konotop, and B. A. Malomed, 2013, *J. Opt.* **15**, 064010.
- Bludov, Yu. V., C. Hang, G. Huang, and V. V. Konotop, 2014, *Opt. Lett.* **39**, 3382.
- Bludov, Yu. V., V. V. Konotop, and B. A. Malomed, 2013, *Phys. Rev. A* **87**, 013816.
- Brazhnyi, V. A., and V. V. Konotop, 2004, *Mod. Phys. Lett. B* **18**, 627.
- Burlak, G., and B. A. Malomed, 2013, *Phys. Rev. E* **88**, 062904.
- Caliceti, E., F. Cannata, and S. Graffi, 2006, *J. Phys. A* **39**, 10019.
- Caliceti, E., and S. Graffi, 2005, *J. Nonlinear Math. Phys.* **12**, 138.
- Caliceti, E., S. Graffi, and J. Sjöstrand, 2005, *J. Phys. A* **38**, 185.

- Cannata, F., J.-P. Dedonder, and A. Ventura, 2007, *Ann. Phys. (Amsterdam)* **322**, 397.
- Cannata, F., G. Junker, and J. Trost, 1998, *Phys. Lett. A* **246**, 219.
- Cao, P., X. Zhu, Y. He, and H. Li, 2014, *Opt. Commun.* **316**, 190.
- Cartarius, H., D. Haag, D. Dast, and G. Wunner, 2012, *J. Phys. A* **45**, 444008.
- Cartarius, H., and G. Wunner, 2012, *Phys. Rev. A* **86**, 013612.
- Castaldi, G., S. Savoia, V. Galdi, A. Alù, and N. Engheta, 2013, *Phys. Rev. Lett.* **110**, 173901.
- Cavaglia, A., and A. Fring, 2012, *J. Phys. A* **45**, 444010.
- Cavaglia, A., A. Fring, and B. Bagchi, 2011, *J. Phys. A* **44**, 325201.
- Chang, L., X. Jiang, S. Hua, C. Yang, J. Wen, L. Jiang, G. Li, G. Wang, and M. Xiao, 2014, *Nat. Photonics* **8**, 524.
- Chen, H., S. Hu, and L. Qi, 2014, *Opt. Commun.* **331**, 139.
- Chen, Y., 1996, *Opt. Lett.* **21**, 462.
- Chen, Y., A. W. Snyder, and D. N. Payne, 1992, *IEEE J. Quantum Electron.* **28**, 239.
- Chen, Y.-X., C.-Q. Dai, and X.-G. Wang, 2014, *Opt. Commun.* **324**, 10.
- Chen, Z., J. Huang, J. Chai, X. Zhang, Y. Li, and B. A. Malomed, 2015, *Phys. Rev. A* **91**, 053821.
- Chen, Z., J. Liu, S. Fu, Y. Li, and B. A. Malomed, 2014, *Opt. Express* **22**, 29679.
- Chestnov, I. Yu., S. S. Demirchyan, A. P. Alodjants, Y. G. Rubo, and A. V. Kavokin, 2016, *Sci. Rep.* **6**, 19551.
- Chiao, R. Y., 1993, *Phys. Rev. A* **48**, R34.
- Chiao, R. Y., E. Garmire, and C. H. Townes, 1964, *Phys. Rev. Lett.* **13**, 479.
- Chong, Y. D., L. Ge, H. Cao, and A. D. Stone, 2010, *Phys. Rev. Lett.* **105**, 053901.
- Chong, Y. D., L. Ge, and A. D. Stone, 2011, *Phys. Rev. Lett.* **106**, 093902.
- Christodoulides, D. N., and R. I. Joseph, 1989, *Phys. Rev. Lett.* **62**, 1746.
- Chtchelkatchev, N. M., A. A. Golubov, T. I. Baturina, and V. M. Vinokur, 2012, *Phys. Rev. Lett.* **109**, 150405.
- Chun-Yan, L., H. Chang-Ming, and D. Liang-Wei, 2013, *Chin. Phys. B* **22**, 074209.
- Cooper, F., A. Khare, and U. Sukhatme, 1995, *Phys. Rep.* **251**, 267.
- Cuevas, J., P. G. Kevrekidis, A. Saxena, and A. Khare, 2013, *Phys. Rev. A* **88**, 032108.
- Cuevas-Maraver, J., A. Khare, P. G. Kevrekidis, H. Xu, and A. Saxena, 2015, *Int. J. Theor. Phys.* **54**, 3960.
- Curtright, D. L., and D. B. Fairlie, 2008, *J. Phys. A* **41**, 244009.
- Dai, C.-Q., and W.-H. Huang, 2014, *Appl. Math. Lett.* **32**, 35.
- Dai, C.-Q., X.-G. Wang, and G.-Q. Zhou, 2014, *Phys. Rev. A* **89**, 013834.
- Dai, C.-Q., and Y. Wang, 2014a, *Opt. Commun.* **315**, 303.
- Dai, C.-Q., and Y. Wang, 2014b, *J. Opt. Soc. Am. B* **31**, 2286.
- Dai, C.-Q., and Y.-Y. Wang, 2014c, *Laser Phys.* **24**, 035401.
- Daley, A. J., 2014, *Adv. Phys.* **63**, 77.
- Dalibard, J., F. Gerbier, G. Juzeliūnas, and P. Öhberg, 2011, *Rev. Mod. Phys.* **83**, 1523.
- D'Ambroise, J., P. G. Kevrekidis, and S. Lepri, 2012, *J. Phys. A* **45**, 444012.
- D'Ambroise, J., P. G. Kevrekidis, and B. A. Malomed, 2015, *Phys. Rev. E* **91**, 033207.
- D'Ambroise, J., S. Lepri, B. A. Malomed, and P. G. Kevrekidis, 2014, *Phys. Lett. A* **378**, 2824.
- D'Ambroise, J., B. A. Malomed, and P. G. Kevrekidis, 2014, *Chaos* **24**, 023136.
- Dana, B., A. Bahabad, and B. Malomed, 2015, *Phys. Rev. A* **91**, 043808.
- Darboux, G., 1882, *C. R. Acad. Sci. (Paris)* **94**, 1456.
- Dast, D., D. Haag, H. Cartarius, and G. Wunner, 2013, *J. Phys. A* **46**, 375301.
- Dast, D., D. Haag, H. Cartarius, G. Wunner, R. Eichler, and J. Main, 2013, *Fortschr. Phys.* **61**, 124.
- Degiron, A., S. Y. Cho, T. Tyler, N. M. Jokerst, and D. R. Smith, 2009, *New J. Phys.* **11**, 015002.
- Demirkaya, A., D. J. Frantzeskakis, P. G. Kevrekidis, A. Saxena, and A. Stefanov, 2013, *Phys. Rev. E* **88**, 023203.
- Demirkaya, A., T. Kapitula, P. G. Kevrekidis, M. Stanislavova, and A. Stefanov, 2014, *Stud. Appl. Math.* **133**, 298.
- Desyatnikov, A. S., M. R. Dennis, and A. Ferrando, 2011, *Phys. Rev. A* **83**, 063822.
- Dias, J.-P., M. Figueira, V. V. Konotop, and D. A. Zezyulin, 2014, *Stud. Appl. Math.* **133**, 422.
- Djakov, P., and B. S. Mityagin, 2006, *Usp. Mat. Nauk* **61**, 77 [Russ. Math. Surv. **61**, 663 (2006)].
- Dmitriev, S. V., S. V. Suchkov, A. A. Sukhorukov, and Yu. S. Kivshar, 2011, *Phys. Rev. A* **84**, 013833.
- Dmitriev, S. V., A. A. Sukhorukov, and Yu. S. Kivshar, 2010, *Opt. Lett.* **35**, 2976.
- Dodd, R. K., J. C. Eilbeck, J. D. Gibbon, and H. C. Morris, 1982, *Solitons and Nonlinear Wave Equations* (Academic Press, New York).
- Dohnal, T., and P. Siegl, 2015, [arXiv:1504.00054](https://arxiv.org/abs/1504.00054).
- Dorey, P., C. Dunning, and R. Tateo, 2001, *J. Phys. A* **34**, 5679.
- Driben, R., and B. A. Malomed, 2011a, *Europhys. Lett.* **96**, 51001.
- Driben, R., and B. A. Malomed, 2011b, *Opt. Lett.* **36**, 4323.
- Driben, R., and B. A. Malomed, 2012, *Europhys. Lett.* **99**, 54001.
- Duanmu, M., K. Li, R. L. Horne, P. G. Kevrekidis, and N. Whitaker, 2013, *Phil. Trans. R. Soc. A* **371**, 20120171.
- Dubard, P., P. Gaillard, C. Klein, and V. B. Matveev, 2010, *Eur. Phys. J. Spec. Top.* **185**, 247.
- El-Ganainy, R., K. G. Makris, D. N. Christodoulides, and Z. H. Musslimani, 2007, *Opt. Lett.* **32**, 2632.
- Facchi, P., and S. Pascazio, 2008, *J. Phys. A* **41**, 493001.
- Faddeev, L. D., and L. A. Takhtadjan, 1987, *Hamiltonian Methods in the Theory of Solitons* (Springer-Verlag, Berlin).
- Faisal, F. H. M., and J. V. Moloney, 1981, *J. Phys. B* **14**, 3603.
- Fan, L., J. Wang, L. T. Varghese, H. Shen, B. Niu, Y. Xuan, A. M. Weiner, and M. Qi, 2012, *Science* **335**, 447.
- Fan, S., *et al.*, 2012, *Science* **335**, 38.
- Fang, L., J. Gao, Z. Shi, X. Zhu, and H. Li, 2014, *Eur. Phys. J. D* **68**, 298.
- Feijoo, D., D. A. Zezyulin, and V. V. Konotop, 2015, *Phys. Rev. E* **92**, 062909.
- Feng, L., M. Ayache, J. Huang, Y.-L. Xu, M.-H. Lu, Y.-F. Chen, Y. Fainman, and A. Scherer, 2011, *Science* **333**, 729.
- Feng, L., Z. J. Wong, R. Ma, Y. Wang, and X. Zhang, 2014, *Science* **346**, 972.
- Feng, L., Y.-L. Xu, W. S. Fegadolli, M.-H. Lu, J. E. B. Oliveira, V. R. Almeida, Y.-F. Chen, and A. Scherer, 2013, *Nat. Mater.* **12**, 108.
- Fleischhauer, M., C. H. Keitel, M. O. Scully, C. Su, B. T. Ulrich, and S. Y. Zhu, 1992, *Phys. Rev. A* **46**, 1468.
- Fring, A., 2007, *J. Phys. A* **40**, 4215.
- Fring, A., H. F. Jones, and M. Znojil, 2008, Eds., *J. Phys. A Special Issue*, Vol. **41**, No. 24 [<http://iopscience.iop.org/issue/1751-8121/41/24>].
- Fushchych, W. I., N. I. Serov, and T. Amerov, 1991, *Proc. Acad. Sci. Ukraine* **12**, 15 (in Russian, English abstract) [http://www.imath.kiev.ua/~fushchych/papers/1991_11.pdf].

- Gaididei, Yu. B., 2013 (unpublished).
- Galitski, V., and I. B. Spielman, 2013, *Nature (London)* **494**, 49.
- Galley, C. R., 2013, *Phys. Rev. Lett.* **110**, 174301.
- Gallo, C., and D. E. Pelinovsky, 2014, *Stud. Appl. Math.* **133**, 398.
- Gao, T., *et al.*, 2015, *Nature (London)* **526**, 554.
- Garcia, S. R., E. Prodan, and M. Putinar, 2014, *J. Phys. A* **47**, 353001.
- Gasymov, M. G., 1980, *Funkts. Anal. Prilozh.* **14**, 14 [*Funct. Anal. Appl.* **14**, 11 (1980)].
- Ge, L., M. Shen, C. Ma, T. Zang, and L. Dai, 2014, *Opt. Express* **22**, 29435.
- Gericke, T., P. Würtz, D. Reitz, T. Langen, and H. Ott, 2008, *Nat. Phys.* **4**, 949.
- Geyer, H., D. Heiss, and M. Znojil, 2006, Eds., *J. Phys. A Special issue*, Vol. **39**, No. 32 [<http://iopscience.iop.org/issue/0305-4470/39/32>].
- Ginzburg, V. L., and L. D. Landau, 1950, *Zh. Eksp. Teor. Fiz.* **20**, 1064, English translation in *Collected Papers of L. D. Landau*, edited by D. Ter Haar (Pergamon Press, Oxford, 1965), p. 546 [<https://dx.doi.org/10.1016/B978-0-08-010586-4.50078-X>].
- Graefe, E.-M., 2012, *J. Phys. A* **45**, 444015.
- Graefe, E. M., U. Günther, H. J. Korsch, and A. E. Niederle, 2008, *J. Phys. A* **41**, 255206.
- Graefe, E.-M., and H. F. Jones, 2011, *Phys. Rev. A* **84**, 013818.
- Graefe, E.-M., H. J. Korsch, and A. E. Niederle, 2008, *Phys. Rev. Lett.* **101**, 150408.
- Graefe, E.-M., and C. Liverani, 2013, *J. Phys. A* **46**, 455201.
- Greenberg, M., and M. Orenstein, 2004, *Opt. Lett.* **29**, 451.
- Guo, A., G. J. Salamo, D. Duchesne, R. Morandotti, M. Volatier-Ravat, V. Aimez, G. A. Siviloglou, and D. N. Christodoulides, 2009, *Phys. Rev. Lett.* **103**, 093902.
- Guo, B., L. Ling, and Q. P. Liu, 2012, *Phys. Rev. E* **85**, 026607.
- Gupta, S. K., and A. K. Sarma, 2014a, *Europhys. Lett.* **105**, 44001.
- Gupta, S. K., and A. K. Sarma, 2014b, *J. Mod. Opt.* **61**, 227.
- Hang, C., G. Huang, and V. V. Konotop, 2013, *Phys. Rev. Lett.* **110**, 083604.
- Hang, C., Y. V. Kartashov, G. Huang, and V. V. Konotop, 2015, *Opt. Lett.* **40**, 2758.
- Hang, C., D. A. Zezyulin, G. Huang, V. V. Konotop, and B. A. Malomed, 2014, *Opt. Lett.* **39**, 5387.
- Hang, C., D. A. Zezyulin, V. V. Konotop, and G. Huang, 2013, *Opt. Lett.* **38**, 4033.
- Haus, H. A., 1984, *Waves and Fields in Optoelectronics* (Prentice-Hall, Englewood Cliffs, NJ).
- He, Y., and D. Mihalache, 2012, *Rom. Rep. Phys.* **64**, Supplement p. 1243 [http://www.rpp.infim.ro/2012_supliment/art09Mihalache.pdf].
- He, Y., and D. Mihalache, 2013, *Phys. Rev. A* **87**, 013812.
- He, Y., D. Mihalache, X. Zhu, L. Guo, and Y. V. Kartashov, 2012, *Opt. Lett.* **37**, 2526.
- He, Y., X. Zhu, D. Mihalache, J. Liu, and Z. Chen, 2012a, *Opt. Commun.* **285**, 3320.
- He, Y., X. Zhu, D. Mihalache, J. Liu, and Z. Chen, 2012b, *Phys. Rev. A* **85**, 013831.
- He, Y.-J., and B. A. Malomed, 2013, "Spatial Solitons in Parity-Time-Symmetric Photonic Lattices: Recent Theoretical Results," in *Spontaneous Symmetry Breaking, Self-Trapping, and Josephson Oscillations*, edited by B. A. Malomed (Springer, Berlin).
- Heiss, W. D., 2012, *J. Phys. A* **45**, 444016.
- Hesmer, F., E. Tatartschuk, O. Zhuromskyy, A. A. Radkovskaya, M. Shamonin, T. Hao, C. J. Stevens, G. Faulkner, D. J. Edwards, and E. Shamonina, 2007, *Phys. Status Solidi B* **244**, 1170.
- Hodaie, H., M.-A. Miri, M. Heinrich, D. N. Christodoulides, and M. Khajavikhan, 2014, *Science* **346**, 975.
- Hong, W.-P., and Y.-D. Jung, 2015, *Phys. Lett. A* **379**, 676.
- Horne, R. L., J. Cuevas, P. G. Kevrekidis, N. Whitaker, F. Kh. Abdullaev, and D. J. Frantzeskakis, 2013, *J. Phys. A* **46**, 485101.
- Hu, S., and H. Chen, 2014, *Phys. Lett. A* **378**, 3079.
- Hu, S., and W. Hu, 2013a, *Opt. Commun.* **294**, 311.
- Hu, S., and W. Hu, 2013b, *Physica B (Amsterdam)* **429**, 28.
- Hu, S., D. Lu, X. Ma, Q. Guo, and W. Hu, 2012, *Europhys. Lett.* **98**, 14006.
- Hu, S., X. Ma, D. Lu, Z. Yang, Y. Zheng, and W. Hu, 2011, *Phys. Rev. A* **84**, 043818.
- Hu, S., X. Ma, D. Lu, Y. Zheng, and W. Hu, 2012, *Phys. Rev. A* **85**, 043826.
- Hu, S. M., and W. Hu, 2012, *Eur. Phys. J. D* **66**, 266.
- Hu, S.-M., and W. Hu, 2013, *Chin. Phys. B* **22**, 074201.
- Huang, C., C. Li, and L. Dong, 2013, *Opt. Express* **21**, 3917.
- Huang, C., F. Ye, Y. V. Kartashov, B. A. Malomed, and X. Chen, 2014, *Opt. Lett.* **39**, 5443.
- Infeld, L., and T. E. Hull, 1951, *Rev. Mod. Phys.* **23**, 21.
- Jackson, R. K., and M. I. Weinstein, 2004, *J. Stat. Phys.* **116**, 881.
- Jin, L., and Z. Song, 2009, *Phys. Rev. A* **80**, 052107.
- Jing, H., S. K. Özdemir, X.-Y. Lü, J. Zhang, L. Yang, and F. Nori, 2014, *Phys. Rev. Lett.* **113**, 053604.
- Jisha, C. P., A. Alberucci, V. A. Brazhnyi, and G. Assanto, 2014, *Phys. Rev. A* **89**, 013812.
- Jisha, C. P., L. Devassy, A. Alberucci, and V. C. Kuriakose, 2014, *Phys. Rev. A* **90**, 043855.
- Joglekar, Y. N., D. Scott, M. Babbey, and A. Saxena, 2010, *Phys. Rev. A* **82**, 030103(R).
- Jones, H., 1999, *Phys. Lett. A* **262**, 242.
- Jørgensen, M. F., and P. L. Christiansen, 1994, *Chaos Solitons Fractals* **4**, 217.
- Jørgensen, M. F., P. L. Christiansen, and I. Abou-Hayt, 1993, *Physica D (Amsterdam)* **68**, 180.
- Karjanto, N., W. Hanif, B. A. Malomed, and H. Susanto, 2015, *Chaos* **25**, 023112.
- Kartashov, Y. V., 2013, *Opt. Lett.* **38**, 2600.
- Kartashov, Y. V., V. V. Konotop, and L. Torner, 2015, *Phys. Rev. Lett.* **115**, 193902.
- Kartashov, Y. V., V. V. Konotop, and D. A. Zezyulin, 2014, *Europhys. Lett.* **107**, 50002.
- Kartashov, Y. V., B. A. Malomed, and L. Torner, 2011, *Rev. Mod. Phys.* **83**, 247.
- Kartashov, Y. V., B. A. Malomed, and L. Torner, 2014, *Opt. Lett.* **39**, 5641.
- Kartashov, Y. V., V. A. Vysloukh, V. V. Konotop, and L. Torner, 2016, *Phys. Rev. A* **93**, 013841.
- Kato, T., 1966, *Perturbation Theory for Linear Operators* (Springer-Verlag, Berlin).
- Kevrekidis, P. G., 2009, *The Discrete Nonlinear Schrödinger Equation: Mathematical Analysis, Numerical Computations, and Physical Perspectives* (Springer-Verlag, Berlin, Heidelberg).
- Kevrekidis, P. G., 2014, *Phys. Rev. A* **89**, 010102(R).
- Kevrekidis, P. G., V. V. Konotop, A. Rodrigues, and D. J. Frantzeskakis, 2005, *J. Phys. B* **38**, 1173.
- Kevrekidis, P. G., D. E. Pelinovsky, and D. Y. Tyugin, 2013a, *J. Phys. A* **46**, 365201.
- Kevrekidis, P. G., D. E. Pelinovsky, and D. Y. Tyugin, 2013b, *SIAM J. Appl. Dyn. Syst.* **12**, 1210.
- Khare, A., S. M. Al-Marzoug, and H. Bahlouli, 2012, *Phys. Lett. A* **376**, 2880.
- Khare, A., and U. Sukhatme, 1989, *J. Phys. A* **22**, 2847.

- Kharif, C., E. Pelinovsky, and A. Slunyaev, 2009, *Rogue waves in the ocean* (Springer, Heidelberg).
- Kirr, E. W., P. G. Kevrekidis, E. Shlizerman, and M. I. Weinstein, 2008, *SIAM J. Math. Anal.* **40**, 566.
- Kivshar, Yu. S., T. Alexander, and S. K. Turitsyn, 2001, *Phys. Lett. A* **278**, 225.
- Klaiman, S., U. Günther, and N. Moiseyev, 2008, *Phys. Rev. Lett.* **101**, 080402.
- Konotop, V. V., D. E. Pelinovsky, and D. A. Zezyulin, 2012, *Europhys. Lett.* **100**, 56006.
- Konotop, V. V., and L. Vázquez, 1994, *Nonlinear Random Waves* (World Scientific Publishing, Singapore).
- Konotop, V. V., and D. A. Zezyulin, 2014a, *Opt. Lett.* **39**, 1223.
- Konotop, V. V., and D. A. Zezyulin, 2014b, *Opt. Lett.* **39**, 5535.
- Kreibich, M., J. Main, H. Cartarius, and G. Wunner, 2013, *Phys. Rev. A* **87**, 051601(R).
- Kulishov, M., J. Laniel, N. Bélanger, J. Azaña, and D. V. Plant, 2005a, *Opt. Express* **13**, 3068.
- Kulishov, M., J. Laniel, N. Bélanger, and D. V. Plant, 2005b, *Opt. Express* **13**, 3567.
- Lamb, G. L., 1980, *Elements of Soliton Theory* (Wiley, New York).
- Landau, L. D., and E. M. Lifshitz, 1977, *Quantum Mechanics. Nonrelativistic Theory* (Pergamon Press, New York).
- Lawrence, M., N. Xu, X. Zhang, L. Cong, J. Han, W. Zhang, and S. Zhang, 2014, *Phys. Rev. Lett.* **113**, 093901.
- Lazarides, N., M. Eleftheriou, and G. P. Tsironis, 2006, *Phys. Rev. Lett.* **97**, 157406.
- Lazarides, N., and G. Tsironis, 2013, *Phys. Rev. Lett.* **110**, 053901.
- Lee, J. M., T. Kottos, and B. Shapiro, 2015, *Phys. Rev. B* **91**, 094416.
- Lee, T. D., and G. C. Wick, 1969, *Nucl. Phys. B* **9**, 209.
- Leonhardt, U., 2006, *Science* **312**, 1777.
- Lévai, G., F. Cannata, and A. Ventura, 2001, *J. Phys. A* **34**, 839.
- Lévai, G., and E. Magyari, 2009, *J. Phys. A* **42**, 195302.
- Leykam, D., V. V. Konotop, and A. S. Desyatnikov, 2013, *Opt. Lett.* **38**, 371.
- Li, C., C. Huang, H. Liu, and L. Dong, 2012, *Opt. Lett.* **37**, 4543.
- Li, C., H. Liu, and L. Dong, 2012, *Opt. Express* **20**, 16823 [<https://www.osapublishing.org/oe/abstract.cfm?uri=oe-20-15-16823>].
- Li, H., X. Jiang, X. Zhu, and Z. Shi, 2012, *Phys. Rev. A* **86**, 023840.
- Li, H., X. Zhu, Z. Shi, B. A. Malomed, T. Lai, and C. Lee, 2014, *Phys. Rev. A* **89**, 053811.
- Li, H.-j., J.-p. Dou, and G. Huang, 2013, *Opt. Express* **21**, 32053.
- Li, K., and P. G. Kevrekidis, 2011, *Phys. Rev. E* **83**, 066608.
- Li, K., P. G. Kevrekidis, D. J. Frantzeskakis, C. E. Rüter, and D. Kip, 2013, *J. Phys. A* **46**, 375304.
- Li, K., P. G. Kevrekidis, and B. A. Malomed, 2014, *Stud. Appl. Math.* **133**, 281.
- Li, K., P. G. Kevrekidis, B. A. Malomed, and U. Günther, 2012, *J. Phys. A* **45**, 444021.
- Li, K., D. A. Zezyulin, P. G. Kevrekidis, V. V. Konotop, and F. Kh. Abdullaev, 2013, *Phys. Rev. A* **88**, 053820.
- Li, K., D. A. Zezyulin, V. V. Konotop, and P. G. Kevrekidis, 2013, *Phys. Rev. A* **87**, 033812.
- Li, P., L. Li, and B. A. Malomed, 2014, *Phys. Rev. E* **89**, 062926.
- Li, X., and X.-T. Xie, 2014, *Phys. Rev. A* **90**, 033804.
- Lien, J., Y. Chen, N. Ishida, H. Chen, C. Hwang, and F. Nori, 2015, *Phys. Rev. B* **91**, 024511.
- Lin, Y. J., K. Jiménez-García, and I. B. Spielman, 2011, *Nature (London)* **471**, 83.
- Lin, Z., H. Ramezani, T. Eichelkraut, T. Kottos, H. Cao, and D. N. Christodoulides, 2011, *Phys. Rev. Lett.* **106**, 213901.
- Liu, X., S. D. Gupta, and G. S. Agarwal, 2014, *Phys. Rev. A* **89**, 013824.
- Longhi, S., 2009a, *Phys. Rev. B* **80**, 165125.
- Longhi, S., 2009b, *Phys. Rev. Lett.* **103**, 123601.
- Longhi, S., 2010, *Phys. Rev. A* **81**, 022102.
- Longhi, S., 2011, *Phys. Rev. A* **83**, 055804.
- Lu, N., P. G. Kevrekidis, and J. Cuevas-Maraver, 2014, *J. Phys. A* **47**, 455101.
- Lu, Z., and Z. Zhang, 2011, *Opt. Express* **19**, 11457.
- Lumer, Y., Y. Plotnik, M. C. Rechtsman, and M. Segev, 2013, *Phys. Rev. Lett.* **111**, 263901.
- Lupu, A., H. Benisty, and A. Degiron, 2013, *Opt. Express* **21**, 21651.
- MacKay, R. S., 1987, "Stability of equilibria of Hamiltonian systems," in *Hamiltonian Dynamical Systems*, edited by R. S. MacKay and J. Meiss (Adam Hilger, Bristol), pp. 137–153.
- MacKay, R. S., and S. Aubry, 1994, *Nonlinearity* **7**, 1623.
- Makris, K. G., R. El-Ganainy, D. N. Christodoulides, and Z. H. Musslimani, 2008, *Phys. Rev. Lett.* **100**, 103904.
- Makris, K. G., R. El-Ganainy, D. N. Christodoulides, and Z. H. Musslimani, 2010, *Phys. Rev. A* **81**, 063807.
- Makris, K. G., R. El-Ganainy, D. N. Christodoulides, and Z. H. Musslimani, 2011, *Int. J. Theor. Phys.* **50**, 1019.
- Makris, K. G., Z. H. Musslimani, D. N. Christodoulides, and S. Rotter, 2015, *Nat. Commun.* **6**, 7257.
- Malomed, B. A., 2013, Ed., *Spontaneous Symmetry Breaking, Self-Trapping, and Josephson Oscillations* (Springer, Berlin).
- Malomed, B. A., and P. G. Kevrekidis, 2001, *Phys. Rev. E* **64**, 026601.
- Manakov, S. V., 1973, *Zh. Eksp. Teor. Fiz.* **65**, 505 [*Sov. Phys. JETP* **38**, 248 (1974), http://www.jetp.ac.ru/cgi-bin/dn/e_038_02_0248.pdf].
- Maytevarunyoo, T., B. A. Malomed, and A. Reksabutr, 2013, *Phys. Rev. E* **88**, 022919.
- Meng, Y., and Y. Liu, 2013, *J. Opt. Soc. Am. B* **30**, 1148.
- Midya, B., 2015, *Nonlinear Dyn.* **79**, 409.
- Midya, B., B. Roy, and R. Roychoudhury, 2010, *Phys. Lett. A* **374**, 2605.
- Midya, B., and R. Roychoudhury, 2013, *Phys. Rev. A* **87**, 045803.
- Midya, B., and R. Roychoudhury, 2014, *Ann. Phys. (Amsterdam)* **341**, 12.
- Miri, M., M. Heinrich, and D. N. Christodoulides, 2013, *Phys. Rev. A* **87**, 043819.
- Miri, M. A., A. B. Aceves, T. Kottos, V. Kovanis, and D. N. Christodoulides, 2012, *Phys. Rev. A* **86**, 033801.
- Miri, M.-A., A. Regensburger, U. Peschel, and D. Christodoulides, 2012, *Phys. Rev. A* **86**, 023807.
- Miroshnichenko, A. E., B. A. Malomed, and Yu. S. Kivshar, 2011, *Phys. Rev. A* **84**, 012123.
- Moiseyev, N., 2011, *Non-Hermitian Quantum Mechanics* (Cambridge University Press, Cambridge, England).
- Moiseyev, N., and S. Friedland, 1980, *Phys. Rev. A* **22**, 618.
- Moreira, F. C., F. Kh. Abdullaev, V. V. Konotop, and A. V. Yulin, 2012, *Phys. Rev. A* **86**, 053815.
- Moreira, F. C., V. V. Konotop, and B. A. Malomed, 2013, *Phys. Rev. A* **87**, 013832.
- Mostafazadeh, A., 2002a, *J. Math. Phys. (N.Y.)* **43**, 205.
- Mostafazadeh, A., 2002b, *J. Math. Phys. (N.Y.)* **43**, 2814.
- Mostafazadeh, A., 2002c, *J. Math. Phys. (N.Y.)* **43**, 3944.
- Mostafazadeh, A., 2003a, *J. Phys. A* **36**, 7081.
- Mostafazadeh, A., 2003b, *J. Math. Phys. (N.Y.)* **44**, 974.
- Mostafazadeh, A., 2008, *J. Phys. A* **41**, 055304.
- Mostafazadeh, A., 2009a, *Pramana J. Phys.* **73**, 269.
- Mostafazadeh, A., 2009b, *Phys. Rev. Lett.* **102**, 220402.
- Mostafazadeh, A., 2009c, *Phys. Rev. A* **80**, 032711.
- Mostafazadeh, A., 2010, *Int. J. Geom. Methods Mod. Phys.* **07**, 1191.
- Mostafazadeh, A., 2011a, *Phys. Rev. A* **83**, 045801.
- Mostafazadeh, A., 2011b, *Phys. Rev. A* **84**, 023809.

- Mostafazadeh, A., 2012, *J. Phys. A* **45**, 444024.
- Mostafazadeh, A., 2013a, *Phys. Rev. Lett.* **110**, 260402.
- Mostafazadeh, A., 2013b, *Phys. Rev. A* **87**, 063838.
- Mostafazadeh, A., 2014, *Stud. Appl. Math.* **133**, 353.
- Mostafazadeh, A., 2015, *Trends in Mathematics 145* (Springer International Publishing, Switzerland).
- Mostafazadeh, A., and H. Mehri-Dehnavi, 2009, *J. Phys. A* **42**, 125303.
- Muga, J. G., J. P. Palao, B. Navarro, and I. L. Egusquiza, 2004, *Phys. Rep.* **395**, 357.
- Muslimani, Z. H., K. G. Makris, R. El-Ganainy, and D. N. Christodoulides, 2008a, *Phys. Rev. Lett.* **100**, 030402.
- Muslimani, Z. H., K. G. Makris, R. El-Ganainy, and D. N. Christodoulides, 2008b, *J. Phys. A* **41**, 244019.
- Naimark, M. A., 1954, *Trudy Moscov. Mat. Obsc.* **3**, 181 [Transl.-Am. Math. Soc. **16**, 103 (1960)].
- Nazari, F., N. Bender, H. Ramezani, M. K. Moravvej-Farshi, D. N. Christodoulides, and T. Kottos, 2014, *Opt. Express* **22**, 9574.
- Nazari, F., M. Nazari, M. K. Moravvej-Farshi, and H. Ramezani, 2013, *IEEE J. Quantum Electron.* **49**, 932.
- Nazari, M., F. Nazari, and M. K. Moravvej-Farshi, 2012, *J. Opt. Soc. Am. B* **29**, 3057.
- Nixon, S., L. Ge, and J. Yang, 2012, *Phys. Rev. A* **85**, 023822.
- Nixon, S., and J. Yang, 2013, *Opt. Lett.* **38**, 1933.
- Nixon, S., and J. Yang, 2014, *Stud. Appl. Math.* **133**, 373.
- Nixon, S., and J. Yang, 2016a, *Phys. Rev. A* **93**, 031802(R).
- Nixon, S., and J. Yang, 2016b, *Stud. Appl. Math.* (to be published).
- Nixon, S., Y. Zhu, and J. Yang, 2012, *Opt. Lett.* **37**, 4874.
- Noginov, M. A., V. A. Podolskiy, G. Zhu, M. Mayy, M. Bahoura, J. A. Adegoke, B. A. Ritzo, and K. Reynolds, 2008, *Opt. Express* **16**, 1385.
- Nötzold, D., 1987, *Phys. Rev. D* **36**, 1625.
- Novikov, S. P., S. V. Manakov, L. P. Pitaevskii, and V. E. Zakharov, 1984, *Theory of Solitons: The Inverse Scattering Method* (Springer-Verlag, Berlin).
- Nozva, D., B. A. Malomed, H. Michinel, and V. M. Pérez-García, 2008, *Phys. Rev. Lett.* **101**, 144101.
- O'Brien, C., P. M. Anisimov, Y. Rostovtsev, and O. Kocharovskaya, 2011, *Phys. Rev. A* **84**, 063835.
- Ohta, Y., and J. Yang, 2012, *Proc. R. Soc. A* **468**, 1716.
- Pare, C., and M. Florjanczyk, 1990, *Phys. Rev. A* **41**, 6287.
- Pelinovsky, D. E., 2011, *Localization in Periodic Potentials: From Schrödinger Operators to the Gross-Pitaevskii Equation* (Cambridge University Press, New York).
- Pelinovsky, D. E., P. G. Kevrekidis, and D. J. Frantzeskakis, 2013, *Europhys. Lett.* **101**, 11002.
- Pelinovsky, D. E., D. A. Zezyulin, and V. V. Konotop, 2014, *J. Phys. A* **47**, 085204.
- Pelinovsky, D. E., D. A. Zezyulin, and V. V. Konotop, 2015, *Int. J. Theor. Phys.* **54**, 3920.
- Pendry, J. B., D. Schurig, and D. R. Smith, 2006, *Science* **312**, 1780.
- Peng, B., Ş. K. Özdemir, S. Rotter, H. Yilmaz, M. Liertzer, F. Monifi, C. M. Bender, F. Nori, and L. Yang, 2014, *Science* **346**, 328.
- Peng, B., Ş. K. Özdemir, F. Lei, F. Monifi, M. Gianfreda, G. L. Long, S. Fan, F. Nori, C. M. Bender, and L. Yang, 2014, *Nat. Phys.* **10**, 394.
- Peregrine, D. H., 1983, *J. Aust. Math. Soc. Series B, Appl. Math.* **25**, 16.
- Pérez-García, V. M., P. J. Torres, and V. V. Konotop, 2006, *Physica D (Amsterdam)* **221**, 31.
- Pickton, J., and H. Susanto, 2013, *Phys. Rev. A* **88**, 063840.
- Pitaevskii, L., and S. Stringari, 2003, *Bose-Einstein Condensation* (Clarendon Press, Oxford).
- Poladian, L., 1996, *Phys. Rev. E* **54**, 2963.
- Popa, B.-I., and S. A. Cummer, 2014, *Nat. Commun.* **5**, 3398.
- Proite, N. A., B. E. Unks, J. T. Green, and D. D. Yavuz, 2008, *Phys. Rev. Lett.* **101**, 147401.
- Psiachos, D., N. Lazarides, and G. P. Tsironis, 2014, *Appl. Phys. A* **117**, 663.
- Ramezani, H., T. Kottos, R. El-Ganainy, and D. N. Christodoulides, 2010, *Phys. Rev. A* **82**, 043803.
- Ramezani, H., H.-K. Li, Y. Wang, and X. Zhang, 2014, *Phys. Rev. Lett.* **113**, 263905.
- Reed, M., and B. Simon, 1980, *Methods of Modern Mathematical Physics I: Functional Analysis* (Academic Press, San Diego).
- Regensburger, A., C. Bersch, B. Hinrichs, G. Onishchukov, A. Schreiber, C. Silberhorn, and U. Peschel, 2011, *Phys. Rev. Lett.* **107**, 233902.
- Regensburger, A., C. Bersch, M.-A. Miri, G. Onishchukov, D. N. Christodoulides, and U. Peschel, 2012, *Nature (London)* **488**, 167.
- Ren, X., H. Wang, H. Wang, and Y. He, 2014, *Opt. Express* **22**, 19774.
- Robins, N. P., P. A. Altin, J. E. Debs, and J. D. Close, 2013, *Phys. Rep.* **529**, 265.
- Rodrigues, A. S., K. Li, V. Achilleos, P. G. Kevrekidis, D. J. Frantzeskakis, and C. M. Bender, 2013, *Rom. Rep. Phys.* **65**, 5 [http://www.rpp.infim.ro/2013_65_1/art01Rodrigues.pdf].
- Rosenau, P., 1994, *Phys. Rev. Lett.* **73**, 1737.
- Rosenau, P., and J. M. Hyman, 1993, *Phys. Rev. Lett.* **70**, 564.
- Rotter, I., 2009, *J. Phys. A* **42**, 153001.
- Rubinstein, J., P. Sternberg, and Q. Ma, 2007, *Phys. Rev. Lett.* **99**, 167003.
- Ruschhaupt, A., F. Delgado, and J. G. Muga, 2005, *J. Phys. A* **38**, L171.
- Rüter, C. E., K. G. Makris, R. El-Ganainy, D. N. Christodoulides, M. Segev, and D. Kip, 2010, *Nat. Phys.* **6**, 192.
- Rysaeva, L. K., S. V. Suchkov, and S. V. Dmitriev, 2014, *JETP Lett.* **99**, 577.
- Sacchetti, A., 2009, *Phys. Rev. Lett.* **103**, 194101.
- Sarma, A. K., 2014, *J. Opt. Soc. Am. B* **31**, 1861.
- Sarychev, A. K., and V. M. Shalaev, 2004, *Proc. SPIE Int. Soc. Opt. Eng.* **5508**, 128.
- Schäfer, T., and C. E. Wayne, 2004, *Physica D (Amsterdam)* **196**, 90.
- Schindler, J., A. Li, M. C. Zheng, F. M. Ellis, and T. Kottos, 2011, *Phys. Rev. A* **84**, 040101(R).
- Scott, D. D., and Y. N. Joglekar, 2011, *Phys. Rev. A* **83**, 050102(R).
- Scully, M. O., 1991, *Phys. Rev. Lett.* **67**, 1855.
- Serkin, V. N., and A. Hasegawa, 2000, *Phys. Rev. Lett.* **85**, 4502.
- Shchesnovich, V. S., and V. V. Konotop, 2010, *Phys. Rev. A* **81**, 053611.
- Shi, Z., X. Jiang, X. Zhu, and H. Li, 2011, *Phys. Rev. A* **84**, 053855.
- Shi, Z., H. Li, X. Zhu, and X. Jiang, 2012, *Europhys. Lett.* **98**, 64006.
- Simmons, Z. J., N. A. Proite, J. Miles, D. E. Sikes, and D. D. Yavuz, 2012, *Phys. Rev. A* **85**, 053810.
- Slonczewski, J. C., 2002, *J. Magn. Magn. Mater.* **247**, 324.
- Sluka, V., A. Kákay, A. M. Deac, D. E. Bürgler, R. Hertel, and C. M. Schneider, 2011, *J. Phys. D* **44**, 384002.
- Smith, D. R., J. B. Pendry, and M. C. K. Wiltshire, 2004, *Science* **305**, 788.
- Snyder, A. W., and D. J. Mitchell, 1997, *Science* **276**, 1538.
- Solombrino, L., 2002, *J. Math. Phys. (N.Y.)* **43**, 5439.
- Song, Q., Z. Shi, Y. Li, and H. Li, 2014, *Opt. Commun.* **331**, 105.
- Spreeuw, R. J. C., T. Pfau, U. Jianicke, and M. Wilkens, 1995, *Europhys. Lett.* **32**, 469.
- Stanescu, T., B. Anderson, and V. Galitski, 2008, *Phys. Rev. A* **78**, 023616.

- Stegeman, G. I., D. J. Hagan, and L. Torner, 1996, *Opt. Quantum Electron.* **28**, 1691.
- Suchkov, S. V., S. V. Dmitriev, B. A. Malomed, and Yu. S. Kivshar, 2012, *Phys. Rev. A* **85**, 033825.
- Suchkov, S. V., B. A. Malomed, S. V. Dmitriev, and Yu. S. Kivshar, 2011, *Phys. Rev. E* **84**, 046609.
- Suchkov, S. V., A. A. Sukhorukov, S. V. Dmitriev, and Yu. S. Kivshar, 2012, *Europhys. Lett.* **100**, 54003.
- Suchkov, S. V., A. A. Sukhorukov, J. Huang, S. V. Dmitriev, C. Lee, and Yu. S. Kivshar, 2016, *Laser Photonics Rev.* **10**, 177.
- Sukhorukov, A. A., S. V. Dmitriev, S. V. Suchkov, and Yu. S. Kivshar, 2012, *Opt. Lett.* **37**, 2148.
- Sukhorukov, A. A., Z. Xu, and Yu. S. Kivshar, 2010, *Phys. Rev. A* **82**, 043818.
- Sulem, C., and P. Sulem, 2000, *The Nonlinear Schrödinger Equation: Self-focusing and Wave Collapse* (Springer, Berlin).
- Sun, Y., W. Tan, H.-q. Li, J. Li, and H. Chen, 2014, *Phys. Rev. Lett.* **112**, 143903.
- Truong Vu, Y. N., J. D'Ambrose, F. Kh. Abdullaev, and P. G. Kevrekidis, 2015, [arXiv:1501.00519v1](https://arxiv.org/abs/1501.00519v1).
- Tsironis, G. P., and N. Lazarides, 2014, *Appl. Phys. A* **115**, 449.
- Tsoy, E. N., I. M. Allayarov, and F. Kh. Abdullaev, 2014, *Opt. Lett.* **39**, 4215.
- Tsoy, E. N., S. S. Tadjimuratov, and F. Kh. Abdullaev, 2012, *Opt. Commun.* **285**, 3441.
- Tsutsumi, M., 1984, *SIAM J. Math. Anal.* **15**, 357.
- Tsuzuki, T., 1971, *J. Low Temp. Phys.* **4**, 441.
- Unanyan, R. G., 1992, *Sov. Phys. JETP* **74**, 781 [*Zh. Eksp. Teor. Fiz.* **101**, 1463 (1992), http://www.jetp.ac.ru/cgi-bin/dn/e_074_05_0781.pdf].
- Vysloukh, V. A., and Y. V. Kartashov, 2014, *Opt. Lett.* **39**, 5933.
- Wadati, M., 2008, *J. Phys. Soc. Jpn.* **77**, 074005.
- Wadati, M., and K. Ohkuma, 1982, *J. Phys. Soc. Jpn.* **51**, 2029.
- Walasik, W., C. Ma, and N. M. Litchinitser, 2015, *Opt. Lett.* **40**, 5327.
- Wan, W., Y. Chong, L. Ge, H. Noh, A. D. Stone, and H. Cao, 2011, *Science* **331**, 889.
- Wang, D. H., and A. B. Aceves, 2013, *Phys. Rev. A* **88**, 043831.
- Wang, H., W. He, S. Shi, X. Zhu, and Y. He, 2014, *Phys. Scr.* **89**, 025502.
- Wang, H., W. He, L. Zheng, X. Zhu, H. Li, and Y. He, 2012, *J. Phys. B* **45**, 245401.
- Wang, H., S. Shi, X. Ren, X. Zhu, B. A. Malomed, D. Mihalache, and Y. He, 2015, *Opt. Commun.* **335**, 146.
- Wang, H., and J. Wang, 2011, *Opt. Express* **19**, 4030.
- Wang, H.-C., D.-X. Ling, S.-Q. Zhang, X. Zhu, and Y.-J. He, 2014, *Chin. Phys. B* **23**, 064208.
- Wang, Y. Y., C. Q. Dai, and X. G. Wang, 2014a, *Nonlinear Dyn.* **77**, 1323.
- Wang, Y. Y., C. Q. Dai, and X.-G. Wang, 2014b, *Ann. Phys. (Amsterdam)* **348**, 289.
- Wasak, T., P. Szankowski, V. V. Konotop, and M. Trippenbach, 2015, *Opt. Lett.* **40**, 5291.
- Wen, Z., and Z. Yan, 2015, *Phys. Lett. A* **379**, 2025.
- Wigner, E., 1959, *Group Theory and Its Application to Quantum Mechanics of Atomic Spectra* (Academic, New York).
- Wimmer, M., A. Regensburger, M.-A. Miri, C. Bersch, D. N. Christodoulides, and U. Peschel, 2015, *Nat. Commun.* **6**, 7782.
- Witthaut, D., F. Trimborn, H. Hennig, G. Kordas, T. Geisel, and S. Wimberger, 2011, *Phys. Rev. A* **83**, 063608.
- Wright, E. M., G. I. Stegeman, and S. Wabnitz, 1989, *Phys. Rev. A* **40**, 4455.
- Xie, J., Z. Shu, W. Chen, G. Chen, J. Lv, D. Mihalache, and Y. He, 2014, *Opt. Commun.* **313**, 139.
- Xu, H., P. G. Kevrekidis, and A. Saxena, 2015, *J. Phys. A* **48**, 055101.
- Xu, X.-W., Y.-X. Liu, C.-P. Sun, and Y. Li, 2015, *Phys. Rev. A* **92**, 013852.
- Xu, Y.-J., and C.-Q. Dai, 2014, *Opt. Commun.* **318**, 112.
- Yan, Z., 2008, *Phys. Scr.* **77**, 025006.
- Yan, Z., 2012, *J. Phys. A* **45**, 444035.
- Yan, Z., 2013, *Phil. Trans. R. Soc. A* **371**, 20120059.
- Yan, Z., 2015, *Appl. Math. Lett.* **47**, 61.
- Yan, Z., Z. Wen, and C. Hang, 2015, *Phys. Rev. E* **92**, 022913.
- Yan, Z., Z. Wen, and V. V. Konotop, 2015, *Phys. Rev. A* **92**, 023821.
- Yan, Z., B. Xiong, and W. M. Liu, 2010, [arXiv:1009.4023v1](https://arxiv.org/abs/1009.4023v1).
- Yang, J., 2010, *Nonlinear Waves in Integrable and Nonintegrable Systems* (SIAM, Philadelphia).
- Yang, J., 2012, *Stud. Appl. Math.* **129**, 133.
- Yang, J., 2014a, *Stud. Appl. Math.* **132**, 332.
- Yang, J., 2014b, *Phys. Lett. A* **378**, 367.
- Yang, J., 2014c, *Opt. Lett.* **39**, 1133.
- Yang, J., 2014d, *Opt. Lett.* **39**, 5547.
- Yang, J., 2015, *Phys. Rev. E* **91**, 023201.
- Yavuz, D. D., 2005, *Phys. Rev. Lett.* **95**, 223601.
- Yin, C., Y. He, H. Li, and J. Xie, 2012, *Opt. Express* **20**, 19355.
- Yulin, A. V., and V. V. Konotop, 2013, *Opt. Lett.* **38**, 4880.
- Zakharov, V. E., and A. B. Shabat, 1971, *Zh. Eksp. Teor. Fiz.* **61**, 118 [http://www.jetp.ac.ru/cgi-bin/dn/e_034_01_0062.pdf][*Sov. Phys. JETP* **34**, 62 (1972)].
- Zeng, J., and Y. Lan, 2012, *Phys. Rev. E* **85**, 047601.
- Zezyulin, D. A., Y. V. Kartashov, and V. V. Konotop, 2011, *Europhys. Lett.* **96**, 64003.
- Zezyulin, D. A., and V. V. Konotop, 2012a, *Phys. Rev. A* **85**, 043840.
- Zezyulin, D. A., and V. V. Konotop, 2012b, *Phys. Rev. Lett.* **108**, 213906.
- Zezyulin, D. A., and V. V. Konotop, 2013, *J. Phys. A* **46**, 415301.
- Zhang, X., J. Chai, J. Huang, Z. Chen, Y. Li, and B. A. Malomed, 2014, *Opt. Express* **22**, 13927.
- Zharov, A. A., I. V. Shadrivov, and Y. S. Kivshar, 2003, *Phys. Rev. Lett.* **91**, 037401.
- Zheng, M. C., D. N. Christodoulides, R. Fleischmann, and T. Kottos, 2010, *Phys. Rev. A* **82**, 010103(R).
- Zhong, W.-P., M. R. Belić, and T. Huang, 2012, *Nonlinear Dyn.* **70**, 2027.
- Zhu, X., P. Cao, L. Song, Y. He, and H. Li, 2014, *J. Opt. Soc. Am. B* **31**, 2109.
- Zhu, X., H. Li, H. Wang, and Y. He, 2013, *J. Opt. Soc. Am. B* **30**, 1987.
- Zhu, X., H. Ramezani, C. Shi, J. Zhu, and X. Zhang, 2014, *Phys. Rev. X* **4**, 031042.
- Zhu, X., H. Wang, H. Li, W. He, and Y. He, 2013b, *Opt. Lett.* **38**, 2723.
- Zhu, X., H. Wang, L. X. Zheng, H. Li, and Y.-J. He, 2011, *Opt. Lett.* **36**, 2680.
- Zibrov, A. S., M. D. Lukin, L. Hollberg, D. E. Nikonov, M. O. Scully, H. G. Robinson, and V. L. Velichansky, 1996, *Phys. Rev. Lett.* **76**, 3935.
- Znojil, M., 1999, *Phys. Lett. A* **259**, 220.
- Znojil, M., 2000, *J. Phys. A* **33**, L61.